Compliant Grids

Theory, Design and Realization

Jonas Schikore

Technical University of Munich

TUM School of Engineering and Design

TUM

Compliant Grids

Theory, Design and Realization

Jonas Schikore

Chair:

Prof. Dr. Pierluigi D'Acunto

Examiners:

1. Prof. Dr.-Ing. Rainer Barthel
2. Prof. Dr.-Ing. Kai-Uwe Bletzinger
3. Prof. Dr.-Ing. Julian Lienhard

Acknowledgements

Abstract

This thesis investigates the mechanical behavior and planning methods for transformable lightweight structures. In scope are spatial grid structures for support, that perform semi-compliant transformations, including both rigid-body and compliant mechanisms. These structures are based on quadrilateral grids of initially straight, partly compliant beams, that are coupled by hinges.

The aim is to understand the geometric and mechanical interrelations for practical use. This work looks for conceptual, mechanical, and constructive approaches as well as suitable planning methods.

The state of the art presents the theoretical, constructive, and architectural basis, and describes adapted methods for modeling and simulation, that are applied in this work.

A series of mechanical studies forms the theoretical framework. Firstly, all relevant components and parameters are displayed. The decisive kinematic, kinetic, and static phenomena and relations are elaborated using analytical and computational analyses: These include the orthogonal deflection and force ratios of kinematic grids, the spatial transformability and morphology of semi-compliant systems, the inner energetic proportions during transformation, as well as decisive static, global and local stiffness proportions. The parameters of compliant grid structures are referred to individual characteristics. Physical model studies show the conceptual, morphological, and mechanical freedom of design and demonstrate general feasibility.

The architectural implementation involves conflictive mechanical requirements and parameters. These are revealed, and appropriate strategies for an iterative planning process is developed. Several case studies inform this development in a "Research by Design"-process, that introduces constructive requirements. Firstly, the one-time erection of asymptotic gridshells is in scope.

The *Kinetic Umbrella* marks the first reversible transformable structure of its kind. Actuated by a cable pulley system, the compliant grid structure made of GFRP lamellas deploys from a bundled, closed shape into an open umbrella. This project demonstrates the feasibility at architectural scale and shows mechanical and constructive challenges and potentials. The mechanical findings and planning methods are fully incorporated and validated in this project.

This work determines fundamental mechanical phenomena of semi-compliant, doubly curved grid structures and presents useful engineering strategies for practical use. Thereby, this work provides a comprehensive basis for the development of semi-compliant support structures for architectural use.

Zusammenfassung

Diese Arbeit untersucht das mechanische Verhalten und Planungsmethoden transformierbarer Tragstrukturen für den Leichtbau. Gegenstand sind räumliche Gitterstrukturen mit der Fähigkeit zur teilnachgiebigen Formänderung, welche sowohl starr-körper Mechanismen als auch nachgiebige Mechanismen vereinen. Im Fokus stehen vorwiegend vierseitige Gitter aus geraden, und axial eingeschränkt nachgiebigen Stäben, welche untereinander gelenkig gekoppelt sind.

Ziel ist es, die geometrischen und mechanischen Zusammenhänge dieser Tragsysteme zu verstehen, und für die Anwendung zu erschließen. Gesucht werden konzeptionelle, mechanische und konstruktive Lösungsansätze, sowie geeignete Planungsmethoden.

Der Stand der Technik bildet die theoretische, konstruktive und architektonische Grundlage. Zudem werden angepasste Methoden der Modellbildung und Simulation beschrieben, welche hier zum Einsatz kommen.

Eine Reihe mechanischer Studien bildet das theoretische Rahmenwerk. Zunächst werden alle relevanten Komponenten und Parameter systematisch aufbereitet. Mittels analytischer und computergestützter Untersuchungen werden wesentliche kinematische, kinetische und statische Phänomene und Zusammenhänge ausgearbeitet: Diese umfassen die orthogonalen Verschiebungs- und Kraftverhältnisse kinematischer Gitter, die räumliche Transformierbarkeit und Morphologie teilnachgiebiger Systeme, die inneren energetischen Verhältnisse bei der Formänderung, sowie wesentliche statische, lokale und globale Steifigkeitsverhältnisse. Den unterschiedlichen Systemparameter werden dabei individuelle Eigenschaften zugeordnet. Physische Modellentwürfe zeigen den konzeptionellen, morphologischen und mechanischen Gestaltungsspielraum und die generelle physikalische Umsetzbarkeit.

Für die bautechnische Umsetzung im architektonischen Maßstab werden die teils gegensätzlichen mechanischen Anforderungen und Zielgrößen hergeleitet und entsprechende Strategien für einen iterativen Planungsprozess entwickelt. Mehrere Fallstudien begleiten diese Entwicklung In einem *„Research by Design"*-Prozess, wobei auch konstruktive Anforderungen einfließen. Dabei stehen die einmalige Formänderung und Statik asymptotischer Gitterschalen im Fokus.

Der *„Kinetic Umbrella"* hingegen ist die erste reversibel wandelbare Konstruktion ihrer Art. Angetrieben durch ein Seilzugsystem entfaltet sich die nachgiebige Gitterstruktur aus GFK-Lamellen von einer gebündelten, geschlossenen Form in einen offenen Schirm. Dieses Projekt demonstriert die Umsetzbarkeit solcher Systeme im architektonischen Maßstab und zeigt die mechanischen und konstruktiven Herausforderungen und Potenziale auf. Die theoretischen Erkenntnisse und Planungsmethoden sind in diesem Projekt gänzlich umgesetzt und validiert.

Diese Arbeit erfasst grundlegende mechanische Aspekte teilnachgiebiger, gekrümmter Gitter. Für die Praxis werden umfassende ingenieursmäßige Arbeitsstrategien aufgezeigt. Damit bildet diese Arbeit eine belastbare Grundlage für die Entwicklung teilelastischer Gitterstrukturen für das Bauwesen.

Content

Figure 1 *The Kinetic Umbrella inside view*

1 INTRODUCTION

This thesis is written at the *Technical University of Munich*, at the *Chair of Structural Design*, led by Prof. Dr.-Ing R. Barthel, and later at the followed professorship of Prof. Dr. P. D'Acunto. It was conducted between 2017 and 2022. The topic of compliant grid structures and mechanisms emerged from extensive work in the field of formfinding and parametric modeling, and in collaboration with Prof. Dr.-Ing. Eike Schling, investigating asymptotic gridshells.

Object of this research are smooth transformable grid structures. These systems combine compliant deformation and kinematic freedom to perform fluent transformations of doubly curved shapes. This mechanical concept is applied to an architectural environment, including its scale, constructive criteria, and structural requirements on load-bearing.

The technical challenges for this structural innovation are to manage several complexities: the geometry of doubly curved grids structures, the integration of mechanical systems, the spatial transformation and its progression, and the constructive implementation.

How to meet these challenges? The first step is to capture the current state of the art, to identify relevant fundamentals, methods and developments, and potential interrelations (chapter 2). The second step is to formulate the structural problem and investigate key phenomena to provide a theoretical base (chapter 3). The last step is the architectural implementation including the development of design strategies, verified in physical case studies (chapter 4).

Motivation

Structural transformability is a powerful quality, potentially useful in any field, application, or scale, and has always fascinated engineers and designers. However, the benefits of transformability conflict with the mechanical complexity associated. If complex geometries are to be transformed using conventional rigid-body mechanisms, hinges or sliding devices, the constructive effort may outbalance the benefits of transformability. This conflict motivates the idea of compliant mechanisms, that operate without friction and with less components. At small objects scale, compliant mechanisms are part of our everyday life.

The idea of transformability in an architectural context expands the design space of architects. It allows differing functions at different times, or adaption to user's needs. Technical development in the field of transformability supports this idea. Moreover, structural transformability can be a part of the construction process and support rapid erection or packing for mobile structures.

This work deals with doubly curved grid structures, also called gridshells, considering a specified load-bearing behavior. These structures are classified as lightweight structures, known for remarkable efficiency and architectural quality. An advanced type utilizes elastic deformation to generate curvature: Strained gridshells. This concept simplifies the constructive and fabrication effort.

In the field of differential geometry, findings have revealed geometrical transformability of networks on smooth surfaces with constrained geometric parameters, and these relationships

were brought in context with mechanical constraints of grid structures. The topic of compliant grid structures picks up on these findings. It combines the potentials of compliant mechanisms, grid structures, and transformability.

However, compliant mechanisms require sophisticated engineering strategies. The balance of geometry and force requires computer aided design tools and coordinated workflows. The increase of computational abilities in the past decades has now prepared the path for such systems, to be integrated in the build environment.

Objective

This research aims to develop compliant grid structures for architectural implementation and use. Therefore, full understanding of the geometric and mechanical phenomena is essential. This includes the morphology of such systems and the internal progression of forces, stresses, and energies. Furthermore, this theoretical understanding must be applicable in terms of suitable engineering workflows, strategies, and tools, that handle the systems complexity. It is a major goal of this work, to provide such solutions.

Several research questions arise for compliant grid structures and inherent mechanisms:

- What are the components and parameters?

- Which elastic mechanisms are suitable for grid structures?

- Which geometric principles apply and what shapes can be generated?

- How do such mechanisms perform mechanically, and how are they controlled?

- How are such mechanisms designed, model and simulated?

- How do requirements of transformability and load-bearing interrelate?

- Which architectural scales are suitable for implementation?

Methodology

The substantial research is conducted in chapter 3 and 4, using the following methodology:

Chapter 3 involves both deductive and inductive approaches. The deductive character results from geometric relations, provided by differential geometry. Findings in this field are used as a starting point for mechanical implementation. The inductive approach is used in various analyses. Selected mechanical systems are simulated or physically modeled to test and derive decisive relations and behavior patterns or to verify morphological expectations.

Chapter 4 follows a "Research by Design" strategy. During various case studies, decisive parameters, criteria, and requirements are identified and an engineering process is developed iteratively. The physical outcome of these case studies is furthermore verifying theoretical expectations.

Structure

This thesis is organized in five chapters. Framed by an introduction (chapter 1) and a summary (chapter 5), the actual content is given in chapters 2, 3 and 4, that represent basis, theory, and practice. These chapters are further subdivided into 11 sections in total, that are organized using subordinated numbering.

Chapter 2 displays the state of art. It bundles geometric and mechanical fundamentals in the first sections (2.1, 2.2), displays methods for modeling and simulation that are used in this work (section 2.3), and provides insight into the research environment and associated developments (section 2.4).

Chapter 3 contributes a theoretical basis to design and simulate semi-compliant grids. The structural components of semi-compliant grid structures are defined in section 3.1. In various analyses, associated kinematic and kinetic phenomena are investigated to reveal specific geometric and mechanical interrelations (section 3.2). The third section (3.3) investigates the structural performance at static states. In the last section (3.4), four physical designs at model scale are analyzed regarding its components and performance.

Chapter 4 contributes practical design strategies. The first section (4.1) presents key aspects of engineering semi-compliant grid structures. The second section (4.2) gives insight to build asymptotic gridshells, erected using semi-compliant mechanisms. The last section (4.3) presents the *Kinetic Umbrella*, a deployable semi-compliant grid structure at architectural scale.

Tools

The tools used in this work involve physical testing models and computational modeling and simulation software:

Multiple strip models are extensively used for mechanical explorations and testing (see section 3.4 and 4.3.3). These models are mostly built from thin laminated timber sheets that are laser cut and plug connected at nodes. Other models made from GFRP utilize extruded profiles, manually prepared. Various models include 3D-printed plastic details (*Formlabs* Stereolithography) (see section 2.3.3).

For computational analyses, the following software products are used:

- Parametric 3D modeling: *Rhino6/7 by McNeel, Grasshopper*

- Isogeometric Analysis: *Carat++ by TUM / KIWI* (*Grasshopper* Plugin by *str.ucture GmbH*)

- Finite Element Methods: *R-FEM 5 by Dlubal Software GmbH*

Terminology

Several technical terms used may allow differing interpretations or detailed specifications. The following list includes some terms with distinct specifications, valid for this work:

Compliancy	Property of a structural element that is a necessary condition for mechanisms, to perform intended, large elastic deformations.
Deflection	Elastic deformation caused by loads and gravity. In addition to the intentional change of geometry by mechanisms, deflections can also occur unintentionally, and are usually minimized by design measures to ensure the integrity of mechanisms.
Deformation	Change of shape, involving purely elastic strain.
Deployment	Structural transformation from a packed into a service state.
Grid Structure	A load-bearing system of beams (members), that is referenced to a surface. The load-bearing performance may include grillage like and/or shell like behavior.
Mechanism	A transformable system, that has a function and performs in a controlled way. Inherent transformations are reactions to actuations.
Morphology	Change of shape in a transformation process, or the collective geometric spectrum within a transformation.
Transformation	Change of the state of a structural system including geometrical and mechanical change

Publications and Theses

Parts of this work have been published in collaborative conference papers or specialized books. Some contents are part of bachelor or master theses at the *Technical University of Munich*, supervised by the author of this work.

In the following publications, Jonas Schikore contributed as guiding author:

- *Schikore, Jonas; Schling, Eike; Oberbichler, Thomas; Bauer, Anna Maria (2020): Kinetics and Design of Semi-Compliant Grid Mechanisms. In: Olivier Baverel, Cyril Douthe, Romain Mesnil, Caitlin Mueller, Helmut Pottmann und Tomohiro Tachi (Publ.): AAG 2020 // Advances in architectural geometry 2020. Advances in Architectural Geometry 2020. Paris, France. Ecole des Ponts ParisTech. Paris: Ecole des Ponts ParisTech; Université Gustave Eiffel dDL 2021, p. 108–129.*

  (Associated sections 3.2, 4.2, 4.3)

- *Schikore, Jonas (2020): Mobile, wandelbare und adaptive Tragwerke. In: Eberhard Möller (Hg.): Atlas Tragwerke. München: Detail Business Information, p. 136–141.*

  (Associated sections 2.4.2 and 2.4.3)

- *Schikore, Jonas; Bauer, Anna M; Barthel, Rainer; Bletzinger, K.-U. (2019): Large torsion on elastic lamella grid structures. In: International Centre for Numerical Methods in Engineering (Hg.): Proceedings of the IASS Annual Symposium 2021. Form and Force. IASS. Barcelona, p. 807–814.*

  (Associated sections 2.2.3 and 4.2.2)

In the following publications, Jonas Schikore contributed as co-author author:

- *Schling, Eike; Kilian, Martin; Wang, Hui; Schikore, Jonas; Pottmann, Helmut (2018): Design and Construction of Curved Support Structures with Repetitive Parameters. In: Lars Hesselgren, Axel Kilian, Samar Malek, Karl-Gunnar Olsson, Olga Sorkine-Hornung und Chris Williams (Hg.): AAG 2018. Advances in Architectural Geometry 2018, Bd. 7. Gothenburg, Sweden. Wien: Klein Publishing GmbH; Klein Publishing GmbH (Ltd), p. 140–165. Online verfügbar unter www.mediatum.ub.tum.de/doc/1468900/file.pdf, last access: 09.04.2020.*

  (Associated sections 2.4.1, 4.2.1)

- *Schling, Eike; Hitrec, Denis; Schikore, Jonas; Barthel, Rainer (2017): Design and Construction of the Asymptotic Pavilion. In: K.-U. Bletzinger, E. Onate, B. Kröplin (Hg.): Structural Membranes 2017, Bd. 8. VIII International Conference on Textile Composites and Inflatable Structures. Munich, 7.-11.10.2017. International Center for Numerical Methods in Engineering (CIMNE). 9 Bände. Barcelona: Artes Gráficas Torres S.L., Huelva 9, 08940 Cornellà de (8), p. 178–189.*

  (Associated sections 4.2.1)

- *Schling, Eike; Schikore, Jonas; Oberbichler, Thomas (2020/21): D-Nets on rotational surfaces. Equilibrium gridshell layout, symmetric to the principal stress directions. In: International Centre for Numerical Methods in Engineering (Publ..): Proceedings of the IASS Annual Symposium 2021. IASS. Surrey.*

  (Associated sections 3.2.1)

- *Schling, Eike; Schikore, Jonas (2022): Morphology of Kinetic Asymptotic Grids. In: Christoph Gengnagel, Olivier Baverel, Giovanni Betti, Mariana Popescu, Mette Ramsgard Thomsen und Jan Wurm (Hg.): Towards radical regeneration. Design Modelling Symposium Berlin 2022. Cham, Switzerland: Springer, p. 374–393.*

  (Associated sections 3.2, 4.3)

As an academic council, the author of this work was supervising several related theses:

- *Forker, Felix Konstantin (2020): Minimal Energy Modes of Transformable Compliant Grid Structures. Master Thesis. Technical University of Munich, Munich. Chair of Structural Design (Prof. R. Barthel).*

- *Isildak, Eda Ayla (2020): Scherengelenke elastischer Gitterstrukturen. Beziehungen zwischen Rotationsachse und Verformungsverhalten. Master Thesis. Technical University of Munich, Munich. Chair of Structural Design (Prof. R. Barthel).*

- *Lindner, Clemens; Sun, Tao (2021): Transformable Cladding Systems. Research, Design and Fabrication. Bachelor Thesis. Technical University of Munich, Munich. Professorship of Structural Design (Prof. P. D'Acunto).*

Projects and Contribution

The practical part in chapter 3.3 includes several built projects (case studies), that were developed, supported, and executed in close collaboration with various actors. The contribution of these actors is specified below:

Inside\Out **Pavilion (2017)**

Project lead:	Eike Schling (*TUM*)
Design and modeling:	Eike Schling, Denis Hitrec
Static Analysis and official proof:	Jonas Schikore
Details and Dimensioning:	Eike Schling, Jonas Schikore
Assembly and Construction:	Beatrix Huff, Denis Hitrec, Andrea Schmidt, Viktor Späth, Miquel Lloret Garcia, Maximilian Gemsjäger
Manufacturing, Sponsoring and Consultation:	*BRANDL Eitensheim GmbH*

Hotel Intergroup **Canopy (2019)**

Contractor:	*BRANDL Eitensheim GmbH*
Architect:	Eike Schling
Static Analysis and official proof:	Jonas Schikore
Details and Dimensioning:	Eike Schling, Jonas Schikore
Manufacturing, Assembly and Construction:	*BRANDL Eitensheim GmbH*
Membrane:	*Liz-Boa* (Nick Seise)
Prices:	*Deutscher Metallbaupreis 2020,* category*:* Steel Structures

Kinetic Umbrella (2021)

Project lead:	Jonas Schikore (*TUM*)
Academic Partner and Consultation:	Eike Schling (*HKU*), Pierluigi D'Acunto, Rainer Barthel
Design, modeling, static analysis, Dimensioning:	Jonas Schikore
Industrial Partners and Sponsors:	*BRANDL Eitensheim GmbH* (steel), *Farcturee* (aluminium nodes), *Gepotex GmbH* (Textile Cover System)
Manufacturing and Industrial Partners:	*Holzbau-Amann GmbH* (Timber), *BRANDL Eitensheim GmbH* (Steel)
Assembly and Construction:	Merlin Bieling, Frederic Chovghi, Sebastian Dietrich, Sebastian Hoyer, Clemens Lindner, Maria Rau, Fabian Matella, Sanziana Maximeasa, Sarah Sendzek, Tao Sun, Frauke Wilken
Project grants	*STO Stiftung* (*Design Built Research*), *Dr. Marschall* scholarship

Asymptotic Timber Vault (2022)

Project lead:	Eike Schling, Zongshuai Wan (*The University of Hong Kong | HKU*)
Academic Partner:	*Technical University of Munich* (*TUM*): Chair of Structural Design: Prof. Pierluigi D'Acunto Jonas Schikore, Julian Trummer, Sebastian Hoyer *King Abdullah University of Science and Technology* (*KAUST*): Applied Mathematics and Computational Science: Prof. Helmut Pottmann, Dr. Hui Wang
Static Analysis:	Zongshuai Wan
Engineering Support:	Jonas Schikore (Project Consultation), Joram Tutsch (Approval Planing), Máté Péntek, (Wind Consultant), Jörg Rehm (Approval Planing and Fire Safety)
Manufacturing and Industrial Partners:	*Holzbau-Amann GmbH* (Timber)*, BRANDL Eitensheim GmbH* (Steel)
Assembly and Construction:	Josef Eglseder, Anne Ambrosy, Clemens Lindner Laura Lehle, Martina Gruzlewski, Gabriele Felici, Desiré Agostini, Davide Binci, Aida Domingo Losa, Andrea Albalate Pérez, Anna Gaudin, Axel Rasmussen, Belén Ruiz, Camilla Evangelisti, Davide Piccolo, Elisa Cordaro, Esteban Álvarez Balogh, Federico Ferrero, Lavinia Krick, María García, Maria Pancewicz, Mathilde Larose, Philip Schneider, Rémi Koumakpayi, Valentina Ficca

Section 3.3 includes four selected physical model studies that have been developed by and with master students in an architectural design studio at the TUM. This studio was supervised by Jonas Schikore in 2019. The following projects contributed:

The **Active Grillage** by Fredrik Justnes (Acknowledgement *Stuttgarter Leichtbaupreis 2019*)

The **Sail** by Barbara van Waarden

The **Blooming Flower** by Chiara Saccomanno and Noemi Thierens

The **EXX-Dome** by Alberto Ortensi (1. Price *Competition Online Campus 2020*)

Figure 2 *The Hoberman Sphere*

2 STATE OF THE ART

This chapter includes the current state of art that directly relates to this work. It is subdivided into the following sections:

- Section 2.1 presents the **geometric fundamentals** related to surface-based networks.

- Section 2.2 explains the **mechanical fundamentals** with focus on large elastic beam deformation and nonlinear behavior.

- Section 2.3 describes methods of **modeling and simulation**, that are applied in this work.

- Section 2.4 presents preparatory **research and developments** in the field of structural engineering and architecture.

2.1 Geometric Fundamentals

This work is deals with grid structures based on surface embedded networks. The following sections describe the basic geometric components such as points, curves and surfaces, and the characteristics of surface embedded curves and networks, that represent the geometric reference of the compliant grid structures. Special attention is given to the geometric definitions of curvature, which is later related to compliant bending.

2.1.1 Points and Curves

Points are infinitely small and have no own characteristics except its position in space. A point is the basic element in geometry.

Curves describe a continues and infinite number of points, or a trace of a moving point in space. In general, there are smooth and discrete curves. Smooth curves are crucial for this work, as these are referred to continues beams in a mechanical context. Discrete curves (Polygons) are used to approximate smooth curves in conventional numerical methods (see section 2.3.2 p.33).

The parameter t is conventionally used to define any position along the curve. The *Frenet-Serret*-frame (TNB-frame) is a powerful apparatus to handle the curves curvature. It can be set up at any point of the curve and it is defined by the curves tangent **t**, normal **n**, and bi-normal vector **b**. The curvature $\kappa_{(t)}$ at any location t can be expressed by the curvature-circle with radius $r_{(t)}$:

$$r_{(t)} = \frac{1}{\kappa_{(t)}}$$

<div align="right">*Equation 1*</div>

The circle of curvature is located within the **n-t**-plane. Figure 3 shows an arbitrary spatial curve with the curvature circle and the *Frenet-Serret*-frame applied at parameter t.
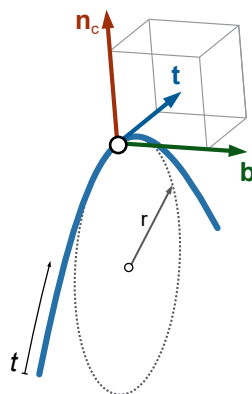

Figure 3 *The Frenet-Serret-frame on an arbitrary curve at parameter t*

Note, for straight lines (or polygon curves) this frame remains undefined, as curvature for frame orientation does not exist.

2.1.2 Smooth Surfaces

Smooth surfaces are two-dimensional spaces that are differentiable in mathematical context. The surface parameters (U, V) can be used to allocate any position on the surface. At any location, the normal vector **n** exists, that is perpendicular to the surface, or its local tangential plane.

Normal Curvature

The surface's normal curvature can be measured at any point on the surface, in any direction. The principal curvatures are the minimum and maximum curvatures, always given in perpendicular directions $\mathbf{k}_1$ and $\mathbf{k}_2$. Figure 4 illustrates an arbitrary surface with two embedded points, one at a synclastic (positive) surface area, one at an anticlastic (negative) area.
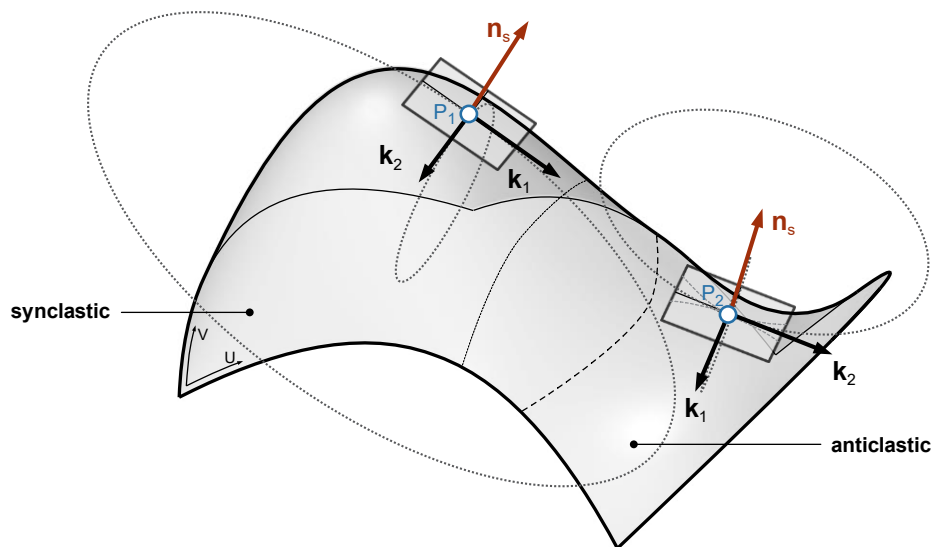
Figure 4 *Smooth surface, normal vectors and tangential planes, and principal curvature directions and curvature-circle at a positively (P_1) and negatively curved position on the surface (P_2)*

The Gaussian curvature K and mean curvature H are fundamental quantities of curved surfaces, defined at any point using the principal curvatures:

$$K = \kappa_1 \cdot \kappa_2 \; ; H = \frac{1}{2}(\kappa_1 + \kappa_2)$$

Equation 2

If κ_1 and κ_2 are of same sign, the Gaussian curvature becomes positive and the surface is synclastic. If both are of opposite sign, the Gaussian curvature is negative and the surface is anticlastic. Accordingly, the curvature circles of the principal curvatures are located at same side (see Figure 4, P_1) or opposite side of the surface (P_2). Surfaces with zero Gaussian curvature are developable.

The Gaussian curvature is used for classification of grid structures (see section 3.1.1), and for geometric analyses in section 3.2.2.

Types

There are numerous types of smooth surfaces, that can be classified according to their geometric or even physical qualities:

- **Traditional surfaces** are generated using simple geometric operations (e.g., translation or rotation of curves)

- **Free-form surfaces** require more complex geometric operations, but they allow high flexibility to designers. A network of control points defines these surfaces. Bezier-, B-splines, and NURBS-surfaces are commonly used.

- **Physical surfaces** also follow geometric constraints. However, they are related to physical phenomena that occur naturally, such as soap-films (minimal surfaces) or hanging shapes.

A selection and detailed descriptions are given in Figure 5, set up by Schling, 2018 (based on Bentley et al., 2007 and Barthel, 2019).
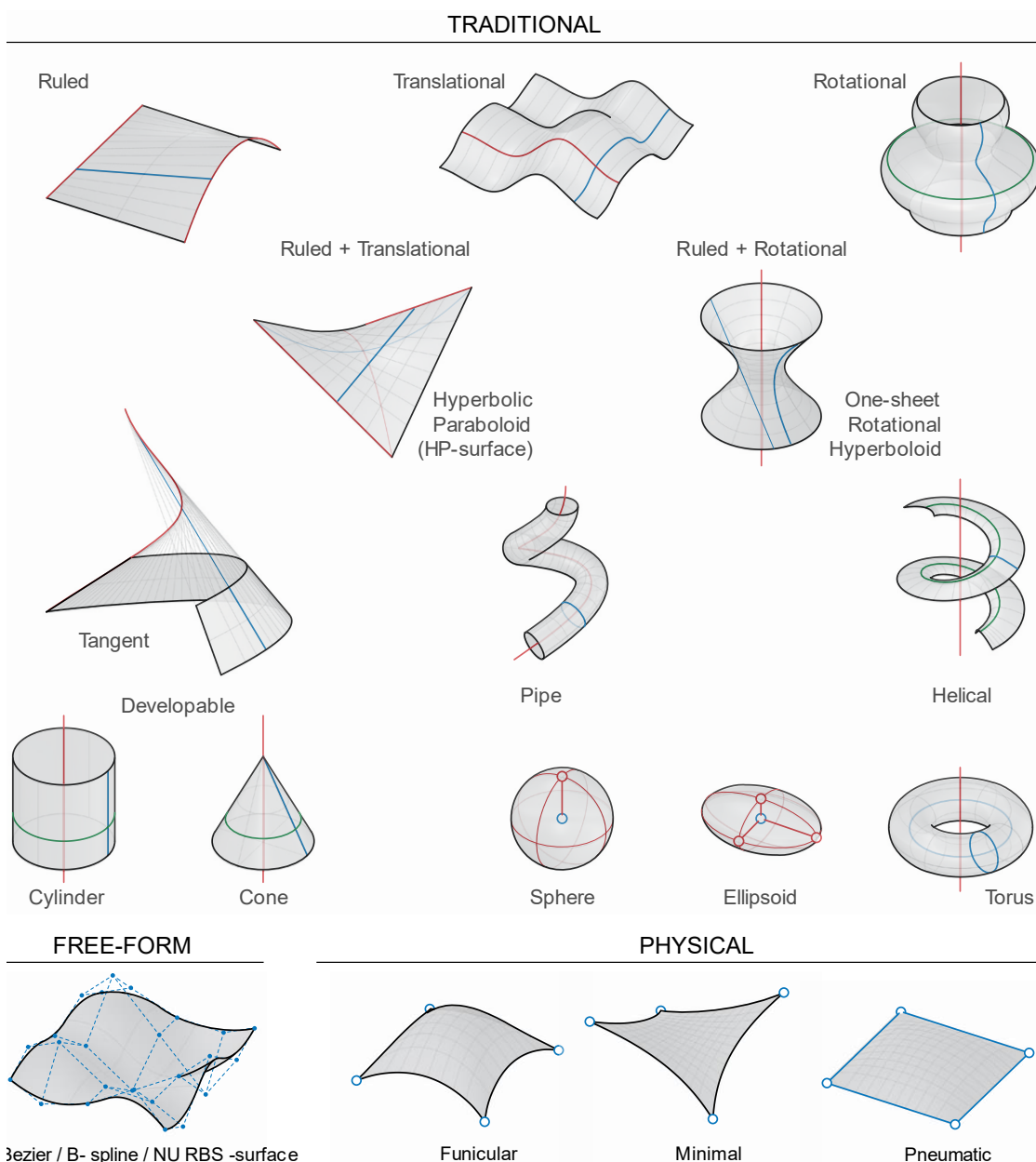

Figure 5 *Overview of surface classes (Schling, 2018, p. 12)*

Topology
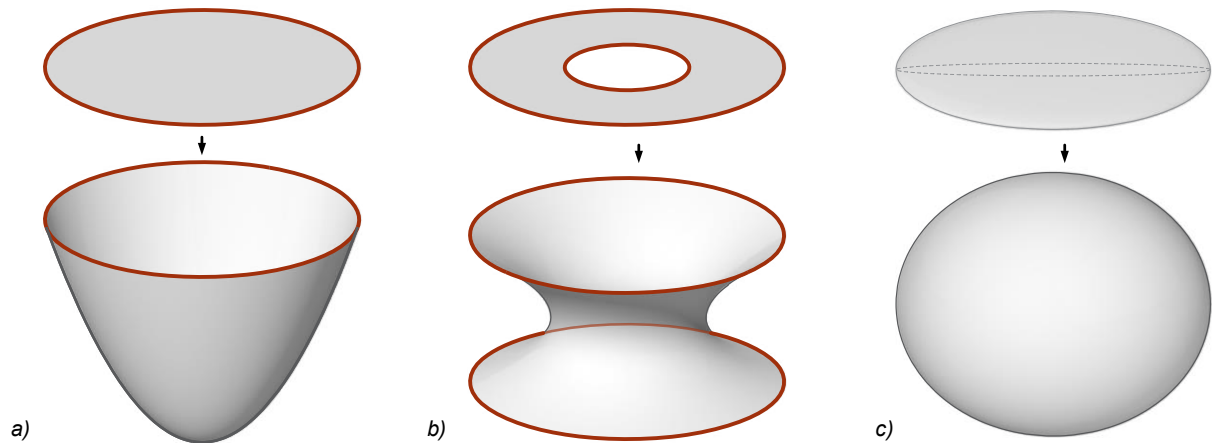
Figure 6 *Surface topologies: Exemplary homeomorphisms of different topologies: a) Disc surface (one edge), b) Disc with one hole (two edges), c) Closed surface (zero edges and holes)*

The typology of surfaces addresses the existence of boundaries and holes, their configuration and number. The topology has an impact on the continuous deformability of surfaces in a mathematical context. Two surfaces are topologically identical (or homeomorphic), if they can be deformed to match each other by stretching or changing curvature only, without cutting or seaming edges (Kinsey, 1993).

Deformation
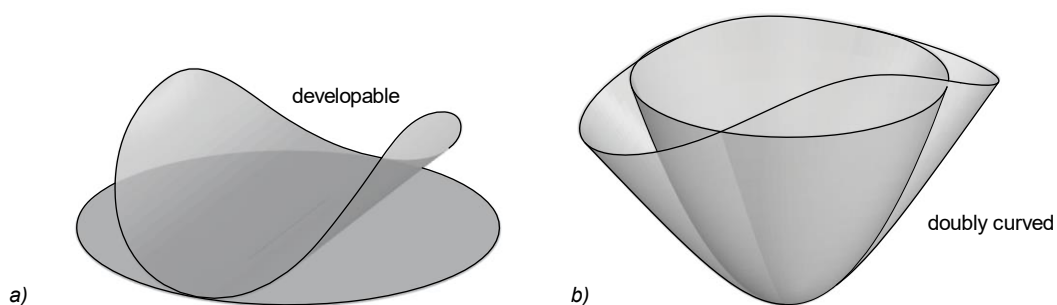
Figure 7 *Inextensional surface deformation: a) deformation of a deployable surface, b) deformation of a doubly curved surface*

Another characteristic regarding **surface deformation** addresses the change of the surface's curvature and/or area. In this work, a specific distinction is relevant: There is extensional and inextensional surface deformation, referred to local changes of area. These terms have a mechanical background. They are used to describe shell deformation (Chris Williams, 2014, p. 25), involving stretching or bending only.

Extensional deformations are shown in Figure 6. These include area and curvature changes.

Inextensional deformations involve curvature change only and may apply to single or doubly curved surfaces. The term "developable" relates to surfaces that inextensionally deform into planar states. Such surfaces have zero Gaussian curvature. Figure 7 shows inextensional deformations of a developable (a) and doubly curved surface (b).

2.1.3 Curves on Surfaces

For a curve embedded in a surface, the *Darboux*-frame provides another powerful apparatus, that orientates the curves to the surface normal. This orthogonal system is defined by the curves tangent **t**, the surface normal **n**$_s$, and the bi-normal **u**, located in the tangential plane. Accordingly, the three curvatures geodesic torsion τ_g, geodesic curvature κ_g and normal curvature κ_n can be measured.
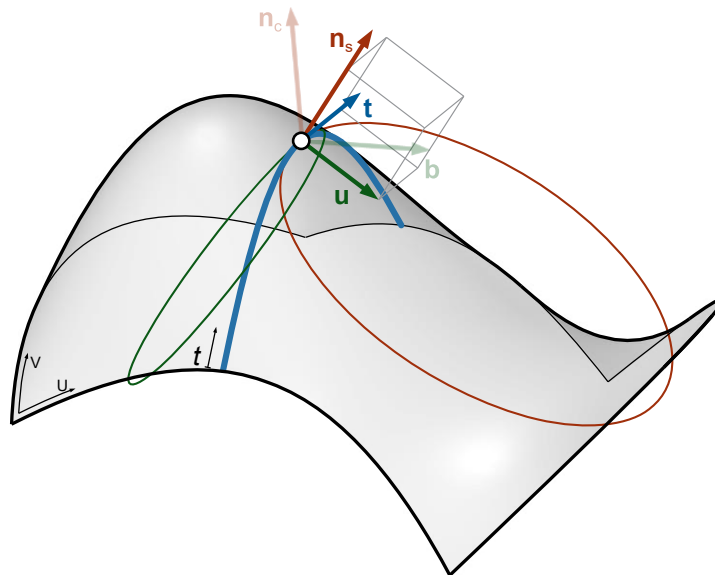
Figure 8: Curve embedded in a surface, the Darboux-frame and curvature-circles of the geodesic and normal curvature. For comparison, the TNB-Frame is also shown (pale colors)

There are several approaches to create surface embedded curves with different references used for the definition.
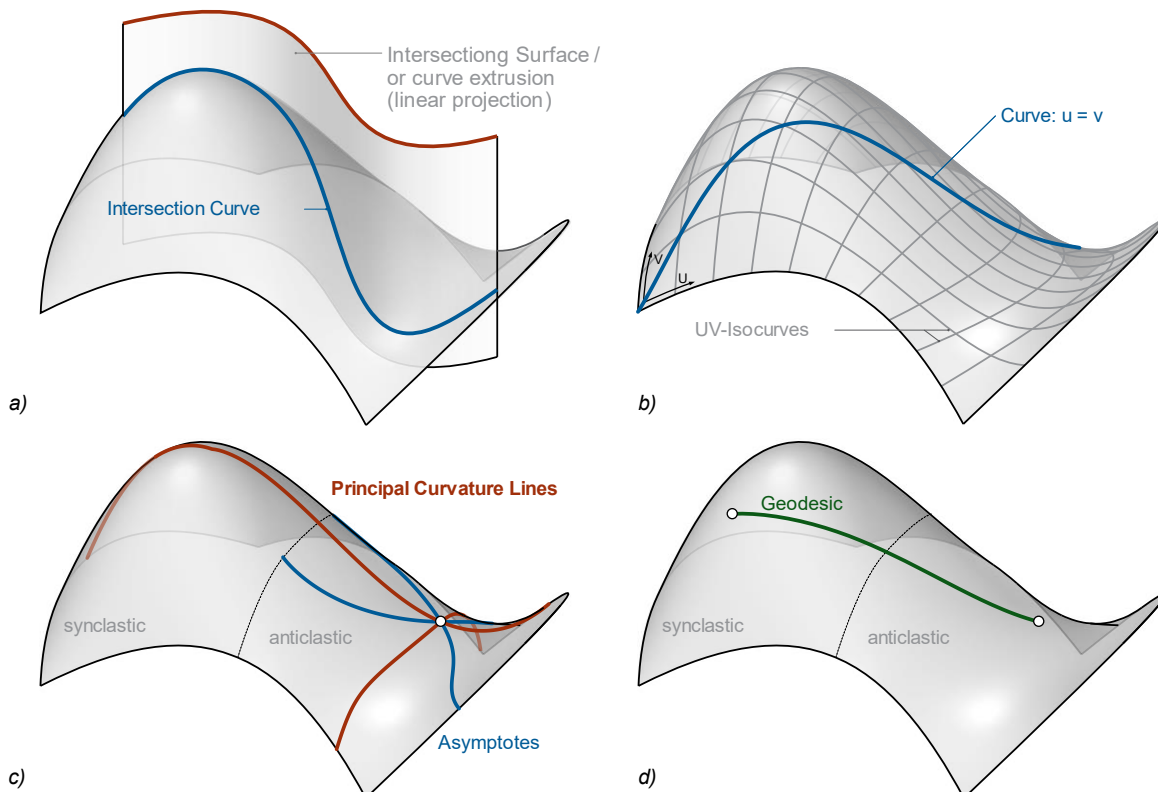
Figure 9 Selected types of definition for curves on surfaces: a) Intersection curves, b) Surface parameter curves, c) Normal curvature orientated curves (Principal curvature lines and Asymptotic Curves), d) Geodesic curve

Some basic types are presented below and illustrated in Figure 9:

- **Intersection curves** are defined by intersecting surfaces or planes, hence, an external reference object. Projections of curves onto surfaces also match this group (e.g. when the projection is interpreted as intersection of the surface with the extrusion of the curve).

- **Surface parameter curves** are defined by functions of the surface parameters (U,V). With constant surface parameter, these are called *Isocurves*. The UV-system can be used for the definition of freeform curves on surfaces.

- **Normal curvature orientated curves** are paths on surfaces that are oriented towards the surface's curvature field:

  Principal curvature lines follow the directions of the surface's principal curvatures. They can be found on any smooth surface, and the pair of curves given for a point on the surface is always orthogonal. The geodesic torsion is zero.

  Asymptotic curves define the path of zero normal curvature. This pair of curves are found on anticlastic surfaces only. The curves become orthogonal on surfaces with zero mean curvature (minimal surfaces). The direction of zero normal curvature $\kappa_n = 0$ on a given point on a surface can be derived from the principal curvatures κ_1 and κ_2, using a basic formula:

$$\kappa_{n(\mu)} = \kappa_1 (\cos \mu)^2 \cdot \kappa_2 (\sin \mu)^2$$

<div align="right">*Equation 3*</div>

(μ is the deviation angle between the principal curvature direction and the direction looked at)

- **Geodesic curvature orientated curves** are not driven by the surface's normal curvature field, but by an initial direction and a geodesic curvature constraint. Geodesic curves (or geodesics) have zero geodesic curvature. They are equivalent to straight lines on a planar surface or the shortest connection between two points on a surface.

Smooth Networks on Surfaces

Networks describe a set of curves (or lines) and their intersections (nodes). In context with surfaces, networks can be described as segmentation of surfaces. This work focusses on smooth networks with traversal nodes, meaning that the networks' smooth curves are passing continuously through nodes without any kinks or endings within the surface.

Among infinite strategies to generate networks on surfaces, some common types and characteristics in an architectural or structural context are summarized in the following:

In general, there are regular patterns of faces and/or nodes (valance) or irregular configurations. The connectivity of networks is also called topology. Figure 10 shows an exemplary selection of network typologies.
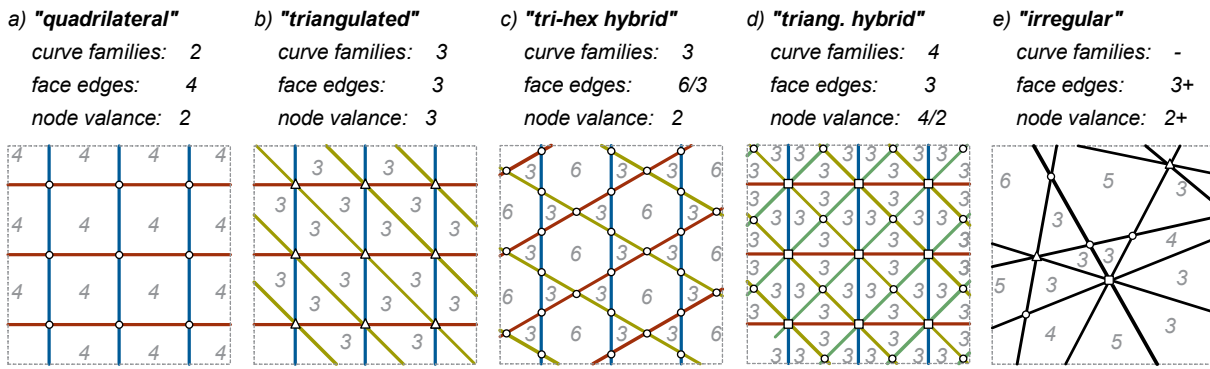
Figure 10 *Selection of different network topologies*

The edges of equilateral networks are of same length. Quadrilateral nets of this kind are also called Chebyshev nets can be constructed on smooth spatial surfaces using two initial, intersecting curves.

2.2 Mechanical Fundamentals

This chapter provides mechanical fundamentals, focusing on Elastostatics of beams, stability, and large bending deformations. There is a lot of literature that describes these fundamentals. For detailed descriptions, the reader is be referred to Dankert & Dankert, 2006 or Pflüger, 1964.

2.2.1 Elasticity

Linear elastic deformation is a reversible deformation with a constant stress σ to strain ε relation. Hookes Law relates elastic strain to stresses via the Modulus of Elasticity E:

$$E = \frac{\sigma}{\varepsilon}$$

Equation 4

In analogy, the Modulus of Shear G is defined by shear τ and distortion γ:

$$G = \frac{\tau}{\gamma}$$

Equation 5

For linear elastic, isotropic materials, Modulus of Elasticity and Shear are coupled by the Poisson's ratio ν:

$$\nu = \frac{E}{2G} - 1$$

Equation 6

There is a multitude of material parameters, well adapted to individual material characteristics. For each material type, specific parameters, boundaries, and evaluation methods have been developed. However, all solid materials show elastic behavior in general, although the range is limited, and the distribution may not be linear. Depending on a brittle or ductile material behavior, the material either fails or yields after crossing the materials "elastic" strength. Figure 11 shows simplified diagrams of the linear elastic stress-strain relations and its boundaries.
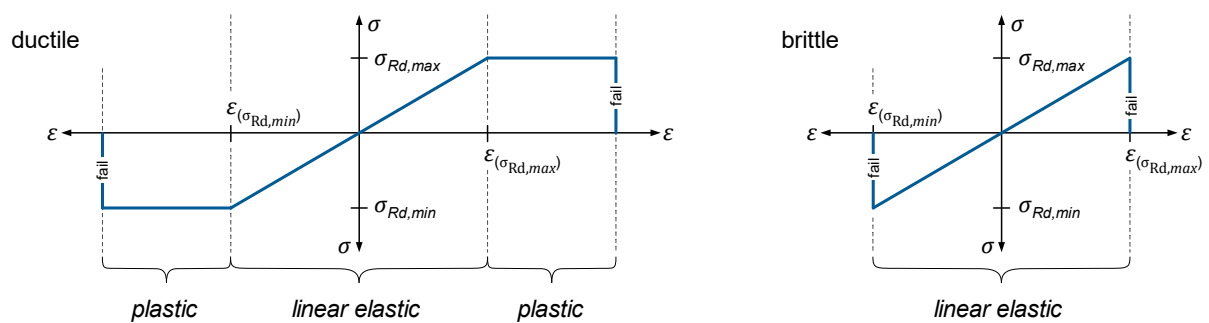
Figure 11 *Simplified Stress-Strain-Graph of ductile (left) and brittle(right) material behavior*

In this work, the elastic boundaries are expressed by the maximum elastic strain $\varepsilon_{\sigma_{Rd,max}}$, furthermore called "strain at failure" and the maximum elastic stress σ_{Rd}[1] , furthermore called "strength" of material. These boundaries define the materials elastic capacity. They are coupled by Hooke's Law.

---

[1] *For simplification, if not explicitly defined, there is no differentiation between the compressive or tensile strength.*

2.2.2 Bending

Bending of beams describes the elastic portion of curvature, caused by moments acting perpendicular to the local beam axis. Based on the assumptions of Bernoulli and Euler[1], presuming that the profile planes of bent beams remain perpendicular to the beam's axis, the curvature-strain relation can be derived geometrically. Figure 12 shows a schematic description of bending related geometric definitions.

Figure 12 Geometric relation of bending radius and profile strain

The curvature κ of an originally straight beam refers to the neutral fiber of the profile. The bending radius describes the inverse value:

$$\kappa_y = \frac{1}{r_0}$$

<div align="right">Equation 7</div>

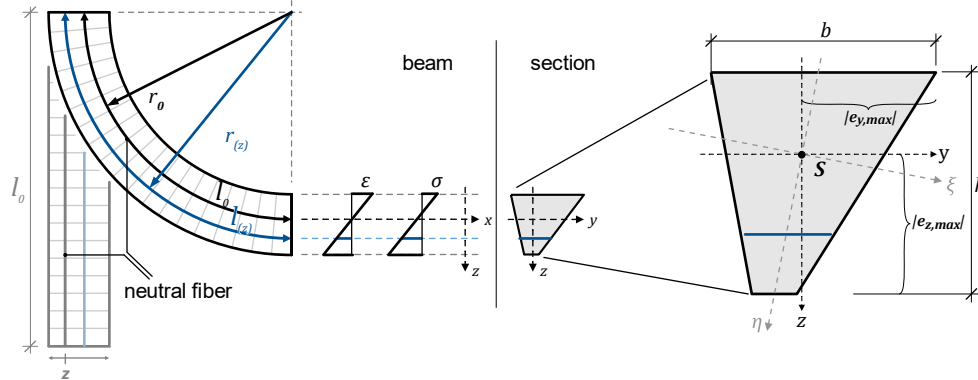All fibers with distance z from the neutral fibre hold the curvature radius $r_{(z)} = r_0 + z$. Radius and arclength are in linear relationship $U = 2\pi r$. Accordingly, across the profile's height h, strain ε_z is linearly distributed:

$$\varepsilon_{(z)} = \frac{z}{r_0} = \kappa_y z$$

<div align="right">Equation 8</div>

With the Elastic Modulus E, normal stresses σ result to:

$$\sigma_{(z)} = E\kappa_y z$$

<div align="right">Equation 9</div>

From this stress distribution, the bending moment can be derived by integrating all fibers' stresses, multiplied by their lever arm:

$$M_y = \int_A \sigma_{(z)} z \, dA = E\kappa_y \int_A z^2 \, dA$$

<div align="right">Equation 10</div>

The moment of inertia I might be interpreted as auxiliary quantity to describe the profiles stiffness geometrically. It results from the integration of all lever arms squared across the profile area.

---

[1] *These assumptions go back to the work of Various members of the Bernoulli Family (e.g.: Jakob B. 1655-1705; Johan I B. 1667-1748) and Leonhard Euler (1707 – 1783). The first formulations go back to Jakob Bernoulli.*

$$I_y = \int_A z^2 \, dA$$

<div align="right">*Equation 11*</div>

Inserted to Equation 10, we receive:

$$M_y = EI_y \kappa_y$$

<div align="right">*Equation 12*</div>

Combining Equation 9 and Equation 12 results in the stress distribution in dependence of the applied bending moment:

$$\sigma_{(z)} = \frac{M_y}{I_Y} z$$

<div align="right">*Equation 13*</div>

The maximum stress can be calculated using the section modulus W_y, an auxiliary quantity based on Equation 13, with the maximum distance $|e_{max}|$ inserted for z:

$$\sigma_{max} = \frac{M_y}{I_Y} |e_{max}| = \frac{M_y}{W_Y} \; ; \; W_Y = \frac{I_y}{|e_{max}|}$$

<div align="right">*Equation 14*</div>

Considering biaxial bending, strains and stresses are superimposed.

Note, the profile axes defined must not necessarily align with the principal bending axes. Figure 12 shows the profile axes (y, z) and the principal bending axes (ξ, η) of this asymmetric section.

2.2.3 Torsion

The theory of torsion requires more complex mechanical models compared to bending. Torsion involves multiple mechanical effects, both generating shear and normal stresses. The internal torsional moment caused by an external load M_T is split into portions accordingly:

$$M_T = \sum_x M = M_{x,St.V.T.} + M_{x,Warping\,T.} + M_{x,Helix\,T.}$$

<div align="right">*Equation 15*</div>

This section gives an overview on St. Venant ($M_{x,St.V.T.}$), warping ($M_{x,Warping\,T.}$) and helix torsion ($M_{x,Helix\,T.}$). While St. Venant torsion generates shear stresses in theory, warping and helix torsion are additionally activating normal stresses. Note, warping torsion is not occurring in this work, as the preconditions for this phenomena are not fulfilled.

St. Venant Torsion

According to the theory of St. Venant, torsional moments are transferred via a closed flow of shear stresses across the profile, and shear distortions result in a twist. In analogy to bending (see Equation 12), the relation of twist κ_x, St. Venant torsional moment $M_{x,St.V.}$ and the torsional moment of inertia I_T is given by the equation:

$$M_{x,St.V.} = GI_T \kappa_x$$

<div align="right">*Equation 16*</div>

However, the distribution of torsional shear stresses and hereby the torsional moment of inertia depend on the profile type. This results from the necessity of a closed shear flow and a nonlinear distribution of shear stresses accordingly. A major distinction can be made between "full", "closed thin-walled" or "open thin-walled" profiles. Among various profile shapes within

these types, the following formulas describe the profile's shear for circular profiles exemplarily.
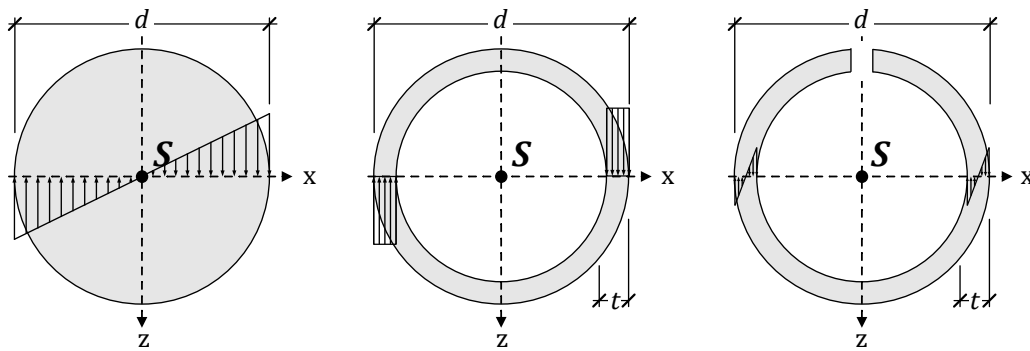
a) Full profile   b) Closed thin-walled profile   c) Open thin-walled profile

$$\tau_{max} = 16\frac{M_{x,St.V.}}{\pi d^3} \qquad \tau_{max} = 2\frac{M_{x,St.V.}}{\pi d^2 t} \qquad \tau_{max} = 2\frac{M_{x,St.V.}}{\pi d t^2}$$

Equation 17

Note: $\frac{\pi d^2}{4}$ = inner profile Area

$$I_T = I_P = \frac{\pi}{32}d^4 \qquad I_T = I_P \approx \frac{\pi}{4}d^3 t \qquad I_T \approx \frac{\pi}{3}dt^3$$

Equation 18

For t << d   Valid for a small slot within profile.

Full profiles' torsional shear stresses increase with the distance to the center of rotation. For circular sections, the stress distribution is linear. For any others, an analogy helps to understand the distribution: Considering a soap film across the profile section, with constant inner "air" pressure, the soap-film would bulge out of plane and form a hill. The torsional shear stresses are then proportional to the hill's gradient and the torsional moment of inertia is proportional to the hills volume. The calculation of maximum shear and moment of inertia are rather time-consuming and various approximations for simple profile shapes are provided in literature (see Equation 17 and Equation 18).

Closed thin-walled profiles have a circumferential flow of stresses. They can be solved using the Bredt's formulas. Approximately, the stresses in the profile walls are constant across the thickness. The maximum stress occurs at the thinnest region of the profile wall. The profiles enclosed section area is a decisive magnitude for the torsional behavior.

Open thin-walled profiles the torsional shear flow turns at the wall's edges. This results in an approximately linear distribution of shear stresses across the walls thickness. This distribution causes a comparatively low stiffness. In contrast to closed thin-walled profiles, the maximum shear occurs on the thickest profile wall.

The differences in torsional stiffness of full, closed, or open thin-walled profiles are shown in Equation 18. E.g.: The torsional moment if inertia for the thin-walled closed profile in a cubic function of the diameter, for the open version, it is a cubic function of thickness. These differences are potentials to modify the torsional stiffness.
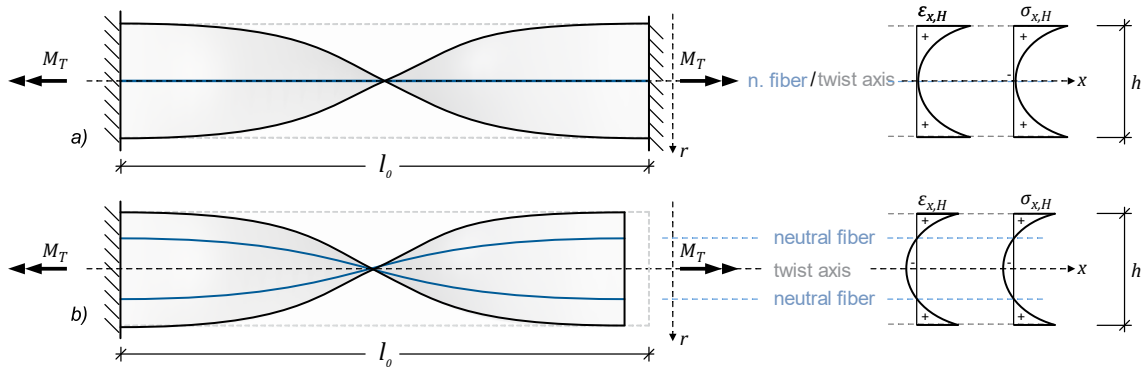
Helix Torsion

Figure 13 *Helix stress distribution of a beam (Lamella) with 180° twist: a) The beam is fixed in length: The length of the center line remains, the edge fibers are stretched, only tension occurs b) The beam is not fixed in length: The central area is compressed, the edge fibers are stretched, tensile and compressive stresses are in equilibrium*

The concept of helix torsion (Lumpe & Gensichen, 2014) follows the geometric model of a twisted beam with fibers following a helix curve around the beam's longitudinal axis accordingly. Hereby, deviations in fiber lengths arise, which are equalized by strain and corresponding stresses. If the twisted beam is constrained in length, all fibers, except the fiber on the rotational axis must elongate (Figure 13a). If the beam is free to change length, internal compressive stresses occur, to create an equilibrium. The total length is shortened. The "neutral fiber" is then in between the central rotation axis and the outer fiber. This theory is described using the following formulas:

The elongation $\varepsilon_{x,H}$ due to helix torsion in fibers with distance r to the rotational axis (longitudinal axis) is expressed in a quadratic function:

$$\varepsilon_{x,H} = \frac{1}{2}r^2\kappa_x^2$$

Equation 19

For small twists, this effect is neglectable. For large twists of profiles with large polar moment of inertia, the internal torsional moment due to helix stresses becomes significant:

$$M_{x,H} = \frac{1}{2}EK_r\kappa_x^3$$

Equation 20

The auxiliary quantity K_r describes the "reduced" helix area moment. It integrates an adjustment of the original helix area moment to achieve an equilibrium of total tensile and compressive stresses across the profile (Figure 13b).

$$K_r = I_r - i_p^2 I_p$$

Equation 21

With i_p is the radius of inertia.

The helix area moment is biquadratic:

$$I_r = \int_A r^4 \, dA = \int_z \int_y (y^2 + z^2)^2 dydx$$

Equation 22

The normal stresses due to helix torsion result to:

$$\sigma_{x,H\,(x,y,z)} = \frac{1}{2}E(y^2 + z^2 - i_p^2)\kappa_x^2$$

Equation 23

The minimum and maximum stresses result to:

$$\sigma_{x,H,min} = -\frac{1}{2}E i_p^2 \kappa_x^2 \quad ; \quad \sigma_{x,H,max} = -\frac{1}{2}E\left(r_{max}^2 - i_p^2\right)\kappa_x^2 \qquad \textit{Equation 24}$$

There are additional effects and stresses in the context of helix torsion, e.g., shear stresses, whenever helix stresses are not constant, or coactions of normal forces, etc. In this work, we set these effects aside, as they are expected to be of neglectable impact.

The theory of helix torsion is simplified for the case of lamella profiles in section 4.1.2 p.112. Furthermore, helix torsion is considered within the build case studies in section 4.2 and 4.3. In section 4.2.2 p.128, the proportions of helix torsion and St. Venant torsion are displayed in a case study for the specific profile used.

Warping Torsion

Warping is an out of plane deformation of the profile. Whether warping occurs, depends on the profile geometry and the support condition. Warping torsion causes shear and normal stresses. It is usually referred to thin-walled profiles.

Figure 14 *Thin-walled profile shapes that can activate a pair of forces (left) or not (right)*

For the phenomena of warping torsion, the following preconditions must be fulfilled:

- The profile activates a pair forces. These are thin-walled profiles with straight parts that intersect in more than one point (e.g., H-profiles, Z-profiles, etc.). Such profiles include at least two flanges, stiff enough to generate a pair of forces to act on torsional moments (see Figure 14).

- Warp stresses are activated, if warp is restrained or if the torsional moment is not constant along the beam. If not, warping occurs without generating warp stresses, as the profile is "free to warp".

- The theory of warping torsion is limited to small twists.

If warping stresses are activated, the torsional moment applied to a beam is split into portions of St. Venant and warping Torsion.

The theory of warping torsion is rather complex and associated to structural steelwork. In this work, it is not relevant, as the profiles used do not activate warping torsion.

2.2.4 Energy

The law of energy conservation is of fundamental significance for physical relations in general. It interconnects various subareas of physics. Work or energy Π in general mechanics is be described as the product of force F and path u:

$$\Pi = Fu$$

In the context of this work, strain and potential energy are used to describe the kinetic behavior, and further explained:

Potential Energy

Kinetic structures exposed to gravity may change their potential energy to large extends during transformation. The basic expression is:

$$\Pi_{pot} = mgh$$

This linear relation is displayed in Figure 15. The mass m and gravity constant g result to the constant force G, equal to the opposing, external force F, considering static equilibrium. The potential energy Π_{pot} (shaded area) is linearly dependent on the elevation height h.
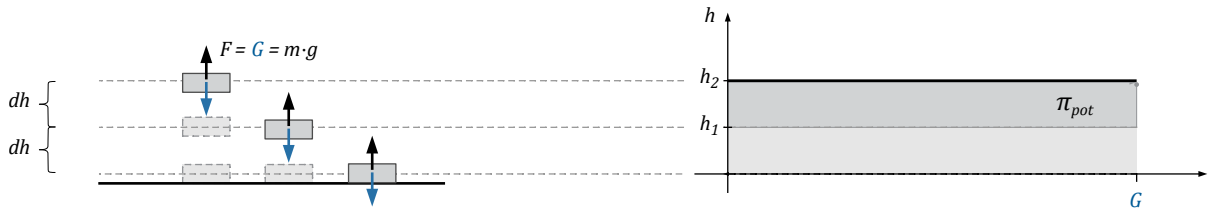

Figure 15 *The relation of potential energy, height, and gravity*

Strain Energy

Strain energy Π_i is stored by elastic deformation (strain ε and distortion γ) under stress. It results from the elastic and shear moduli E and G and the deformations respectively:

$$\Pi_i = E\,\frac{1}{2}\underbrace{\int_V \varepsilon^2 \, dV}_{\text{strain}} + G\,\frac{1}{2}\underbrace{\int_V \gamma^2 \, dV}_{\text{distortion}}$$

In elastostatics, energy methods are applied to solve indeterminate systems. Strain energy is induced by external work Π_e. It is the product of F and its path or a moment M and a rotation φ performed respectively:

$$\Pi_e = \underbrace{\int_u F \, du}_{\text{force}} + \underbrace{\int_\varphi M \, d\varphi}_{\text{moment}}$$

The energy theorem provides the basic equation:

$$\Pi_i = \Pi_e$$

The quadratic character can be explained using the prevalent analogy to springs. The internal force S of a spring is proportional to its deflection (using the spring constant C), and equal to the opposing external force F, considering static equilibrium. In Figure 16, the linear relation of deflection and force are displayed in a graph. The stored strain energy Π_i is represented by the shaded area underneath. Strain energy is in a quadratic dependency on deflections du. Note, there is a direct analog of springs and beams: The spring constant refers to the beam's stiffness.
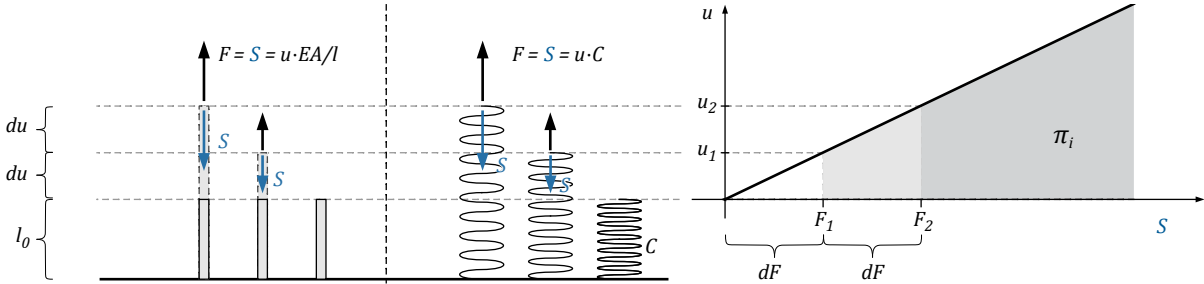

Figure 16 *The relation of Stiffness and strain energy and the analogy of springs and beams.*

The strain energy, stored by "Euler-Bernoulli"-beam is decomposable into directional portions of normal- and shear forces, bending and torsion. From the internal forces, it results to:

$$\Pi_i = \frac{1}{2}\left[\int_c \underbrace{\frac{N^2}{EA^2}}_{\text{normal force}} + \underbrace{k_y\frac{Q_y^2}{GA} + k_z\frac{Q_z^2}{GA}}_{\text{shear force}} + \underbrace{\frac{M_t^2}{GI_T}}_{\text{torsion}} + \underbrace{\frac{M_y^2}{EI_y} + \frac{M_z^2}{EI_z}}_{\text{bending}}\ ds\right]$$

Equation 30

$$\text{with: } k_y = \frac{A}{I_z^2}\int_A \frac{S_z^2}{h^2}dA\ ,\ k_z = \frac{A}{I_z^2}\int_A \frac{S_z^2}{b^2}dA$$

For long beams ($l \gg h$), portions due to shear are neglectable, and for large bending, portions from normal forces become neglectable. This assumption simplifies the energy term:

$$\Pi_i = \frac{1}{2}\left[\int_c \frac{M_t^2}{GI_T} + \frac{M_y^2}{EI_y} + \frac{M_z^2}{EI_z}\ ds\right]$$

Equation 31

Using Equation 12, this term can be expressed using the beam's curvature of deformations:

$$\Pi_i = \frac{1}{2}\left[\underbrace{GI_T\int_c \kappa_x^2\ ds}_{\text{twist}} + \underbrace{EI_y\int_c \kappa_y^2\ ds + EI_z\int_c \kappa_z^2\ ds}_{\text{bending}}\right]$$

Equation 32

For large twists, strain energy due to helix torsion (section 2.2.3) becomes significant (Schikore et al., 2019).

$$\Pi_{i,Helix-Torsion} = \frac{1}{18}EI_r\int_c \kappa_x^4\ ds$$

Equation 33

Equation 32 is then supplanted by strain energy through helix torsion:

$$\Pi_i = \frac{1}{2}\left[\underbrace{\frac{1}{9}EI_r\int_c \kappa_x^4\ ds + GI_T\int_c \kappa_x^2\ ds}_{\text{twist}} + \underbrace{EI_y\int_c \kappa_y^2\ ds + EI_z\int_c \kappa_z^2\ ds}_{\text{bending}}\right]$$

Equation 34

2.2.5 Stiffness

Stiffness describes the relation between force and deformation. The stiffness of a structural system involves some distinguished phenomena, relevant for large deformations:
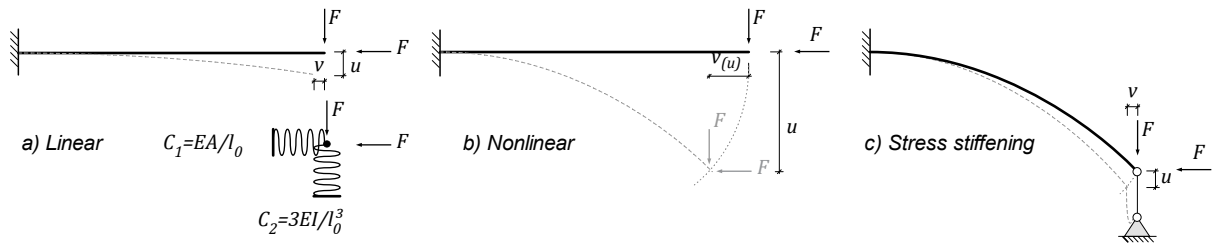

Figure 17 *Characteristics of stiffness: a) Linear beam stiffness for small deflections b) Nonlinear stiffness under large deformations c) Stress stiffening effect of an initially stressed beam*

- **Elastic stiffness** of beams involves material (see section 2.2.1) and profile stiffness (e.g., Area, Moment of Inertia). For a linear elastic material, the "elastic stiffness" in a static system remains constant. This context can be illustrated using the analogy of beams and a spring. The spring constant C can be referred to a beam's stiffness and length parameters. It is derived using the strain energy (see 2.2.4). Considering small deflections, the beam in Figure 17a can be replaced by linear springs.

- **Geometric stiffness** involves the nonlinear effect of deformations. It depends on load and geometry of a structure. While tension forces in general increase geometric stiffness, it is lowered by compressive forces (Lienhard, 2014). Figure 17b shows a largely deformed cantilever. The stiffness of this setup becomes dependent on the current state of deformation and calculations of 3rd order become necessary.

- **Stress stiffening** occurs if internal stresses are already present when additional loads are applied. This effect is coherent with a linear, initially deflected spring. Any further deflection requires higher forces as if the deflection was measured starting from an unstressed spring. This directly relates to the work and strain energy involved (see 2.2.4).

Compliant grid structures are characterized by large deformations and initial strains. Through this, nonlinear effects and stress stiffening are likely and considered within nonlinear numerical simulation methods (see section 2.3.2).

Stress stiffening is identified for elastically curved grid members in section 3.3.2.

2.2.6 Stability

Stability problems are cases of ambiguity. These occur, when for a system in static equilibrium, another, neighboring equilibrium exists. These phenomena typically occur in systems under compression, as these may pose various deformation modes. However, there are different types of stability problems, as shown exemplarily in Figure 18.
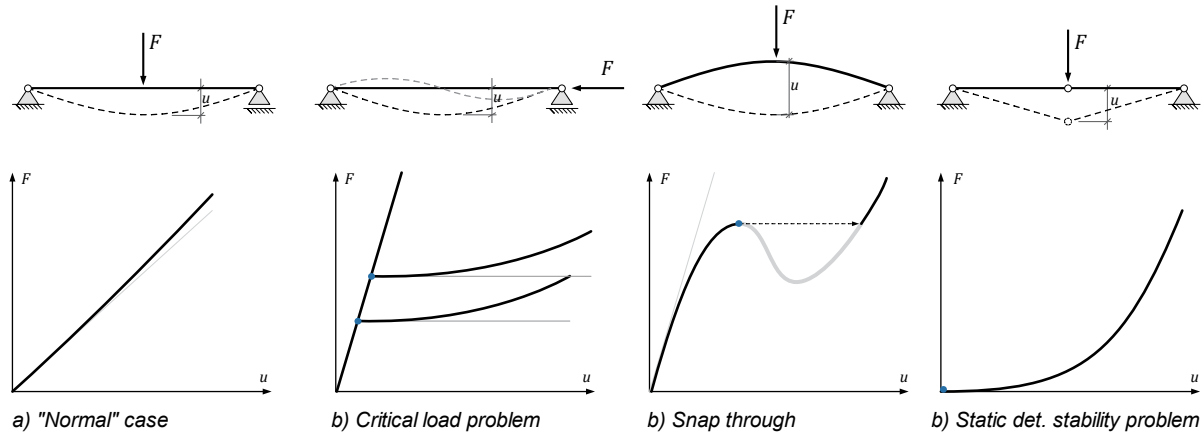

Figure 18 *Basic types of stability problems (Pflüger, 1964, p. 27)*

The load-displacement graphs illustrate the problems:

a) represents the "normal" case. There is only one equilibrium state for a given load.

b) shows a typical buckling problem. When a critical load is reached, the system is indifferent and when further loaded, the system becomes instable. Any disturbance will cause a transition into a secondary equilibrium state. In practice, such disturbances might be imperfections or lateral loads. The problem shown can be referred to the well-known critical "Euler"-load $F_{crit.}$:

$$F_{crit.} = \frac{EI\pi^2}{s_k^2}$$

Equation 35

This formula includes the buckling length s_k that indicates the shape of deformation mode. Note, that several buckling modes are theoretically possible, but only the first one is likely, as modes of higher order involve higher strain energy.

c) shows a "snap through"-problem. When a critical load is reached, the system is indifferent, and further loading leads to a sudden, inevitable conversion of the system.

d) Shows a special case that is classified as "kinematic" in 1st order static analysis. The unloaded state is indifferent.

Simple stability problems can be solved using the equilibrium methods on a deformed system. Also energy methods are used (Lehmann, 1985, p. 262). For complex problems, numerical calculations (e.g., FEM) of 3rd order are commonly used.

Investigations in section 3.3.2 identify the critical "Euler"-load and snap through phenomena within compliant grid structures. Furthermore, buckling refers to the next section (2.2.7): The Elastica curve can be referred to a beam in a post buckled state.

2.2.7 The Elastica Curve

The Elastica curve represents the shape of a bent beam under given geometric constraints. It has fascinated famous scientists since centuries, such as Galileo, Bernoulli, Euler and others (Levien, 2008).
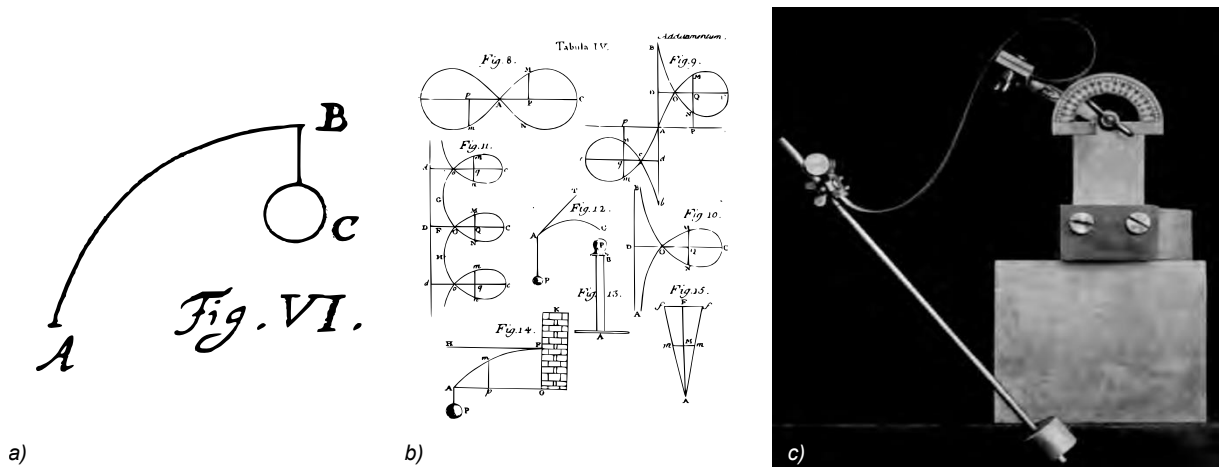

a)   b)   c)

Figure 19 *Historical developments of the Elastica curve: a) The Elastica problem posed by James Bernoulli 1691, b) Family of Elastica curves by L. Euler 1744, c) Experimental apparatus for measuring the Elastica by Max Born 1906 (Levien, 2008)*

Figure 19 shows three investigations on the elastic curve exemplarily, from James Bernoulli in the 17th century to Max Borns studies at the beginning 20th century. Today, the Elastica can be simulated using numerical methods.

Central issue is finding a curve that minimizes strain energy under given constraints. Assuming that axial compression and shear energy portions are neglectable, and the beams stiffness is constant along the beam, in a 2D space, the strain energy from Equation 30 is reduced to:

$$\Pi_i = \frac{1}{2} EI \int_c \kappa^2 \, ds$$

Equation 36

The equilibrium shape of minimal strain energy is found when the integrated curvature-squared ($\int_c \kappa^2 \, ds$) is minimal. The problem becomes purely geometrical.

For given constraints, several equilibrium states can be found. States of higher order may be instable as they involve higher total strain energy. There is an analogy to eigenvalue problems and buckling shapes, as these possess various solutions. However, this cannot be generalized.

In the following, a progressive simulation[1] of two modes of the Elastica on a largely compressed two-span beam is performed exemplarily to track basic phenomena (Figure 20). The simulation path-controlled. Shape, force, and strain energy are tracked.

---

[1] *The simulation is performed using Isogeometric Analysis (see section 2.3.2). To induce deformation, small imperfections are installed.*
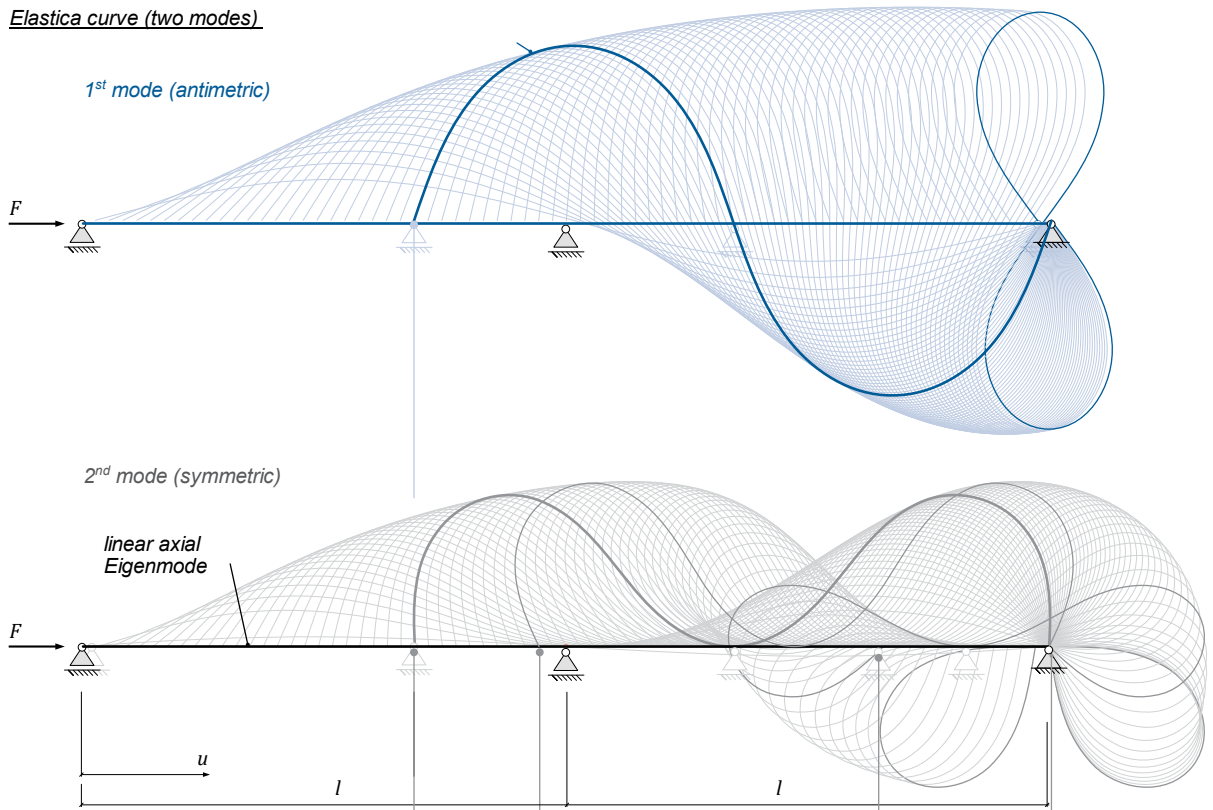
This progression displays some crucial phenomena of large bending deformations, regarding large bending, ambiguity, and non-linearity:

1) Marks the range before buckling (axial deformation only). The systems stiffness is constant (see also Figure 17a), until a critical load is reached. The critical loads for a first and second eigenmode according to the "Euler"-load (Equation 49) are mapped in the diagram[1]. In conventional engineering, this load is referred to the beam's resistance against buckling.

2) Shows a state of larger deformation. The system's relation of load and displacement is non-linear, rising for both modes. The second modes energy level is higher, and thus it is more unlikely.

3) Marks another critical state of the second mode. Any further loading (in case of a force-controlled system) would result in a sudden "snap-through" (see also Figure 18b). Mode 1 does not feature this stability phenomena (there is no other deformation mode involving less strain energy)

4) Shows a change in sign for the load in mode 2. It is a state in unstable equilibrium in a local energy maximum. External forces are not necessary to hold this deformation (apart from the support forces).

5) At this state, both modes are equal in strain energy. In both modes a double-drop-like shape emerges. In mode 1 the signs are opposite, in mode 2, both drops are of same curvature sign. For mode 1, this state is the global energy maximum. For mode 2, this state is a local energy minimum (in the range of deflection shown).
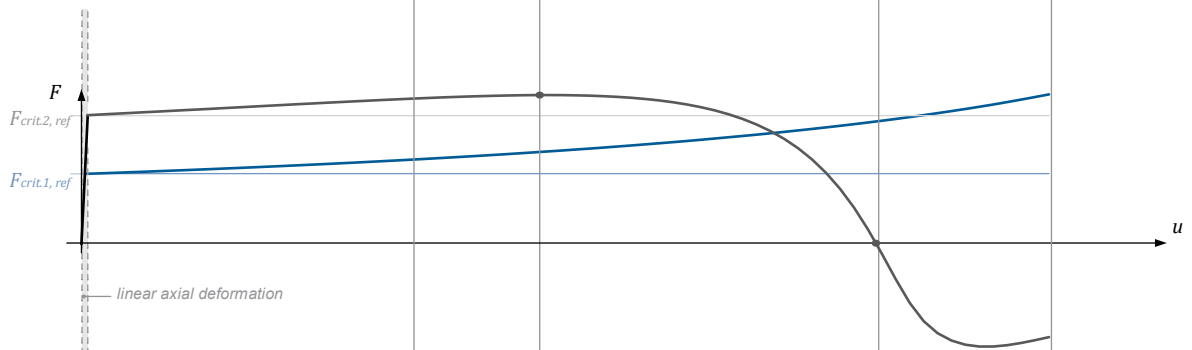
The multispan beam is used as reference system for local investigations of compliant grid members in this work (see section 3.3.2).

---

[1] *For the first mode, the buckling length $s_k = l$; For the second mode, the buckling length $s_k = 0{,}7l$ is used.*

Elastica curve (two modes)

1st mode (antimetric)

2nd mode (symmetric)

linear axial Eigenmode

F

u

l

l

Load-displacement graph

F

$F_{crit.2, ref}$

$F_{crit.1, ref}$

u

linear axial deformation

Strain Energy

π_i
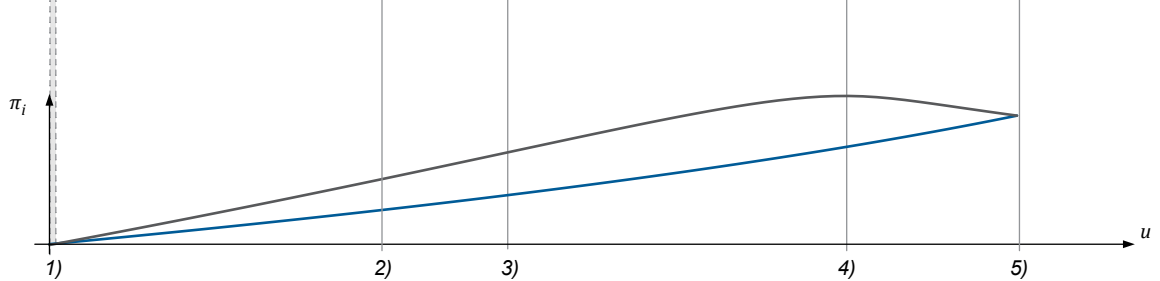
u

1)   2)   3)   4)   5)

Figure 20 Numerical simulation of an Elastica curve (two modes)

2.3 Modelling and Simulation

Models are crucial for the design, analysis, evaluation, fabrication, and assembly of structures. The following sections describes novel developments in geometric and mechanical modeling and simulation, both physical and digital, and suitable for spatial grids involving large deformation. The methods presented in this section are extensively used for investigations in sections 3.2 and 3.3, and furthermore part of the computer aided engineering process developed in section 4.1.4.

2.3.1 Computational Modelling

This chapter describes the fundamental representation of curved objects in *Computer Aided Design* (CAD) and gives insight to the powerful tools of computational modeling. Lastly, the important role of geometric modelling for the comprehensive engineering process is highlighted.

Geometric Objects in CAD

The basic geometric objects in CAD are points, curves (or lines) and surfaces. For the object's descriptions, there are various approaches and options provided by CAD software.

Points are commonly defined by Euclidean X,Y and Z-coordinates. Furthermore, cylindrical, or spherical coordinates are used. The result, a location in space, is the same.

Curves are defined using various descriptions available with distinct qualities. Different types of description may not be able to perfectly describe the same geometry, but at least provide an approximation. A fundamental distinction is between discrete and smooth (continues) curves. While discrete curves in CAD are polygons, smooth curves are mostly described by *Non-Uniform Rational B-Splines* (NURBS), which became standard for CAD systems (Borrmann et al., 2015, p. 37). The curve is defined by control points and a polynomial degree sets the continuity of the curve[1]. Figure 21 illustrates the description of a NURBS with polynomial degree 3 and polygonised curve, both using 7 points for definition.
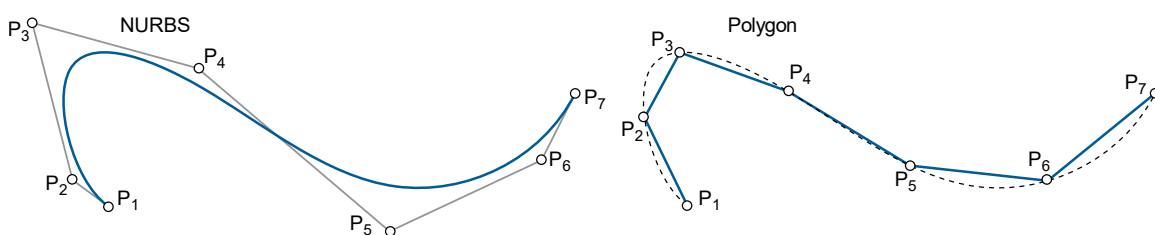

Figure 21 Spatial NURBS (left) and polygonised curve (right) described by 7 points

Surfaces are described analogous, but two-dimensional. NURBS-surfaces are described by a control net, and meshes are described by points and edges.

Volumes are usually described using *Boundary Representation* (B-Rep). In this method, a set of boundary surfaces describes a closed volume.

---

[1] *Note, the polygonised curve matches a NURBS of polynomial degree 1.*

Generation of Curvature Lines on Surfaces

Curvature lines are paths on surfaces, following curvature constraints (*Darboux*-Frame, see chapter 2.1.3). For the determination of these curves, algorithms are necessary, which are not yet standard in conventional CAD applications.

Working on asymptotic networks, E. Schling developed an algorithm applicable in the Rhino/Grasshopper environment. The algorithm iteratively finds the zero normal curvature direction and follows this, walking in small steps across the surface. Later, Oberbichler, 2021 published the plugin *BOWERBIRD (Oberbichler, 2021)*, giving users even more flexibility for the design of various curvature orientated curves on surfaces. The latter method is used in this work.

Parametric and adaptive Modelling

Parametric modelling is an important trend in the building sector. Geometric objects can be defined using selected object parameters and dependencies between them. These dependencies need to be programmed. Parametric models are flexible and able to quickly adapt to changing key inputs, without large modelling effort (Borrmann et al., 2015).

Figure 22 gives an example: A 2D-square is defined using three different parametric descriptions (parameter sets) with varying number of necessary inputs (blue). From those inputs, the geometry is generated by programmed operations. For less inputs, the design space of the geometric objects decreases.
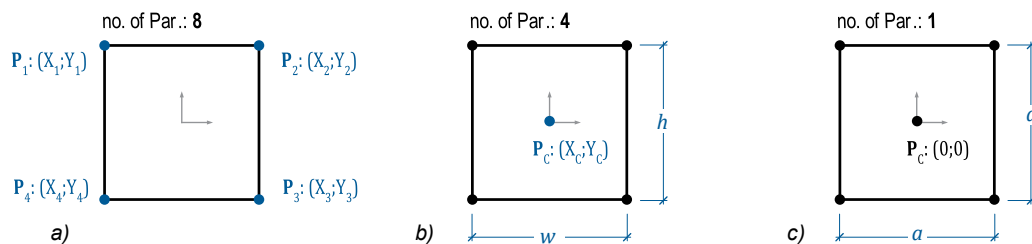

Figure 22 Exemplary parametric definition inputs of a 2D-square: a) Definition of 4 corner points, b) Definition of center point, width and height, c) Definition of corner edge length

Further nesting of parametric objects allows complex adaptive models that are extremely useful for repetitive geometric models.

Modern structural analysis software also includes the parametrization of structural parameters such as support constraints, stiffness parameters, etc. This allows complex structural models and optimization algorithms for specific goals.

Visual Programming

The definition of parametric models requires programming. This is conventionally done using appropriate scripting. The language *Python*, exemplarily, is widely used for geometric scripts, and some geometric modelling software offer interfaces to script software specific commands. This applies also to numerical software for static analysis. *SOFiSTiK*[1] exemplarily, includes an own syntax to create parametric structural models.

---

[1] *SOFiSTiK is a commercial FEM software*

In the past decades, a more intuitive process for scripting was developed: Visual programming provides a graphically represented script (also called "definition"), in which parameters, objects, computational operations and the data flow are displayed graphically.

Figure 23 shows exemplarily the graphic definition of a parametric square in the visual programming environment of the 3D-modelling software *Rhino/Grasshopper*[1]. Closed operations are displayed as "components" (grey boxes) and data is passed in-between using wires.
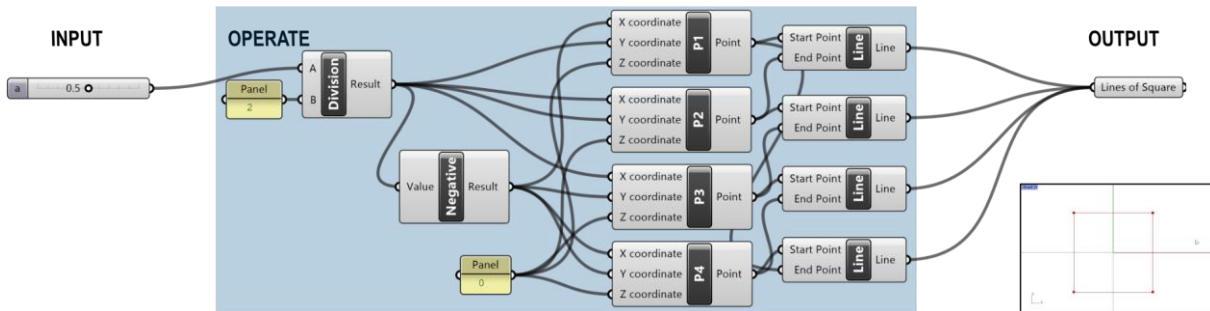
***Figure 23** Visual Programming Interface: The parametric definition of a square (According to **Figure 22**c) in the visual programming interface of Rhino/Grasshopper. From an input length parameter "a", a square is modelled.*

Computer Aided Design (CAD) in the Engineering Workflow

In the last decades, the importance of CAD in engineering and design processes increased rapidly, together with the fast-developing *Information Technology* (IT). Nowadays, CAD does not only support geometric modelling as a separated task. Furthermore, CAD connects to several engineering tasks, including physics, mechanics, visualization, data management and so on, with geometry as common denominator. In the Building Industry, this led to the development of *Building Information Modelling* (BIM), a comprehensive approach, to interconnect various disciplines in the whole lifecycle of buildings, from planning to demolition.
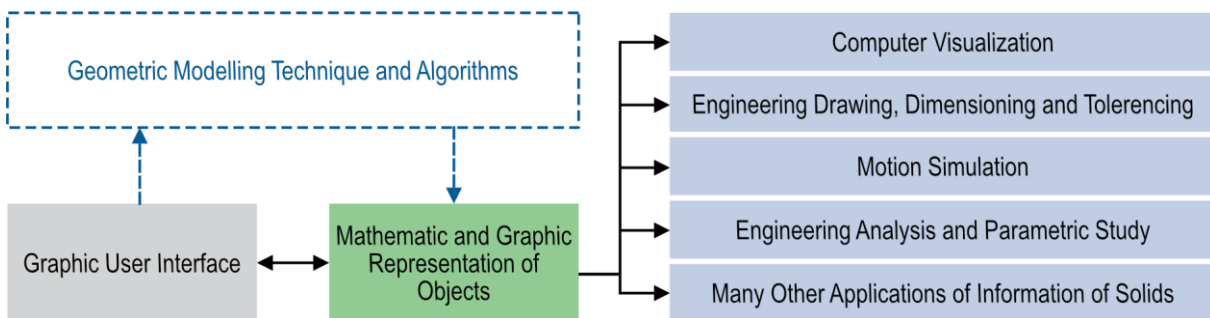

***Figure 24** Role of geometric modelling in Computer Aided Systems (CAD) (Bi, 2020)*

Figure 24 displays the role of geometric modelling within computer aided design processes. The geometric representation provides the basis for several design tasks:

" […] For example, virtual geometric models can be used by computer graphics to visualize the designs before physical products are made. Engineering drawings needed in manufacturing processes can be directly generated from solid models of products, and all of the annotations relating to dimensioning and tolerance can be included in the drawings. If a product is a machine with relative

---

[1] *Rhino is a commercial 3D modelling software, and Grasshopper is a plugin for visual programming. For Grasshopper, again, various plugins are available, and many are open source.*

motions among system components, a motion study can be defined upon the computer aided design (CAD) model to investigate the relations of driving forces and motions. In addition, engineering analysis can be performed at any stage of the product design process. [...]" (Bi, 2020, p. 37)

For highly iterative and interdependent design processes, a fluid workflow becomes essential. This led to novel developments of CAD integrated design tools and cycles. Exemplarily, Goldbach & Bletzinger, 2019 proposed a design cycle for membrane structures. Included are various tasks such as the definition of constraints, formfinding, structural analysis and the cutting pattern generation. In the parametric environment of *Rhino/Grasshopper*, all these tasks are connected in a fluid data stream (Goldbach & Bletzinger, 2019).

This work uses a similar approach that adapts to compliant grid structures (see section 4.1.4 and 4.3.2).

2.3.2 Numerical Methods

Numerical methods are widely used for mechanical analysis. These are based on mechanical models, translated into equation systems, and solved by algorithms (solvers).

The structural analysis of actively bent structures requires some rather sophisticated approaches:

In a classical **"forward"**-approach, the simulation starts from an initially unstressed state, iteratively applying loads or displacements and couplings. This method may lead to a complex simulation process, but potentially covers the whole assembly stepwise.

In the **"inverse"**-approach, the input geometry is already bent, and residual stresses, derived from the curved geometry are applied. For complex active bending structures with coupled elements, this approach simplifies the analysis, as the simulation process from an unstressed and possibly uncoupled setup into a largely bent and coupled configuration is skipped.

In the following, two "inverse" approaches are described: One is based on the conventional *Finite Element Method* (FEM), the other is based on *Isogeometric Analysis* (IGA). These methods have been presented in Schikore et al., 2020 and Anna Maria Bauer, 2020.
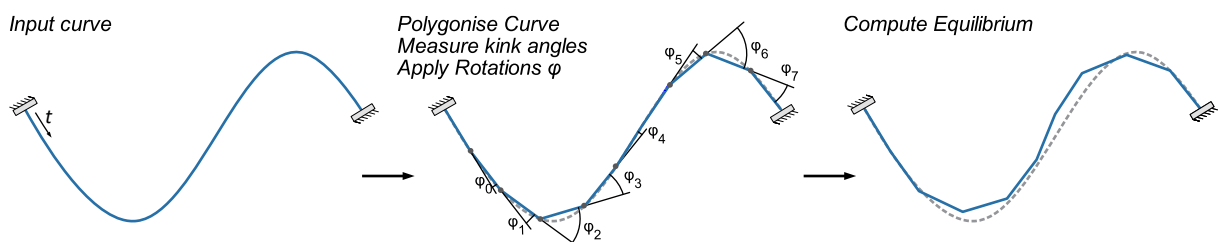
FEM "inverse"

Figure 25 *Computational steps of the FEM-inverse Method (Schikore et al., 2020, p. 114)*

FEM software applications are well developed, and became standard in commercial structural engineering. They offer user friendly modelling, stable numerical solving and even integrate national standards for buildings. Within FEM, curved beams are often approximated by polygons, but also curved elements are formulated.

To calculate a bent beam from an arbitrary deformed state, the following steps are computed: First, an arbitrary input curve is defined (system curve). The length of this curve needs be of an unstressed state. This curve is discretized to a polygon, and each segment orientated in twist. At all kinks, the angle and twist are measured, and applied as local rotations to reset the kinks. In spatial cases, all three local angles of the polygon's kinks need to be considered respectively. When computing equilibrium, the natural shape emerges.

All other elements, supports, loads, etc. of the calculation model are treated in a conventional way. This workflow allows the use of conventional FEM-software and therefore gives access to well developed software features, especially valuable for practical applications.

Note: This approach can be interpreted as a special assembly method. E.g.: Instead of deforming a continues straight beam into a constrained shape, the beam is divided into pieces, attached to final constraints (supports or couplings) and rigidly reconnected.

IGA "inverse"

In IGA, curves are not polygonised, but represented by NURBS. Similar to the FEM-inverse approach, also IGA can be performed using initially bent geometry inputs. The internal moments are computed by the curvature and torsion of the curve, and the geometrically nonlinear problem is then solved like the conventional FEM approach. This method was developed by Anna M. Bauer (Anna M. Bauer et al., 2019; Anna Maria Bauer, 2020).
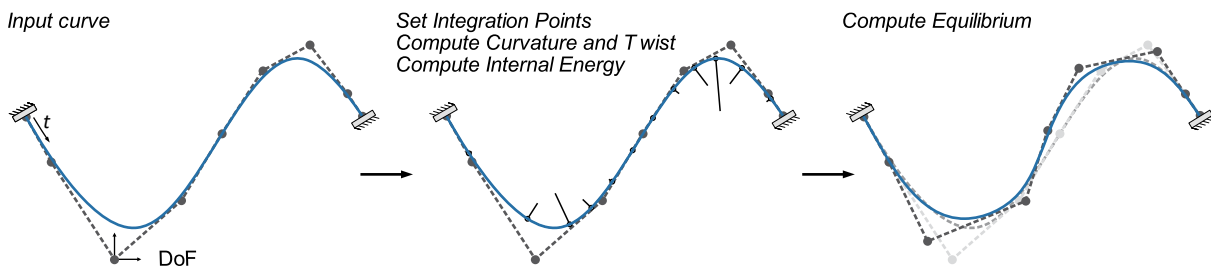

Figure 26 *Computational steps of the IGA-inverse Method (Schikore et al., 2020, p. 114)*

IGA allows a more fluent workflow when working with smooth curves, since the NURBS curves from CAD are directly used in the analysis as inputs and results.
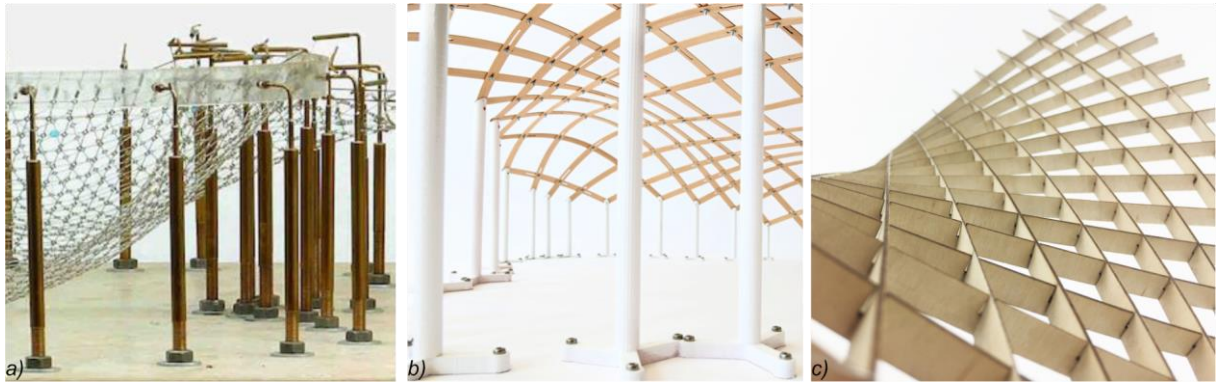
2.3.3 Physical Modelling Techniques

Figure 27 *Physical models for structural investigation: a) Hanging model of the Multihalle Mannheim (Photo: Uwe Dettmas; Kleefisch-Jobst, 2017), b) 3D-printed supports for investigations on geodesic mechanisms (Pillwein & Musialski, 2021), c) Laser cut lamellas for asymptotic lamella grid models*

Physical models are an inherent part in structural research, used for experimental investigations, for validation and demonstration. Models of structural applications are usually of smaller scale and thus the miniaturization of components is required. Furthermore, scaling leads to decisive effects in the mechanical behavior and cannot be ignored.

Besides traditional handcraft techniques, in the past decades, some novel fabrication techniques have been developed to create small, individualized components, based on digital input data. Most relevant in context of this work is laser cutting and 3D-printing. The advantages of these are the fast fabrication, the direct integration into the digital design workflow, and small tolerances.

Laser cutting allows the fabrication of planar elements from steel, timber, or specific plastics. 3D-printing is nowadays a substantial technique for individual manufacturing in many design fields. There is a wide range of materials, being integrated in 3D-printing technologies, such as various kinds of plastic, metals, ceramics, concrete, clay, etc.

This work includes model studies where lamella profiles are laser cut and details are made of 3D printed (stereolithography) plastic components (see section 3.4 and 4.3.3)

Figure 27 shows the hanging model for the *Multihalle Mannheim (see section 2.4.6 p.46)*, made of metal components (a), a compliant gridshell model with 3D-printed plastic supports (b) and laser cut timber lamellas with individualized slots (c).

2.4 Research and Developments

This section includes selected findings and developments from related research areas. The content results from extensive literature review on scientific publications, mainly published in the last decades. The following topics provide an overview on related geometric, mechanical, and architectural fields.

2.4.1 Networks in Architectural Geometry

Although geometry has always been an inherent part of architecture, the geometric and constructive complexity in modern architecture, and novel numerical methods have formed a new research area:

"[…] One has to decompose the skins into manufacturable panels, provide appropriate support structures, meet structural constraints and last, but not least make sure that the cost does not become excessive. Many of these practically highly important problems are actually of a geometric nature and thus the architectural application attracted the attention of the geometric modeling and geometry processing community. This research area is now called Architectural Geometry." (Pottmann et al., 2015)

The architectural possibilities for design are extended using freeform, doubly curved surfaces, and curvature allows shell-like behavior. Structurally, these are often realized as gridshells or grillages, which poses design questions about network layout, face planarity, constructive implementation and component fabrication, which are closely connected.

Eike Schling systematically analyzed geometric parameters of selected networks, allocated constructive strategies of built gridshells, and derived novel ones (Schling, 2018).
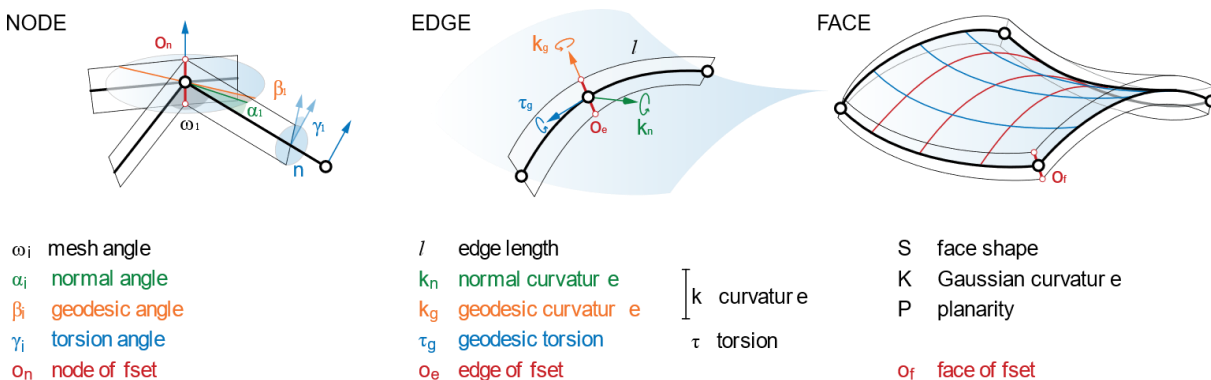
Repetitive Parameters of Curved Support Structures

NODE		EDGE			FACE	
ω_i	mesh angle	l	edge length		S	face shape
α_i	normal angle	k_n	normal curvature	k curvature	K	Gaussian curvature
β_i	geodesic angle	k_g	geodesic curvature		P	planarity
γ_i	torsion angle	τ_g	geodesic torsion	τ torsion		
o_n	node of fset	o_e	edge of fset		o_f	face of fset

Figure 28 *Geometric parameters of discrete and/or smooth networks (Schling, 2018, p. 53)*

According to the theoretical framework for curved support structures given by Schling, 2018, key parameters at node, edge and face can be determined (displayed in Figure 28). A characterization of networks can be derived by a qualitative evaluation of these parameters. E.g.: The parameter is "null", "constant", or "variable".

Accordingly, constructive strategies are applied to meet the geometric characteristics. E.g.: A variable intersection angle at node can be implemented using a hinge, variable curvature can

be implemented using curved prefabrication, or elastic deformation, some geometric relations can be handled by tolerances.

In an analysis of repetition, build structures or structures from novel geometric investigations, curved grid structures can be evaluated regarding these parameters and constructive or geometric strategies.

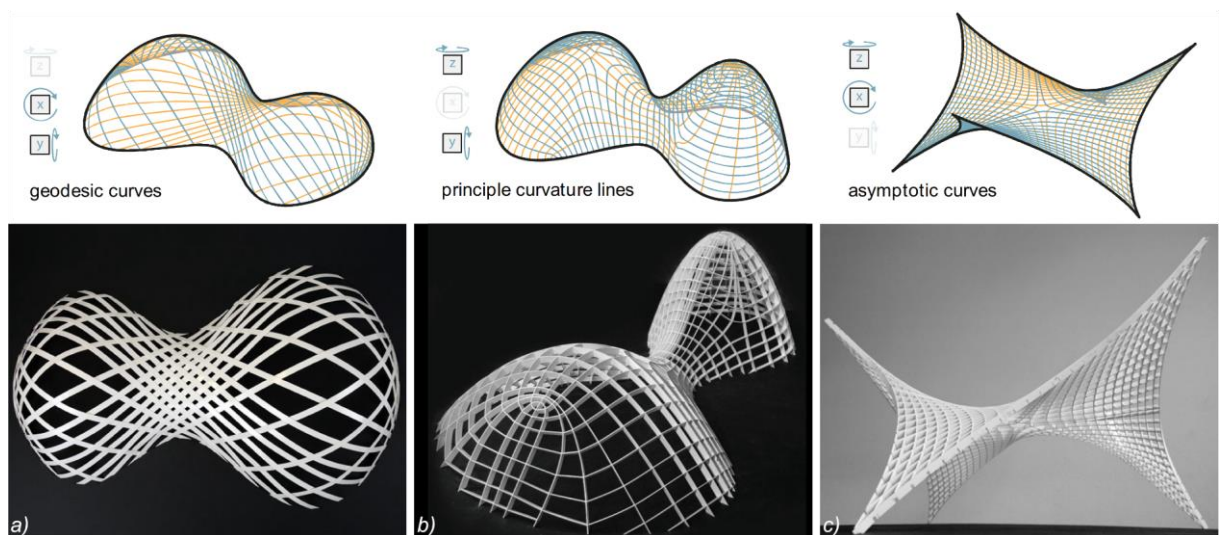## Strips on Smooth Curvature Networks

Figure 29 Smooth networks with biaxially curved curves: a) Geodesic network, b) Principal-Curvature Network, c) Asymptotic Network (Schling, Hitrec, & Barthel, 2018)

Networks that are geometrically derived using zero curvature constraints can be matched with (nearly) developable strips (Chengcheng Tang et al., 2016). Some basic examples are given in Figure 29. For each of these networks, one of three curvature quantities is zero (*Darboux*-Frame, see chapter 2.1.3).

Figure 29a shows a geodesic network on a both syn-, and anticlastic surface. The curves have zero geodesic curvature, and the strips are initially straight. Figure 29b shows a principal curvature network with no geodesic torsion. Note, the strips have normal curvature and thus are precurved. Figure 29c shows an asymptotic network on an anticlastic surface with zero normal curvature. The strips are initially straight.

In his dissertation, Schling, 2018 contributes the approach of geometrically and mechanically superimposed strained lamella gridshells:

"[…] We focus on the use of straight, bendable strips to construct strained lamella gridshells and demonstrate the mathematical background and physical application of such designs. […]" (Schling, 2018, p. 160)

2.4.2 Transformable Structures

Structural transformability in architecture is commonly interpreted as a reversible process. It is used for various applications and functions: Convertible building skins (roofs, facades – adaption to user's needs), Erection of structures[1] (as part of the construction process), Mobile (deployable) structures (packing and transportation), Adaptive structures (geometric adaption to varying loads), Convertible bridges on water routes (adaption traffic).

Literature provides numerous characteristics of transformable structures to be possibly used for classification (Šljivić et al., 2021). For a wide overview on this topic, the reader is referred to Schikore, 2022. In the following, three basic classification principles are described, that also apply to compliant grid structures, the scope of this work.

Geometry of Movement and Structural Type

BAUART/ CONSTRUCTION SYSTEM	ART DER BEWEGUNG/ TYPE OF MOVEMENT	BEWEGUNGSRICHTUNG/DIRECTION OF MOVEMENT			
		PARALLEL/PARALLEL	ZENTRAL/CENTRAL	ZIRKULÄR/CIRCULAR	PERIPHER/PERIPHERAL
MEMBRANEN, TRAGKONSTRUKTION FESTSTEHEND/ MEMBRANES, SUPPORTING STRUCTURE STATIONARY	RAFFEN/ BUNCHING				
	ROLLEN/ ROLLING				
MEMBRANEN, TRAGKONSTRUKTION BEWEGLICH/ MEMBRANES, SUPPORTING STRUCTURE MOVABLE	SCHIEBEN/ SLIDING				
	KLAPPEN/ FOLDING				
	DREHEN/ ROTATING				
STEIFE KONSTRUKTIONEN/ RIGID CONSTRUCTIONS	SCHIEBEN/ SLIDING				
	KLAPPEN/ FOLDING				
	DREHEN/ ROTATING				

Figure 30 *Classification Matrices of transformable structures (suggested by Blümel, 1972)*

A classification principle, set up by the former Institute of lightweight Structures in Stuttgart (Blümel, 1972, pp. 44–45) organizes entire structures according to the structural type (e.g. rigid structures or membranes), the type of movement (rolling, folding, bunching, etc.), and the path of transformation (linear, circular, etc.).

---

[1] Note: Erection in this context does not include the assembly, but structural forming.

Figure 30 shows various combinations. This collection is limited to systems involving membranes or stiff components, but the principles are potentially applicable to other structural types.

Types of Mechanisms

The expression "mechanism" is widely spread in any fields. In general, it describes a system of action and reaction. In a mechanical context, mechanisms are processes, involving time, states, controlled motion of parts and actuators. There is a large variety of mechanical approaches in the field of transformable structures, that may be classified into three main classes (based on Novacki, 2014): Rigid, compliant and soft.
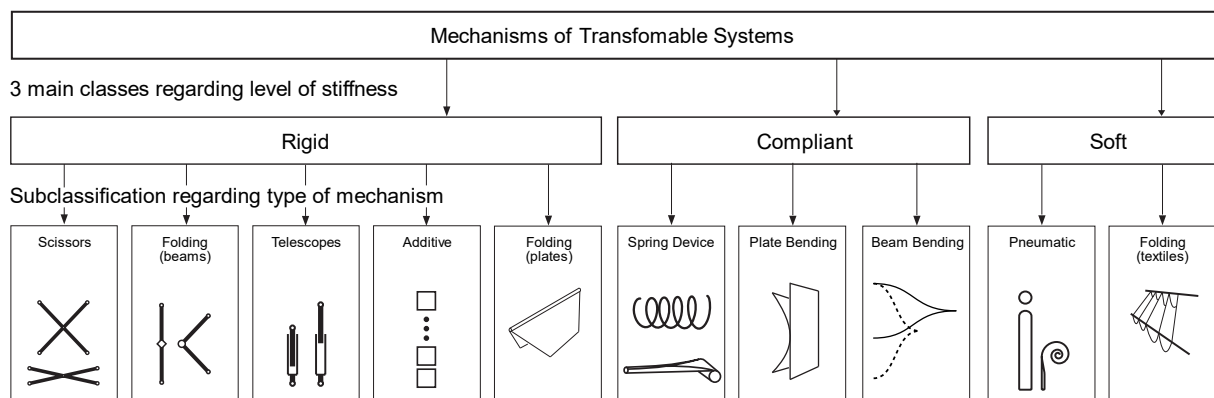
Figure 31 *Classification of mechanisms for transformable structures (Novacki, 2014, extended by J. Schikore)*

- **Rigid** mechanisms are compound by stiff elements. Transformability is achieved by hinges or through addition. Such types are widely used and well developed. Transformations follow kinematic principles and can be described by geometric operations only.

- **Compliant** mechanisms transform using controlled elastic deformation and thus require the consideration of forces. Spiral or leaf springs are commonly used as controlled "path-force"-devices. In the last decades, compliant mechanisms are continuously developed and thus can be found in various applications. They offer advantages high precision, low weight, low friction, low part count, the ability to miniaturize, etc. (Howell, 2001).

- **Soft** mechanisms take advantage of the softness of textiles or cables and stiffen through tension.

Transformable structures may include various types of mechanisms. Such "hybrids" are common (e.g., springs assembled within rigid-link structures). Hybrid configurations of hinged, compliant beams are furthermore called "semi-compliant". In Figure 32, an exemplary version of a simple mechanism using the folding, compliant, and semi-compliant approach are shown.
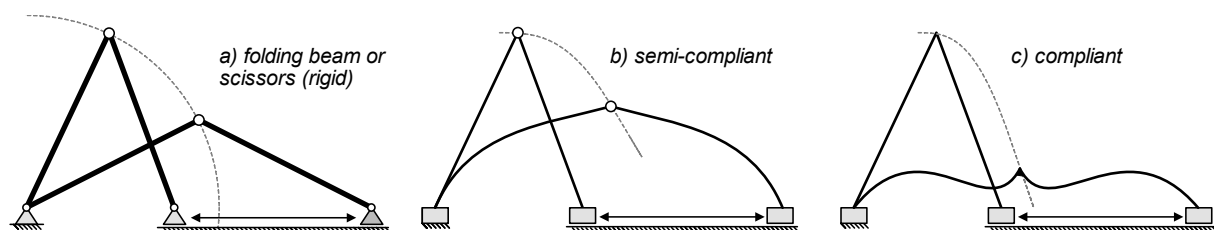
Figure 32 *Folding (a), compliant (c), and hybrid configuration (b) of a two-beam-mechanism (based on Lienhard, 2014, p. 15)*

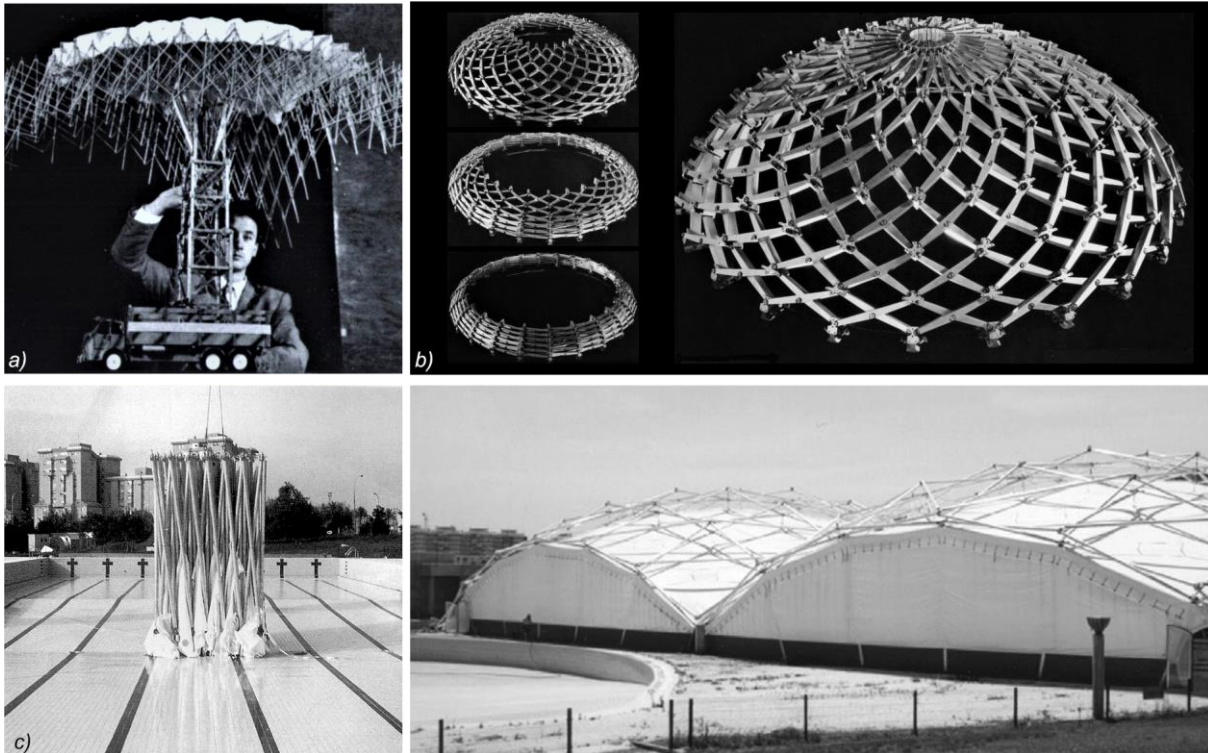## 2.4.3 Scissor Systems

Figure 33 *Architectural scissor systems: a) The movable Theatre concept, presented by Emilio Pérez Piñero in 1961 (Fernández-Serrano) b) The "Iris Dome" Model 1:100 by Chuck Hoberman 1993 (Hoberman, 1993) , c) A deployable roof for the San Pablo Olympics Swimming Pool in Seville by F. Escrig in Seville 1996 (Kassabian et al., 1999)*

Scissors, in a structural context, are rigid body systems of intersecting bars, linked by a pivot. Configurations of scissor chains and grids allows complex and spatial transformations.

The kinematics of scissors is integrated in the structural transformations of semi-compliant grids, treated in this work. The architectural context of the research conducted in this field also applies to compliant structures.

The utilization of scissors can be traced back for centuries. This mechanism is found in notes from Leonardo da Vinci (Escrig, 1996). In 1631, it was utilized by Christoph Scheiner for a copying device (von Braunmühl, 1891). The basic mechanism of a scissor unit is referred to a pantograph mechanism. This mechanical principle was brought into architecture in 1961, when Emilio Pérez Piñero, a Spanish architect, presented the famous "Movable Theatre", a concept for a deployable and mobile roof structure (Fernández-Serrano). In the past decades, this field has been extensively investigated by the research groups related to the engineers and scientists Sergio Pellegrino, Felix Escrig and Chuck Hoberman.

Figure 33 shows some well-known examples developed by the engineers mentioned: The *Movable Theater* by Emilio P. Pinero (a) was supposed to open from a truck. It marks a famous milestone in this research field. The *Iris Dome* by Chuck Hoberman (b) is a mechanical survey. The geometric principle is picked up in section 3.4.4 (A closer look at this approach follows on p. 42). Figure 33c shows a deployable roof for a swimming pool in Seville by Felix Escrig (c) at packed and deployed state. This project shows the potentials of scissors at architectural scale.

Geometric Basics

There are two basic groups of scissor units: Those with straight, and those with angulated legs. The lengths of the scissor's legs offer extensive possibilities to guide and control the transformation path of scissor systems.
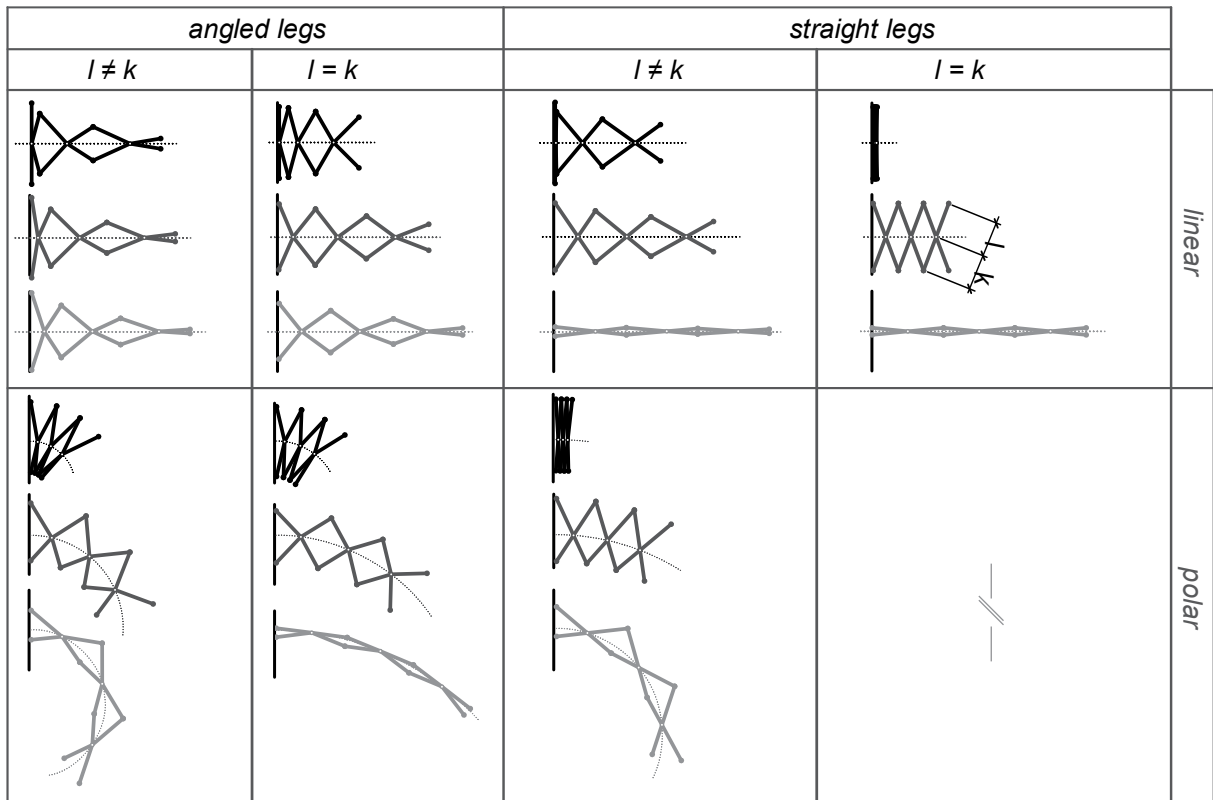

angled legs		straight legs		
l ≠ k	*l = k*	*l ≠ k*	*l = k*	*linear*
				polar

Figure 34 *A selection of straight and angled scissor chains in different transformation states*

Figure 34 shows a selection of scissor chains using repetitive units with straight or angled scissor legs, equal or unequal leg length. Their transformation paths are linear or curved. These diagrams also display the range of transformability, considering that the scissors' legs do not overwind (locking at 0° leg-angle).

Scissor Systems are often used to pack structures. The ability to fully retract can be satisfied for scissor chains with straight legs using a simple geometric condition:

$$l'_i + k'_i = l'_{i+1} + k'_{i+1}$$

Equation 37
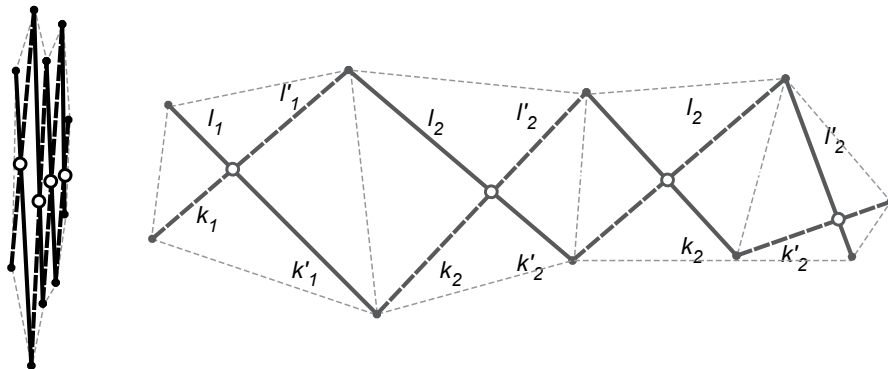
Figure 35 *Arbitrary scissor chain using units with straight legs*

Rotational Scissor Grids

Chuck Hoberman demonstrated the potentials of scissor grids to generate rotational symmetric deployable grid structures with the *Iris Dome* (Figure 33b). These structures consist of coupled, angulated scissor chains. At couplings (hubs), these systems require multiaxial hinges. Figure 36 shows the structures details, implemented for a demonstrator exhibited at the *MoMA*[1] in 1994, with angulated scissors, and hubs with four rotational axes.

Figure 36 *Detail view of the Iris Dome model, exhibited in 1994 at Museum of Modern Art in New York (Photo: Mali Olatunji, Museum of Modern Art Archives, 1994)*

Later, Krishnan & Li, 2019 investigated geometric design strategies for axisymmetric spatial structures using planar angulated members. Emerging shapes and their morphology can be controlled using the geometric parameters of scissor units and the grid density. Their work underlines the spectrum of possible shapes for deployable structures of this kind. Figure 37 shows exemplary shapes that can be configured. These include synclastic, developable, or anticlastic shapes.
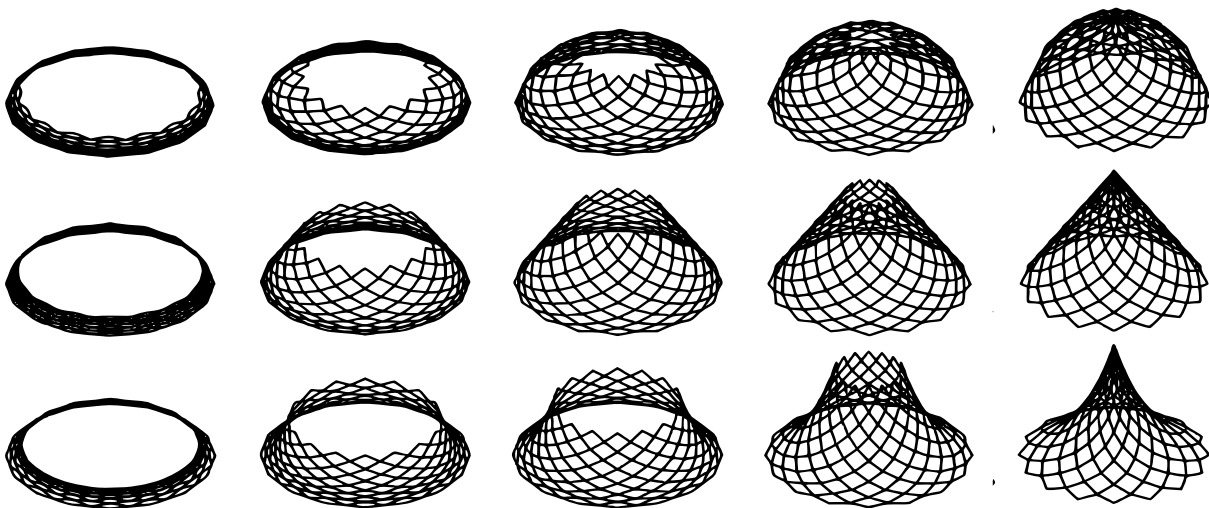
Figure 37 *Rotational symmetric shapes of scissor grids on a synclastic (top), developable (middle), and anticlastic (bottom) reference surface "Deployment sequence for fully compact forms" (Krishnan & Li, 2019)*

The concept of rotational scissor grids is picked up in a design study in section 3.4.4.

---

[1] *The Museum of Modern Art in New York, US*

2.4.4 Bending-Active Structures

Figure 38 *Built bending-active Structures, designed using varying approaches: a) Mudhif house in Southern Iraq. The building technic is still used today (Lienhard, 2014, p. 53), the design is "behavior"-based, b) Multihalle Mannheim build 1974, designed using a geometry based approach (Burkhardt & Bächer, 1978), c) The AA/ETH-Pavilion build 2011 at the ETH, designed using the integral approach (D'Acunto & Kotnik, 2013)*

Bending-active describes an approach of elastic formation, applicable to various structural types. The term has been defined by Julian Lienhard:

"Bending-active structures are structural systems that include curved beam or shell elements which base their geometry on the elastic deformation from an initially straight or planar configuration. […] Bending-active structures are understood to be an approach rather than a distinct structural type!" (Lienhard, 2014, p. 13)

There is differentiation of three design approaches for bending-active Structures:

- *"In a **behavior-based** approach bending is initially used intuitively; the system's geometry and structural behavior is studied empirically. Material limitations are tested physically.*

- *In a **geometry-based** approach the system's geometry is predefined based on analytical geometry or experimental form-finding methods, both of which are used as a controlled means to approximate the actual bending geometry. Material limitations are considered analytically based on moment curvature relation.*

- *In an **integral approach** the elastic bending deformation is analyzed through numerical form finding, which enables full control of material behavior-based geometry. Material characteristics and limitations are included in the numerical analysis model."* (Lienhard, 2014, p. 50)

Designing bending-active structures requires careful consideration of deformability and load-bearing capacities, which are opposing characteristics. This leads to a paradox, that underlies all bending-active structures. The induced residual stresses affect the load-bearing behavior in terms of capacity and stiffness. Whether these effects are advantageous or not, depends on the specific configuration of initial prestress, external loads, and geometry. Activating stress-stiffening effects is a key strategy to create structurally sound systems (Lienhard, 2014, p. 141)

The compliant structures in scope of this work can be classified as bending-active structures, designed using both geometry-based (initial design), and integral approaches (transformation).

2.4.5 Compliant Mechanisms

Figure 39 *Various applications of compliant mechanisms: a) Compliant catapult, sketched by Leonardo da Vinci (Howell, 2001, p. 9), b) Inextensional deformation of the "Spring-Back Reflector" used for the M-SAT2 satellite (Tan & Pellegrino, 2006) c) Thematic Pavilion at the Expo 2012 in South Korea by SOMA architects and Knippers Helbig (Schleicher, 2016, p. 48)*

Compliant mechanisms are part of our everyday life. Larry L. Howell, a famous researcher in this field, gives a far-reaching definition:

"If something bends to do what it is meant to do, then it is compliant. If the flexibility that allows it to bend also helps it to accomplish something useful, then it is a compliant mechanism." (Howell, 2001)

Compliant mechanisms are widely found in nature, and for humans, the use reaches back to ancient times (e.g., compliant scissors or bow and arrow). Today, various small tools take advantage of such mechanisms (e.g., plastic clips). Larger applications are found in notes from Leonardo da Vinci (Figure 39a), and compliant mechanisms are used for deployment in space. The *M-SAT2* satellite uses a compliant spring-back Reflector (see Figure 39b). In architecture, only few applications exist, and the development started at beginning of the 21st century. The *Thematic Pavilion* is built or the *EXPO* 2012 in South Korea (*SOMA Architects* and *Knippers Helbig* engineers) has a kinetic façade with GFRP-panels that open through controlled buckling (Figure 39c).

Compliant mechanisms hold various advantages, compared to traditional rigid mechanisms:

- Low number of components (no hinges with bolts, etc.)

- Low maintenance (no friction – no need for lubricants)

- Strain energy integration (advantages of energy storage, e.g., spring back)

- Possibilities of miniaturization and mass production (3D- printing or plastic casting)

The design of compliant mechanisms requires careful synthesis of freedom and constraint in terms of elastic stiffness.

2.4.6 (Strained) Gridshells and Erection in Architecture

Gridshells are a special type of shell structures, that, unlike continues shells, are compound by a grid of beams, and strained gridshells are a subtype of those, and they relate to bending-active structures (see chapter 2.4.4). Elisa L. Hernández provides a clear definition with validity to this work:

"[…] The definition of elastic gridshell corresponds to a shell structure composed of a single- or multi-layer grid of continuous profiles, which are initially straight and will be progressively bent until achieving an architecturally and structurally satisfactory geometry. This form-giving bending process induces important residual stresses on the grid profiles; reason why these structures are also known as strained gridshells" (Hernandez, 2016)

Gridshells, and especially strained gridshells, are a niche in architecture. The main advantage is to generate doubly curved shell structures from initially straight elements. The main challenge relates to the paradox for bending-active structures: to manage stiffness, load-bearing and deformability.

Another challenge addresses the erection process. Mostly, the entire gridshells, or patches, are transformed from a flat assembly state into special shapes. The emerging shapes are either formfound in advance or predefined and adjusted by supports and bracings. Gregory Quinn defines four practical erection strategies, if the grid is assembled flat: "Lift up", "Push up", "Ease-down" and "Inflate" (Quinn, 2018b, 13–24).
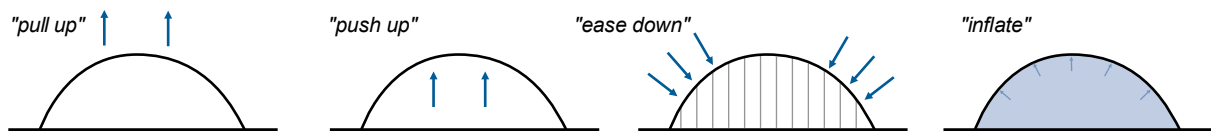
Figure 40 Erection strategies for strained gridshells from flat to spatial: "pull up!, "push up", "ease down" and inflate (based on (Quinn, 2018b, p. 13)

The following sections address built structures, starting from early steel structures designed by Vladimir Šuchov, followed by strained timber gridshells, and temporary structures made from GFRP.

Šuchovs' Steel Structures

Figure 41 Steel gridshells from Vladimir Šuchov: a) Hyperboloid shaped Water Tower in Niznij Novgotod with twisted L-profiles (Beckh, 2012) b) Workshop in Vyksa (RU 1897) (Picture in public domain, taken from MARCH, 2020)

Vladimir Šuchov was a pioneer in gridshell design in the 19th century. His work is not typically referred to strained gridshells, but elastic deformation was at least partly applied in assembly. In numerous hyperbolic lattice structures (towers), straight L-profiles are twisted to align the profiles' orientations at the grid's nodes. This deformation (twist) in this case was not used to shape the global geometry, but rather to satisfy constructive criteria (see Figure 41a).

The workshop in Vyksa is a doubly curved gridshell and marks a milestone in lightweight structures in general. The structural drawings and geometric investigations imply, that the profiles were most likely fabricated planar and deformed to fit the complex spatial geometry (Beckh, 2012; Schling & Barthel, 2021).

Strained Timber Gridshells

Figure 42 *Strained timber Gridshells: a) Multihalle Mannheim (GER, 1974, Architect: Mutchler&Partner, Engineering: Ove-Arup&Partner and Frei Otto), b) Weald and Downland Museum (Johnson, 2002) c) The Savill Building (b, c: Du Peloux de Saint Romain, 2017).*

In the 20th century, the German engineer and scientist Frei Otto investigated strained timber gridshells. The **Multihalle Mannheim**, *a prominent milestone for gridshells in architecture,* was designed and built in 1974 for the "Bundesgartenschau" (see Figure 41a). This project involved extensive research in formfinding, load-bearing and construction (Burkhardt & Bächer, 1978). It inspires engineers and architects up to the present. Later examples for strained timber gridshells are the **Weald and Downland Museum** (Figure 41b, 2002, UK, Architect: *E. Cullinan*, Eng.: *Buro Happold,* UK), or the **Savill Building** (Figure 41c, 2006, Architect: *Glenn Howells*, Eng.: *Buro Happold*, UK).

The *Multihalle Mannheim* is explained more detailed: The roof has a funicular, formfound shape and spans up to 60m. The equilateral grid (50cm mesh) is compound out of layered, square timber profiles (50x50mm, hemlock fir). The structure is stiffened by diagonal steel bracings and covered by a PVC membrane. Figure 43a shows the complete building, covering 7500m^2.

The grid of the Multihalle Mannheim was assembled flat and could be packed. After placing the grid, it was erected following a "push-up"-strategy, using temporary stands (see Figure 43 b-e). Once shaped into the desired funicular geometry, the supports were fixed, the nodes (scissor hinges) were tied, and the bracing was attached (Figure 43b). Thereby, the geometry was locked, and the stiffness of the double layered members was activated.
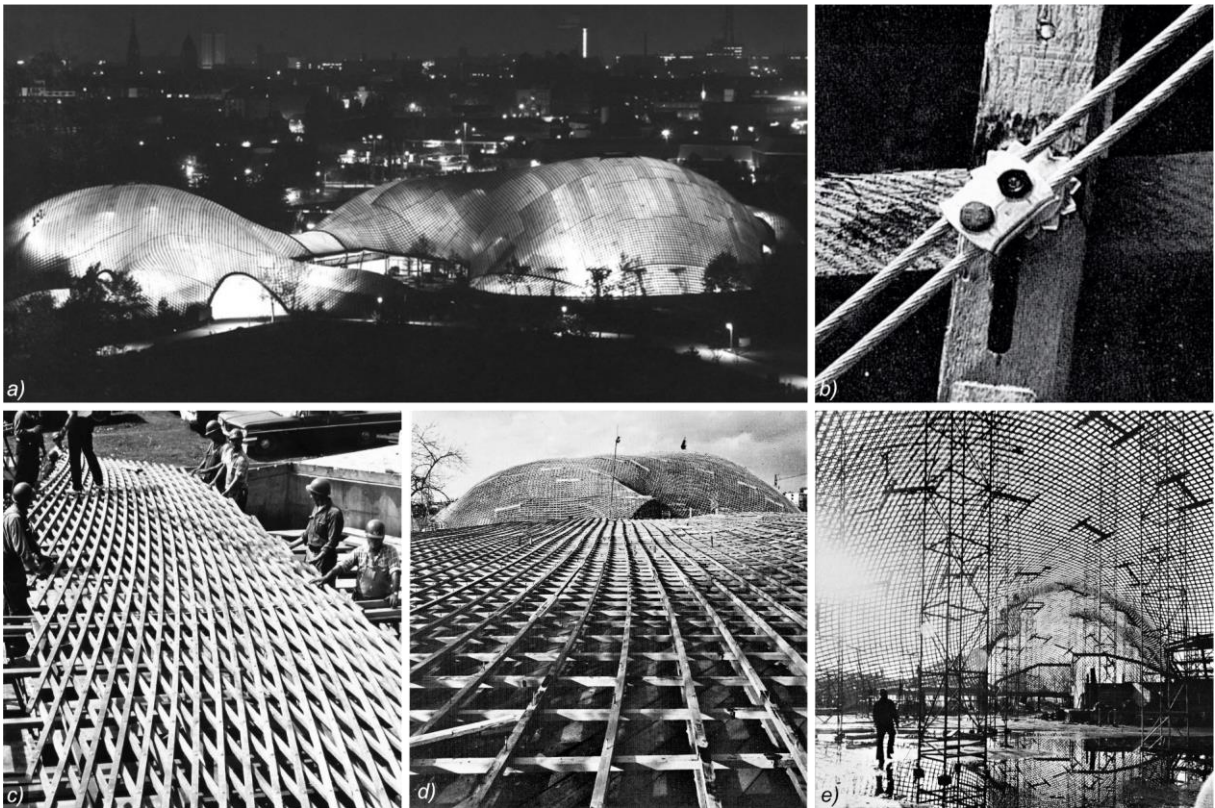
Figure 43 The Multihall Mannheim: a) Night view of the building b) Node detail, c) Packed timber grid (Kleefisch-Jobst, 2017), d) Placing of flat grid, partly lifted, e) Lifting grid using temporary stands (Source.a,b,d,e: Burkhardt & Bächer, 1978)

GFRP Gridshells

Novel developments of the past years show the potentials of GFRP to create ultralight strained gridshells.

The **Soliday Forum** in Paris (June 2011) was a temporary gridshell, designed by *UR Navier*, *Ecole des Ponts* (Paris) and *T/E/S/S atelier d'ingénierie*, and covered 300 m^2. The triangulated, three-layered grid is made of GFRP-tubes (D=41,7 mm), that are laterally clamped. The erection process refers to the *Multihalle Mannheim*, but a crane was able to lift the lightweight structure. Figure 44 shows the building and construction on site.

Figure 44 Gridshell at the Soliday Festival: a) View from outside, b) Inside view, c) Detail view d) Flat Assembly of the equilateral grid (two layers), e) Pull-up erection of the quadrilateral grid, f) Bracing (triangulation) at final geometry with third layer of GFRP tubes (TESS, 2011).

Another approach for gridshell erection was investigated by Gregory Quinn: In this method, a cushion is inflated to push the flat grid structure into spatial shape. After inflation, the grid structure is fixed to its supports and the cushion can be removed. This concept has been proven by various prototypes. Figure 45 show the **SheltAir** pavilion, erected in Berlin in 2018.

Figure 45 *SheltAir Pavilion, erected using inflation: a) Outside view, b) Interior view, c) Flat assembly state, d) Inflation using cushion for erection, e) fixed and supported grid, the cushion is removed. (Quinn, 2018a)*

The last example is a patented, vegetated grid structure, developed at the ENPC[1] in France (Bavarel et al., 2020). The structure can be placed as "garden furniture". The **Corolle** is made of 18 mm circular GFRP profiles and has a diameter of 8 m. The grid structure is based on a Chebyshev net. The structure is assembled flat and bound into a cylindric shape. Pulling the edge nodes downward, the structure transforms into a funnel shape. At desired shape, the structure is locked using bracings. Figure 46 shows the key steps from assembly to use.

Figure 46 *Funnel shaped gridshell for the support of climbing plants (ENPC, 2020)*

The geometric and mechanical concept of the *Corolle* is similar to the *Kinetic Umbrella*, a practical case study in section 4.3.

---

[1] *École Nationale des Ponts et Chaussées (Grande école in Champs-sur-Marne, France)*

2.4.7 Research on Compliant Grid Transformation

The transformation of compliant grids has been investigated on different levels, from differential geometry to numerical calculations and physical research. In the following, selected investigations, that highly relate to this work are briefly summarized.

The work of S. Finsterwalder: *"Mechanical Relations of Surface Deformation"*
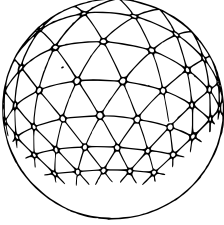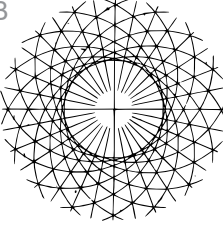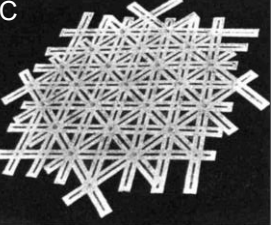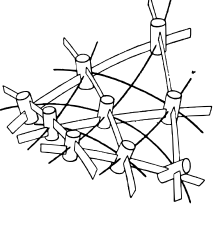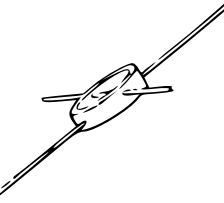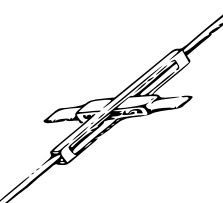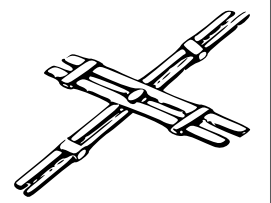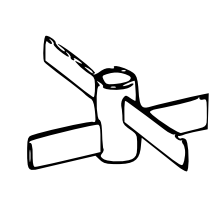
	A	B	C	D
Network Setup				
	Surface: Free Form Curve Fam.: 3	Surface: Rotational Curve Fam.: 3	Surface: Sphere Curve Fam.: 4	Surface: Minimal Curve Fam.: 2
Mechanical Interpretation				
Geometric Constraints	$\kappa_n \neq 0$ $\kappa_g \neq 0$ *(free curved)* $\tau_g \neq 0$ φ = constant l = variable	$\kappa_n \neq 0$ $\kappa_g = 0$ *(geodesic)* $\tau_g \neq 0$ φ = variable l = constant	$\kappa_n \neq 0$ $\kappa_g = 0$ *(geodesic)* $\tau_g \neq 0$ φ = variable l = variable	$\kappa_n = 0$ $\kappa_g \neq 0$ *(asymptotic)* $\tau_g \neq 0$ φ = 90° l = constant
Srf.	any smooth surface	Rotational Surfaces / Plane	Spheres / Pseudosp., Plane	Minimal Surfaces / Plane

Table 1 *Four selected cases of network deformability investigated by S. Finsterwalder. (Figures/drawings are taken from Finsterwalder, 1899)*

The deformation of networks in a geometric context describes changes of curvature and/or curve lengths, without topological changes. Fundamental relations on such deformations, combining geometric and mechanical aspects have been studied by Sebastian Finsterwalder in the 19th century (Finsterwalder, 1899). He describes the deformability of various networks with specific geometric constraints regarding curvature or nodal degree of freedom. Furthermore, geometric constraints are allocated to mechanical limitations, e.g., introducing lamella profiles as mechanical equivalent for uniaxial zero-curvature preservation or thin circular sections as capable for free biaxial bending and torsion. A selection of four cases, individual characteristics, constraints, and deformation restrictions are summarized in Table 1 exemplarily.

The significance of S. Finsterwalders work lies in the correlation of differential geometry, kinematics, and kinetics of grid structures, that opens new perspectives and potential applications.

Self-Shaping Gridshells

In the past decade, various research groups picked up the topic of deployable and self-shaping grid structures. In the following paragraphs, some highly related projects are summarized exemplarily:

In 2014, a flat collapsible geodesic mechanism was applied for a demonstrator at architectural scale. The "Neula"-pavilion, exemplarily, is an anticlastic geodesic gridshell, and the shape emerges naturally when deployed from an initially planar state (Soriano et al., 2019, p. 1896).

Figure 47 Erection of the "Neula"-pavilion in 2014 by Scientists of the UPC and CODA[1](Photo: Andrés Flajszer)

Scientists at the UPC (LiTA)[2] in investigated "G-Shells", grids of "flat" orientated lamellas on geodesic networks. These structures are restrained in deformability due to their members strong axis. Soriano et al., 2019 categorizes such mechanisms into "pantograph" (2D), "geodesic" (3D) and "flat collapsible geodesic" (or "G-Shells") (2D to 3D).
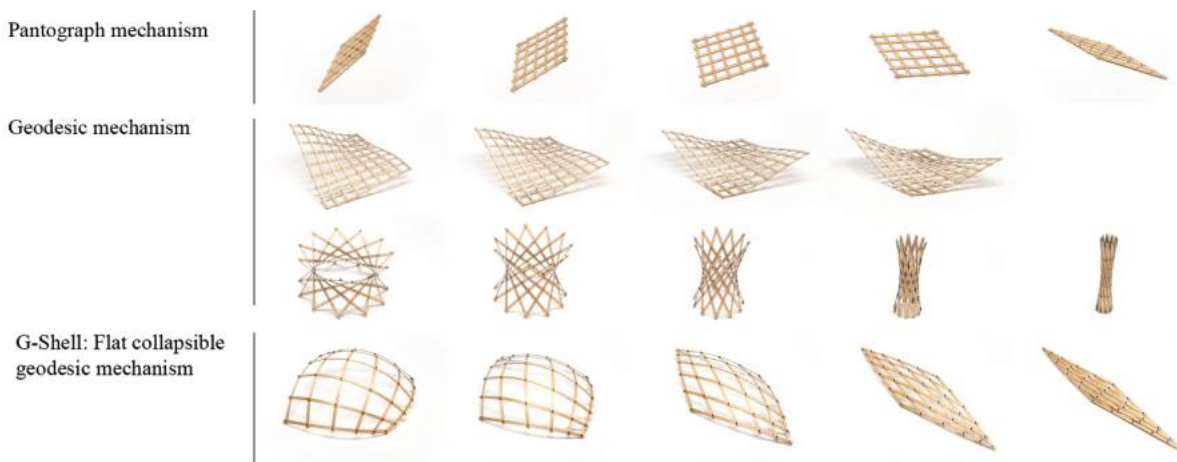
Figure 48 Physical models displaying the subcategorization of deployable geodesic grid systems (Soriano et al., 2019, p. 1897)

In 2019, scientists at the EPFL in Switzerland introduced "X-shells" as new class of deployable structures. These comprise grids with compliant beams and hinged joints. Using numerical optimization, deployable configurations were found, and the diversity of such structures was displayed. Emerging shapes are controlled by the grid layout and stiffness parameters (Panetta et al., 2019).

---

[1] *CODA is an engineering firm in Barcelona working closely together with the UPC.*

[2] *The "LiTA" is the "Laboratory of Innovation and Technology in Architecture" at the Polytechnic University of Catalonia.*
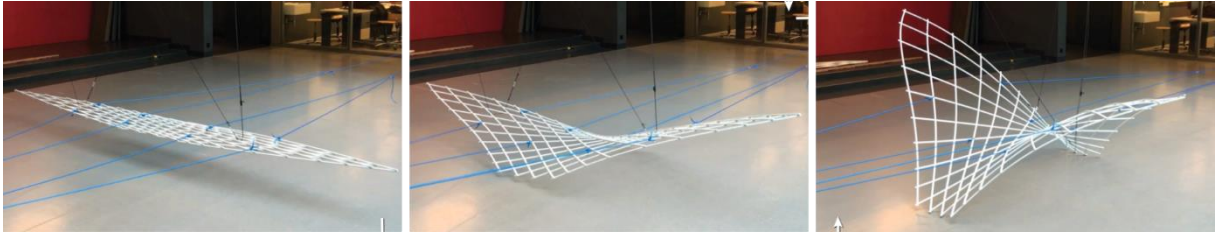
Figure 49 *Actuation into spatial of an "X-Shell" (Panetta et al., 2019)*

In 2020, researchers at TU-Wien published digital methods and algorithms to find flat geodesic configurations that deploy into predefined design surfaces (Pillwein, Leimer, et al., 2020; Pillwein & Musialski, 2021). On a free-form surface, a quadrilateral patch is defined, and using algorithms, the patch is filled with a quadrilateral geodesic network. The deployment is based on the changing angle $\bar{\alpha} \to \alpha$, and requires additional translational DoFs (notches in the physical model, see Figure 50b).

Figure 50 *Physical model showing a) Flat to spatial deployment of a geodesic grid, b) Notches, necessary to provide a translational DoF at nodes to allow transformation (Pillwein, Kübert, et al., 2020)*

Deformation with Constant Normal Curvature

In 2018, the deformability of networks with constant normal curvature was identified and numerically simulated by the research group of Helmut Pottmann (Schling, Kilian, et al., 2018). Figure 51 shows three states of deformation.

Figure 51 *Paper model of the deformation of a rotational network with constant normal curvature (Schling, Kilian, et al., 2018).*

Bundled quadrilateral Gridshells

Bundable Mesh on Design Surface   *Relaxed and loaded Gridshell (self-weight)*   *Bundled state*
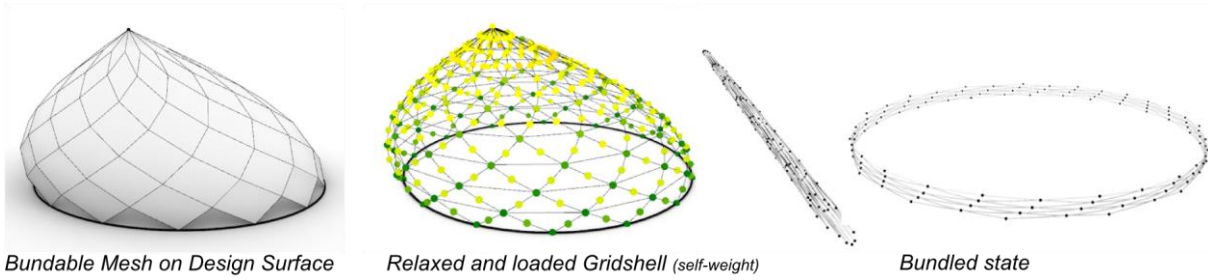
***Figure 52** Bundlable Gridshells: Bundable mesh on a design surface, relaxed and loaded gridshell, and bundled states*

In 2022, Xavier Tellier (EPNC Paris) developed a novel approach to find spatial quadrilateral grid layouts on design surfaces, that can be fully packed into a bundle. The criteria for fully closing scissor chains, described by F. Escrig (see Figure 35 and Equation 37) are applied to smoothly curved spatial networks on surfaces. This property is generally valid for any Chebychev net. An exemplary network on a given design surface, the mechanically relaxed and loaded (self-weight) gridshell, and two possible bundled states are shown in Figure 52.

Summary and Research Gap

The presented topics include the research areas of architectural geometry, transformable, scissor, compliant, active bending and strained or self-shaping structures. These topics have a common ground but originate from different perspectives. All topics involve transformation.

Specific types of mechanisms are found in any transformable support structures: Rigid-body, compliant or soft mechanisms. Furthermore, transformable structures can be classified by the type of movement and the path of transformation These basic classifications may be referred to grid structures.

Scissor systems were developed that allow grid transformation, following geometric design rules. These systems involve rigid-body mechanisms (section2.4.3). The question arises, to what extend scissor systems can be combined with compliant mechanisms?

Architectural geometry provides approaches to design smooth strained gridshells (section 2.4.1). A selection of build strained gridshells demonstrates feasibility and quality at architectural scale (section 2.4.6). Strained gridshells can be seen as bending-active structures, as elastic deformation is used for shaping (section 2.4.4). The process of erection of these structures can be interpreted as a semi-compliant mechanism (section 2.4.5). However, the erection involves transformation as part of the construction process only, and the transformation is barely constrained. The question arises, how semi-compliant grid transformation can be constrained to generate controlled transformations?

Several research groups investigated compliant grid structures, developing self-shaping grid structures. The increasing interest in this research field underlines the significance and potentials of such mechanisms and structures. However, this topic is still in its infancy.

The research presented in section 2.4.7 was conducted parallel to this work. The numerous approaches for specific mechanisms, aiming at selected structural parameters and behaviors are not embedded in a comprehensive theoretical framework.

All research subjects involve quadrilateral grids with uniaxial hinges and compliant members. However, essential kinematics of quads or uniaxial hinges, or the internal energy balances throughout transformation of compliant members remain unclear.

A focus is given on geodesic networks and inherent compliancy. The general transformability of asymptotic configurations is identified but barely investigated.

A large research gap opens for practical implementation. The research briefly presented remains on a theoretical, morphological level, with only few prototypes that take the step forward into application and architectural scale. The challenges of suitable engineering workflows, dimensioning with the stiffness paradox, constructive implementation and actuation remain rather unexplored. The question arises: Are compliant grid structures generally feasibly at architectural scale?

Figure 53 *Actuation model detail for the Hotel Intergroup*

3 MECHANICAL STUDIES

This chapter investigates geometric and mechanical characteristics, and the performance of semi-compliant structures as both static, and transformable structures. It is subdivided into the following sections:

- Section 3.1 provides a framework to classify compliant grid structures and refers the scope of this work to this framework. It defines the **research object**.

- Section 3.2 reveals basic kinematic rules of quadrilateral grid cells and the kinetic performance of structures with restricted compliancy in three **transformation analyses**. These analyses aim to systematically clarify the transformation process in morphology, kinematics, and kinetics. It introduces the curvature-square analysis as a method to evaluate the internal kinetic relations of transformation.

- Section 3.3 investigates global stiffness and local stability in a **static analysis**. This section aims at load-bearing, necessary at both static service states and throughout transformations. These investigations reveal decisive local and global phenomena regarding stiffness and stability.

- Section 3.4 includes **physical model studies** of compliant grid structures developed in a design studio. Four exemplary designs are classified according to the framework of section 3.1. Furthermore, the mechanical approaches that were developed in a creative process are analyzed.

3.1 Research Object

In the first part of this section, the structural components and related parameters of semi-compliant grid structures are systematically displayed, providing a framework for classification. Secondly, the scope of this work is defined within this framework.

3.1.1 Structural Components
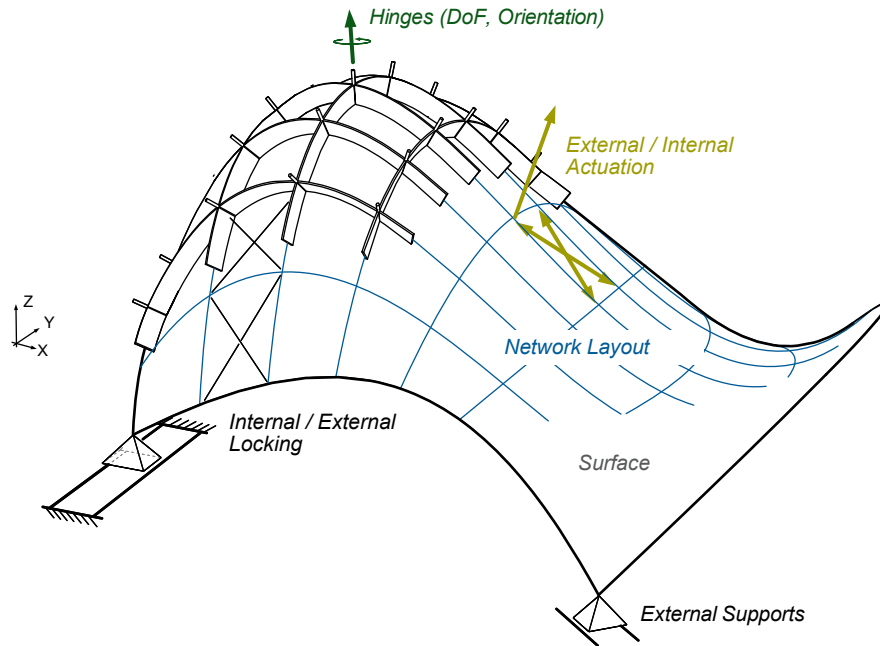
Figure 54 *Schematic overview on structural components and characteristics of semi-compliant grid structures*

Semi-compliant grid structures show distinct geometric and mechanical characteristics. In the following sections, key components are systematically described and classified. This comprehensive description reveals the total design spectrum of such structures as a combination of its component parameters. Figure 54 displays those components in a schematic overview.

Note, these parameters do not aim to give a full and detailed description of compliant structures, but help to provide classification of full systems.

Surface

The reference surface is the geometric basis for grid structures treated in this work. Fundamental types of doubly curved surfaces are shown in section 2.1.2 (Figure 5). Other distinctions address curvature and topology.

The key characteristics/parameters are summarized below:

- TYPE: ruled, rotational, freeform, …
- CURVATURE: e.g. Gaussian curv.: zero, negative, positive (syn.- and/or anticlastic)
- TOPOLOGY: zero (closed), one, two, … closed edge loops

Network (Layout)

Networks on smooth surfaces are a collection of curves, which follow distinct definitions. In section 2.1.3, some basic types of definitions are displayed. A distinction is made between curves defined by an external geometric reference (e.g. intersecting surfaces or planes, "free-form" curve on surface), or curves that are driven by the internal surface's parameters (e.g. curvature orientated paths). Other basic characteristics are the curvature and topology of the network.

The key characteristics/parameters are summarized below:

- REFERENCE: external (e.g., intersecting objects), surface, curve
- CURVATURE: from *Darboux-,* or *Frenet-Serret-Frame*: zero, constant, variable
- TOPOLOGY: quadrilateral, triangulated, irregular, …

Beams (Orientation and Compliancy)

The beam's system curves are given by the network (layout). In context with compliant grids, beams are decisively characterized by their orientation and local compliancy.

The orientation of beams defines the beams torsion. Besides a variable (free) orientation, beams may be aligned to distinct references. Again, a reference can be taken from: an external object (e.g. global orientation or orientation to a point in space), the reference surface (e.g. the surface normal vector – the *Darboux-Frame*), or the curve itself (e.g. the curves curvature vector – the *Frenet-Serret-Frame*).

a) external   *b) surface*   *c) curve*
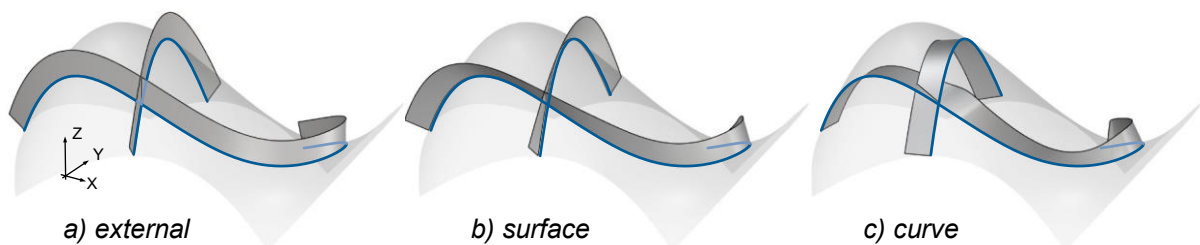
Figure 55 *Three different references for a beam's orientation. The blue curves mark the beam system lines. The strips display the different orientations: a) global orientation (global z-vector), b) Surface orientation (normal vector, see section 2.1.2), c) curve orientation (bi-normal vector orientation, see section 2.1.1)*

Another parameter is the beams compliancy, defined by the beams local stiffnesses. There are three orthonormal components of bending stiffness, refereed to the beam's axes (EI_T, EI_y, EI_z). The relation of these affects the compliant morphology and can be used for control. The deformability can be "restricted" to selected axial components, using relatively high axial stiffness where no compliant deformation is desired. In terms of compliant functionality, a general distinction between rigid and compliant behavior is used. This leads to various combinations of axial compliancy (Table 2).

The beams may involve an initial curvature, that is present in an unstressed state. This initial curvature may apply to either rigid or compliant beam axes.

Compliancy		GI_t	EI_y	EI_z	Section Geometry Example
No compliancy	No Bending/Torsion (rigid)	**r**	**r**	**r**	large circular section
Uniaxial compliancy	Torsion only	c	**r**	**r**	T-section / L-section (warp-free open thin profiles)
	Uniaxial Bending (no Torsion)	r	c	r	geometrically infeasible
		r	r	c	
Biaxial compliancy	Biaxial Bending (no Torsion)	r	c	c	
	Uniaxial Bending and Torsion	c	**r**	c	Lamella section
		c	c	**r**	
Triaxial compliancy	Bending and Torsion	c	c	c	Small circular section

Table 2 *Combinatorics of rigid or compliant beam axes ("r" = rigid, "c" = compliant)*

The key characteristics/parameters are summarized below:

- ORIENTATION: external (e.g., intersecting objects), surface, curve

- TORSION: zero, constant, variable / smooth, discrete

- COMPLIANCY: rigid, compliant (x,y,z)

- INIT. CURV: zero, constant, variable / smooth, discrete

Hinges

The grids' hinges are located the intersection points of the beam system lines. Their degree of freedom defines the kinematic quality of semi-compliant grid structures. However, there is a large spectrum for the setup of hinges, regarding axial orientation and topology.
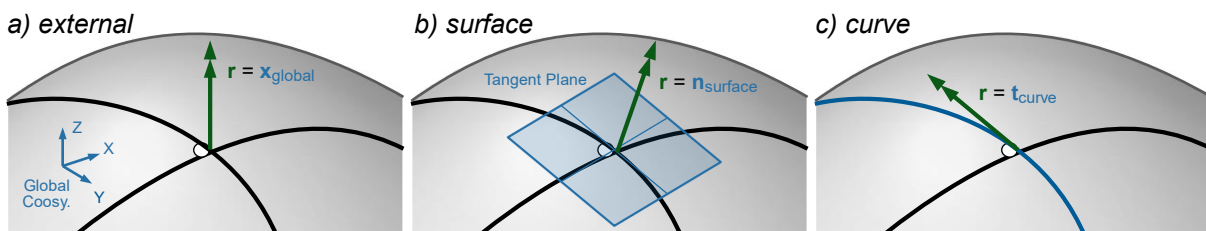
Figure 56 *Exemplary rotational axis orientations at a traversal node: a) Externally (globally) orientated axis, b) Axis aligned with surface normal, c) Axis aligned to system curve tangent.*

Generally, there are six possible DoFs in 3D space for a given object: three rotational axes and three translational directions. Grid structures are characterized by system curve intersections, and thus, any kinematic translation, disjointing these intersections, violates this character. Consequently, any translational freedom, normal to the grids reference plane at intersection is invalid. The only translational DoF, that does not violate this boundary condition are translations in the beam's local x-axes, also referred to "sliding" hinges. Rotational DoFs do not violate the network's intersecting character.

Rotational axes can be chosen freely and exemplarily reference to external objects, global vectors, surface normal (*Darboux*-Frame), or local beam axes. Figure 56 shows three examples of rotational axis orientation: global vector, surface normal and curve tangent.

In total, there are four applicable DoFs left: Three rotational DoFs, and the longitudinal beam translation (sliding). From those optional DoFs, many combinations can be assembled: Uniaxial or multiaxial rotational hinges, with or without sliding freedoms.

Another key quality of hinges is their topology (also called connectivity), that defines, which members at intersection are connected by which DoF. The topology becomes significant, when more than two members are connected at nodes (e.g. triangulated networks of smooth curves).

The key characteristics/parameters are summarized below:

- DoF: rotational, sliding

- ORIENTATION: external (e.g.: global vector), reference surface, curve

- TOPOLOGY: connectivity of freedom and constraints between members (valance > 2)

Supports

Supports are part of any structural system. In semi-compliant grid structures, they are part of the mechanism to restrict and control the global transformability and thus influence the mechanisms performance. Supports may block rotation or translation in suitable directions.

The key characteristics/parameters are summarized below:

- CONSTRAINT: rotational, translational

- AXIAL REF.: external object: Vector, Surface, Curve

Actuation

Actuation systems set transformable structures in motion. For this process, mechanical energy must be induced (or released). In the context of semi-compliant grid structures at architectural scale, the following portions of energy may compound this energy:

- lifting structural mass (potential energy)

- deform compliant members (strain energy)

- overcome friction (friction energy)

- accelerating structural mass (kinetic energy)

Figure 57 shows an abstract mechanical model that includes forces that relate to these portions. Two cases display different movement scenarios. The actuation force results from the equilibrium condition.

$$\text{F}_{Strain} + \text{F}_{Self-weight} + \text{F}_{Friction} + \text{F}_{Actuation} = 0 \qquad \textit{Equation 38}$$

Note, forces due to friction change according to the direction of movement, and thus, the direction of movement has an impact on the force equilibrium. The kinetic energy due to acceleration is not considered here, as these are assumed to be neglectable for the scope of this work.
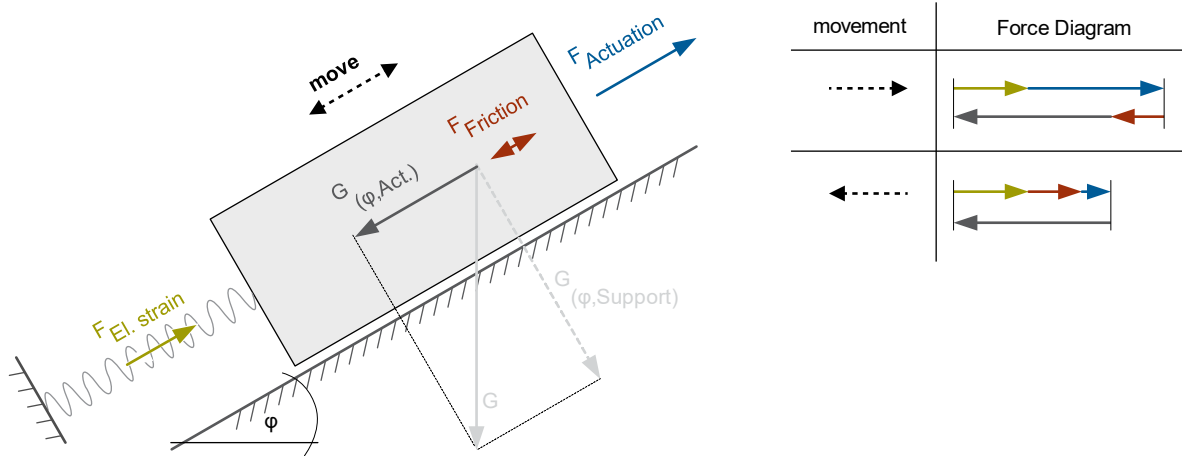
Figure 57 *Abstract mechanical model of a compliant system. Forces are displayed for two directions of movement.*

Actuation can be controlled via two principles: In a path controlled actuation, a defined path or displacement (or rotation) per time is applied. The force adapts to this constraint. In a force controlled actuation, a defined force (or moment) per time is applied. The displacement (or rotation) is corresponding. However, the functionality of compliant grid structures is to perform geometric transformations, and thus, only path controlled actuations are reasonable.

A distinction is made for the references of actuation systems: The **internal** actuation integrates the actuation system in the grid structure and follows its movement (e.g. cable systems as part of the grid structure, or nodal rotational actuation). The **external** actuation applies displacements following an external path (e.g. moving selected nodes along a predefined path).

Throughout transformation, the actuation force may change its direction, a decisive quality that may impact the devices used for actuation. E.g.: Cables only perform in tension, and thus are not able to change in force direction. This quality is described by either **uni-** or **bidirectional** actuation.

The key characteristics/parameters are summarized below:

- ACT.REF.: internal/external
- DIRECTION: unidirectional, bidirectional

Locking

Transformable structures serve as static structures at predefined states of geometric transformation (service states). At these states, the structures might be exposed to additional loads and locked accordingly. Locking systems have two basic functions:

- **Limitation of transformation:** The transformation is geometrically limited to a predefined transformation domain.

- **Service load-bearing:** At service state, additional loads may require a structural reconfiguration for load-bearing.

Locking is a geometric constraint, in which displacements or rotations are limited. In context of semi-compliant grid structures, there are two basic reference types in analogy to actuation

systems: **Internal** locking systems are integrated in the grid structure and lock at predefined states (e.g. cable activation within the grid structure, or nodal rotational locking at prescribed angles). **External** locking systems utilize external supports (e.g. locking selected nodes at predefined states)

The key characteristics/parameters are summarized below:

- CONSTRAINT: rotational (angular limitation), translational (distance limitation)

- LOCK REF.: internal, external

3.1.2 Structural Scope of Analysis

The structural components described in section 3.1.1 allow manifold configurations that possibly suit a semi-compliant mechanism. However, the structural research of this work focusses on a narrow subset of those, that geometrically and structurally refer to strained gridshells and related research (see section 2.4).

In scope of this work are structures with the following characteristics:

- All grid structures are based on quadrilateral networks (section 2.1.3).

- All beam orientations align with the reference surface's normal (section 2.1.2).

- All beams are straight in an unstressed (undeformed) state.[1]

- All hinges are uniaxial and align with the reference surface's normal.

- All profiles are either compliant or rigid (not deformable) in bending/torsion.

- All beams with rigid axes follow corresponding zero-curvature paths (section 2.4.1).

Further restrictions, that relate to the transformation processes:

- Forces due to acceleration (inertial forces) are not part of this work. These are assumed to be very small (low accelerations).

- All transformations relate to homeomorphisms: The grids reference surfaces change shape only in curvature and area, not in topology (see 2.1.2 p.13).

---

[1] *An exception is given in section 3.4.1, the "Active Grillage" design of F. Justnes does include pre-curved members to tune the natural state of the structure.*

These limitations are furthermore summarized in Table 3, addressing the structural components, characteristics and parameters described in section 3.1.1.

Component	Parameter	Scope
SURFACE	TYPE	ruled, rotational, freeform
	CURVATURE	Gaussian curv.: zero, negative, positive, pos. and negative
	TOPOLOGY	one and two edge surfaces
NETWORK	REFERENCE	surface curvature (*Darboux*-Frame)
	CURVATURE	zero and variable curvature components (*Darboux*-Frame)
	TOPOLOGY	quadrilateral
BEAMS	ORIENTATION	network Alignment (*Darboux*-Frame)
	TWIST	
	COMPLIANCY	uni-, bi- and triaxial compliancy
	INIT. CURVATURE	zero (no initial curvature)
HINGES	DoF	rotational
	ORIENTATION	surface normal
	TOPOLOGY	(bilateral connections only)
SUPPORTS	CONSTRAINT	translational
	AXIAL REF.	global vectors
ACTUATION	ACT.REF.	internal, external
	DIRECTION	uni-, bidirectional
LOCKING	CONSTRAINT	translational (distance limitation)
	LOCK REF.	internal, external

Table 3 *Parameter Scope of Investigation (grey: Qualities that are not varying in this work)*

3.2 Transformation Analyses

Semi-compliant transformations involve both kinematic rotations or translations and compliant beam deformation. Among a large spectrum of possible structures and transformations, this section investigates selected structural systems using analytical methods and numerical simulation.

Section 3.2.1 treats purely kinematic rigid body transformations at unit cell, and grid level. Parts of this content is published by Schling et al., 2021.

Section 3.2.2 reveals and validates basic expectations on grid transformability of structures with restricted compliancy. Geometric characteristics are compared with the results of mechanical simulations.

Section 3.2.3 characterizes selected types of semi-compliant systems regarding their kinetic behavior. In this context, the curvature-square analysis is proposed. Parts of this content is published by Schikore et al., 2020.

3.2.1 Rigid-Body Transformation

This section investigates the two-dimensional kinematic transformation of quadrilateral, kite-shaped unit cells. In scope are translational relations that result from the cells shape and orientation in principal coordinate system (X,Y). The kinematic performances and orthogonal force relations of the unit cells relocate in entire grid structures. From this perspective, the intersection angles of quadrilateral grid structures define the normal force relations within the grid. In context to actuation, this angle acts like a gear box.

Unit Cell Kinematics
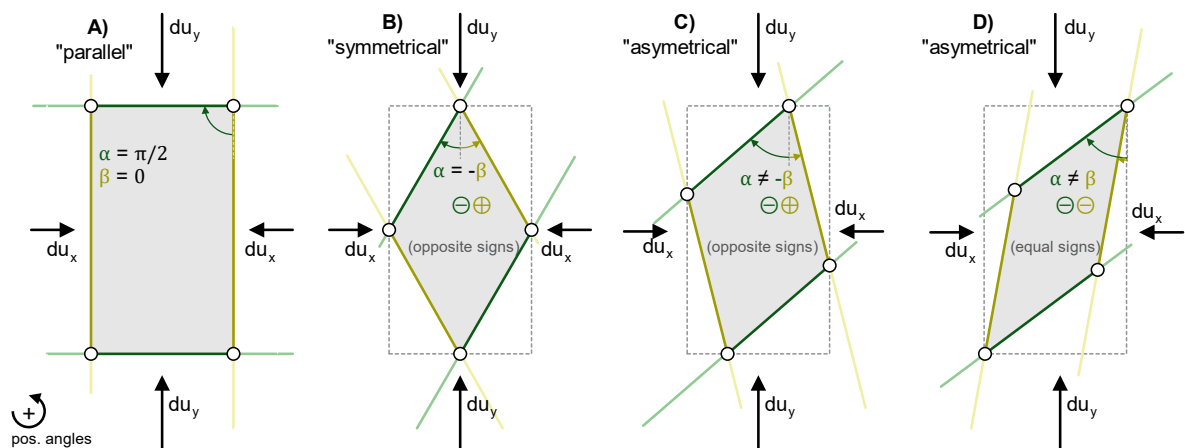
Figure 58 Four basic cases A,B,C and D of a quadrilateral unit cell regarding angular orientation towards the direction of actuation

Figure 58 shows four basic cases of unit cells (A, B, C and D) with varying intersection angles (corner angles) and orientations in a principal coordinate system. The parallel pairs of cell edges represent the smooth networks curve families (yellow and green). For a given displacement du_x, the orthogonal displacement du_y is derived from the initial setup, described by the angles between the respective cell edges (curve families) and the principal coordinate

axis Y. The edges in these basic setups are:

A) parallel to the principal axes.

B) symmetrical to the principal axes and the angles

C) asymmetrical with opposite angular signs (contrary directed).

D) asymmetrical with equal angular signs (equally directed).

With given angles between edge and principal axis α and β, the relation between infinitesimal translations in X and Y direction is given by:

$$d_{uy} = -\frac{\sin\beta}{\cos\alpha}\,d_{ux} \qquad\qquad \text{Equation 39}$$

Due to the angular sum in a quad, α and β are limited:

$$|\alpha| + |\beta| \leq 180° \qquad\qquad \text{Equation 40}$$

Based on Equation 39, the following relations result with respect to cases A-D:

A) The system is in equilibrium and does not move.

$$d_{uy} = 0 \,; d_{ux} = 0 \qquad\qquad \text{Equation 41}$$

with: $\alpha \leq {}^{\pi}/_{2}$ and $\beta = 0$

B) The relation in Equation 39 can be simplified by the tangent. The infinitesimal displacements d_{uy} and d_{ux} are always of opposite sign. Compression in Y-direction always leads to expansion in X-direction.

$$d_{uy} = \tan\alpha\,d_{ux} \text{ or } d_{uy} = -\tan\beta\,d_{ux} \qquad\qquad \text{Equation 42}$$

with: $\alpha = -\beta$

C) The infinitesimal displacements d_{uy} and d_{ux} are always of opposite sign. Compression in Y-direction always leads to expansion in X-direction.

D) The infinitesimal displacements d_{uy} and d_{ux} are always of equal sign. Expansion in Y-direction always leads to expansion in X-direction. The structure is "auxetic".

Grid Transformation

The kinematic relations shown for unit cells in the section above can be transferred to grids of straight members. Figure 59 shows grid layouts on a squared region with the geometric characteristics of cases A-D (see Figure 58). In a kinematic analysis these grids are transformed, applying a defined displacement in one principal axis (in Figure 59 the "vertical" axis). The grids are either compressed (red) or expanded (blue), if kinematically possible, and the transformed geometries are evaluated.
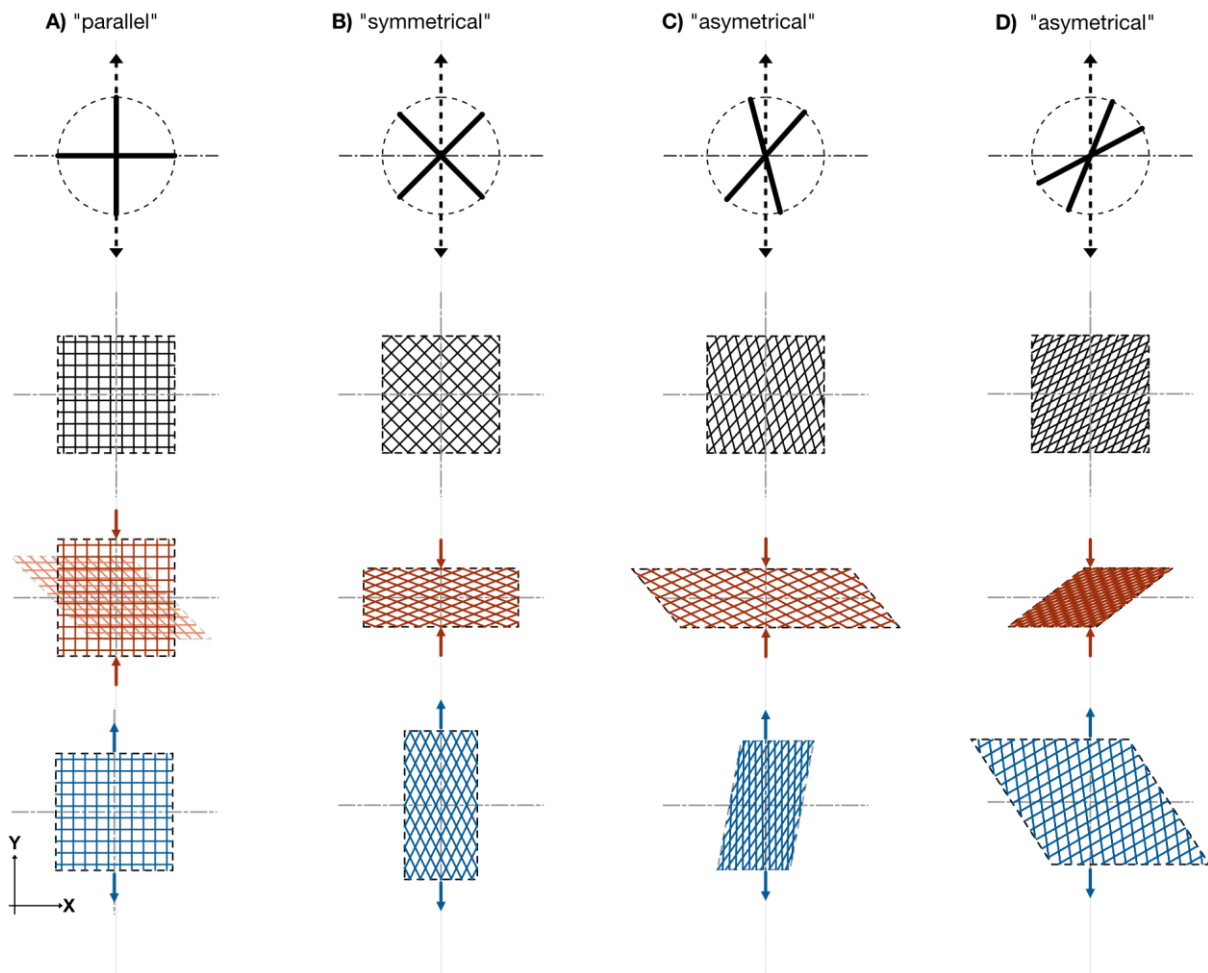
Figure 59 Kinematic transformation of a quadratic grid section. The grids are orientated towards the actuation direction according to four basic cases (see Figure 58)

The transformed grid regions show the following geometric characteristics:

A) The grid is in equilibrium. In this case, the grid is not expanding or compressed in X-direction. Expansion in Y-direction is not possible. However, compression in Y-direction is possible if the grid is shearing.

B) Compression in Y-direction leads to expansion in X-direction and vice versa. There is no shear.

C) If compressed in Y-direction, the grid expands in X-direction and vice versa. In addition, there is shear transformation.

D) The grid is either compressed or expanded in both directions, showing an auxetic behavior. Additionally, the grid is shearing.

These observations match with the unit cells kinematic behavior, as these represent a repetition of cells.

The kinematic relation also applies for static equilibrium. If the infinitesimal displacements d_{uy} and d_{ux} are replaced by forces F_y and F_x in a static system, the relation of forces results to:

$$F_y = -\frac{\sin\beta}{\cos\alpha}F_x$$

<div style="text-align: right">*Equation 43*</div>

65

Conclusion

The layout of grid structures defines the intersection angles. For quadrilateral grids, these angles are the decisive parameter for the kinematic performance. The unit cell can be used to describe the kinematic relations of lateral extension and contraction. This ratio is expressed by a simple equation (see Equation 39).

Four basic cell configurations are identified that that show distinct kinematic qualities regarding their lateral extension: Case A is in equilibrium and does not generate movement. Case B and C cause lateral extension. C and D include additional shear. Case D shows an unusual characteristic: The cell (or grid) shows an auxetic behavior (extension leads to lateral extension). These characteristics can be shown at the unit cell and at entire grid configurations (see Figure 59).

The kinematic relations directly express the static force relations within the grid, and thus influences the actuation and static performance. From this perspective, the intersection angle (the network layout) can be used as a design parameter.

Although these are purely kinematic relations, they are likely to exist also within compliant, curved configurations, that also (at least partly) perform through axial forces.

3.2.2 Semi-Compliant Transformation

This section investigates the spectrum of semi-compliant transformability. In scope are grid structures with restricted beam compliancy (see section 3.1.1 p.58). Non-compliant beam axes are assumed rigid, as their deformations are small and not part of the shape transformation. These grids include tri-, bi- or uniaxially compliant members, and their spectrum of morphology decreases in this order (e.g.: beams that are fully compliant have a larger spectrum of morphology than beams with only one compliant axis). The term morphology in this context describes all shapes that emerge within a transformation process.

Restrictions in axial compliancy create morphological subsets: The spectrum of uniaxially compliant morphologies is a subset of biaxially compliant morphologies, and biaxially compliant morphologies are a subset of triaxially morphologies.

Figure 60 Subsets in the morphological spectrum of semi-compliant grid structures with restricted compliancy

In the following analysis, a simple structural setup is chosen, and differing configurations of local compliancy are applied. The grid structure's transformations are simulated using selected nodal actuations or by eigenmode analyses, and the emerging curvatures are compared to geometric expectations.

This analysis aims to verify geometric expectations using mechanical simulations and to test the structures qualities to be actuated. Furthermore, it reveals the morphological spectrum.

Investigation Setup

The different levels and types of beam compliancy are numerically analyzed using a simple structural study-setup: A planar, squared, equilateral grid structure with four supports located in the middle of the grids' edges, that only allow central sliding. All connections are uniaxial hinges, with a rotational axis normal to the planar grid. The setup of supports is chosen to create an important characteristic: The system locks a kinematic collapse but allows a large spectrum of transformations. The simulated transformed morphologies are then compared to geometric expectations. Figure 61 shows the structural system.
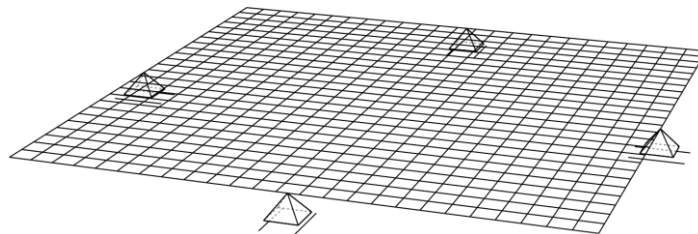
Figure 61 Structural system used for numerical investigations of tri-, bi- and uniaxially compliant morphologies

Triaxial Compliancy

If beams are fully compliant in bending and torsion, they can be deformed to match any smooth curve on a surface. Hence, grid structures of triaxial compliancy can be transformed into arbitrary smooth shapes. Such transformation is simulated by lifting five nodes of the above-described study-setup exemplarily. Figure 62 shows the actuation setup, transformed

structure, and Gaussian curvature of the transformed reference surface.
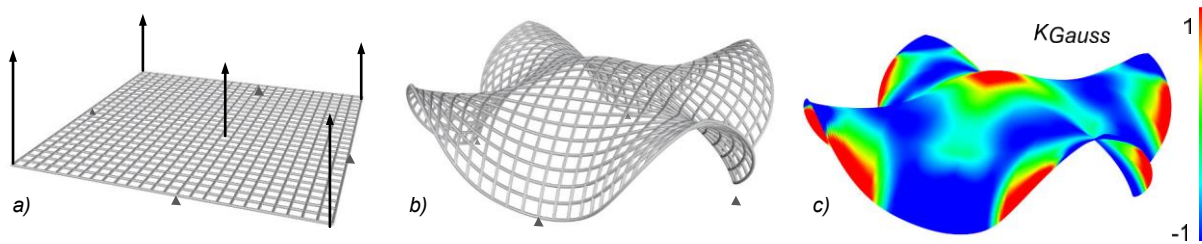
Figure 62 *Arbitrary transformation of a planar equilateral grid structure with triaxial beam compliancy: a) Structural setup, b) Transformed grid structure, c) Gaussian curvature of reference surface*

the Gaussian curvature of the reference surfaces is measured. The surface is colored using a normalized range from -1 (blue) to 1 (red). The transformed reference surface shows, that both anticlastic (negative) and synclastic (positive) curvatures result at different regions.

Note, this type of semi-compliant transformation is applied on various doubly curved strained gridshells, such as the Multihalle Mannheim (see chapter 2.4.6). In this case, the grid was pushed into a previously defined hanging shape, and locked when shaped as planned.

Biaxial Compliancy

The morphological spectrum is restricted, if only two beam axes are compliant: bending, and/or torsion. The study-setup is transformed into spatial by lifting two grid corners only.

There are fundamental geometric relations of smooth equilateral networks with zero curvature constraints and their reference surfaces (see section 2.4.1 and Schling, Hitrec, & Barthel, 2018). The following geometric expectations on transformability can be stated for three possible cases regarding biaxial compliancy:

A) Biaxial Bending: $EI_y; EI_z \ll EI_T$ (mechanically limited profile constraint)

A beam, without torsion, mapped and orientated on a smooth surface matches a principal curvature line. Any curve on a sphere has zero geodesic torsion, and equilateral networks on spheres exist. Any resulting spatial reference surface must be **spherical**.

B) Bending and torsion: $EI_T; EI_z \ll EI_y$ (e.g., "upright" lamella)

The "upright" lamella, mapped and orientated on a smooth surface matches an asymptotic curve. At any transformed state, the network of system curves must represent an asymptotic network, possible only on anticlastic surfaces. Furthermore, equilateral asymptotic networks exist on **pseudospheres** (const. neg. gaussian curvature), which must be the resulting spatial reference surface.

C) Bending and torsion: $EI_T; EI_y \ll EI_z$ (e.g., "flat" lamella)

The "flat" lamella, mapped and orientated on a smooth surface matches a geodesic curve. As only developable surfaces allow equilateral geodesic networks, the resulting reference surface must be **developable**. Note, this is only the case for the equilateral layout. The design spectrum of geodesic curves is high, and spatial, non-developable transformations are generally possible (see section 2.4.7).
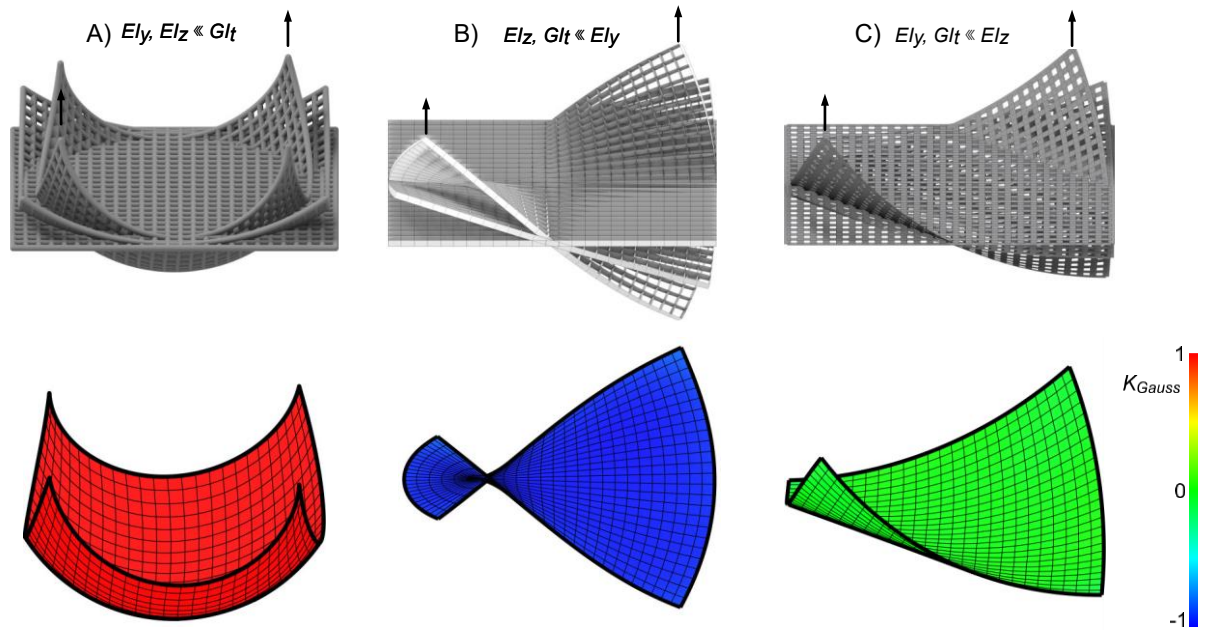
Figure 63 *Gaussian curvature analysis of deformed equilateral grids with varying local stiffness relations (Cases A, B and C)*

Figure 63 shows the transformations of all three cases. From the transformed grids, the reference surfaces are approximated (using the network of system curves) and validated to meet the geometric expectations above. For all cases, the Gaussian curvature of the reference surfaces is measured, providing a clear geometric verification:

A) The Gauss. curv. is constantly positive at all states. The morphology is spherical.

B) The Gauss. curv. is constantly negative at all states. The morphology is pseudospherical.

C) The Gauss. curv. is constantly zero at all states. The morphology is developable.

The geometric expectations are met, as structural transformability matches geometric constraints. These transformations were actuated by the displacement of two nodes only, affecting the entire structure in the presumed way.

Note, profiles with biaxial compliancy are not generally possible. Compliancy in bending and torsion can be easily accomplished by a lamella profile. However, a profile that bends but does not allow torsion are geometrically difficult.

Uniaxial Compliancy

The analysis of uniaxial compliancy is performed using an eigenmode analysis (instead of prescribed nodal deflections). This method is chosen, because these structures are expected to show low morphological freedom, and through the eigenmode analysis, these modes can be identified. Three cases are analyzed, and the following morphological expectations are stated:

A) Compliant bending in local y-direction: $EI_y \ll EI_z, GI_t$

   Any transformed grid and its related network (system-curves) must only show normal curvature and remain equilateral. Both conditions are satisfied only on cylindrical surfaces, a subset of developable surfaces.

B) Compliant bending in local z-direction: $EI_z \ll EI_y, GI_t$

There is no rotational freedom, either kinematic or compliant, that allows rotations out of the initial planar configuration. Any transformation must remain planar.

C) Compliant torsion in local x-direction: $GI_t \ll EI_y, EI_z$

There is no equilateral network known on a smooth surface, that consists of straight lines. Note, it does exist on a hyperbolic paraboloid and on a hyperboloid (non-equilateral).

Figure 64 shows the initial structural setups of case A, B and C and the first eigenmode of each case.

A) *EIy « GIt, EIz* **B)** *EIz « EIy, GIt* **C)** *GIt « EIy, EIz*

Setup:
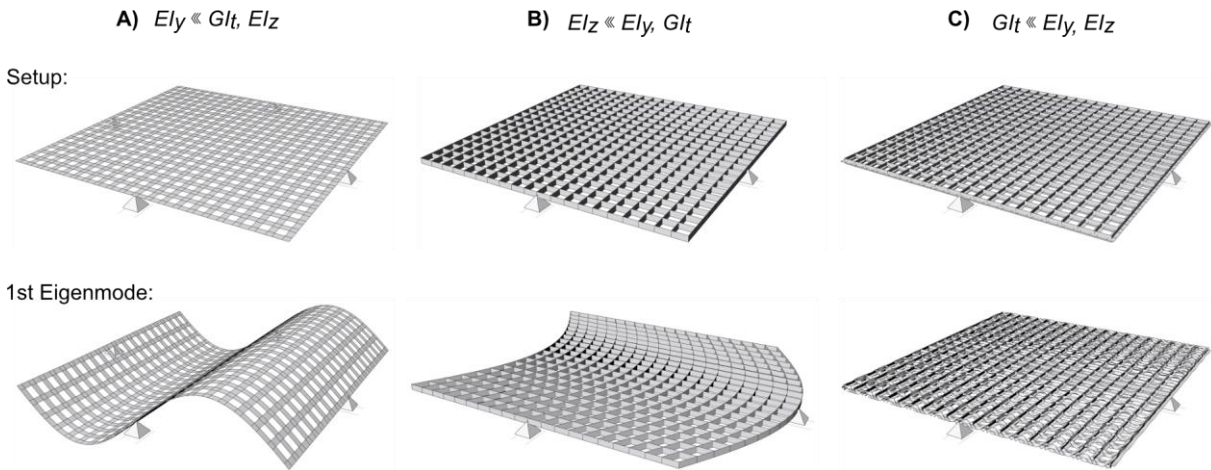
1st Eigenmode:

Figure 64 *Eigenmode analysis of uniaxially compliant planar, equilateral grid structures. The first Eigenmode (bottom) displays one possible "valid" transformation. Note: The beams are visualized as lamella or "cross" profiles, which do not represent the stiffness relations (especially the large torsional stiffness) of this study.*

The eigenmode analysis verifies the geometric expectations. Case A shows a cylindric (developable) surface in its first eigenmode. Case B shows a planar distortion. For case C, global transformability could not be found involving compliant torsion only.

However, a spatial configuration, that allows transformations for torsional only cases is well known: Grids of this quality must be based on the rulings either hyperbolic paraboloids or hyperboloids.

Hyperbolic Paraboloid   Hyperboloid
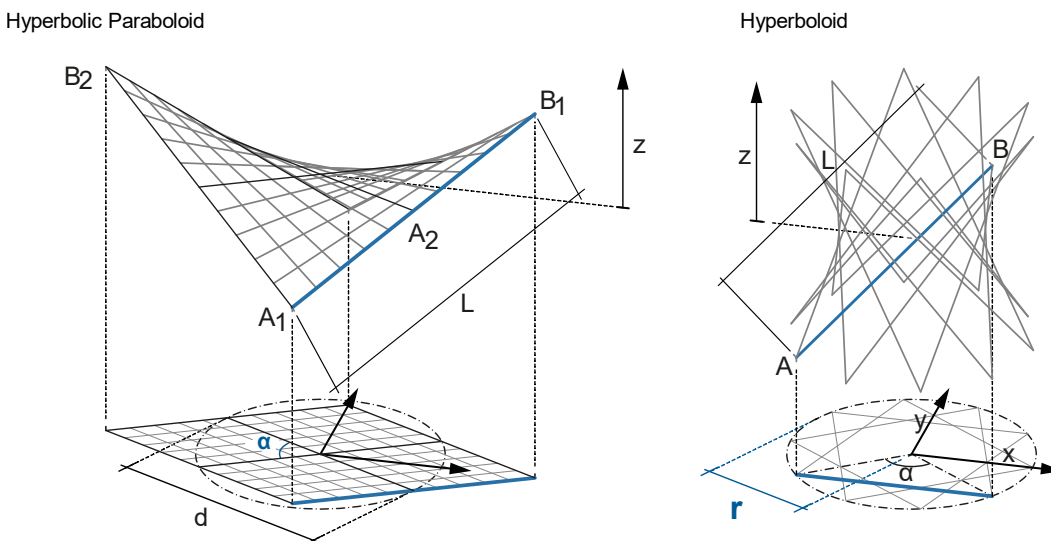
Figure 65 *Parametric model of a hyperbolic paraboloid and a hyperboloid. Any state can be parameterised by a single geometric parameter.*

If torsion is ignored, and joints are fully rotational, the transformability can be described using simple geometric approaches (Maden et al., 2015). Every transformation state can be referred to a single geometric parameter. One approach has been described by Thomas Oberbichler (Schikore et al., 2020), which is briefly described. Figure 65 shows the parametric model.

Every state of the hyperbolic paraboloid shaped grid can be referenced to the projected angle α. The four corner points are then given by the following formula:

$$A_{1,2} = \begin{bmatrix} 0 & \pm d \, \sin\left(\frac{\alpha}{2}\right) & \frac{1}{2}\sqrt{L^2 - d^2} \end{bmatrix} ; \; B_{1,2} = \begin{bmatrix} \mp d \, \cos\left(\frac{\alpha}{2}\right) & 0 & -\frac{1}{2}\sqrt{L^2 - d^2} \end{bmatrix} \qquad \textit{Equation 44}$$

Every state of the hyperboloid shaped grid can be referenced to the radius r. The end points of a single element are then given by the following formula:

$$A,B = \begin{bmatrix} \mp r \, \sin\alpha & r \, \cos\alpha & \mp\frac{1}{2}\sqrt{L^2 - 4\,r^2\,\sin^2\alpha} \end{bmatrix} \qquad \textit{Equation 45}$$

The network is then generated by rotationally copying and mirroring.

At any transformed state, the reference surfaces remain double ruled.

Considering a system with uniaxial hinges and compliant torsion, this torsion can be computed geometrically. Then, the profiles torsion (or orientation) is defined using the reference surfaces normal. This case is further part of the curvature-square analysis in section 3.2.3.

Note, profiles with uniaxial compliancy are geometrically difficult. The only reasonable type is compliancy in torsion, that can be generated by open, thin-walled profiles (e.g.: cross profile)

Conclusion

The geometric expectations for all semi-compliant equilateral grid structures are fulfilled. This verification underlines the suitability of geometrically derived assumptions on structural morphology, not only for selected states, but for entire transformations.

Triaxial compliancy enables a large spectrum of shapes. The geometric expectations on these are not constrained, and thus, specific design shapes cannot be induced by singular actuation. However, built examples have shown the potentials of full compliancy, at least for the erection of gridshells.

For grids with biaxially compliant members, the expected transformations could be initiated via singular actuations at two nodes only. This shows that local actuations can be transmitted within the structure to generate global effects, a key criterion for mechanisms in general.

Uniaxial compliancy enables limited morphology. On section level, uniaxial compliancy is hard to generate.

However, there is still a wide spectrum of global transformability. Exemplarily, transformations shown for uniaxial compliancy (see Figure 64) are also valid for biaxially compliant structures, as these represent a morphological subset.

Altogether, the cases of biaxial compliancy (B, C) and uniaxial compliancy (C) on doubly ruled surfaces show the greatest potentials in their abilities to be punctually actuated and regarding geometric feasibility at section level. These are further investigated (section 3.2.3).

3.2.3 Curvature-Square Analysis

This section introduces the integrated curvature-square value as an important quantity to evaluate and design semi-compliant mechanisms. Tracked throughout transformation, the curvature-square values give insight into internal energy balances (curvature-square graphs). The concept of this analysis and some basic examples are described in this section. The curvature-square analysis has been further used for the evaluation of various asymptotic structures by Schling & Schikore, 2022.

Mechanical Background

As shown in section 2.2.4, the curvature-square value is the geometric factor of the strain energy term, while the beam stiffness parameters $(EI_{y/z}, GI_t)$ represent mechanical factors. When a semi-compliant transformation is simulated, the integrated curvature-square value can be mapped throughout transformation, for each beam axis separately. The progression of curvature-square can be expressed as a function of transformed state, described by the parameter t. The internal strain energy, given by Equation 32 becomes then:

$$\Pi_{i(t)} = \frac{1}{2} GI_T \left(\int_c \kappa_x^2 \, ds \right)_{(t)} + \frac{1}{2} EI_y \left(\int_c \kappa_y^2 \, ds \right)_{(t)} + \frac{1}{2} EI_z \left(\int_c \kappa_z^2 \, ds \right)_{(t)} \qquad \text{Equation 46}$$

Each portion (colored in Equation 46) can be displayed in a curvature-square-graph, providing valuable insight into the internal strain energy progression. This analysis is particularly useful for profile dimensioning and to design the kinetic performance, if a basic condition is satisfied:

The geometric transformation in semi-compliant mechanisms must not depend on the stiffness ratios of the compliant beams' axes, and rigid beam axes do not cause significant strain energy.

In this regard, the semi-compliant system must be constrained accordingly, either by internal restrictions in compliancy, or by external constraints and supports. If this is not the case, and the curvature-square progression does depend on the beam's stiffness parameters, and dimensioning becomes a more iterative process.

Investigation Setup

In the following analysis, six exemplary semi-compliant structures are numerically simulated, and the curvature-square is tracked. The systematic selection of structural configurations used in this analysis is based on previously shown literature research, and morphological analysis (section 3.2.2). In scope are spatial configurations with restricted beam compliancy, realizable on profile level. These are torsional only (uniaxial) and torsional with bending (biaxial) profiles, represented by "cross"- and "lamella"-profiles respectively. Geometrically, these Grids are based on the following network types:

- Rulings (straight lines only on double ruled surfaces)

- Geodesic curves (on both syn- and anticlastic surface parts)

- Asymptotic curves (on anticlastic surfaces only)

Each network type is referenced to two surface topologies: open and rotational surfaces (see also section 2.1.2, p.13). Figure 66 gives an overview on the selected input networks and their categorization.
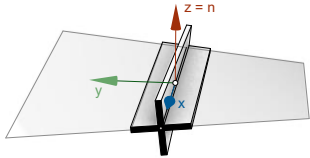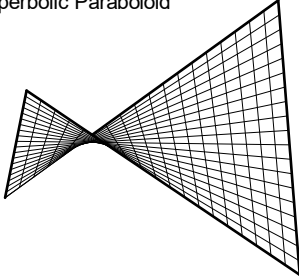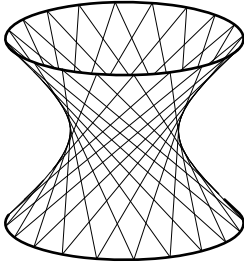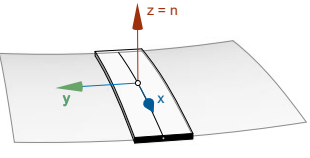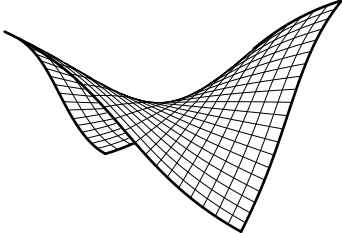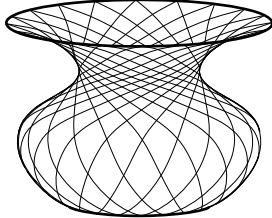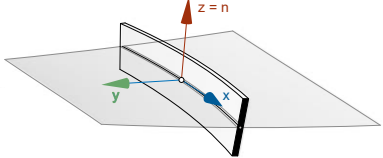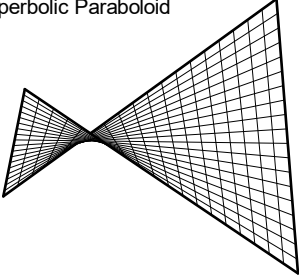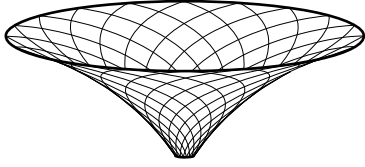
Type	Open	Rotational
Double ruled	Hyperbolic Paraboloid	Hyperboloid
Geodesic	Freeform (double symmetric)	Freeform (rotational symmetric)
Asymptotic	Hyperbolic Paraboloid	Freeform (rotational symmetric)

Figure 66 *Overview on basic semi-compliant grid setups.*

The transformation of each grid structure is simulated using external actuation of selected nodes (e.g. edge nodes, corner nodes). The actuation is path controlled. The dimensions drawn into Figure 67 and Figure 68 also mark the positions of actuation. All simulations are performed in the integrated parametric environment (*Rhino/Grasshopper* – see also 2.3.1).

Structures with biaxial compliancy (uniaxial bending + torsion) are simulated using the IGA-inverse method (see 2.3.2). The axial beam stiffness parameters are derived from a lamella type section with Poisson's ratio $v = 0$. The relation is set to:

EI_{Rigid} / $GI_{T,compliant}$ / $EI_{compliant}$ = 2500 / 2 / 1

Several transformed states, the actuated dimensions, and curvature-square graphs are displayed in Figure 67 and Figure 68. Possibly "natural" states (states of minimum strain energy) are marked blue. Note, that curvature-square graphs are normalized to reach 1,0 at maximum for each curve. This normalization is applied for a qualitative analysis of the kinetic performance.

Results and Observations

In the following, actuation, morphology, and kinetic transformation are briefly described for each simulation. The range of potential natural states is marked blue.

Open surfaces:

- **Double ruled (hyperbolic paraboloid):** The grid structure is based on the rulings of a hyperbolic paraboloid. The transformation is simulated using the geometric rules described in section 3.2.2, p.70. The total integrated curvature-square value is tracked in respect to the edge corner distance $d>0$. The geometric character of a hyperbolic paraboloid remains at any state.

  When the structure "folds" ($d \to 0$), the curvature-square increases, as torsion concentrates in the folding line. At $d = 0$, the curvature-square would be infinite. The state $d = 0$ also marks a geometric limitation, as the corner intersection angle becomes zero.

- **Geodesic disc:** The geodesic network is generated on a double symmetric freeform surface with both syn- and anticlastic regions. The transformation is numerically simulated applying prescribed displacements d at two internal nodes. The transformation is limited when first nodes show an intersection angle of zero.

  The grid performs a spatial, doubly curved transformation. Both bending and torsion find an energetic minimum at the same state, in which corner angles are equal. Consequently, the natural state cannot be manipulated by profile choice.

- **Asymptotic disc:** The grid structure is again based on the rulings of a hyperbolic paraboloid. The transformation is actuated by distance control between opposing grid corners. From the initial hyperbolic paraboloid shape, the distance is shortened to 40% or elongated until the grid becomes flat.

  The grid structure performs a spatial, doubly curved transformation with a purely anticlastic reference surface at any state. The minima of bending and torsion are at differing states. Consequently, the natural state of this structure can be manipulated by the choice of the beams' compliant stiffness parameters (ratio EI_z/GI_T).

Double ruled
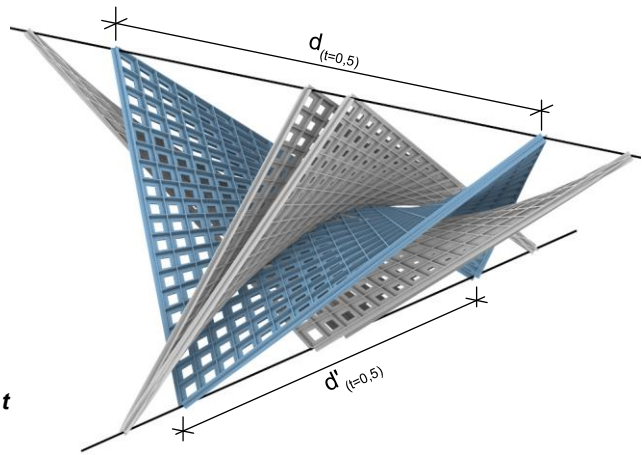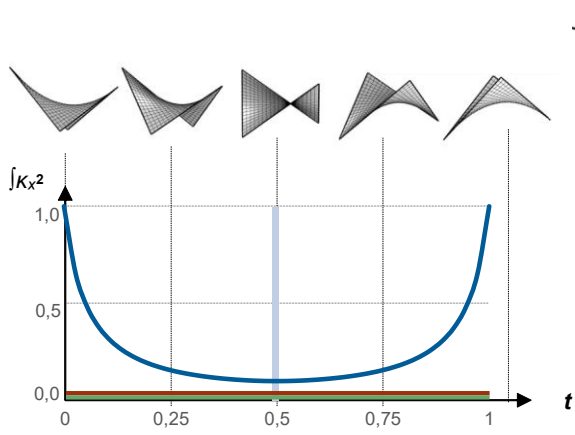
Geodesic
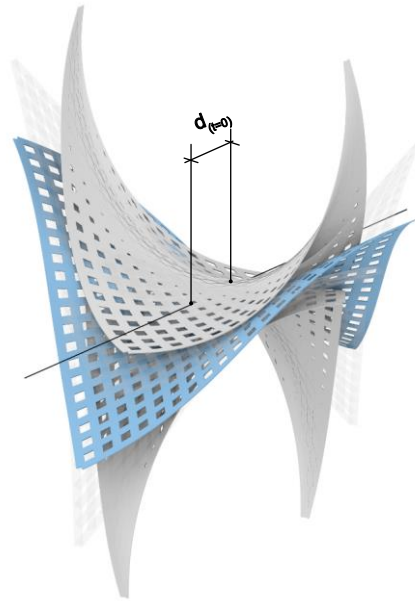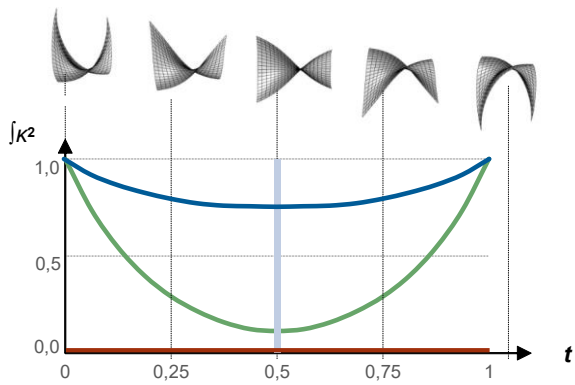
Asymptotic
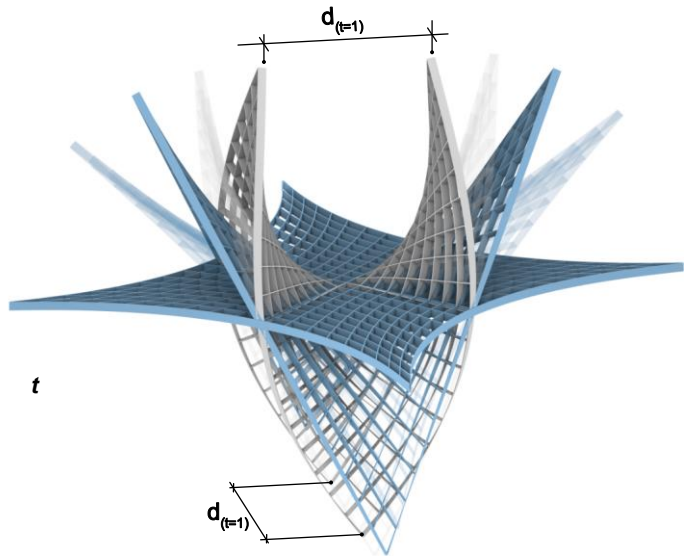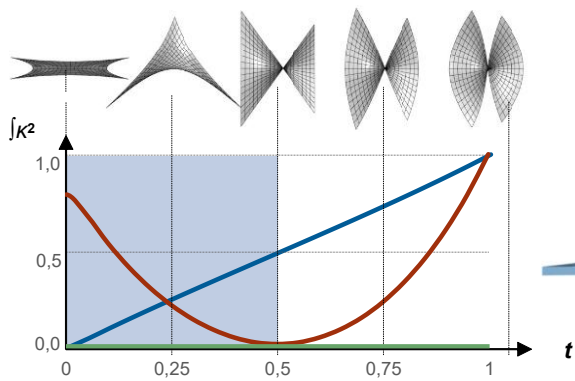
- $\int K_x{}^2$ (torsion)
- $\int K_y{}^2$ (bending)
- $\int K_z{}^2$ (bending)

Figure 67 *Curvature-square analysis on open surfaces*

Rotational surfaces: (All structures investigated here are rotationally symmetric)

- **Double ruled (Hyperboloid):** The grid structure is based on the rulings of a hyperboloid. The transformation is simulated using the geometric rules described in section 3.2.2, p.70. The total integrated curvature-square value is tracked in respect to the diameter $d > 0$. The geometry of a hyperboloid remains at any state.

  Again, when the structure "folds", the curvature-square increases, as torsion concentrates in the folding line. In a totally flat state, torsion would become infinite.

- **Geodesic:** The geodesic network is generated on a rotational symmetric surface with both syn- and anticlastic regions. A single geodesic was drawn from top to bottom and copied and mirrored rotationally. The transformation is numerically simulated applying prescribed diameter d of nodes located in the middle of the structure (black lines Figure 68). The transformation is limited when the first nodes show an intersection angle of zero.

  The grid performs a spatial, doubly curved transformation. The rotational symmetry remains. Both bending and torsion find an energy minimum at the linear, bundled state, and both are increasing when deployed. Consequently, the natural state of this structure cannot be manipulated by profile choice.

- **Asymptotic:** The reference network is generated on a rotational symmetric anticlastic surface. The distance between top and bottom edge nodes is controlled to actuate the transformation ($l_{Beam} > d \geq 0$). The bottom edge is fixed in location.

  The grid structure performs a spatial, doubly curved transformation with a purely anticlastic reference surface at any spatial state. The minima of bending and torsion are at differing states. Consequently, the natural state of this structure can be manipulated by the choice of the beams' compliant stiffness parameters (ratio EI_y/GI_t).

Note, all structures can be bundled into a linear state. For rotationally symmetric structures, this in line with the retractability requirement for scissor chains (Equation 37, p. 41).

Conclusion

The curvature-square analysis gives insight into the internal balance of strain energy portions and their progression. It reveals possibly "natural" states of minimum strain energy, and how profile stiffness ratios can influence the internal strain energy balance.

The "double ruled" structures have their strain energy minimum at bundled state (hyperboloid) or at $d = d'$ (hyperbolic paraboloid).

The natural state of structure with two compliant axes is potentially dependent of the compliant stiffness ratios. Some structures show an increase (or decrease) of both torsion and bending when transformed. Their natural state of equilibrium cannot be modified by tuning the compliant axes bending stiffnesses. Other structures show countering curvature-square graphs. Their natural state can be modified.

The curvature-square analysis can be used for beam dimensioning as part of an iterative engineering process (see section 4.1.4 p.120)

Double ruled
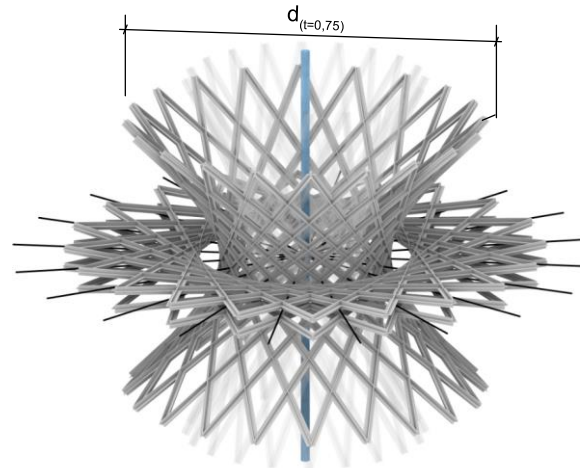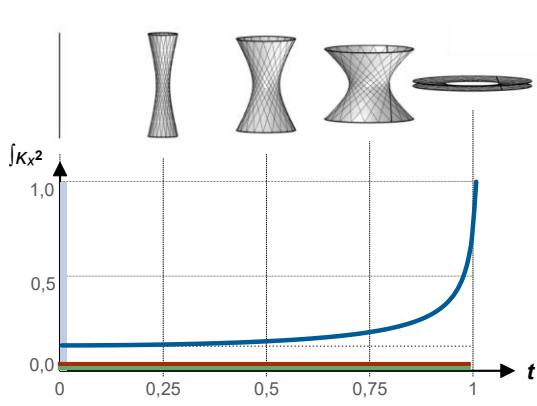
Geodesic
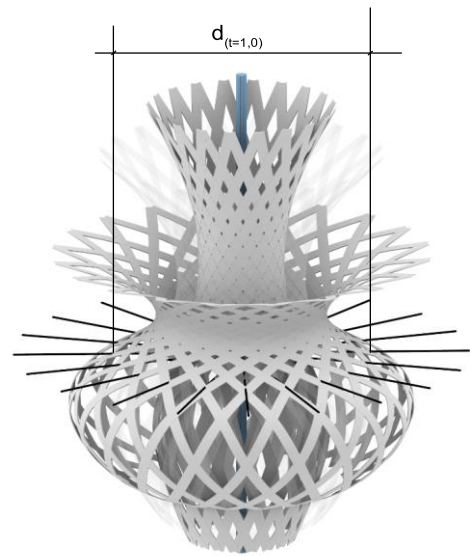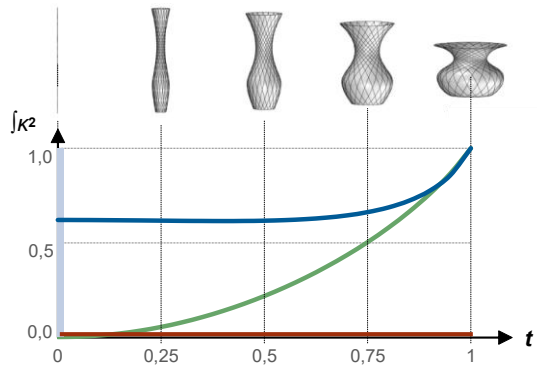
Asymptotic
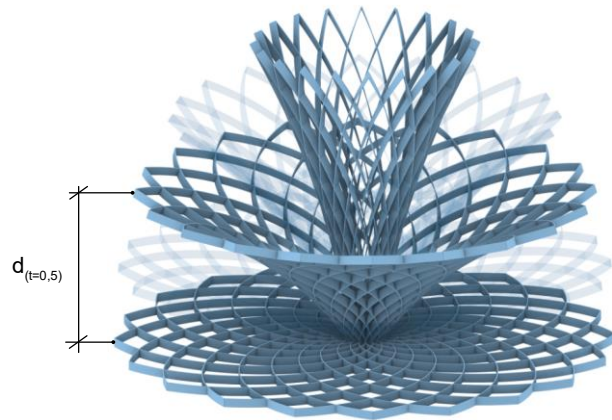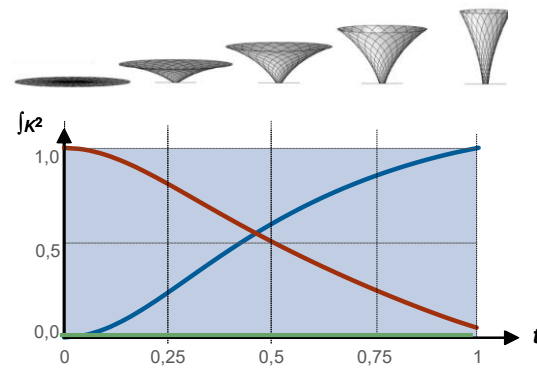
$\int K_x^2$ (torsion)
$\int K_y^2$ (bending)
$\int K_z^2$ (bending)

Figure 68 Curvature-square analysis on rotational surfaces

3.3 Static Analyses

This section addresses the static performance, that might be part of the transformation process, but rather relates to states of service, that potentially require higher load-bearing capacities. In this context, it is crucial to differentiate between stiffness that refers to the compliant function and stiffness referred to load-bearing. The former is discussed in section 3.2, the latter is addressed in this section.

The static analyses investigate global and local stiffness. Global stiffness (section 3.3.1) involves global buckling shapes, and local stiffness (section 3.3.2) addresses internodal buckling. These analyses aim at stiffness ratios, rather than at absolute results. Thus, findings have a qualitative character.

3.3.1 Global Stiffness

The global stiffness of a grid structure is influenced by all structural parameters listed in section 3.1.1. The scope of this investigation is narrowed down to asymptotic and geodesic grid structures with uniaxial hinges.

Strategies for locking or stiffening address internal constraints (e.g., locking node angles or bracing), or external constraints (support conditions). The question arises: Which strategies are suitable for either geodesic or asymptotic configurations? How effective are these strategies? The following investigation evaluates the stiffness of geodesic and asymptotic grid structures with varying in- and external constraints, using natural resonance as indicator.

Investigation Setup

A doubly ruled network of a hyperbolic paraboloid is used, and lamella profiles are applied in both "upright" and "flat" orientation. The resulting grids each represent a geodesic and asymptotic semi-compliant grid structure. The fact, that both grids are based on the same network, allows comparisons that exclude influences of the global shape or layout. The profiles orientation is the only differing parameter. The comparison covers three configurations: The grid structure is

A) supported at the full surrounding edges.

B) supported only at the corners. The edges are free.

C) supported only at the corners and braced. The edges are free.

The eigenmode analysis is a widespread method to evaluate structural stiffness. Eigenmodes reveal potential deformation shapes and dedicated eigenfrequencies represent a reference value to quantify the structural stiffness. This analysis is performed using conventional FEM[1]. The first three modes and frequencies are compared in quality and proportion. The average eigenfrequency of the first three modes is used as reference for comparison. Figure 69 shows the setup und detailed results.

---

[1] *The structural analysis software RFEM 5 and the plugin RF-DYNAM Pro with the "Lanczos"-Method are used. The lamella dimensions are t/h = 2/100 mm; Bracing: D = 8 mm (compression and tension) Material E = 21000 kN/cm² γ=78,5 kN/m³*

Results
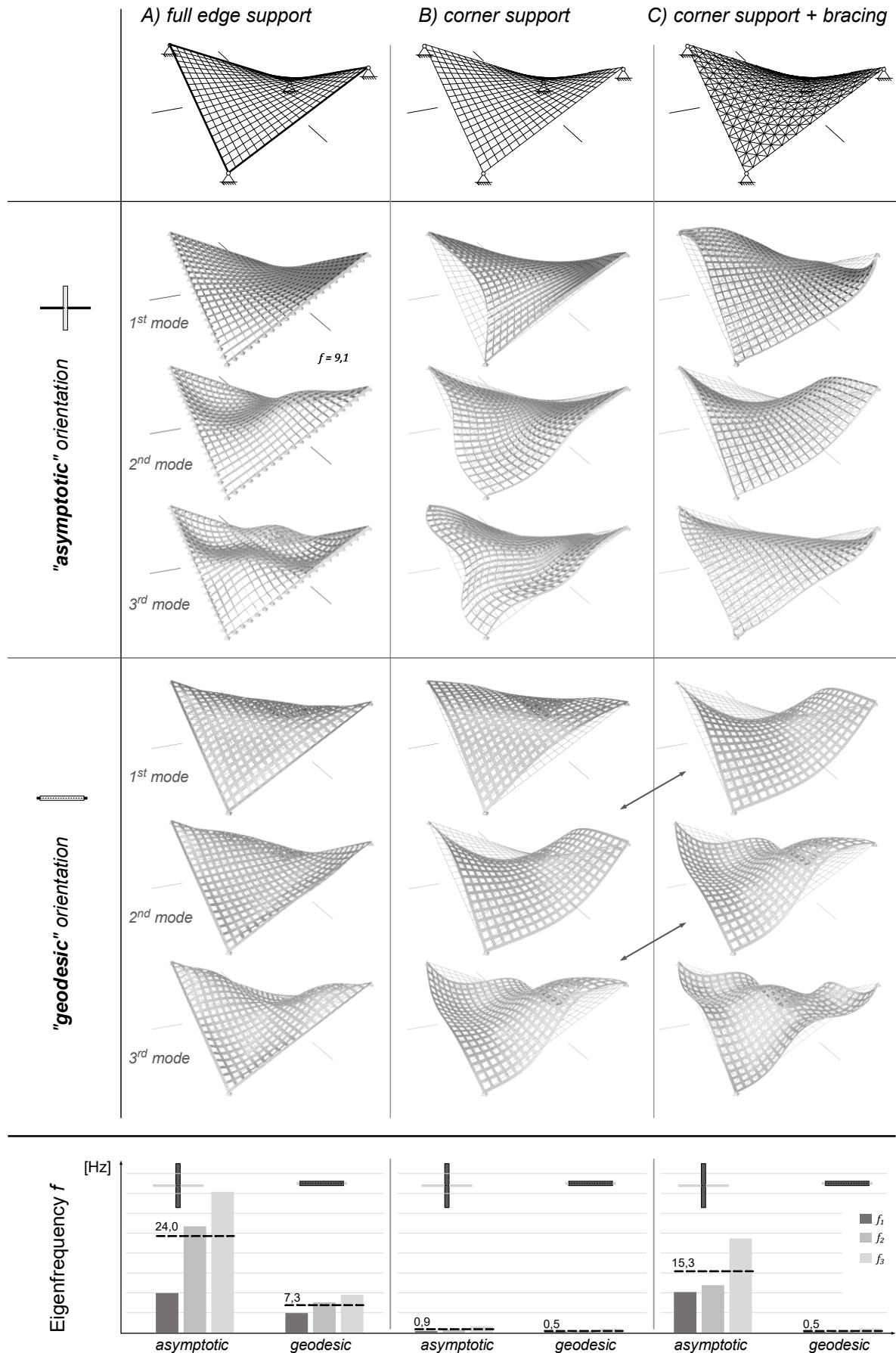
Figure 69 *Global natural eigenmodes and eigenfrequencies of a HP-grid structure with each asymptotic and geodesic beam orientation. Shown are the first three eigenmodes and -frequencies for different setups: A) Full support of grid edges (hinged), B) Supports only at corner points (hinges), and C) Supports as in case "C" with additional bracing.*

79

Observations

The following observations are pointed out:

A) Both the geodesic and the asymptotic configuration show eigenmodes "out of plane". Deflections largely occur in directions normal to the reference surface. The average eigenfrequency of the asymptotic configuration is about 3,3 times higher than the geodesic's frequency. The full edge supported configurations shows the highest frequencies in the overall comparison.

B) The deformations of the asymptotic configuration are predominantly "in plane" in all three modes and the geodesics are "out of plane". The average eigenfrequency of the asymptotic configuration is about 1,7 times higher than the geodesic's frequency. The corner supported configurations shows the lowest frequencies in the overall comparison.

C) The first three eigenmodes of the braced asymptotic configurations are divers. There is no clear "in"- or "out of plane" deformation observable. The geodesic configurations modes are clearly "out of plane" with shape analogies to configuration "b" (without bracing) and the eigenfrequencies of the braced und unbraced geodesic configurations are almost equal. The average eigenfrequency of the asymptotic modes is 28,6 times higher the geodesics frequency.

Conclusion

From those results, the following statements are indicated:

- Asymptotic configurations are globally stiffer compared to the equivalent geodesic configuration.

- Asymptotic configurations globally tend to deform "in plane" and geodesic configurations tend to deform "out of plane".

- Asymptotic configurations can be effectively stiffened using either external or internal constraints. For geodesic configurations, the potentials of stiffening are less, and internal constraints (bracing in this case) are almost non-effective. This can be explained by the fact, that a geodesic configuration already includes "in-plane" stiffness (compared to the asymptotic orientation), and internal constraints in a grid structure have primary effects on the "in-plane" stiffness.

In general, the global stiffness also indicates global stability. In this context, the eigenfrequencies indicate resistance in terms of global stability phenomena and the natural eigenmodes indicate buckling modes.

3.3.2 Local Stiffness

The stiffness and non-linearity of initially bent gid members are affected by various local parameters: curvature, internodal spacing, beam stiffness and residual stress. Under compression, stability phenomena are likely, and the elastically curved members can be characterized as "post-buckled" (see section 2.2.7). This problem is highly non-linear and involves various states of ambiguity (stability problems). Numerical analysis, preferably of 3rd order are suitable to handle this problem. Figure 70 shows selected local deformations at the *Inside/Out* research pavilion, both in 3rd order simulation and in reality.
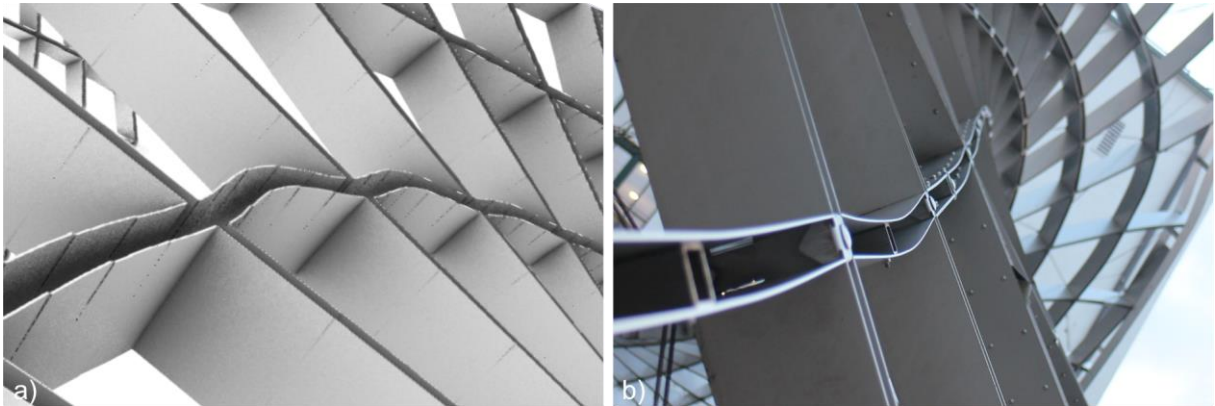
Figure 70 *Local deformations of the Inside\Out Pavilion: a) FEM 3rd order numerical simulation results scaled 10x, b) Deformation on built structure*

The question arises: Is it possible to generalize the local buckling performance using local parameters such as curvature and internodal spacing (grid density)? If answered, this may allow early dimensioning of profile and grid density for practical engineering. And furthermore: How does curvature in context with internodal spacing and prestress affect the non-linear performance and to what extend does the critical "Euler"-load refer to curved configurations?

The following investigation aims at local phenomena regarding load-displacement progression and deformation modes. The local situation is abstracted by a single compressed, cuved, multispan beam and systematically investigated using varying parameters.

Investigation Setup

In this investigation, curved grid members under compression are simulated, and the deformation and the load-displacement progression are tracked (analogous to section 2.2.7, p.29). Abstracted, 2D systems are used to represent single grid members. A set of five beams with varying curvature is chosen. These are punctually supported orthogonal to its axis. Figure 71 displays the abstractions with different constant radii and internodal spacing and gives an overview on all simulated configurations. These structural systems represent any type of compliant member, either asymptotic, geodesic, freeform, or others, that include curvature.

The assessment is carried out using numerical simulations[1]. Supports are applied according to Figure 71, but fixed at one end, the other end is loaded axially. These setups are considered for two cases each: Bent into curvature (initially stressed), or initially curved (unstressed).

---

[1] *For this investigation, IGA is used according to chapter 2.3.2.*
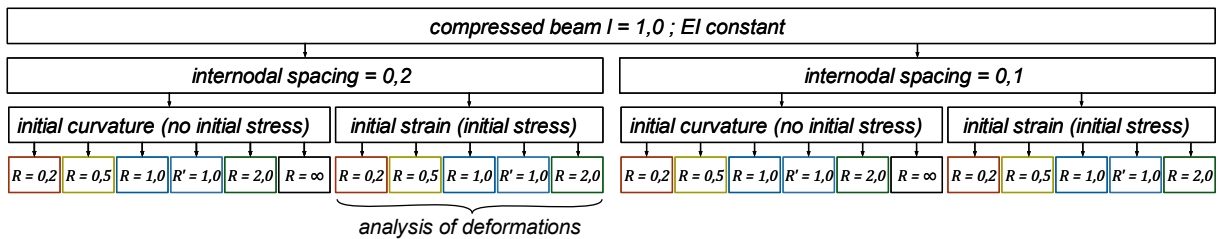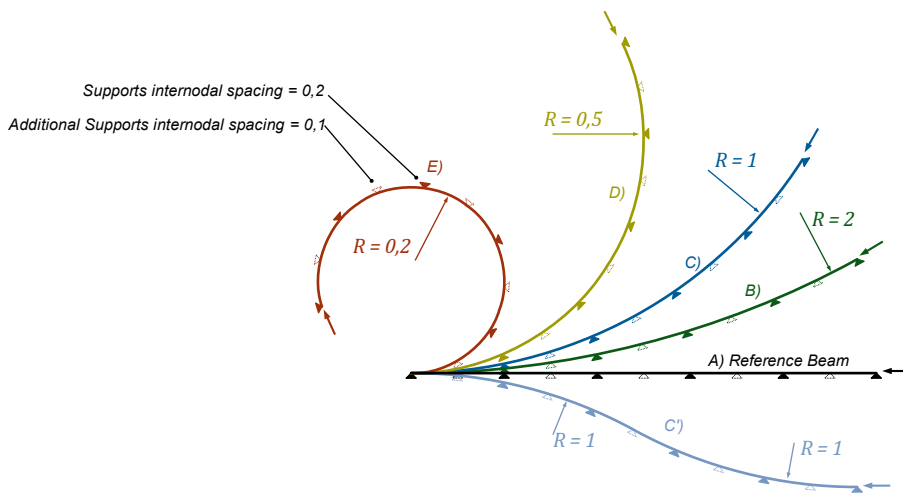
Figure 71 *Schematic overview of the analyzed structural systems (cases) and parameters*

This investigation aims at ratios and qualitative findings. The following numbers describe the setup and proportions:

Total length: $l = 1$

No. of spans: $n = 5\ (10)$

Internodal spacing: $l_i = 0,2\ (0,1)$

Radii: $R_{E)} = 0,2\ ; R_{D)} = 0,5;\ R_{C)C')} = 1,0\ ; R_{B)} = 2,0;\ R_{A)reference} = \infty$

In a second set, the internodal spacing is halved (the number of spans/supports is doubled). Note, configuration c' shows a variation in which the beams curvature is switched in the middle.

The systems are loaded via prescribed tangential displacement of $u = 0,05$ at the beams ends. Deformation and force are tracked along this progressive displacement.

Figure 72 displays the deformations of the initially stressed beams with internodal spacing $l_i = 0,2$. In Figure 73, the load-displacement graphs of all configurations are graphed.

Straight configurations serve as references (see Figure 72 case A). The first three deformation modes and critical loads are assessed via an eigenmode-analysis[1]. The first eigenmode refers to a buckling length equal to the internodal spacing (antimetric waved mode) and to the corresponding critical "Euler"-load $F_{crit.1st,\ li=0,2}$ (see Equation 35 in section 2.2.6). The buckling modes and critical loads of the straight reference setup are displayed within the diagram in Figure 73. The first "Euler"-load of the reference beam with halved internodal spacing results to:

$$F_{crit.1st,\ li=0,1} = 4\ F_{crit.1st,\ li=0,2}$$

<div align="right">

Equation 47

</div>

---

[1] *The eigenmode-analysis is performed using IGA (KIWI)*

Results

A) Reference system

1st buckling mode
2nd buckling mode
3rd buckling mode

l = 1

B)

R = 2

snap through 3rd to 1st mode

C')

arch turning point

R = 1

R' = 1

C)

snap through 2nd to 1st mode

D)

R = 0,5

R = 1

E)

R = 0,2
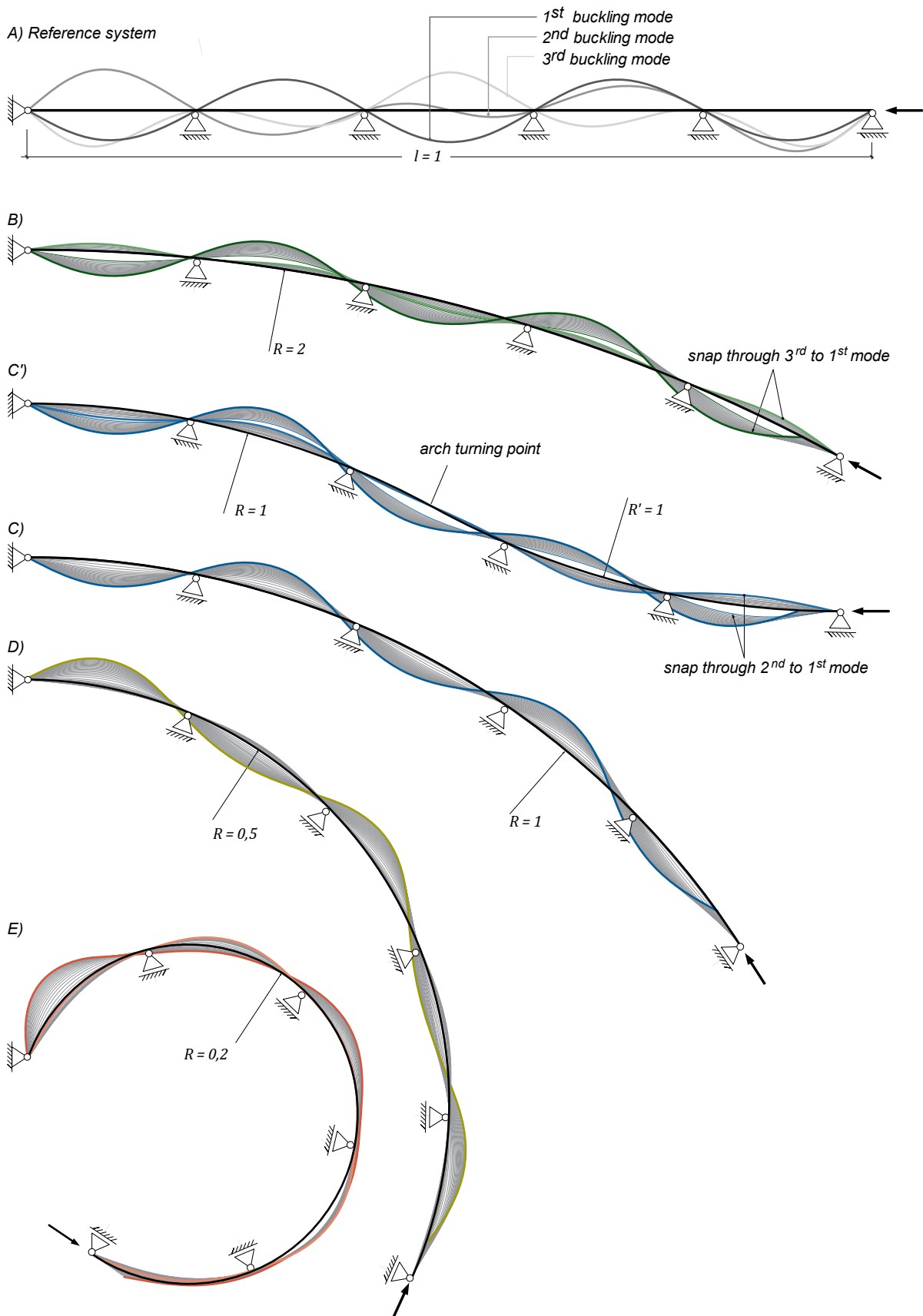
Figure 72 *Deformation of constantly curved beams under compression. All beams are of same length "l" with 5 perpendicular regular spaced supports. The cases differ in curvature: A) Straight Beam (Reference Beam) with 1st, 2nd and 3rd buckling modes, B-E) Varying Radii: 2 / 1 / 0,5 / 0,2 , C') Radius 1 with changing curvature direction at the beams middle point*

Observations

The simulation results provide the following characteristics[1]:

B) **[R=2,0]** The deformations of the stressed configuration show two modes. In the beginning, the deformation relates to the 3rd, and later to the 1st buckling mode of the reference system. Again, this matches with the load-displacement graphs, as they converge to related critical loads respectively.

C) **[R=1,0]** The performance shows qualitative similarities to case "D", but the stiffness until the critical reference load is reached is higher. Differently, the graphs show discontinuities especially in case of smaller internodal spacing $l_i = 0,1$. The stressed configuration with $l_i = 0,2$ converges almost exactly to the critical reference load. With $l_i = 0,1$, there is a slight increase of force after $F_{crit.1st}$ is reached.

C') **[R=1,0]** This variation of case "C" includes a switch in curvature direction. The deformations of the stressed configuration relate to the 2nd reference buckling mode in the beginning, and to the 1st eigenmode in the later progression of displacement. This change in mode matches with the convergency to the 2nd critical reference load, the discontinuity, and an ongoing convergency to the 1st critical load. The unstressed variation performs smooth without any discontinuities. Within the 1st mode (in the later progression of the displacement), case "C'" performs almost equivalent to case "C".

D) **[R=0,5]** The beams deformation mode matches the first buckling mode of the reference beam (antimetric waved mode). Both initially stressed and unstressed versions converge to the reference load but decline slightly compared to the previous radius applied, after turning points are reached. The stiffness is higher than observed for the smaller radius in case "E". The unstressed version converges smoothly, while the stressed version shows a rather sharp kink when the critical reference load is reached. The configuration with halved internodal spacing performs qualitatively analogous.

E) **[R=0,2]** The beam bulges in all spans into outside direction of the circular setup. This deformation does not match any of the first three reference buckling modes displayed in Figure 72 case "A". The force applied increases until a turning point is reached at $F \sim 0,7 F_{crit.1st, \ li=0,2}$. The unstressed version performs similar, but force reaches only $F \sim 0,45 F_{crit.1st, \ li=0,2}$, at larger displacement, providing less stiffness (gradient of the load-displacement graph). The configuration with halved internodal spacing performs qualitatively analogous, but the forces of both initially stressed and unstressed versions are closer to the reference buckling loads.

---

[1] *The deformation shapes are evaluated only for the initially stressed set with internodal spacing $l_i = 0,2$.*
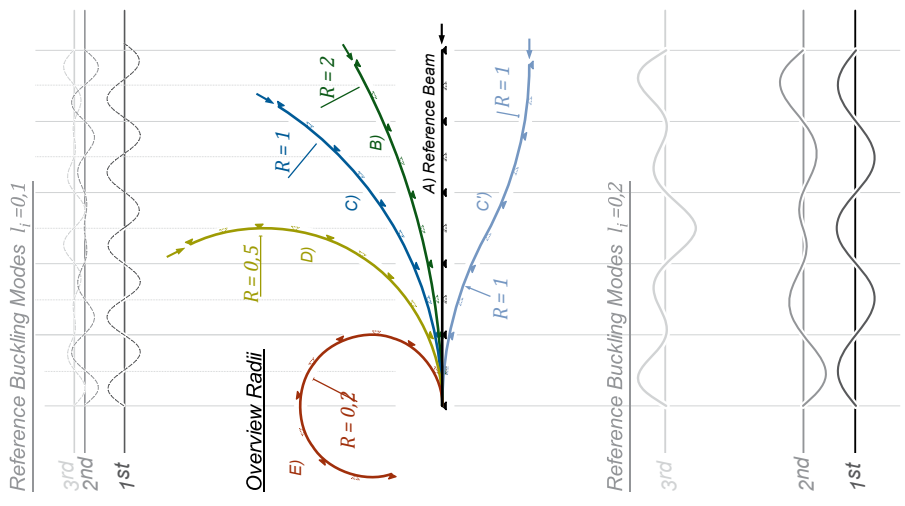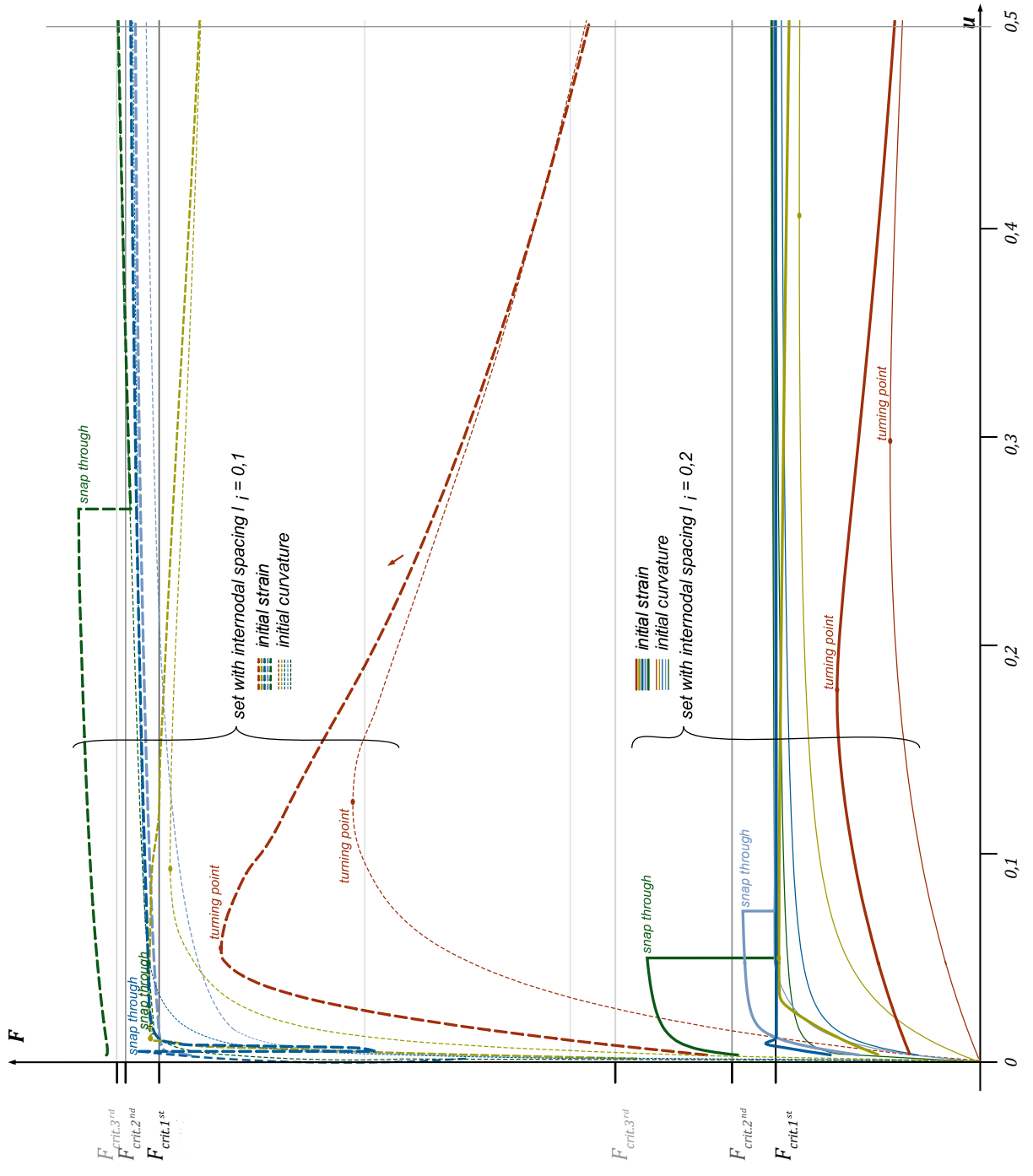
Figure 73 *Load-displacement graphs of multispan beams varying in curvature, init. stress and internodal spacing, and the critical loads and modes of a straight multispan reference beam.*

Conclusion

The observations above, lead to the following generalized statements for curved members under compression:

- Elastically bent members are stiffer than initially unstressed curved members. This is presumably due to stress stiffening effects (see section 2.2.5).

- There are stability problems that involve both critical load problems and snap through phenomena (see section 2.2.6).

- Initially unstressed curved members show less discontinuities and appear smoother in their load-displacement behavior. So far, there is no clear explanation for this phenomenon.

- Curvature does not necessarily decrease the member's critical load. There is a range in curvature, in which load capacities are equal to the critical loads of straight members. When a certain curvature limit is exceeded, the members do not reach that critical load. This phenomenon appears regardless of internodal spacing.

- The buckling modes of straight multispan beams can be allocated to deformation modes of curved beams. This also applies to the related critical loads. In some cases, curved members deform into modes of higher order and thus allow higher loads than the first critical loads. However, such states are ambiguous. Snap through effects between those modes are likely.

- The critical "Euler"-load with a buckling length equal to the internodal span provides a reasonable magnitude to approximate the curved members load capacity:

$$F_{crit.} \sim \frac{EI\pi^2}{l_i^2}$$

<div align="right">Equation 48</div>

However, this simplification is limited to lower curvatures. Further research is required to identify those limitations precisely.

- With respect to the relevance of the "Euler"-load as reference, the internodal spacing, and indirectly the density of a grid has a nearby quadratic impact on load-bearing capacities.

3.4 Physical Model Studies

This section investigates the results of an architectural design studio of master students conducted in 2019 at the Chair of Structural Design (Prof. Rainer Barthel) and supervised by Jonas Schikore. This studio interconnected teaching and research.

The task was to create an architectural idea and a mechanical concept for a compliant grid structure, that had to be implemented in a medium scale model (~ 1,5 mx1,5 m). The structural concepts are inspired by literature review (see section 2.4). All profiles used are biaxially compliant (uniaxial bending and torsion, see section 3.1.1, p.57).

In the following sections, four designs are analyzed and discussed regarding geometry, morphology, and mechanical concept and performance. These analyses systematically cover the components used (section 3.1.1): Surface, Network, Beams, Hinges, Supports, Actuation and Locking. In section 3.4.5, the analyzed designs are systematically compared and evaluated.
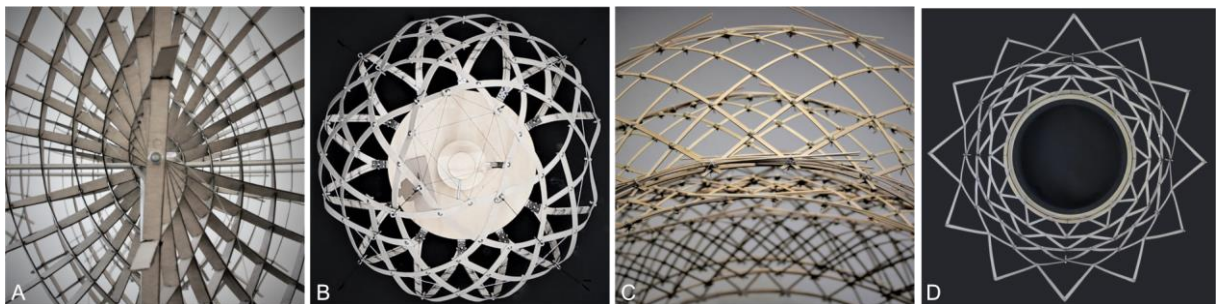
Figure 74 Overview on four selected design studies (Photos by student designers)

Figure 74 shows the four selected designs (A-D), that are shortly introduced below:

A - Asymptotic Discs: The *Active Grillage* by Fredrik Justnes is based on an asymptotic network on a disc surface. (Section 3.4.1)

B - Rotational Geodesics: The *Blooming Flower* by Chiara Saccomanno and Noemi Thierens is based on a geodesic network on a rotational surface. (Section 3.4.2)

C - Deployable Strips: The *Sail* by Barbara van Waarden is based on a geodesic network on a partly developable free-form surface. (Section 3.4.3)

D - Scissor Dome: The *EXX-Dome* by Alberto Ortensi combines compliant deformation and scissor chains. (Section 3.4.4)

All models are geometrically planned and designed using digital design tools such as Rhino/Grasshopper (see section 2.3.1), and the physical implementation utilized digitally referred fabrication techniques, such as laser cutting and 3D-printing (see section 2.3.3). These methods and tools allowed to handle complex geometries from planning to fabrication.

3.4.1 A - Asymptotic Discs
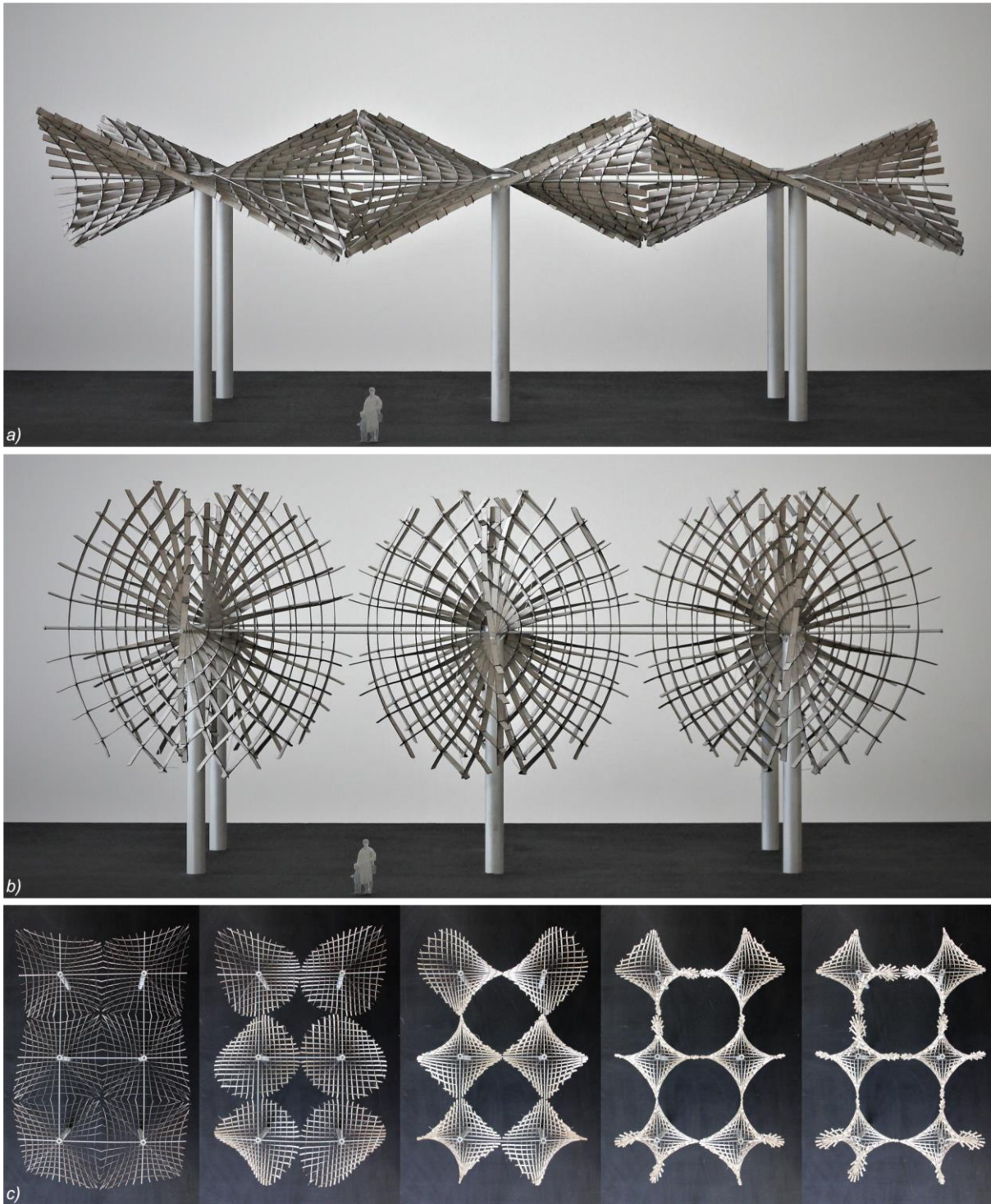
Figure 75 *The "Active Grillage" is an asymptotic grid structure with pre-curved lamellas. The structure is actuated from nearby flat into spatial using cables: a) "Closed" state, b) "Open" state, c) Top view progression of transformation, (Design and Photo: Fredrik Justnes)*

This design aims architecturally on a deployable roof structure, that allows additive modular extension. The structure consists of six equal asymptotic grid modules, each based on an Enneper surface. The mechanical goal is the transformation from a nearby flat into a spatial state.

The project was honored at the *Stuttgarter Leichtbau Preis* in 2019.

Geometry and Morphology

The initial design shape is an Enneper surface, representing an "open" state, and the asymptotic network is derived from this surface. The use of this surface type for an asymptotic lamella structure has been described by Schling et al., 2017. The Enneper surface used is a minimal surface and double symmetric. Figure 76 shows the design process from surface to grid.

From the Enneper shaped grid (Figure 76b)., a near-by flat state that has been numerically derived[1]. The network is cut at all edges to create a planar edge at closed state (Figure 76c). This allows a closed repetition of modules, a valuable quality for transformable roof structures. The network includes two central asymptotic curves that remain straight and only involve torsion (marked green in Figure 76). Figure 76d and e show the cut grid at "closed" and "open" states.

── Actuation Cable
── Support Structure
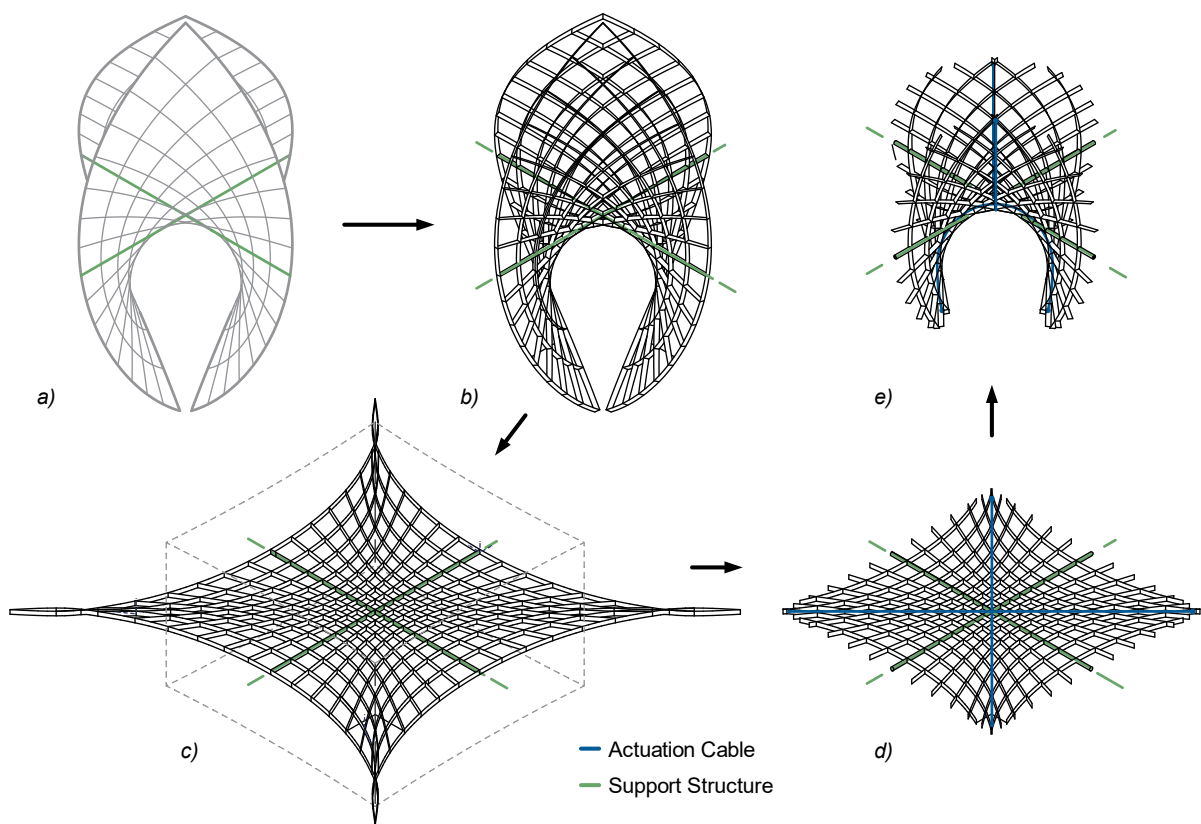
Figure 76 Design process: a) Design of an Enneper surface and asymptotic network. b) Implementation of lamella profiles in asymptotic curve network, c) Flattening of grid structure into "closed" state using simplified simulations (Grasshopper/Kangaroo), and cutting grid using a cube volume, d) Cut grid at flat (closed) state, e) Cut grid at spatial (open) state (Illustration based on Fredrik Justnes 2019)

Mechanical Components and Performance

The "upright" lamella profiles allow biaxial compliancy in bending and torsion, that relates to section 3.2.2 case "B". To manipulate the natural state of the structure, all beams include constant initial curvature in their compliant bending axis (z-axis). This initial curvature promotes a flat natural state, which simplifies the actuation system to perform unidirectional.

---

[1] In this design, the numerical simulation tool Grasshopper/Kangaroo has been used flatten the grid.
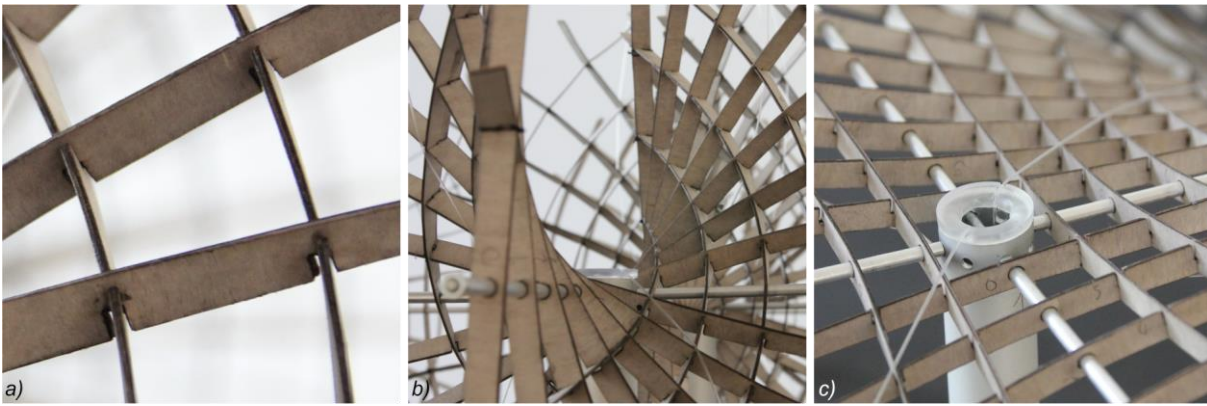
Figure 77 *Details of the Active Grillage model: a) Hinge connection using slots, b) Supporting metal tube c) Actuation cables at central pole. (Design and Photo: Fredrik Justnes)*

The rotational freedom at the hinges is implemented using slots that are laser cut at node locations. The lamellas are interlocking in one grid layer. This connection leads to collision when intersection angles are close to 0° or 180°. Tolerances in the slots extend the rotational range. Figure 77a shows the slotted connection.

Each module is supported at two straight metal pipes that span horizontally and orthogonal. The tubes are placed on the central lines that are geometrically part of the network (marked green in Figure 76, Figure 77b). The compliant grid rotates on these rigid tubes that represent the primary structure.

Actuation and Locking

When the squared grid module transforms, two edges move up, and two move downwards. This mechanism is actuated via four cables for each module, running from the center to the grid's corners. The cables follow the grid diagonally. One pair of cables in attached above the grid, and another below, according to the grid's curvature outside. Hereby the tensioned cable remains in contact with the grid structure. Figure 77c shows the actuation cables running along the grid.
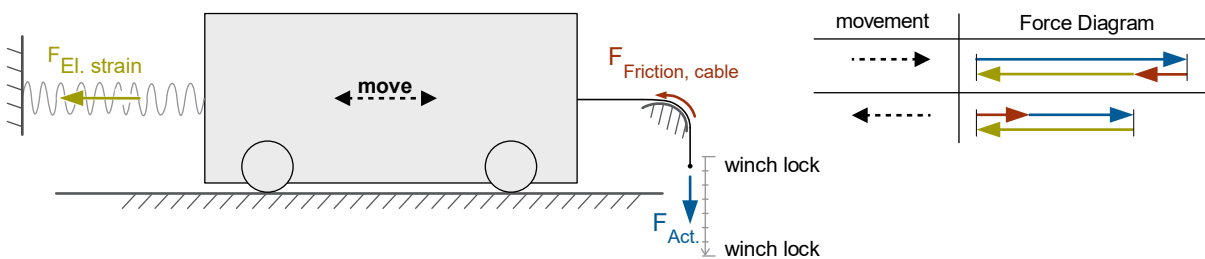
Figure 78 *Schematic mechanical model of the "Active Grillage" including relevant forces and equilibrium*

During transformation, the structural mass of the grid is partly lifted and lowered in a balancing ratio. The center of gravity remains at constant height, and thus, no potential energy must be induced. The internal strain energy pushes the structure in its natural, horizontal state. This is the dominant force in this system. For actuation, friction at cable guidance must be overcome. The actuation cable also inherits the function of mechanic locking, staying in tension at every state. Figure 78 shows a schematic, mechanical model of the structure's transformation and a qualitative force diagram as defined in section 3.1.1.

3.4.2 B - Rotational Geodesics

Figure 79 *The Blooming Flower, a geodesic rotational grid structure: a) Open (bulgy) state – side and top view, b) Closed (slender) state, c) Details at support, locking cable (white) and supporting elastic actuation cables (black) (Photo: C. Saccomanno, N. Thierens)*

The *Blooming Flower* is a synclastic geodesic grid structure that transforms from a slender into a bulgy shaped space. The architectural idea is a transformable space that provides volume whenever used.

Geometry and Morphology

The morphological concept goes back to the geometric deformability of geodesic rotational networks, described by S. Finsterwalder (see section 2.4.7 p. 49, Table 1, column B). However, the meridian curve family in this design is left out. Quadrilateral networks of this kind are generated through copying geodesic curves on a rotational surface around its rotational axis.

The geodesic network layout owns an important characteristic: The initial surface marks the closed state, and the grid requires mechanical capacities to expand and increase its radius to create volume. If the geodesics are nearby horizontal in the closed state, the radial expansion is almost at its limit. Hence, the geodesics are orientated nearby vertical at the closed, initial design state, to allow radial expansion.

Mechanical Components and Performance

The "flat" lamella profiles allow biaxial compliancy in bending and torsion, that relates to section 3.2.2 case "C", and to the structure investigated in the curvature-square analysis (section 3.2.3). The lamellas are made of straight timber strips, perforated at nodes to implement simple scissor hinges using bolted connections. The lateral (double layered) configuration allows theoretically infinite rotation (see section 4.1.4, p.113).

The grid structure is supported at the bottom node row with biaxial rotational hinges (Figure 79c). This configuration of rotational axes at supports ensures the orientation of the lamellas to remain normal to the reference surface but allows scissor like kinematics and adaption to other rotational symmetric states of transformation. However, the support row does not allow changes in base radius and thereby conflicts with necessary freedom in transformation, as demonstrated in the testing model shown in Figure 81.

The transformed, "open" state (Figure 79b) shows the expected increase in radius and volume. However, the bottom part shows concentrated curvature at the first node row (from bottom). This discontinuity is supposed to be an effect of locally increased beam stiffness at bottom part and the locking of the base radius.

Actuation and Locking

The mechanism is actuated using four cables following the rhombi's diagonals, in meridian direction. A circular cable net is highly elastic in tension throughout all states, narrowing the grid into a slender state. The meridian cables can be retracted to enforce a bulgy shape. The transformation is locked, when additional, non-elastic horizontal cables (see Figure 79c, white cables) are activated at "open" state. When reaching the closed state, locking is integrated in the winch, and thus part of the actuation system.

The curvature-square analysis in section 3.2.3 implies, that the natural state of geodesic rotational grid structures is found at "closed" state (linear packed state). The curvature-square becomes minimal when the structure in bundled. Even though, this model does not match the mechanical configuration investigated in section 3.2.3, the structure tends to take shape of the slender state. However, the structural mass is working against, and the circular elastic cable additionally push the structure into the slender shape. This allows the use of actuation cables, as these only act in tension, and thus only apply for either closing or opening actuation. (unidirectional actuation)

Although, friction is not measured in this model, two basic sources of friction are likely: First, the hinges at nodes show contact surfaces that likely generate friction. Secondly, the actuation cables are sliding at connections.
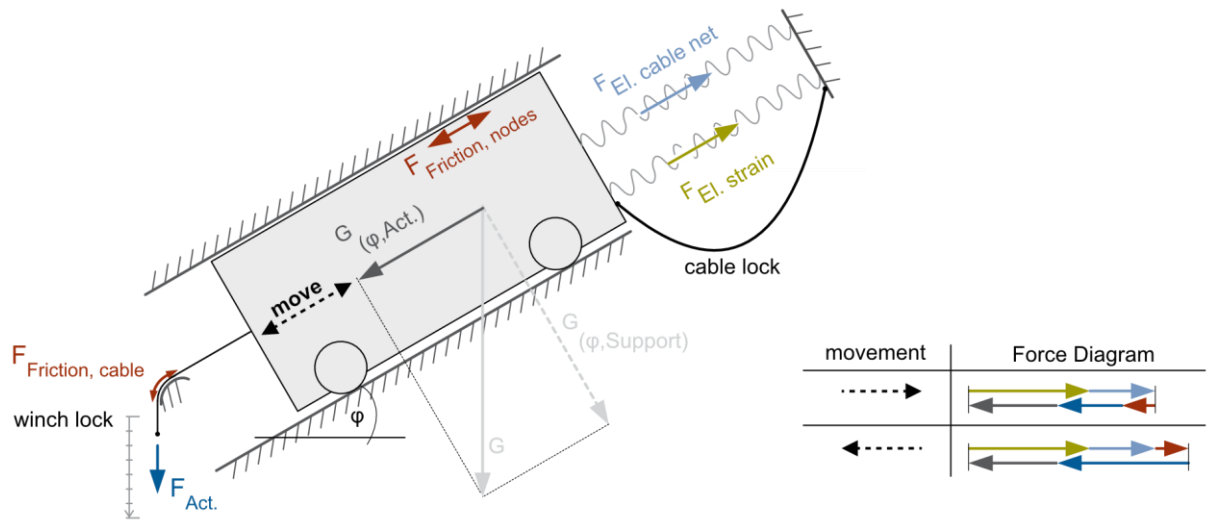
Figure 80 Schematic mechanical of the "Blooming Flower" including relevant forces and equilibrium.

Figure 80 shows the schematic mechanical model of the structure's transformation and a qualitative force diagram as defined in section 3.1.1.

Advanced Studies

Figure 81 Physical model and three states of deformation of a rotational geodesic grid structure. The surface of this demonstration includes both synclastic and anticlastic surface areas.

This setup was furthermore demonstrated by Maria Rau and Sarah Sandzek in a physical model study[1]. Figure 81 shows a rotational geodesic model to test the performance of both anticlastic and synclastic surface areas during transformation. The grid could be actuated by hand. Top and base radii change during transformation. The "natural" state is the bundled state (not perfectly reached due to collision within the model).

---

[1] *This investigation was conducted at the Professorship of Structural Design (Prof. Pierluigi D'Acunto) in 2021 in an architectural master course. This topic was supervised by Jonas Schikore*

3.4.3 C - Developable Strips
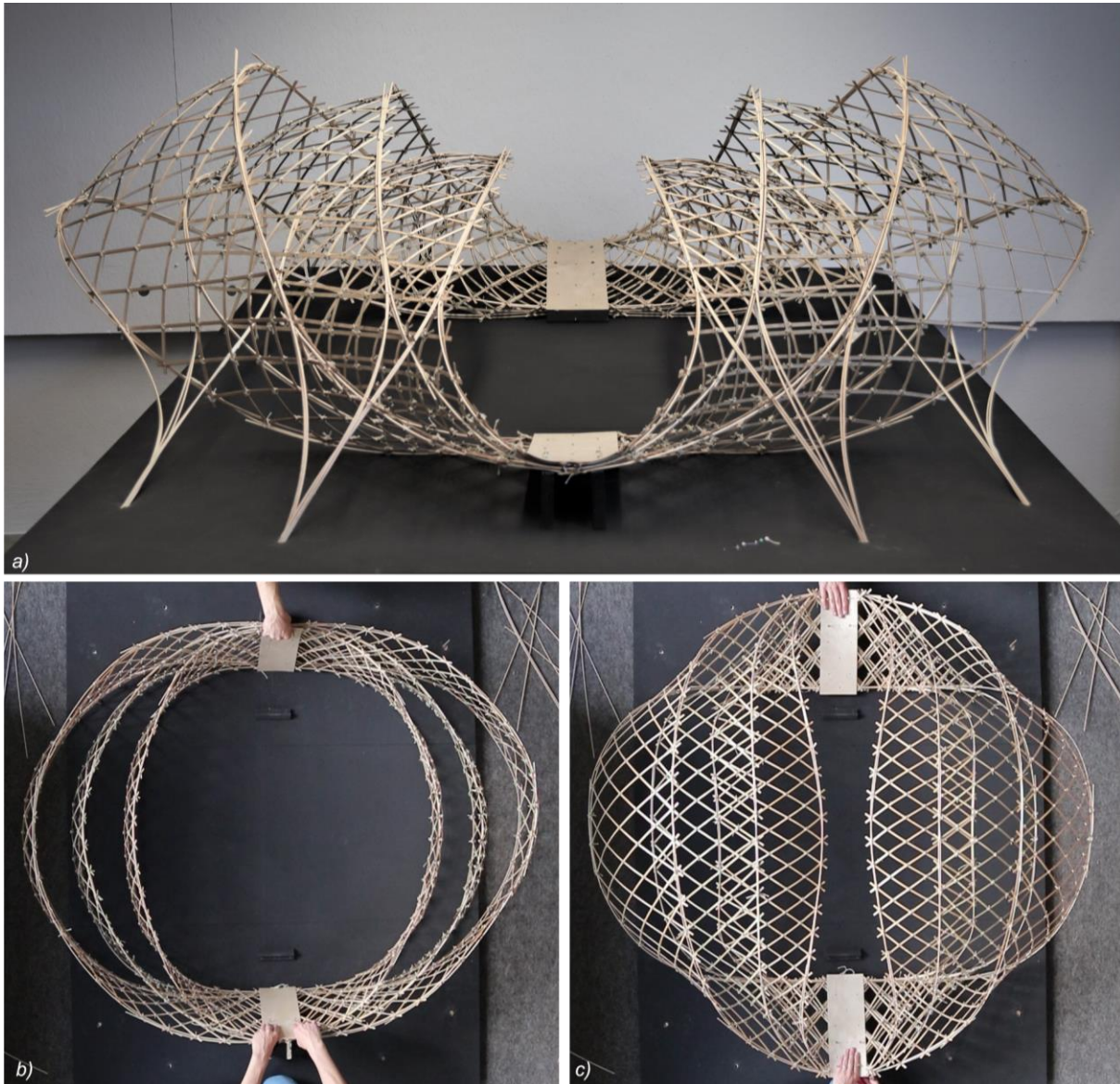
Figure 82 *The Sail, a geodesic grid structure on three partly developable surfaces: a) View at static, locked state, b) Grid structure before actuation (erection), c) Erected Grid structure (Photos: Barbara van Waarden)*

The *Sail,* designed by Barbara van Waarden is a set of three nested quadrilateral geodesic grid structures. The architectural idea is to create a shelter like space for open fires, made from bamboo strips. The mechanical concept of transformation aims at one-time erection.

Geometry and Morphology

The reference surfaces of three nested grid structures are double symmetric. The initial free-form-design surfaces represents the erected state. The surfaces were designed using lofted nurbs, creating three closed loops.

The mechanical concept for transformation utilizes "inextensional" deformation of the shell-like grid structure (see section 2.1.2, Figure 7, p.13). This phenomenon of elastic shell deformation appears on developable surfaces or areas near to free edges. Double curvature reduces such deformation freedoms. Figure 83 shows preliminary explorations on transformability using entirely developable, cylindric strips.
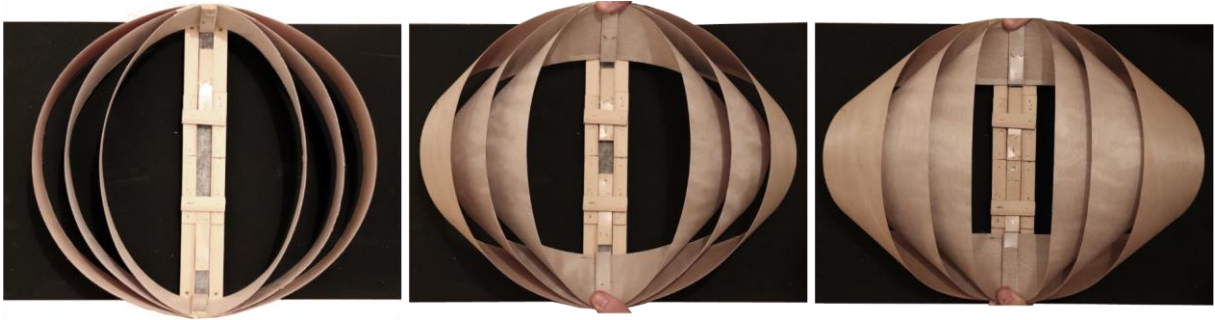
Figure 83 *Preliminary model to explore the compliant transformation of deployable strips. (Photo: Barbara van Waarden)*

In an advanced design step, the reference surfaces were modelled using computational tools, and double curvature was systematically generated at chosen surface parts. Figure 84 shows the Gaussian curvature of the design surfaces, that are the basis for geodesic network generation. The green areas are developable.
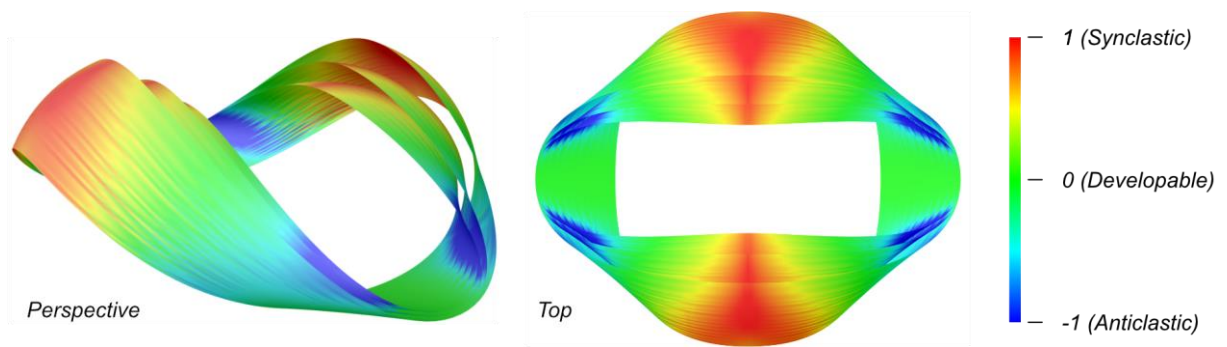
Figure 84 *Gaussian curvature (normalized) of the three nested reference surfaces of the "Sail"*

The developable surface parts aim to promote "inextensional" deformability. The doubly curved parts aim to provide shell-like stiffness.

On these surfaces, quadrilateral geodesic networks form the geometric basis for the grid structure. Together with the edge beams, the grid becomes triangulated at edges. When deformed, the grid's intersection angles do not change.

Mechanical Components and Performance
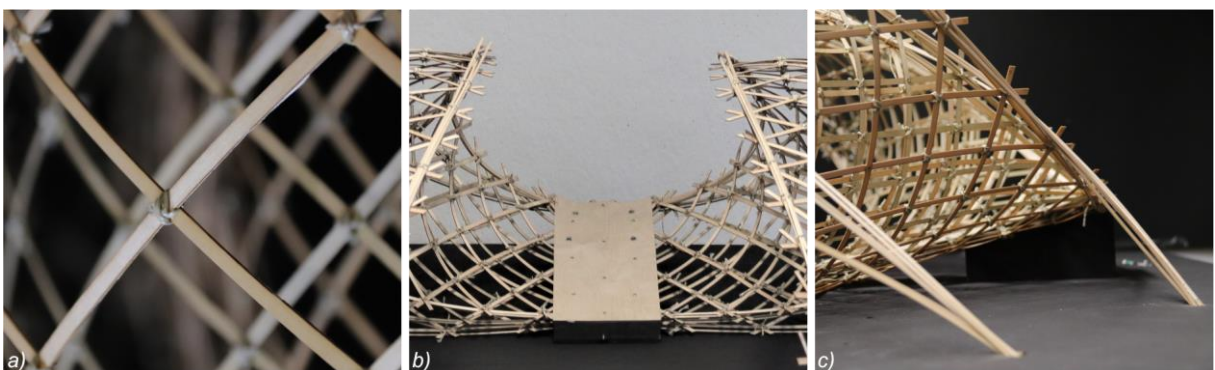
Figure 85 *Details of the "Sail" Gridshell: a) Tied nodes at lateral lamella connection, b) Rigid plate for actuation and support, c) Additional structs for erected state*

The geodesic grid is made by "flat" orientated lamella profiles (related to section 3.2.2 case "C"). The lamellas are made of laser cut timber strips, marked at nodes to implement bolted, lateral connections, that are furthermore tied to create rigid connections (Figure 85a).

The structure is connected to two rigid plates at the bottom part (Figure 85b). When erected, these plates are fixed to the ground. Before, they serve for actuation (erection). At final state, additional struts are implemented for support (Figure 85c).

Actuation and Locking

In this design, actuation and locking are part of an erection process, that is non reversible. The transformation is actuated applying external force. The rigid plates at the bottom perform a rotation and slide inwards. These plates actuate all three grid modules synchronous. Figure 82b and c show how these plates are manually moved. The doubly curved caps of the grid are thereby lifted from an upright position into a more horizontal, sheltering state. (Synclastic areas, see Figure 84 – red area). This requires induction of potential work, as the structural mass must be lifted. Note: There is no rotation at the grid's nodes, and thus, no friction. Although not measured, the grid's members curvature in the erected state appears higher than in the initial state. This implies, that additional strain energy must be induced for erection.

The plates moved for actuation are fixed for locking at erected state and remain as supports together with the additional struts.
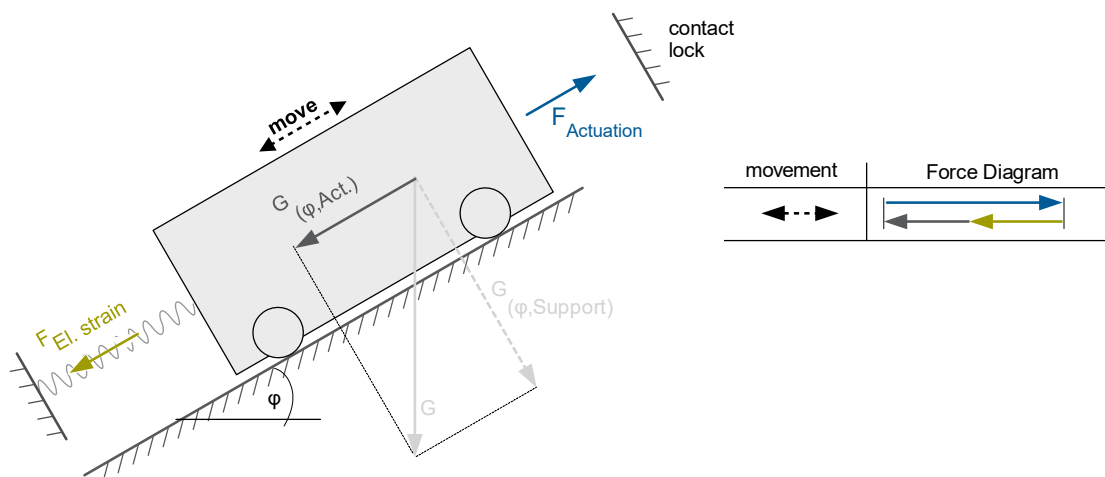
Figure 86 Schematic mechanical of the "Sail" including relevant forces and equilibrium

An abstracted mechanical model according to the definition in section 3.1.1 is shown in Figure 86. The actuation force must overcome both structural self-weight and elastic strain, but no friction.

3.4.4 D - Scissor Dome

Figure 87 *The EXX-dome, designed by Alberto Ortensi. The structure is actuated by highly elastic, (horizontally) and retractable cables (meridian): a) Open state, b) Closed state.*

The *EXX-Dome* was designed by Alberto Ortensi. The architectural intention is to create a deployable dome shaped roof structure that can open like a blossom. This design won the *Competitionline Campus* price in 2020.

The mechanical concept picks up the geometric approach of angulated scissor grids (see chapter 2.4.3), but integrates compliant mechanisms: The *Iris Dome*, a project supported by Chuck Hoberman (see chapter 2.4.3, Figure 33b) represents the purely kinematic reference. The *Iris Dome* required multiaxial hinges to generate a rigid body mechanism. In this semi-compliant version, the rotational degrees of freedom at hinges are replaced by biaxially compliant (bending and torsion) members. Thus, the number of rotational freedoms at hinges is reduced.

Geometry and Morphology

The *EXX-Dome* is a rotational symmetric structure. It is compound by 12 rotationally coupled linear scissor chains forming a scissor grid.

The goal in transformation was to create a closed synclastic state, and an open state, that must not necessarily fully retract the structure, but opens the vertically projected space underneath.

The "open" geometry was used as a starting point for morphological development. In various physical and numerical explorations, different scissor units were applied to varying "open" surfaces, and the "closed" states were determined:

Figure 88 *Physical Exploration of rotational symmetric scissor grids using angulated units on a cylindric reference surface.*

Figure 88 shows an example of a physical study: On a cylindric reference surfaces (representing the "open state"), angulated scissor units are applied. The structure transforms into a dome-shape.
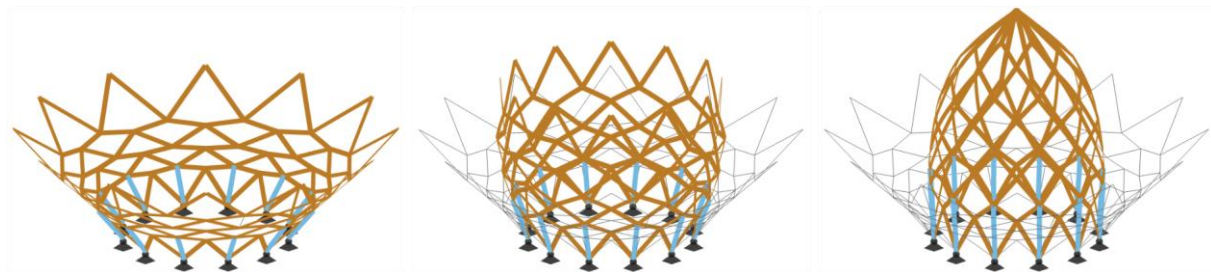
Figure 89 *Numerical investigation and formfinding of a suitable scissor setup for an open to close shape transformation.*

Figure 89 shows a numerical study: This simplified simulation uses non-compliant members and multiaxial hinges (this is a purely kinematic mechanism). This approach was used to quickly test scissor chain setups and their morphology[1]. It transforms into a dome-like closed state. The mechanism in this simulation was actuated using prescribed displacements at the bottom row (marked blue).

Based on this, the final configuration was developed, that is based on a conically open surface. Figure 87 shows both open (a) and closed (b) state of the final model.

---

[1]*This simplified simulation was performed using R-FEM5.*

Mechanical Components and Performance
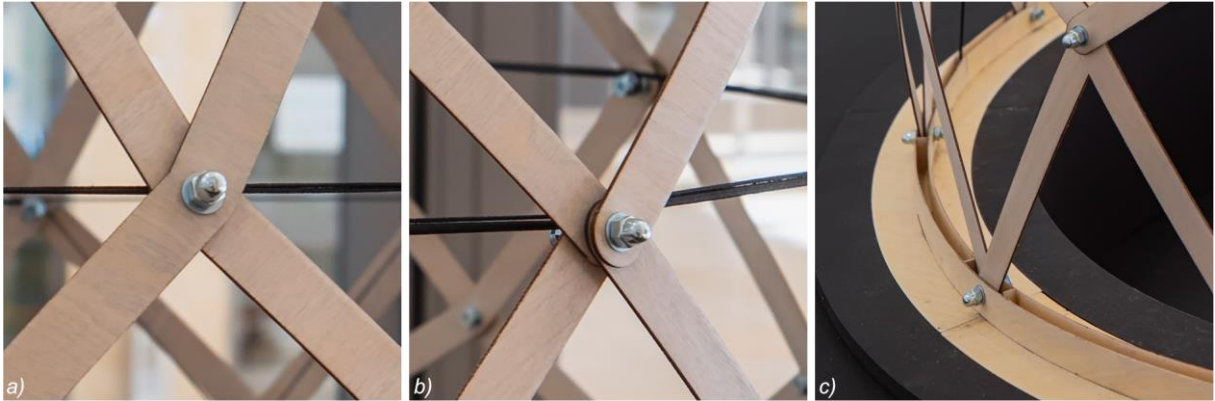
Figure 90 *Details of the EXX-Dome: a) Uniaxial hinge at scissor unit pivots, b) Uniaxial hinge for at coupling of scissor chains, c) Uniaxial hinge at support connection. (Photo: Martina Schikore)*

The grid's scissor units are made of "flat" orientated, laser cut, angulated timber strips. These allow compliant torsion and uniaxial bending. Through their strong axis, these strips transfer shear forces (and dedicated bending moments) within the scissor chain.

There are two types of hinges within the grid structure: The first represents the pivot connection within scissor units (Figure 90a). The second is located at nodes where scissor chains are coupled (Figure 90b) and connects four beams with rotational freedom each.

The bottom row of the grid are single beams. These members provide necessary freedom for the scissor chains to perform radial changes and connect the scissor system to the base supports. These supports are fixed and uniaxially rotational (Figure 90c).

The transformation performs as expected, following the simulated geometry. However, after multiple cycles of actuation, the timber lamellas start creeping under compression, and local buckling emerges. This phenomenon underlines the mechanical challenges between necessary compliancy and buckling failure.

Actuation
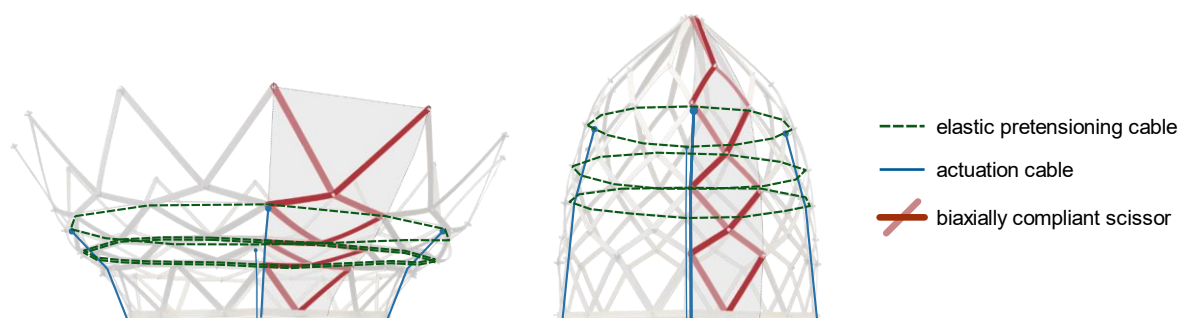
Figure 91 *Components for actuation: actuation and pretensioning cables at open and closed state.*

The mechanism is actuated using two cable sets following the rhombi's diagonals. The horizontal cables are highly elastic and in tension throughout all states. Their tension activates closing the structures. The meridian cables can be retracted to open the dome shaped grid (see Figure 91). The mechanical system can be abstracted equally to the *Blooming Flower's* model (see section 3.4.2, Figure 80).

3.4.5 Summary and Conclusion

The physical model designs shown and analyzed in previous sections were developed in a creative, experimental process. The following statements summarize decisive characteristics and creative developments from a mechanical perspective:

- All designs and transformations originate from an initial design state. The transformed states were found using both computational simulation and physical testing.

- All grid transformations are successfully actuated at only few locations, underlining the structures' qualities to perform controlled transformations (self-shaping quality)

- Models A, B and C demonstrate the physical transformability of the semi-compliant grid structures discussed in section 3.2.2 (biaxial compliancy).

- Model D demonstrates the physical transformability of a semi-compliant version of the concept of the *Iris Dome* (see section 2.4.3 p.42), using lamella profiles (with biaxial compliancy) and reduced nodal DoFs.

- Model A includes asymptotic grids that are cut at edges to allow a closed pattern of modules at closed state. This cutting is not in conflict with the structure's transformability. Hence, the networks' edges must not follow the networks' curves.

- Model B is fixed at the base in radial translation, and thus violates the transformation of rotational geodesic grids, involving radii changes at all locations. Furthermore, the grid members at the bottom part are thicker and stiffer. Thus, the transformed state shows concentrated curvature and appears distorted at the bottom.

- Models A, B and D use cables for actuation. To ensure tension at all states, two strategies were used to modify the structures' natural states, to always counter the cable's tension: In model A, the natural state is modified providing initial curvature in the members compliant axes. In models B and D, the natural state is modified using highly elastic cables.

- Model C aims at one-time transformation (erection). Thus, an external actuation is reasonable, e.g. a crane or lifting device. At final state, locking is realized by additional supports.

The presented designs are evaluated regarding their components according to section 3.1.1. Table 4 gives a comparative overview.

Comp.	Parameter	A	B	C	D
SURFACE	TYPE	disc	rotational	freeform	rotational
	CURV.	negative	positive	variable	zero / positive
	TOP.	1 edge (disc)	2 edges (rot.)	2 edges	2 edges (rot.)
NETWORK	REF.	surface (*Darboux*-Frame)			
	CUR.	$k_n = 0$ (asymptotic)	$k_g = 0$ (geodesic)		
	TOP.	quadrilateral			
BEAMS	ORIENT.	surface normal			
	TWIST	Variable / smooth			
	COMPL. (x/y/z)	c / c / r	c / r / c		
	INIT. CURV.	$k_{z,init.} = constant$	$k_{x,y,z,init.} = 0$		
HINGES	DoF	rotational (1 DoF)		rigid	rotational (1 DoF)
	ORIENT.	surface normal alignment			
	TOP.	bilateral			bilateral (pivot) / quadrilateral (hubs)
SUPPORTS	CONSTR.	fully fixed translation, uniaxial in rotation			
	AX. REF.	surface			
ACTUATION	ACT.REF.	internal	internal	external	internal
	DIRECTION	unidirectional	bidirectional	unidirectional	bidirectional
LOCKING	CONSTR.	Translational (distance limitation)			
	LOCK REF.	internal	internal	external	internal

Table 4 Structural parameters of analyzed physical model designs (comparison)
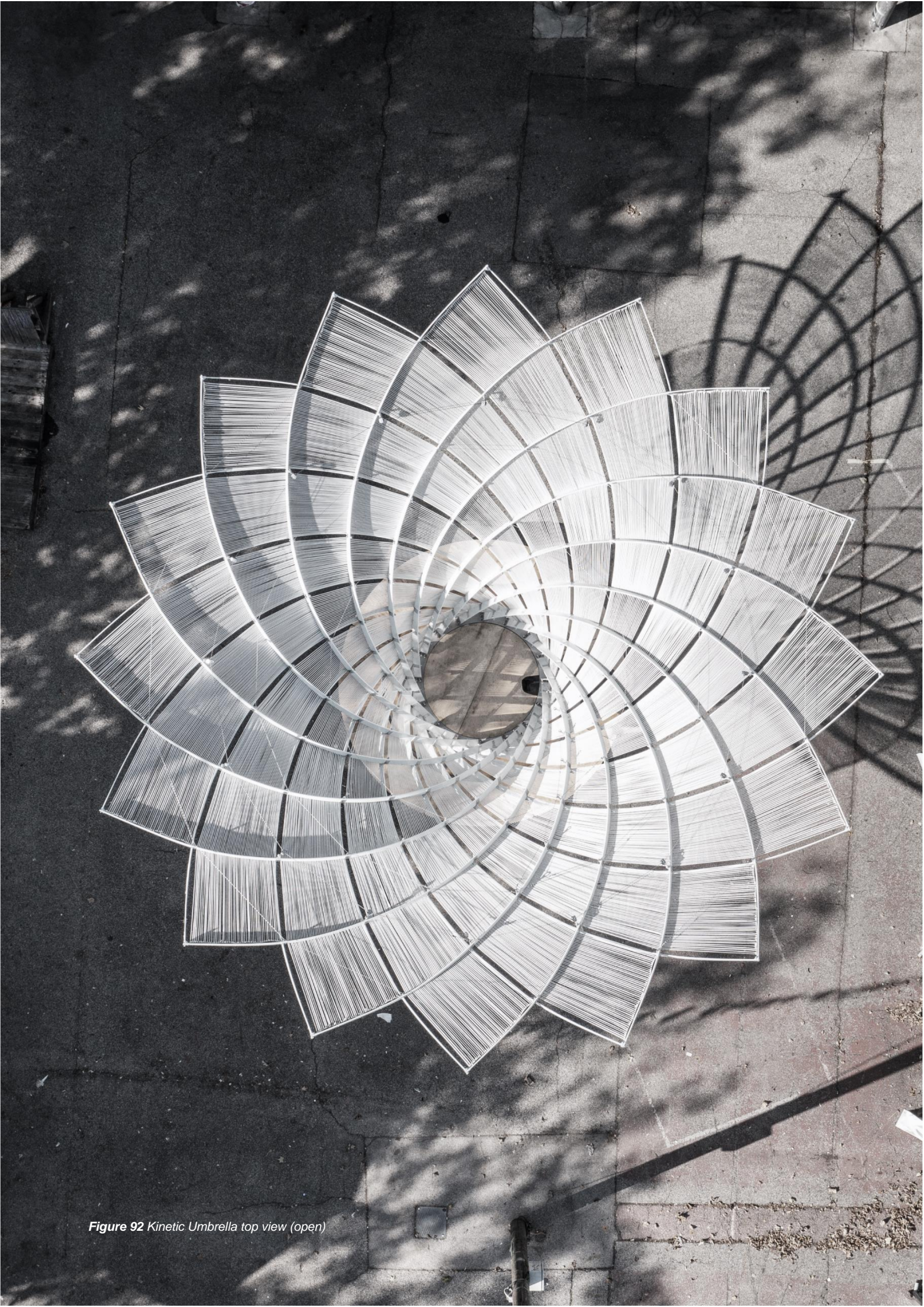
Figure 92 *Kinetic Umbrella top view (open)*

4 ARCHITECTURAL IMPLEMENTATION

This chapter aims at the utilization and realization of semi-compliant grid structures for architectural uses. In various case studies, key challenges are identified, and suitable engineering processes are developed. The chapter is subdivided into the following sections:

- Section 4.1 reveals requirements, strategies and workflows for **structural engineering** that address dimensioning and constructive implementation.

- Section 4.2 displays three **case studies on asymptotic gridshells**, where semi-compliant transformation was used for erection. The experiences gained by these built projects are incorporates in section 4.1.

- Section 4.3 presents the *Kinetic Umbrella*. This built project takes the step forward to incorporate reversible transformability and thus implements the findings of previous chapters.

4.1 Structural Engineering

The challenge of structural engineering is the implementation of architectural concepts into the build environment. Safety, serviceability, material efficiency and feasibility are main goals. When these goals are competing, iterative engineering workflows become inevitable. The development of compliant systems at architectural scale requires an extended consideration of multiple interacting parameters and effects. The complexity of such mechanical problems leads to additional constraints and an even more iterative character in engineering, compared to conventional static support structures or rigid-body mechanisms.

The following sections describe decisive engineering requirements, parameters, relations and performances at material, profile, global and local structural level. Furthermore, constructive criteria are systematically revealed. The last section describes the engineering and modelling process, organized in an iterative workflow.

4.1.1 Requirements and Beam Parameters

Structural design starts with user requirements, to be translated into mechanical qualities and parameter goals. In the following, basic requirements, and their parameter allocations in the context of compliant beams are described. In scope are the most essential relations among many secondary mechanical aspects.
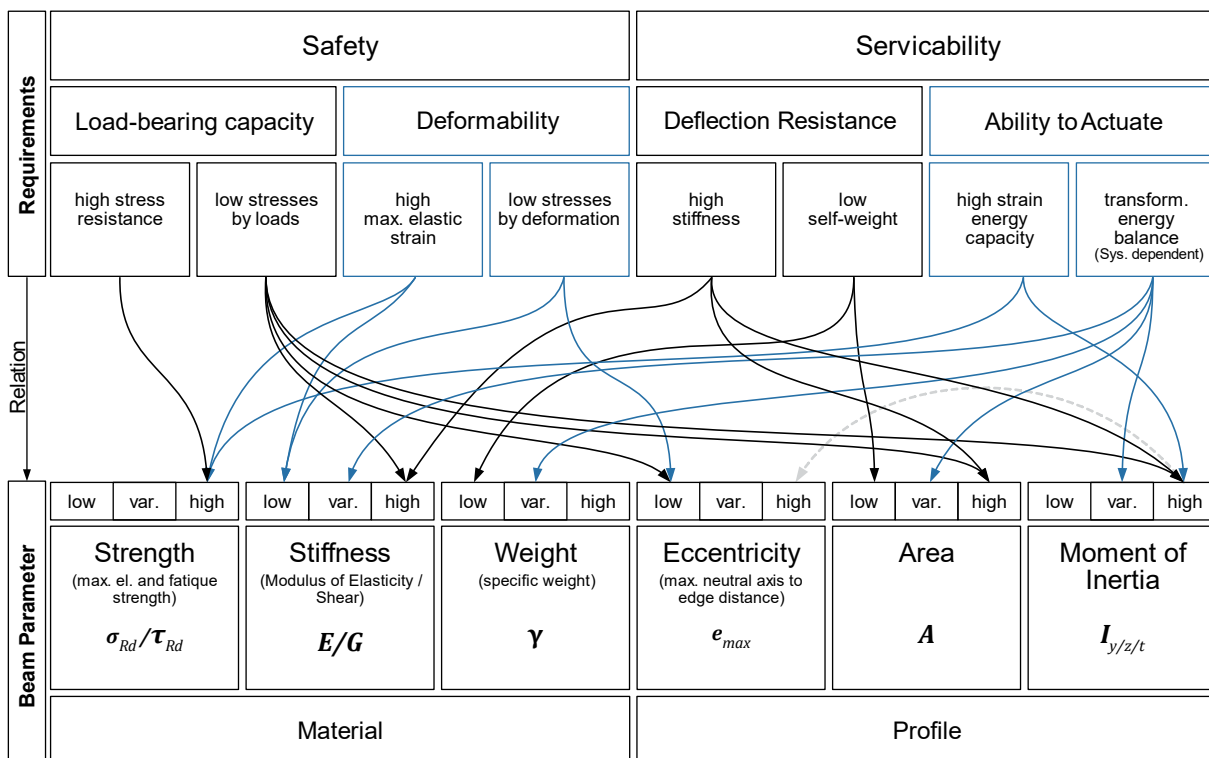
Figure 93 *Connectivity and targets of structural requirements and material parameters*

Safety and serviceability represent decisive user needs. For conventional structures, these refer to load-bearing capacity and deflection resistance respectively. However, compliant structures involve additional technical requirements, raised by the additional tasks to transform. Such structures require deformability to allow transformation, besides resistance on external loads. Also, deformability aims on resistance against collapse (when elastically

104

deforming) and thus aims on safety needs.

Within serviceability, there are limitations for deflections, and for compliant structures in addition, the ability to actuate. This requirement addresses the energy input and usability in terms of transformability.

The mechanical behavior of beams is described using appropriate material and profile parameters. These form an inseparable unit in terms of beam characteristics, engineering, and dimensioning. However, the profile dimensions represent the geometric component, the material parameters introduce stress relations and limitations. Out of many, the most decisive for compliant structure design can be named:

Key Material parameters are:

- Elastic and shear strength "σ_{Rd}"/ "τ_{Rd}" (limit stress of elastic material behavior),

- Elastic and shear modulus "E" / "G" (stiffness)

- Specific weight "γ"

Key Profile parameters are:

- Eccentricity "e_{max}" (max. dimension from the profiles center to edge - perpendicular to a bending axis. This parameter also relates to the auxiliary quantity "section modulus "$W_{y/z/t}$")

- Area "A"

- Moment of inertia "$I_{y/z/t}$"

Requirements of compliant systems can be allocated to beam parameters. Figure 93 provides a connectivity diagram of requirements (top block) and beam parameters (bottom block)[1]. The requirements of conventional only (black) and/or of compliant structures (blue) in addition, refer to parameter goals (e.g. high material strength). The diagram shows multiple relations and even contrary parameter goals.

In the following sections, these structural requirements are described briefly, and dedicated beam parameters are precisely identified:

Load-bearing

Requirements on load-bearing adress the material strength, section modulus and area. It is a fundamental mechanical design goal to keep stresses below material capacities. Out of Equation 14, the bending moment capacity is raised by a high moment of inertia and a low maximum leverarm $|e_{max}|$.

$$M_{y,Rd} = \sigma_{Rd}W_y = \frac{\sigma_{Rd}I_y}{|e_{z,max}|} \; ; \; M_{z,Rd} = \frac{\sigma_{Rd}I_z}{|e_{y,max}|} \qquad \text{\textit{Equation 49}}$$

Load-bearing also relates to stability problems and thus refers to the beam's stiffness EI.

---

[1] *Note, that the relations displayed are to be considered according to local orientations. E.g.: Deformability requirements bending addresses the profile's parameters referred to the bending axis.*

Deformability

Deformability is gained by strain. The limitation of strain $\varepsilon_{(\sigma_{Rd})}$ and shear distortion $\gamma_{(\tau_{Rd})}$ is expressed as follows:

$$\varepsilon_{(\sigma_{Rd})} = \frac{\sigma_{Rd}}{E} \; ; \; \gamma_{(\tau_{Rd})} = \frac{\tau_{Rd}}{G}$$

<div align="right">Equation 50</div>

In this context, a low material stiffness and high strength are beneficial to raise deformability. With a given material and strain at failure $\varepsilon_{(\sigma_{Rd})}$, deformability (bending) can be raised geometrically by lowering the profiles maximum distance from the neutral fiber axis to the profile edge $\left| e_{y,z,max} \right|$. Based on Equation 7, the possible curvature through elastic deformation results to:

$$\kappa_{y,max} = \frac{\varepsilon_{(\sigma_{Rd})}}{\left| e_{z,max} \right|} \; ; \; \kappa_{z,max} = \frac{\varepsilon_{(\sigma_{Rd})}}{\left| e_{y,max} \right|}$$

<div align="right">Equation 51</div>

Equation 51 shows the linear relationship between bending deformability and the profiles dimensions.

Torsional deformations and internal stresses are highly dependent on the type of profile. As described in section 2.2.3, torsion leads to multiple mechanical effects:

For St. Venant torsion, the maximum possible twist is limited by shear strength. For a circular full, closed, and open thin-walled profile exemplarily, the limit twist is given by substitution of Equation 17 into Equation 16:

a) Full circular profile   b) Closed thin-walled tube profile   c) Open thin-walled profiles
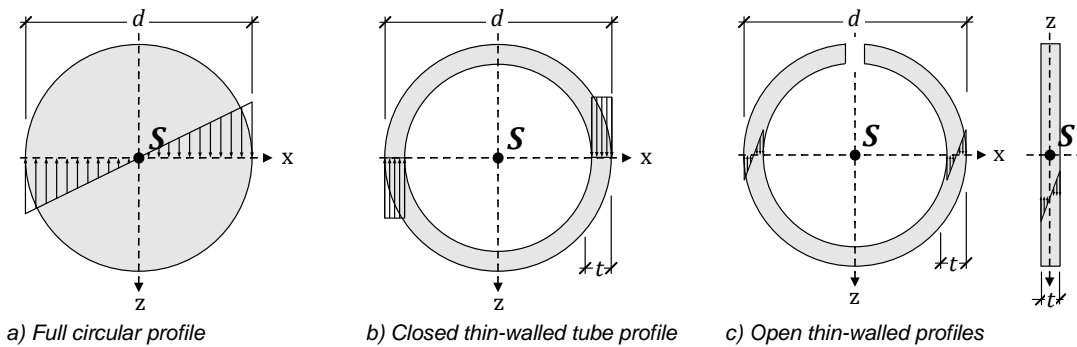
$$\kappa_{x,max} = 2\frac{\gamma_{(\tau_{Rd})}}{d} \qquad\qquad \kappa_{x,max} = 2\frac{\gamma_{(\tau_{Rd})}}{d} \qquad\qquad \kappa_{x,max} = \frac{3}{2}\frac{\gamma_{(\tau_{Rd})}}{t}$$

<div align="right">Equation 52</div>

From Equation 52, some decisive relationships between torsional deformability and profile dimensions can be deduced: For a given material and its specific "distortion at failure" $\gamma_{(\tau_{Rd})}$, there is a linear relationship between the maximum possible twist $\kappa_{x,max}$ and profile dimensions. In analogy to bending deformability, the profile stiffness is not directly significant. A full circular profile and a thin-walled tube of same diameter allow the same twist. For open (thin-walled) profiles, the thickness becomes significant, while the "global" dimension - in this case the diameter d - become irrelevant for torsional deformability.

Deflection and Buckling Resistance

Deflections and buckling are undesired deformations, to be counteracted by stiffness on both material and profile side, raising the elastic or shear modulus E/G or moment of inertia $I_{x,y,z}$

respectively. Furthermore, low self-weight is likely advantageous.

Ability to Actuate

Any actuation system performs according to the systems total energy level during transformation. Compliant Systems include strain energy, which is either released or induced throughout transformation. Additionally, the potential energy, given by the total mass of the system and its height, is possibly changing during transformation. These energy components address the materials stiffness (modulus of elasticity / shear) and specific material weight respectively. It depends on the compliant system, whether a high or low stiffness or material weight is beneficial in terms of actuation. The internal energy level and the actuation system must be designed to fit each other.

The internal strain energy can be used to balance the total energy level by counteracting the potential energy component. In other words: The energy, necessary to move the structures mass (potential energy) might be taken from the stored strain energy. For such strategies, high **energy capacities** are useful. The potential energy capacity is linearly dependent on the mass and accordingly the specific weight. The materials strain energy capacity can be referred to the maximum material strain energy density.

$$max.\,strain\,energy\,density = \frac{1}{2E} \cdot \sigma_{Rd}^2$$

<div align="right">Equation 53</div>

The energy density maximum for shear deformations can be set up accordingly:

$$max.\,shear\,energy\,density = \frac{1}{2G} \cdot \tau_{Rd}^2$$

<div align="right">Equation 54</div>

Equation 53 and Equation 54 show, that the materials capacity to store strain energy is increases by a high strength and low modulus of elasticity/shear. The latter is less intuitive.

4.1.2 Dimensioning with the Stiffness Paradox

This section provides relations strategies for compliant profile dimensioning and material choice. The opposing requirements of high stiffness and deformability are creating a design goal paraoxon (Lienhard, 2014, p. 141). The beams stiffness results from the product of material and section stiffness (EI). These parameters are linked by deformability requirements and cannot be treated separately.

Strategies and Relations for Beam Profile Design

The static analysis in section 3.3.2, and the requirements in section 4.1.1 distinguish the relevance of stiffness for compliant structures. This section reveals theoretical strategies for beam design, considering both load-bearing, and deformability requirements. These strategies are based on beam parameter interrelations and involve specific modifications of material and/or profile parameters.

To explain these strategies, a simple design situation is proposed: A beam with given dimensions (squared profile $w_0 = h_0$) and material ($E_0, \sigma_{Rd,0}$) is chosen as a starting point. The beams deformability ($\kappa_{y,max}$) and mass (profile area A, γ) are chosen to be fixed characteristics. The intention is to increase the beams deflection resistance and stability performance (stiffness EI) by a factor f, without changing the beams deformability and mass. Four strategies are elaborated. Table 5 displays these strategies and includes the parameter factors referred to the stiffness factor f.

			A)	B)	C)	D)
Material	Elastic Modulus	E_0	f	1	1	$1/f$
	Strength	$\sigma_{Rd,0}$	f	$\sqrt{f}$	1	1
Profile	Moment of Inertia	$I_{y,0}$	1	f	f	f^2
	Width	w_0	1	$1/\sqrt{f}$	$\dfrac{1}{\sqrt[3]{2}\cdot\sqrt{(f-\frac{3}{4})}}$	$1/f$
	Height	h_0	1	$\sqrt{f}$	1	f
Beam	Area	A_0			1	
	Deform.	$\kappa_{max,0}$			1	
	Stiffness	$(EI)_0$			f $\quad(f_{max}=3)$	

Table 5 *Stiffness optimization strategies and their factors on beam parameters. Factors marked blue are overall goals (All profiles displayed exemplary with f = 1,5)*

In the following, the parameter interrelations in these strategies are described in more detail:

A) **Increase material strength and elastic modulus (proportionally):**

In conventional engineering, it is an intuitive method to increase the beams stiffness, using material alternatives with higher modulus of elasticity. For compliant structures, this might conflict with necessary capacities on deformation. In consequence, the material strength must be increased proportionally to preserve possible strain at failure. An increase of both E_0 and $\sigma_{Rd,0}$ is proportional to the beams increase of stiffness.

B) **Increase material strength and profile height:**

Higher material strengths allow larger strains at failure. In consequence, the profile height h can be adapted (increased), and deformability requirements are still fulfilled, with increasing effect on profile stiffness. Note, an increase of strength has a quadratic impact on the possible stiffness increase.

C) **Increase profile stiffness (moment if inertia) and preserve material:**

The profile stiffness can be raised, shifting material close to the strain limitations, where $|e_{max}|$ is given by the deformability constraint. There is an analogy to conventional profile design (thinking of H-Profiles in steel structures exemplarily, where profile material is placed at flanges, to generate high moments of inertia).

Theoretically, the beams stiffness can be increased by max. factor 3 using this strategy (All material placed at maximum eccentricity line). However, this profile would then have infinite width, thus, something in between is reasonable.

D) **Lowering material stiffness to create higher profile stiffness:**

In this rather unintuitive strategy, a material with lower elastic modulus is used. Hereby, strain at failure is increased. In consequence, the profile height h can be raised and deformability remains (see also Equation 55). Due to the cubic effect on the profile stiffness (Moment of Inertia I), raising this dimension, the loss of material stiffness can be overcompensated. However, the modification of material stiffness requires preservation of strength.

There are further strategies possible, and some of the explained ones may be combined (E.g.: "C"&"D", "A"&"C", etc.).

Material Design

Elasticity generally applies to any solid material. For conventional building projects, stiff materials with high strength are preferred in a mechanical context, to minimize material input. However, only few building materials are generally suitable for structures involving large deformations, e.g., so called "bending-active" (see section 2.4.4) or "kinetic" structures. The material families timber (incl. bamboo), metal and reinforced plastics are particularly promising in regard to their deformability (Lienhard, 2014, p. 33).

However, it can be questioned, which material allows the largest beam stiffness for given bending radii? There is no general answer valid for any type of profile, but the material strain at failure already provides a useful performance index to evaluate the materials deformability.

Julian Lienhard used Ashby-diagrams[1] to map materials according to their elastic modulus and strength. He identified strain at failure values, suitable for bending-active and kinetic structures. However, this index informs about deformability only, and not about the beam's total stiffness.

To evaluate the materials regarding beam deformability and stiffness, the simple case of a bent plate leads to a helpful indication, especially when using lamella profiles. In the following, a material index is derived that quantifies the potential of a material to design beams with maximum stiffness for elastically curved beams. Figure 94 displays the model for this derivation.
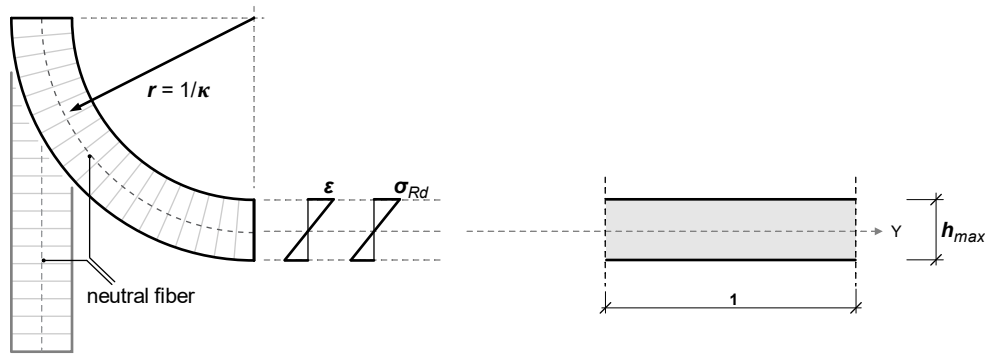
Figure 94 *Mechanical model to identify the decisive material index for bent beams with potentially high stiffness.*

The beam stiffness EI_y can be expressed in dependency of the maximum possible height h_{max}, the corresponding material values E and σ_{Rd}, and the curvature applied κ.

From Equation 50 and Equation 51 we receive a maximum possible height h_{max}:

$$h_{max} = \frac{2\sigma_{Rd}}{E\kappa}$$

Equation 55

The maximum moment of inertia I_y for a unit strip with h_{max} results to:

$$I_{y,hmax} = \frac{h_{max}^3}{12} = \frac{2\sigma_{Rd}^3}{3E^3\kappa^3}$$

Equation 56

The potential beam stiffness EI_y for a given curvature κ results to:

$$EI_{y,h\max} = \frac{2}{3\kappa^3} \cdot \frac{\sigma_{Rd}^3}{E^2}$$

Equation 57

The quotient, marked blue, represents the decisive material index to evaluate the potential stiffness of initially bent beams, when the maximum possible height is applied. In Figure 95, the Ashby-Diagram, set up by Julian Lienhard is shown. The index lines (blue) of the potential stiffness are added for selected case studies (see chapter 4.2 and 4.3).

Timber, metal, and fiber reinforced polymers (GFRP) provide stiffness potentials, raising in this order. However, Hardwoods do meet or even exceed stiffness potentials of lower steel grades. The potential of GFRP, used for the *Kinetic Umbrella* (see chapter 4.3) is about 100 times higher than Steel S355, used for the Hotel Intergroup (chapter 4.2).

Assuming, that the critical Euler-load (Equation 35) is the decisive quantity for structural

---

[1] *Ashley-Diagrams (or Ashley Plots) are material charts to map materials within a two-dimensional property space. These charts help to choose materials for specifically defined mechanical requirements and goals Ashby (2011).*

integrity, and maximum possible profile dimensions are applied (Equation 55), then the quotient of Equation 57 is directly proportional to the beams compressive resistance.
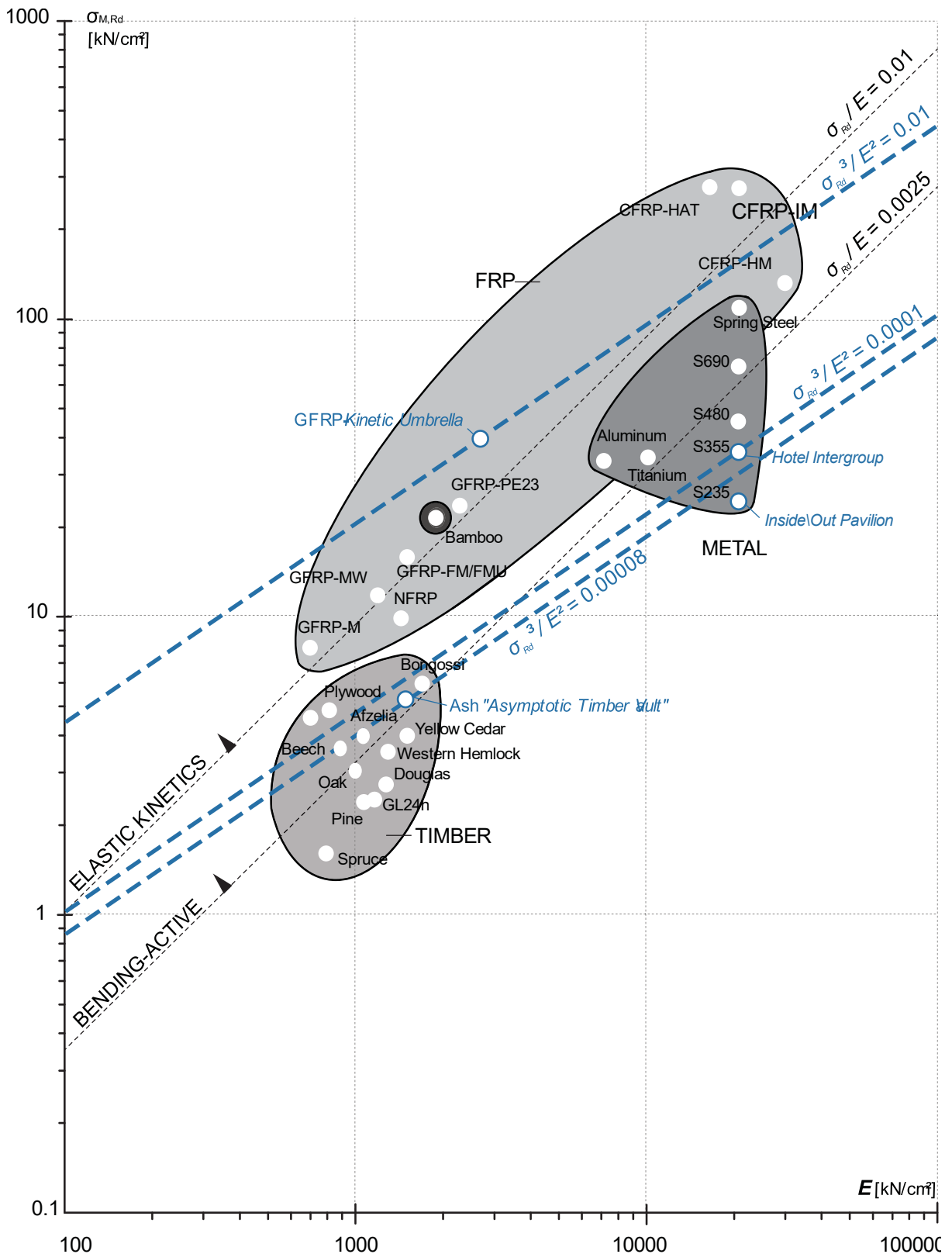
Figure 95 *Strength vs. elastic modulus-Chart by J. Lienhard (Lienhard, 2014, p. 34). Additionally, the Index lines for potential beam stiffness for elastically curved beams are included (marked blue for the "Hotel Intergroup", "Asymptotic Timber Vault", and "Kinetic Umbrella" project.*

The Lamella Profile

Lamella sections are particularly useful for both asymptotic and geodesic configurations, as these hold biaxial compliancy in bending and torsion.

The lamella profile is characterized by large differences in local bending stiffness and consequently useful to activate bending deformations in weak axis direction. Additionally, lamella profiles are "open" without effects of warping torsion, but potentially sensitive for helix torsion effects. Lamella profiles are defined by two dimensions ($h \gg t$). The stiffness ratios (moment of inertia) can be derived analytically:

The moments of inertia result to:

$$I_{t\,(St.V.)} = \frac{1}{3}ht^3 \;;\; I_y = \frac{1}{12}th^3 \;;\; I_z = \frac{1}{12}ht^3$$

<div align="right">Equation 58</div>

The ratios of moments of inertia result to:

$$\frac{I_y}{I_z} = \left(\frac{h}{t}\right)^2 \;;\; \frac{I_y}{I_t} = \frac{1}{4}\left(\frac{h}{t}\right)^2 \;;\; \frac{I_z}{I_t} = \frac{1}{4}$$

<div align="right">Equation 59</div>

These ratios can be applied to perform idealized transformation analysis, as placeholders for planning states before detailed profile dimensioning.

If the local curvatures of a lamella are known, maximum stresses result to:

$$\sigma_{(\kappa y)} = \frac{1}{2}Eh\kappa_y \;;\; \sigma_{(\kappa z)} = \frac{1}{2}Et\kappa_z \;;\; \tau_{(\kappa x)} = \frac{3}{2}Gt\kappa_x$$

<div align="right">Equation 60</div>

The normal strains and stresses induced by helix torsion relate to the radius r. A general description for the helix torsion is given in chapter 2.2.3. For lamella profiles ($h \gg t$), this radius is approximately equal to z (see Figure 96).

$$r \sim |z|$$

<div align="right">Equation 61</div>
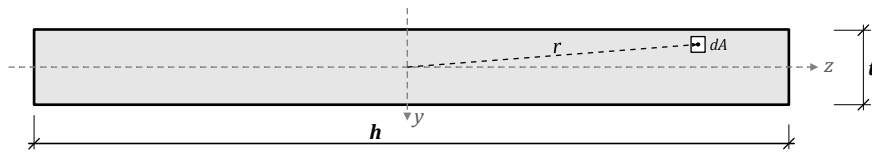
Figure 96 *Parameter definition of the lamella profile (h ≫ t)*

The maximum stresses can be simplified as described by Schikore et al., 2019, p. 809:

$$\sigma_{x,Helix-strain}(\kappa_x) = \frac{1}{12}Eh^2\kappa_x{}^2$$

<div align="right">Equation 62</div>

The helix-area-moment and polar area moment for lamella profiles ($h \gg t$) results to:

$$I_r = \int_A r^4 dA \sim t\int_{-h/2}^{h/2} z^4 dz = \frac{th^5}{80} \;;\; I_p \sim I_y = \frac{th^3}{12}$$

<div align="right">Equation 63</div>

The reduced helix-area-moment results to:

$$K_r \sim 0{,}0069\overline{4}\, th^5$$

<div align="right">Equation 64</div>

4.1.3 Constructive criteria

Constructive criteria define any build object. These are restrictions due to collision, constructional feasibility, fabrication limitations, etc. These criteria may result in eccentricities, tolerances, local discontinuities, additional components, etc.

In the following, some key criteria, regarding beam profiles, grid layering and offsets, nodes and hinges, and local weakening are described, that must be clarified for structural implementation.

Beams and Profiles

Profile dimensions are defined by the beams kinetic and static requirements. However, additional criteria result from constructive aspects:

- Any profile and material refers to specific fabrication methods and its limitations. Exemplarily, GRP profiles have a minimum wall thickness, resulting from the extrusion process and fiber insertion. Furthermore, the length of continuous beams is restricted by fabrication limitations.

- Beams are interconnected and secondary structures are attached. Details for connection may require minimum wall thicknesses, edge distances, feasibility for mounting, etc. In this context, connectivity may become a decisive criterion for profile design. This refers particularly to the type of nodes, hinges, or secondary components.

Offsets and Grid Layering

Offset objects have constant spacing to their original object. For gris structures, two types of offset curves are common: One is an offset in the surface normal direction (Layering), another in bi-normal direction (see *Darboux*-Frame section 2.1.3). In Figure 97, two types of offset curves on a surface are displayed.

a) Layering

b) Offset in tangent normal direction
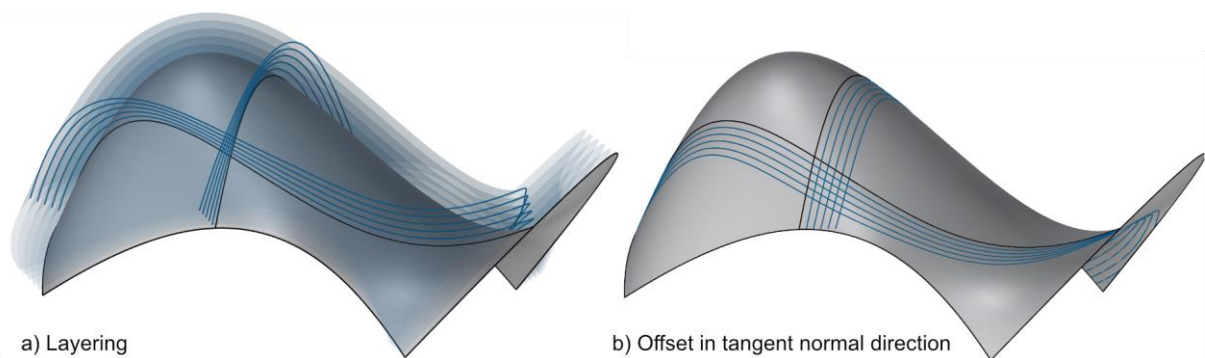
Figure 97 *Offsets of an arbitrary curve on a surface: a) layering – offset in surface normal direction, b) offset in curves (Darboux-Frame) tangent normal direction*

Based on a reference surface, offset surfaces (surfaces with a constant distance in surface normal direction) can be used to assign structural components. Grid structures may be separated into layers to solve collisions or allow beams passing through the structure. This concept is particularly relevant for strained grids structures, where the use of initially straight elements is advantageous, and smooth curvatures are desired.

Layering may also affect kinematic limitations at hinged intersections. Considering two hinged beams in different layers, infinite rotations are theoretically possible without collision.

Figure 98 shows some exemplary configurations of a grid with two beam families (green and blue) and a bracing layer exemplarily. The number of possible configurations rises with number of layers.

Two Layers:

beam-bracing collision (top)   *beam-beam collision, bracing top*   *beam-beam collision, bracing bottom (...)*

Three Layers:

bracing layer in-between   *bracing layer top*   *bracing layer bottom (...)*
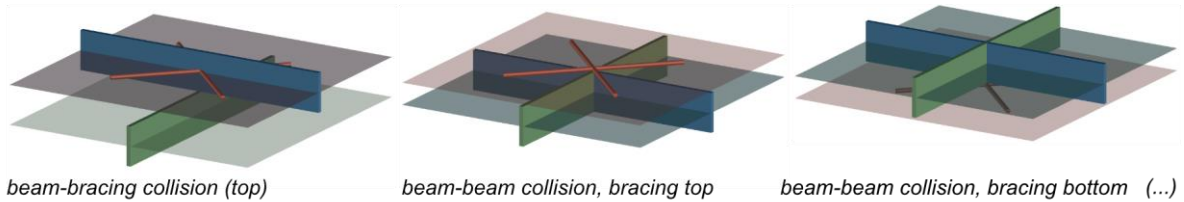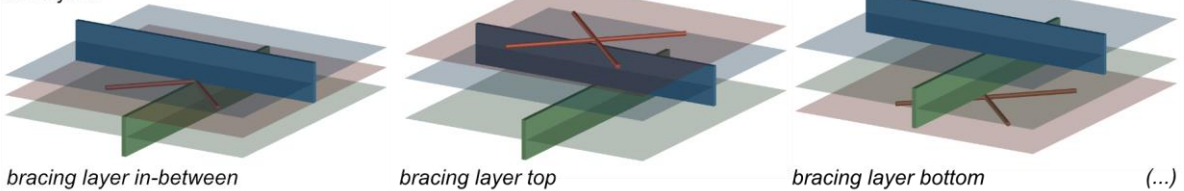
Figure 98 *Exemplary normal offset configurations of double and triple layered grids*

Another possible offset direction is in bi-normal direction of the initial curve on surface (Figure 97b). Such offset curves are nearly on surface, considering small offsets. These offsets might be applied to solve collisions with nodes' detail components, or to generate multi-layered profiles, exemplarily.

beam offset (multi-layered beams)   *bracing offset (double bracings)*   *beam + bracing offset*
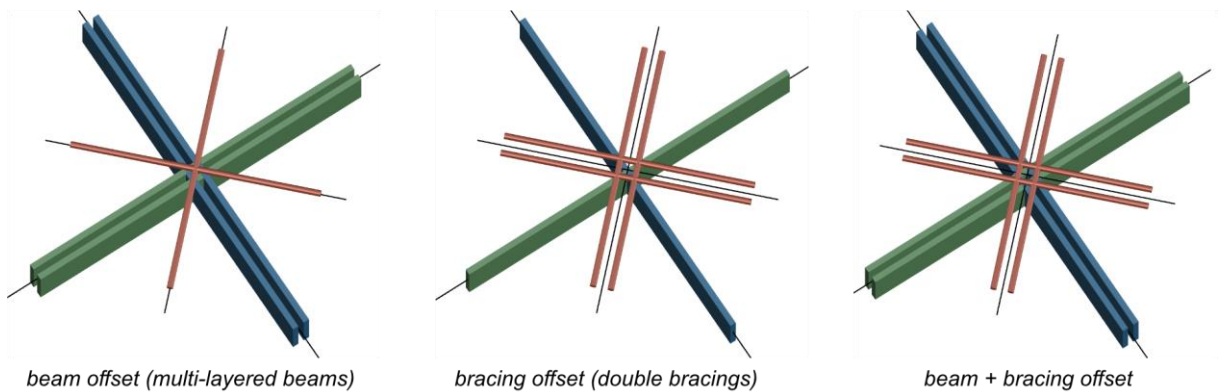
Figure 99 *Exemplary bi-normal-offset configurations of single and doubled grid members*

Figure 99 shows three configurations of bi-normal offsets at a grid node, either applied to beams, bracings, or both. These offsets result from dissolved beams or bracings, often symmetrically, to avoid moments caused by eccentricities.

Using layers and offsets results to various geometric deviations with respect to the initial surface or single layered setup. This also applies to offset curves on surface. The deviation in length of the offset curves results from the curvature of initial curves and surfaces[1]:

The length deviation can be derived using the same geometric approaches that are used to

---

[1] *Note, for a curve on a plane, both offset types do not involve changes in length.*

determine bending (Euler-Bernoulli-Beam, see Figure 12) and helix torsional stresses (see Figure 13). There is an analogous relation between curvature related elongation of beam fibers and length deviations of offset curves. Hence, the fibers of a curved beam are geometrically equal to offset curves. In this analogy, the initial curve relates to the "neutral" fiber, and offset curves relate to stretched or compressed fibers.

The offsets described above are orientated on the *Darboux*-Frame. Length deviations due to normal and geodesic curvature are proportional (linear) to the offset distance. Changes due to geodesic torsion are in quadratic relation.

The offset curves' elongation ε_o due to normal or geodesic curvature with an offset o in surface normal direction is deduced from Equation 8:

$$\varepsilon_o = \kappa_{n/g}\, o$$

<div align="right">Equation 65</div>

The offset curve's elongation ε due to geodesic torsion is deduced from Equation 19:

$$\varepsilon_o = \frac{1}{2}o^2\tau_x^2$$

<div align="right">Equation 66</div>

Using offsets is a constructive strategy for the design of semi-compliant grid structures. However, the geometry of offset curves may differ in length and curvature. Deviations might be relatively small and could be handled by tolerances. In any case, the impact on the structures kinetic and static behavior must be evaluated.

Nodes and Hinges

The design of grid nodes involves the grid members (to be connected) and additional, connective components, that generate appropriate degrees of freedom (e.g., hinges). Nodes can be classified as either central or lateral, according to the member's position.

a) Central Connection *b) Lateral Connection*
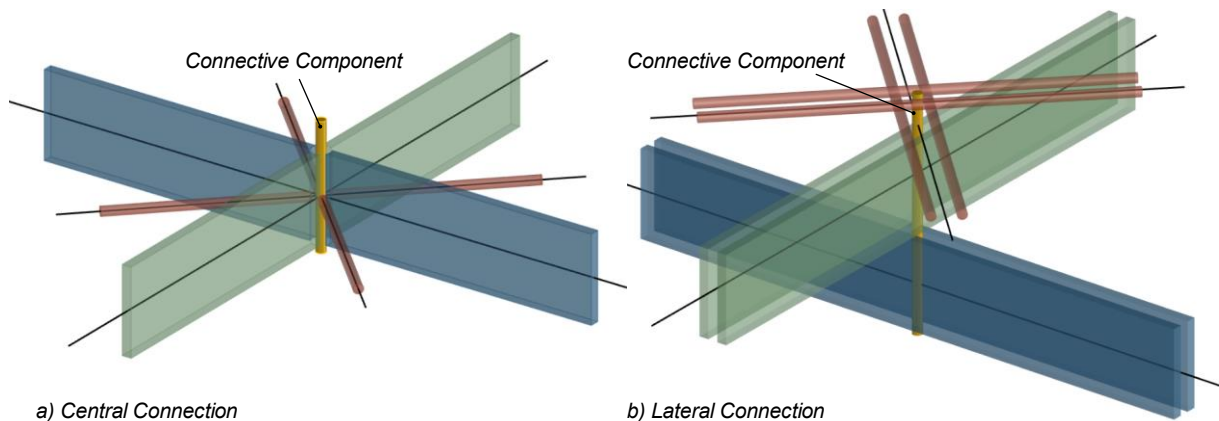
Figure 100 *Schematic concept of a a) Central, and b) Lateral connection*

The previous section describes some strategies for lateral configurations, that allow beams to pass through. The connective component must "bridge" eccentricities between members. In a central node, the grid members must be divided to avoid collision, and the connective component must additionally "bridge" those division, within members. Figure 100 shows a completely central configuration (a), and a lateral configuration in both normal and bi-normal direction (b).

Note, there are two basic geometric approaches for lateral configurations, regarding bi-normal offsets:
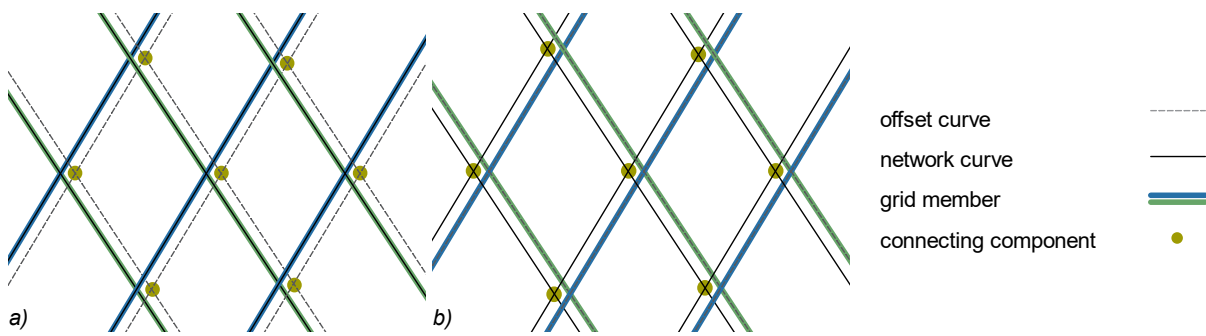
Figure 101 Concepts for lateral node configurations: a) Eccentric connective component, b) Eccentric grid member

The first concept preserves the initial network curves as beam centerlines, and the connective component is places eccentric (Figure 101a). In the second concept, the beams' centerlines are offset with preserved connective components at network intersections (Figure 101b).

Both concepts avoid collision of beams and connective components. If the connective component is hinged, both geometric configurations affect the local kinematic performance, as rotational poles are modified. Such effects need to be considered in planning.

Local beam discontinuities

Grid structures incorporate multiple nodes, and secondary components may require further connections. Such details involve additional components and/or perforations. Figure 102 shows some basic component types schematically: clamps, adapters, bolts, slots, or butt joints. Joint details may compound various of these basic types.
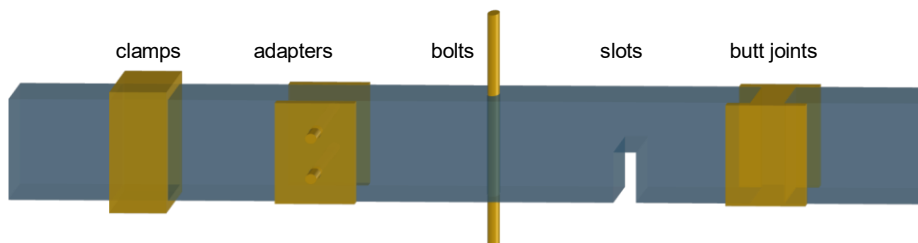
Figure 102 Basic types of joint components with differing effects on the beams local stiffness and load capacity.

Any connection or perforation placed on beams leads to local discontinuities regarding stiffness and load capacity. Slots or additive components exemplarily are influencing the beams mechanical performance locally, even beyond the geometrical position of the discontinuity.

If bending or torsional deformation are geometrically predetermined, stiffness and bending stress are interdependent and need to be considered, and eventually minimized. The local discontinuity can be either softer, equally stiff, or stiffer than the beam itself. On bent beams, this leads to a discontinuous curvature, but not to a discontinues bending moment. However, when the global stiffness of the beam including all local discontinuities is changed, the global, continuous bending moment is changes accordingly. The length of discontinuities is decisive for the change in global beam stiffness and bending moment. Consider, an infinitesimal short discontinuity with infinite local stiffness will not affect the bending performance. And further: An infinitesimal short perforation of a beam (softening) leads to larges strains only in a short area,

that does not affect the global shape of the bent beam (The stiffness of a very short but soft beam segment is high due to the short length). Figure 103 shows the results of a numerical analysis of a circular bent beams (blue) with local stiffness discontinuities (yellow).

Discontinuity	$EI_{Disc.} = 0,1\ EI_{Beam}$	$EI_{Disc.} = 10\ EI_{Beam}$
$l_{Disc.} = 0,01 l_{Beam}$	M ~ 1	M ~ 1
$l_{Disc.} = 0,1 l_{Beam}$	M ~ 0,5	M ~ 1,1
$l_{Disc.} = 1,0\ l_{Beam}$	M ~ 0,05	M ~ 1,8
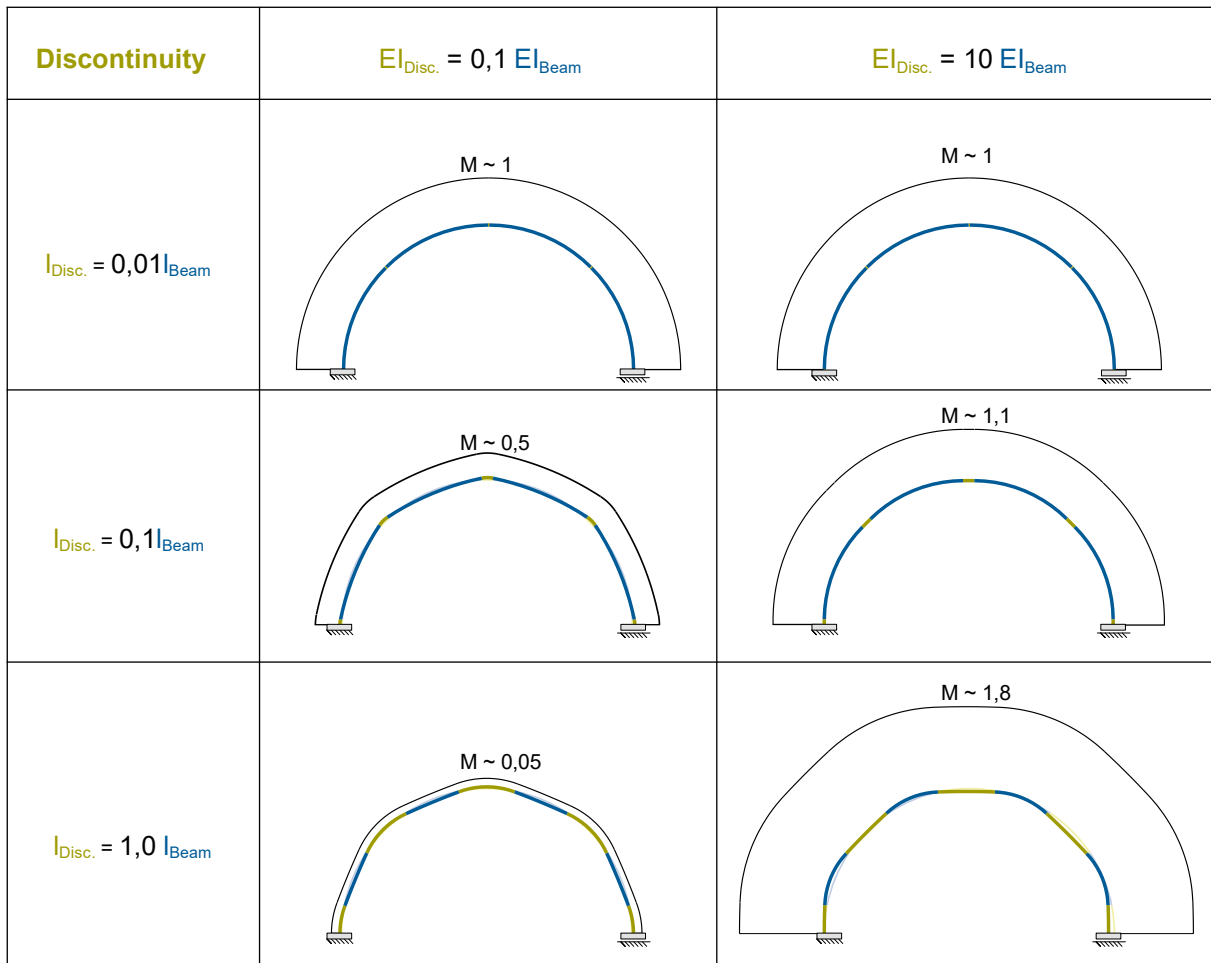
Figure 103 Local stiffness discontinuities on a circular bent beam. The length of the discontinuity is changed from 1% to 10% to 50% of the total beam length (rows). The local stiffness is either softened to 10% (left column) or stiffened to 1000% of the beam stiffness (right column). The results shown are calculated using the IGA inverse method.

The curvature concentrates in areas of relative softness, that are either located in areas of softer discontinuities (left column) or beam segments (right column). With increasing length of discontinuities, the polygonising effect is rising. The constant bending moment is affected, too. It is either de- or increasing according to the global beam stiffness.

From those mechanical relations, practically relevant statements can be summarized:

- If the stiffness of bent beams is discontinuous for a short range only, both shape and bending moment are barely affected. However, the load-bearing capacity of the discontinuity needs to be verified. Example: Perforations such as slots or holes are short. On a bent beam, the perforated areas need to resist the same bending or torsional moments as unperforated areas. This is a matter of strength, not of stiffness.

- If the stiffness of bent beams is discontinuous for a larger range, both shape and bending moment are affected. Softer discontinuities (e.g., long notches) accumulate curvature locally, leading to globally lower bending moments. Stiff discontinuities, such as additive components, plates, etc. lead to a shift of curvature into remaining beam segments. Bending or torsional moments are rising, including the stress on additive components.

4.1.4 The Engineering Process

The development of the engineering process for load-bearing structures began centuries ago and is still ongoing with rising project complexity. Structural engineering is a process. It is characterized as an *"iterative, dynamic optimization with increasing concretion and changing goals in a decentral environment"* (Ihde, 2018). With each iteration, the structure becomes less abstract, and more specific. Iterations are necessary to handle various dependencies that exist throughout the planning sub-processes. This is a general characteristic of structural engineering, that becomes even more significant for compliant structures with their additional requirements (see 4.1.1).

For the design of compliant grid structures, an iterative workflow is developed in course with the case studies shown in chapter 4.2 and 4.3. Key processes and data are organized in an integrated parametric modelling process to efficiently handle the highly iterative character (see chapter 2.3.1). Although the key processes are organized linearly, variable recursive steps are possible and necessary. According to the specific project, the order of processes may even vary. Each process generates data, to be evaluated and integrated into a model environment that integrates and couples geometric and mechanical models. This design process is inspired by the "CAD-integrated Parametric Design Cycle for Structural Membranes", mentioned in chapter 2.3.1.

In the following, key processes, data, and referred models are described chronologically. A systematic overview on this workflow is given in Figure 104.
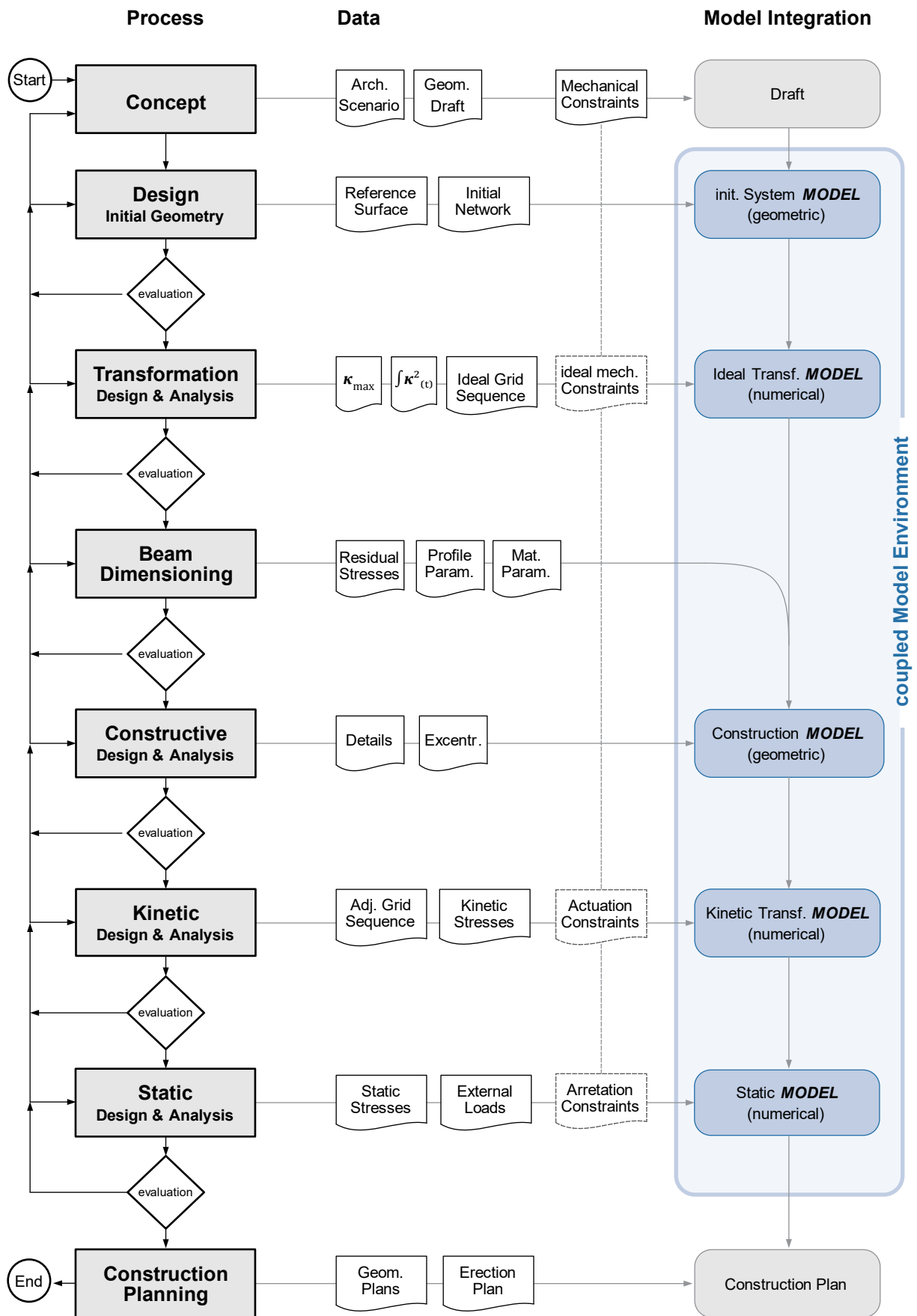
Figure 104 *Engineering workflow split into process, data, and model integration lane.*

Concept

In this first step, an architectural idea is developed that takes advantage of semi-compliant grid mechanisms. This architectural scenario goes with a geometric draft of the structure and a proposed transformation. This concept includes the type of kinetic grid transformability and hereby, mechanical constraints are defined at an early planning state.

Formfinding

Based on conceptual drafts, the reference surface of the curve network, that defines the grid structure needs to be generated. The surface can be defined using geometric operations according to the surface type (e.g., curve rotation for a rotational surface), or using numerical operations for surfaces such as minimal surfaces, hanging shapes, that involve superior geometric constraints (e.g., constant gaussian curvature). Based on this, the network can be found using again geometric operations (e.g., surface-plane intersection) or numerical operations for curves that involve superior geometric constraints (e.g., curvature networks). In addition, the networks density or specific curve locations need to be defined.

The reference surface and referred network are components of the geometric "Initial System Model".

Transformation Design and Analysis

This process aims to find an ideal transformation sequence. Therefore, a numerical simulation is performed. The "initial System Model" is supplemented with ideal mechanical constraints. Although this sequence involves kinetic transformation behavior, mechanical constraints are defined in a relative context. Using numerical methods, such as FEM or IGA, geometric constraints such as zero curvature can be expressed with relative high stiffness exemplarily. The transformation can be controlled via predefined displacements. Such simulations are performed in section 3.2.2 and 3.2.3. From the resulting ideal transformation sequence valuable geometric information can be derived: The curvature-square progression and maximum curvature values are decisive for beam dimensioning.

The ideal transformation sequence is part of the "Ideal Transformation Model". In a coupled model environment, it is connected to the "Initial System Model", and thus, can be efficiently updated. This model provides preliminary insight into the system's transformation.

Beam Dimensioning

In this process, the beams are dimensioned on section level, aiming at requirements on deformability and stiffness only. In contrast to conventional beam dimensioning, where internal forces and bending moments are to be resisted, this dimensioning aims to accommodate maximum curvatures (deformations) within transformation. Some strategies and relations are given in section 4.1.2. It is crucial, that beam's local stiffness relations meet the proposed mechanical concept.

To allow additional stresses, e.g., due to normal forces in a static state and stresses due to external loads, additional profile capacities are necessary.

Furthermore, the strain energy progression can be "tuned" approximately, using the curvature-square diagram from the ideal transformation sequence. This is relevant for the design of actuation.

The process of beam dimensioning at section level can be performed analytically and does not involve any specific model. However, the resulting profile and its' dimensions are part of the geometric "Construction Model".

Constructive Design and Analysis

Constructive criteria may influence the kinetic behavior of semi-compliant grid mechanisms. Especially the design of node details may involve eccentricities or lead to kinematic limitations. This planning process cannot be automated. It involves conceptual development at detail level. Some concepts are given in section 4.1.3.

With resulting eccentricities, the "Initial System Model" and "Ideal Transformation Model" can be updated, and detailed components can be integrated in the "Construction Model". Note, that if the "Construction Model" is parametrically adaptive to the ideal transformation sequence, collision checks are possible.

Kinetic Design and Analysis

This process aims to comprehensively simulate the structure's transformation with respect to applied profiles, materials, self-weights, details, and actuation. The "Kinetic Model" is based on the "Ideal Kinetic Model", but specific profile and material parameters are applied. It allows precise numerical simulation and testing of various actuation concepts. The kinetic behavior is analyzed, including normal forces and stability effects. Deflections or deviations from the "ideal Kinetic Model" are evaluated.

Static Design and Analysis

Transformable structures in architecture serve as static structures at specific states, in which mechanical constraints are active for locking. In these states the structure is exposed to external loads such as wind, snow, or other service loads. The static design and analysis is analogous to conventional engineering of load-bearing structures. From the "Kinetic Transformation Model" specific static states are extracted and the additional locking constraints and external loads are be applied. The load-bearing behavior is analyzed, stresses and stability phenomena are evaluated.

Construction Planning

Basis of the construction planning is the "Construction Model". From this model, fabrication data and construction plans are extracted, and the assembly process is developed.

4.2 Case studies on Asymptotic Gridshell Erection

Semi-Compliant mechanisms can be utilized to erect strained gridshells. The spatial, doubly curved geometry of gridshells can be incorporated within the structure, and thus, substitutes complex formwork. Asymptotic gridshells allow the erection from a planar state.

In the following sections, three projects are presented that incorporate the erection of asymptotic gridshells from a planar state with focus on key facts and aspects regarding construction, kinetic behavior, and numerical analysis.

4.2.1 The Inside\Out Pavilion

The **Inside\Out** pavilion is located at the campus of the *Technical University of Munich (TUM)*. It was built in 2017 and serves as a research pavilion as part of Eike Schling's studies on repetitive structures. The modelling and design were supported by Denis Hitrec. The authors personal involvement included the static analysis and consultations for detail development. The construction was intensively supported by *BRANDL* metal manufacturer. This project is well published (Schikore et al., 2020; Schling, 2018; Schling et al., 2017; Schling, Kilian, et al., 2018).

Design and Construction

Figure 105 *The inside\Out pavilion at TUM Campus, Munich: a) View of the pavilion, b) Node detail, c) Free edge beam and c) Singularity (Photos: Felix Noe)*

The *Inside\Out* pavilion is built from straight, slotted stainless steel lamellas (100x1,5 mm), paired in one layer, and eccentrically braced by cables. Figure 105a shows the pavilion and details. The gridshell is based on a minimal surface, which incorporates an asymptotic network with nodes of 90 degree. The reference surface is a cutout from a modified catenoid, and the asymptotic network incorporates two singularities.

Structural Analysis

The static analysis required some unusual approaches. Due to the geometric complexity of the actively bent grid, the simulation from an initially straight and unstressed configuration would involve extensive effort regarding mechanical modelling. Such approach would require an additive simulation, where each member is separately deformed an attached to the structure. This problem motivated the development of the inverse FEM, described in section 2.3.2. The conventional FEM Software used[1], features dimensioning or loading tools, that are practically valuable for static analysis:

Residual shear stresses due to torsion

Residual normal stresses due to bending
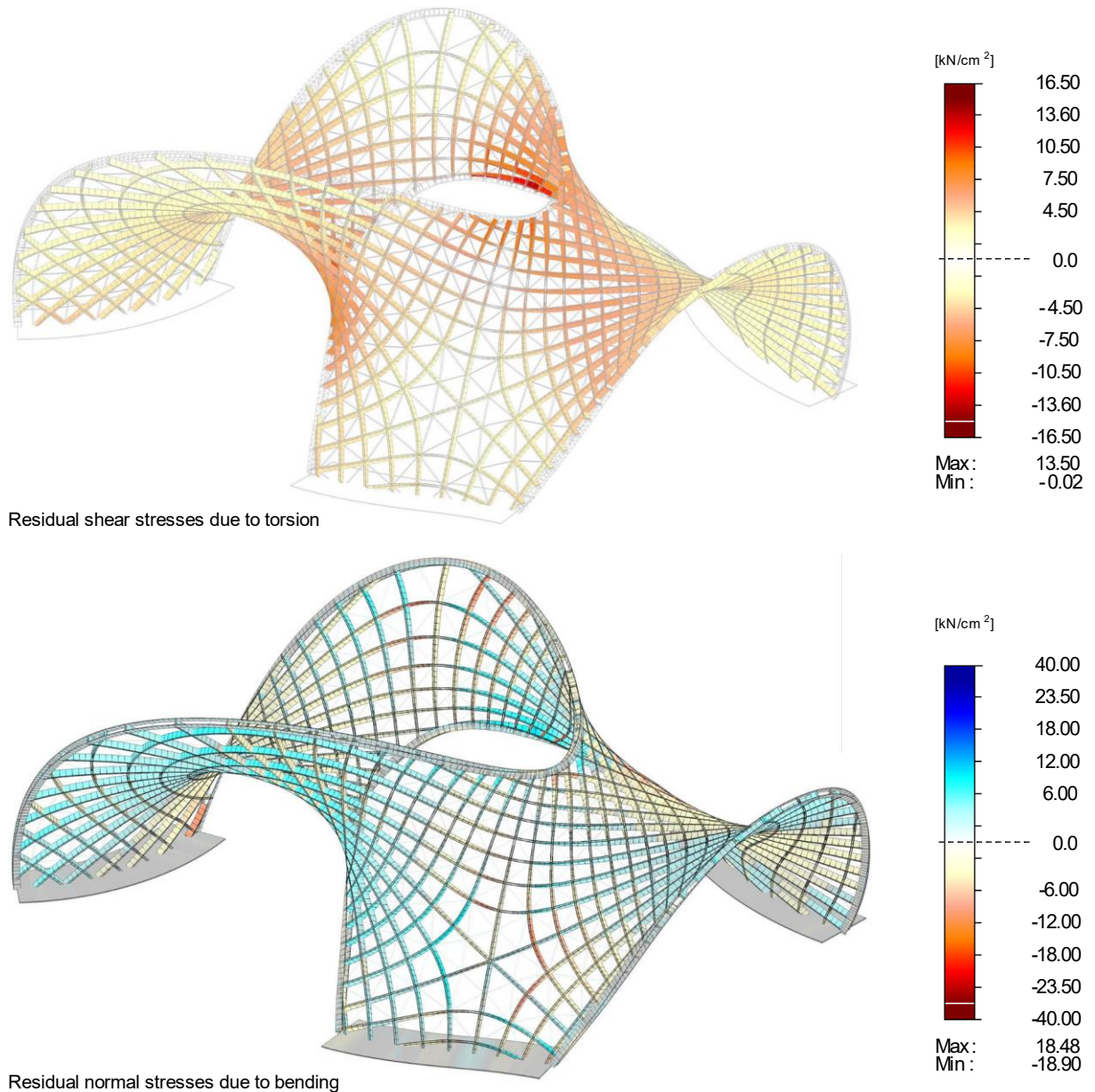
Figure 106 *FEM "inverse" simulation of the Inside\Out pavilion: Residual normal and shear stresses caused by bending and torsion*

Figure 106 shows the residual normal stresses and St. Venant torsional shear stresses. For the stainless steel used, the strength of a standard reference steel S235 (σ_{Rd} = 23,5 kN/cm^2) is used to evaluate the static performance. The maximum utilization of normal stresses

---

[1] *For this project, R-FEM 5 was used.*

(residual stresses) due to deformation results to ~80 %, and shear stresses are utilized by a maximum of about 99 %. However, these maxima occur on singular spots only and plastification is accepted to a very limited extend. Note, that bending and torsion are reciprocal. Positions of large bending involve low torsion and the other way round. The average utilization due to elastic deformation is in a range of 25 % for both normal and shear stresses at the lamellas' surfaces. The FEM analysis also features plastification at the nodes. At these positions, the internal bending moment is limited to the plastic resistance of the halved lamella profile. This potentially allows kinks and the redistribution of loads through plastification to be displayed in the simulation. However, these effects turned out to be neglectable as occurred on few slots only.

In the FEM calculations, normal stresses due to helix torsion (see section 2.2.3) are not included. Manual calculation for a maximum twist of 64 °/m results to normal tensile stresses at the lamella edges of 22,0 kN/cm^2 that utilize 93 % of the material capacity. Again, plastification is accepted to a limited extend (Schling, 2018, p. 155).

For this project, the kinetic performance during transformation from flat to spatial was not numerically simulated and transformability was physically explored on site.

Assembly and Erection
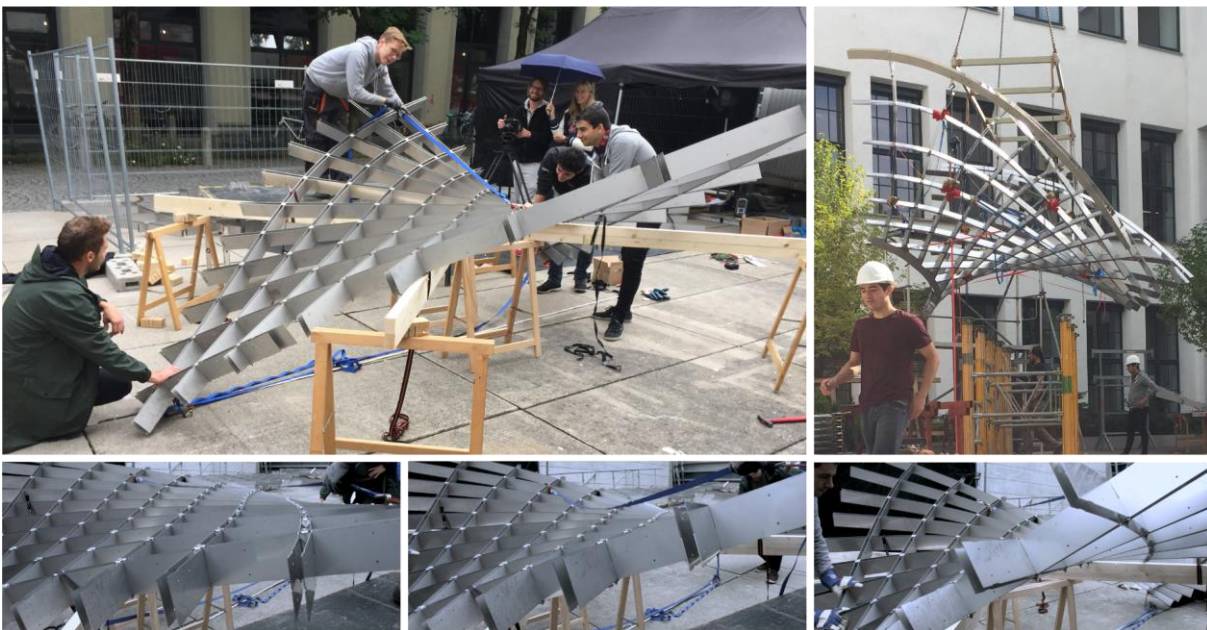
Figure 107 *Curved segments of the Inside/Out Pavilion. The segments are assembled flat and pushed into spatial shape following the design shape naturally. (Photo: Top left and bottom: Eike Schling, Top right: Andrea Schmidt)*

The method of shaping used is the first architectural application of a semi-compliant mechanism for an asymptotic grid. The slotted nodes act as uniaxial hinges to allow transformation. The kinetic behavior shows similar characteristics to the open asymptotic structures (see section 3.2.2, p.68, 3.2.3 and 3.4.1). The mechanism was used to prefabricate nine curved segments, that were assembled flat, hoisted onto suitable supports and deformed by hand. The designed shape emerges naturally, and at final position, the structure is locked. Figure 107 shows the construction and segment deformation. The kinetic performance in this project motivated further research, including this work.

4.2.2 Hotel Intergroup Canopy

The **Hotel Intergroup** in Ingolstadt was completed in December 2019. The entrance canopy is the first commercial asymptotic gridshell. It was designed by Eike Schling and engineered by Jonas Schikore, including dimensioning, official proof of stability and erection simulation and planning. The project was managed, consulted and constructed by *BRANDL* metal manufacturer. There are few publications referring to this building (Anna Maria Bauer, 2020; Schikore et al., 2019; Schikore et al., 2020).

Design and Construction

Figure 108 *The Hotel Intergroup canopy (before membrane assembly): a) Front view b, c) Edge beam detail, d) Concrete foundation*

Figure 108 shows the structure just after placement on site. The canopy is compounded by four symmetric leaf-like, framed grid-segments (a). The grid is bounded by a rectangular frame on top, that adapts to the entrance courtyard (b, c). At the bottom, the structure is supported by two slender concrete foundations (d).

The design of the funnel shaped grid structure requires careful geometric modelling of the reference surface with its connected asymptotic network. The geometric modelling was performed iteratively by Eike Schling until geometric design criteria were fulfilled. The design goal was a horizontal finish of the grid in the top part, a smooth and elegant curvature of the surface and a rather vertical directed network at the bottom. Edge details and additional constructive components adapt to this geometry. The key modelling steps are shown for a single segment in Figure 109.
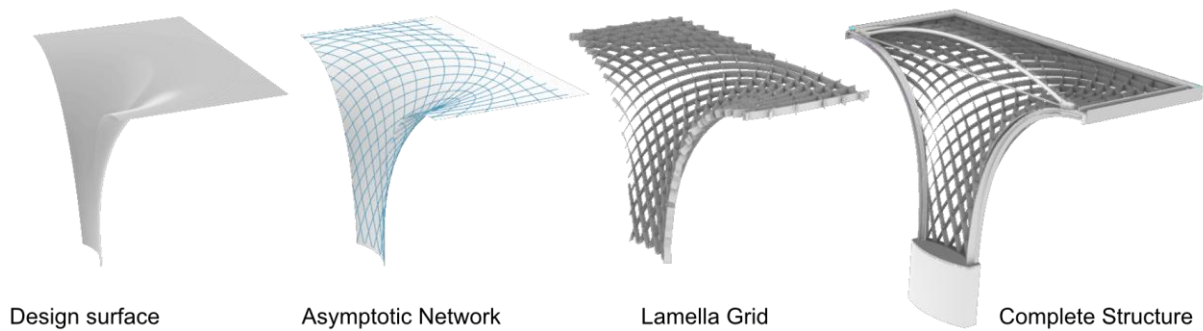
Figure 109 *Geometric modeling of the Hotel Intergroup Canopy. The "Design Surface" is the reference surface for the asymptotic network and lamella orientation. The frame and additional components are adapted.*

The complete canopy covers a rectangular area of 42,5 m² at a height of 3,7 m. The steel structure is composed by 2,5x100 mm stainless steel lamellas that are framed by a steel box profile that integrates water drainage. The lamellas are slotted at nodes to a allow a single-layered configuration. After assembly and erecting, the slots were welded. The top frame anchors a PVC membrane that is tensioned using a steel arch tube. The arches ends are connected by a tensioning cable used to elastically lift the arch through bending like a bow string. The lamella grid is made of stainless steel, comparable to S355 in strength. Figure 110 shows the structural components and dimensions.
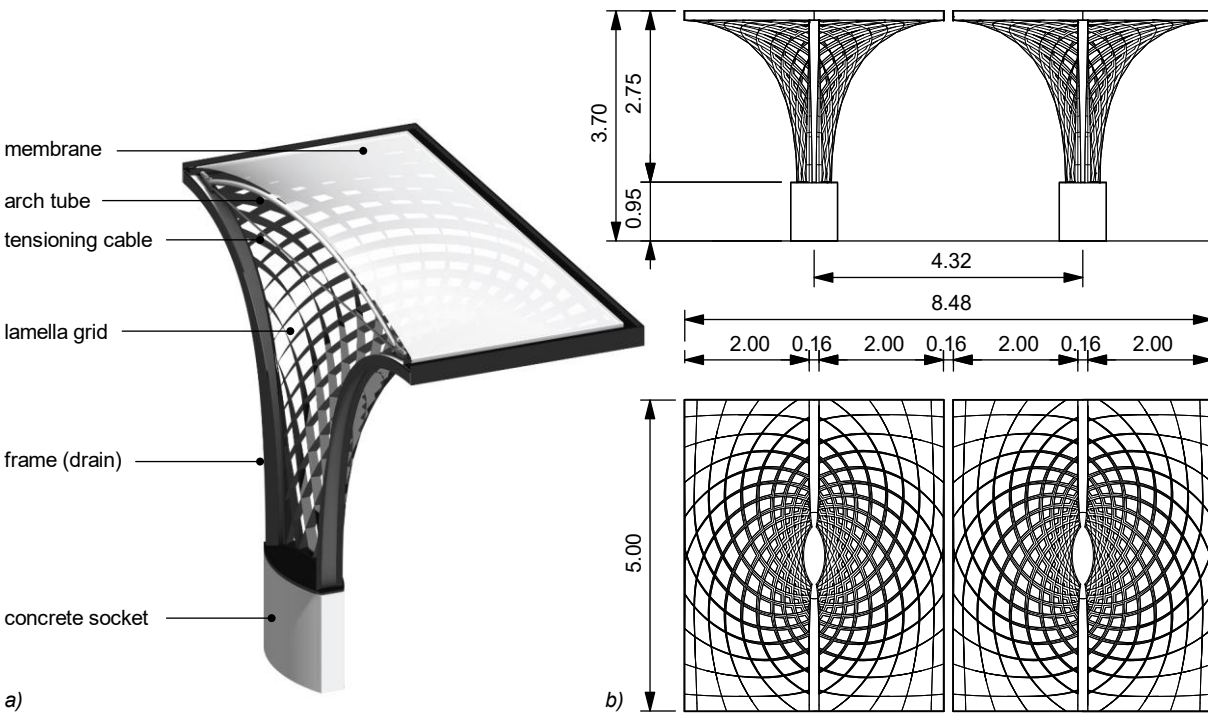
Figure 110 *Structure of the Hotel Intergroup canopy: a) structural components, b) dimensions*

Structural Analysis

In context with this project, analytical and specified numerical calculations were applied to predict and evaluate residual stresses and strain energy through deformation, the erection process, and the static performance. The numerical methods are based on both conventional FEM and IGA. Detailed descriptions of the methods used for the following investigations are given in section 2.3.2 and various publications (Anna Maria Bauer, 2020; Schikore et al., 2019).
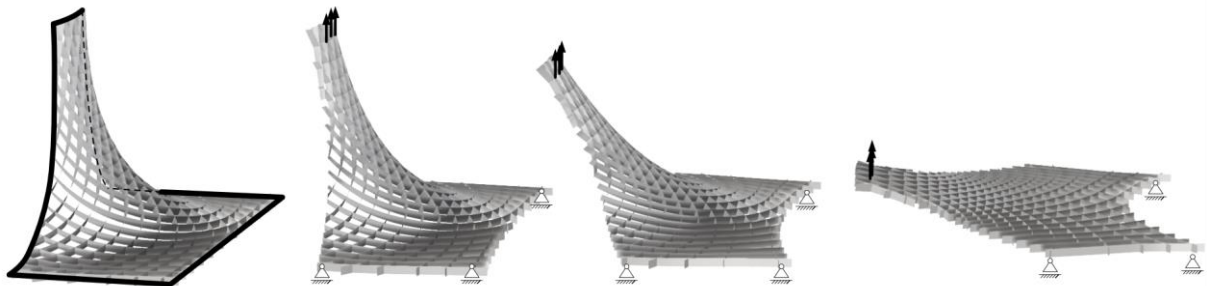
Figure 111 Backwards simulation of the canopy segment erection using IGA "inverse" method and shell elements.

In the first step, the transformation into a flat configuration is simulated and tested. Through this analysis, transformability was evaluated and decisive curvatures and twists at all states of erection are identified for dimensioning. Furthermore, the flat configuration informs the assembly. In practice, the lamella grid was transformed upside down by lifting three nodes at the canopies bottom in upward direction. The slotted connections were acting as uniaxial hinges. However, the simulation was performed in backwards direction, starting from the deformed state.

The IGA-"inverse" method with shell elements was used for this simulation (Anna M. Bauer et al., 2019). First, the residual stresses, computed by the shell's curvature, are applied. Then, without fixed edges, the vertical position of three nodes is released stepwise until the grid is planar. Figure 111 shows the simulation setup and result. The spatial (initial) state shows the highest curvatures and twists within the transformation process. The max. geodesic curvature $\kappa_{g,max}$ is 72 °/m and the max. geodesic torsion $\tau_{g,max}$ is 55 °/m.

It is a decisive design goal, to create smooth curvature, and thus, plastification was avoided or at least, kept under control. The slotted connections at nodes are most likely to plasticize, and detailed investigations on this are necessary. However, the slotted discontinuities are small, and thus the bending moment and curvature is barely affected, assuming, that also the slotted areas are within the elastic range (see section 4.1.3, p.116). This allows a simplified check on plastification: Using Equation 12 with $\kappa_{g,max}$, the max. bending moment at not perforated beam segments results to 3,3 kNcm. At slotted areas, this bending moment exceeds the elastic bending capacities, and the beam plasticizes, and causes kinks. However, this plastification only occurs at few nodes and is accepted. Thinner lamellas were not chosen due to difficulties for welding and higher risk of stability failure. This compromise underlines the thin line for dimensioning compliant steel grids.
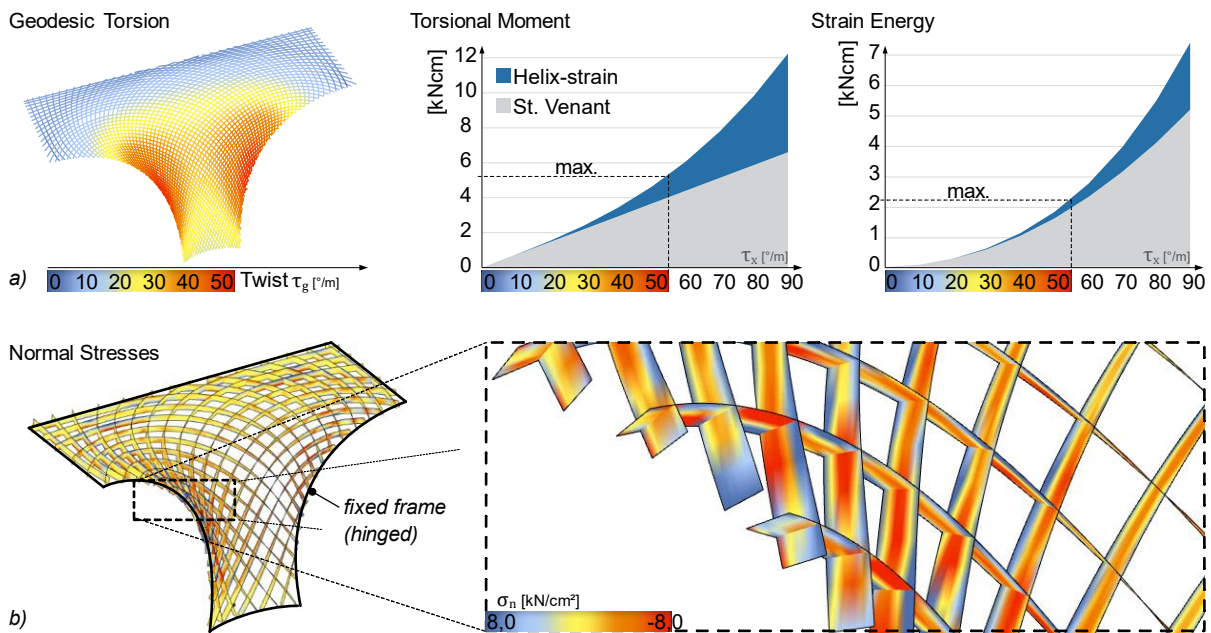
Figure 112 Analytical investigation: a) Geodesic torsion of the asymptotic network, and torsional moment and strain energy portions due to St. Venant Torsion and helix torsion for a 2,5x100 mm steel lamella profile (Schikore et al., 2019) b) Numerical simulation using IGA-inverse method for shell elements

The spatial transformation was analyzed with special focus on torsional stresses, moments, and energies, that are compound by shear and longitudinal stress due to St. Venant torsion and helix torsion effects respectively. The question arose, to what extend lamella torsion influences the erection process, e.g.: How the grid must be constrained and fixed for erection?

The influence and portions of torsion can be determined using analytical calculations described in section 2.2.3. For the *Hotel Intergroup* and the lamella profiles used, the geodesic torsion, the torsional moments and strain energy are displayed in Figure 112a. The maximum torsion of 55 °/m results to a torsional moment of 5,37 kNcm, and 24 % refer to helix torsion. For torsional strain energy, helix torsion makes a portion of 14% of the total torsional energy (86 % St. Venant). As these ratios may not be neglected, a novel "inverse" approach was used to consider helix torsion within numerical investigations for erection (Anna M. Bauer et al., 2019). Shell elements were used to determine the normal stress distribution across the lamella profile due to helix torsion. Figure 112b shows the normal stresses at neutral layer at final state with a fixed frame[1].

The final static analysis was performed using conventional FEM[2]. In this state, the grids nodes are rigid, as the slots were welded. Residual stresses are considered according to the "inverse" FEM-method (section 2.3.2). This analysis includes external loads such as snow, wind, etc., and the results were used for official approval. Note, helix stresses are not displayed in this method and must be considered externally (manually).

---

[1] Note, the stresses displayed are at the inner layer and thus exclude stresses due to weak axis bending
[2] Dlubal R-FEM5

Assembly and Erection

Figure 113 Erection the Hotel Intergroup canopy: a) Pull up of a grid segment, b) Assembly of edge components, c) Framed segment in final shape, c) Lift and transportation of the full steel structure

The segments were designed for an inverted "pull-up" strategy and assembled separately. The stainless-steel lamellas were interlaced via slots and temporarily secured with brackets (Figure 113b). Each segment was then pulled-up by a crane into its design shape. This process originates to an inverted hanging model but involves a compliant mechanism. In shape, the grid was fitted within a rigid steel frame and then welded at each joint (Schikore et al., 2020). The four segments were finally assembled on site to become one structural unit. The steel structure is fitted with two arch supported membranes on top. Figure 113a shows the assembly and the erection process with a similar strategy to the *Inside\Out* pavilion. After welding and edge assembly, each segment becomes a stable unit (c). The final steelwork was mounted in one piece (d).

4.2.3 Asymptotic Timber Vault
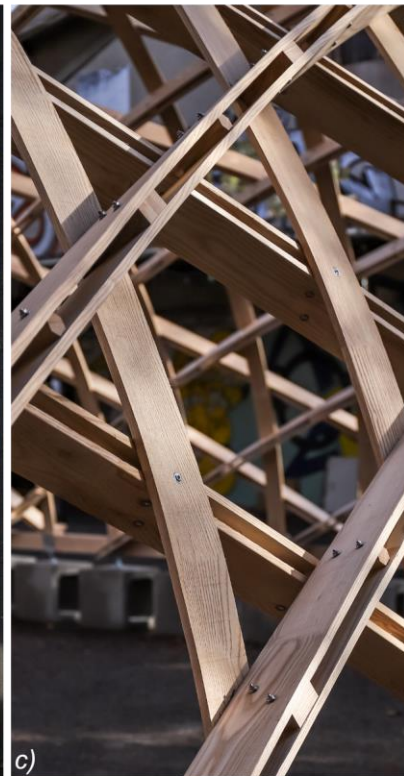
Figure 114 *The Asymptotic Geodesic Timber Vault: a) View of the structure without cladding, b) Top view, (asymptotic curve set), c) Detailed view of the grid (web), including asymptotic ("upright") lamellas and geodesics ("flat") lamellas d) Shaping the grid structure from flat to spatial. e) Prefabricated curved, doubled lamellas.*

The **Asymptotic Geodesic *Timber Vault*** in Munich was conducted in 2022 at the *Kreativquartier* in Munich. The project is led by Eike Schling and Zongshuai Wan in a collaboration of the *Hongkong University* and the *TUM* (Prof. Pierluigi D'Acunto). Jonas Schikore was incorporated in a consulting role. The project was part of the educational master program (architectural).

Three modules are arranged to create an accessible pavilion. The combination of anticlastic patches creates the impression of a vault-like, synclastic structure (Figure 114a,b).

The modules are made from double layered timber lamellas (ash). The timber web systematically combines both asymptotic and geodesic curves. The resulting web is triangulated. All members and components are assembled completely lateral (Figure 114c, see also section 4.1.3, Figure 100b).

During construction, the asymptotic paired and curves beams are mounted planar on the ground. The shape emerges naturally when the grid is lifted and carefully pushed into shape (Figure 114c). The spatial geometry is locked when the geodesic, triangulating set of lamellas are attached.

The Asymptotic Timber Vault involves several engineering strategies, discussed in previous sections:

- With the set of geodesics, the buckling length is halved, thus rising local buckling capacities (see section 3.3.2).

- The grid structure combines layering in surface normal direction (three layers, two asymptotic layers and one geodesic layer in between), and offsets in bi-normal direction (doubled lamellas). Thus, continuous members are possible (see section 4.1.3, p.113).

- The grid members are interconnected using adapters and eccentric bolts. Thus, the impact of discontinuities is kept minimal (see section 4.1.3, p. 116)

- The edge beams and geodesics are locking the grid in its final shape. This can be referred to "internal" locking. The actuation, however, is performed manually by hand, and can be referred to "external" actuation. This is typical for non-reversible mechanism, used for erection.

The grid is transformed from flat to spatial, using initially curved, double layered members. This incorporates stiffness, that allows only limited deformation. Furthermore, the nodes are not ideal hinges. However, the transformation performs, as only limited curvature changes are necessary, and the bolted connections include tolerances.

This project demonstrates the usability of timber tor this structural type. The combination of asymptotic and geodesic curves marks a novel geometric approach. The transformability of this combination is hereby tested practically, but not fully investigated in theory.

4.3 The *Kinetic Umbrella*

Figure 115 *Side- and topview from open (left) to closed state (right) of the "Kinetic Umbrella" at the Kreativquartier Munich. (Photos: Martina Schikore)*

The *Kinetic Umbrella* is a transformable grid structure located at the *Kreativquartier* in Munich. It is placed at an outdoor cultural event space and used for shading. The structure is a research project following the principles of "Research by Design" [1]. The goal of this project is the architectural implementation of semi-compliant grid mechanisms at architectural scale. The kinetic structure is derived from the theoretical framework described in chapter 3. The rotational asymptotic grid structure is covered with an adaptive shading system. It performs a reversible semi-compliant transformation from a slender cylindric (closed) to a open funnel shape whenever needed. Figure 115 shows the structure and the different states of transformation.

The following sections provide insight into the developments and final solutions from basic concept to detailing in an iterative process, followed by investigations to evaluate tolerances in geometry and force distribution:

Section 4.3.1 describes concept and components.

Section 4.3.2 displays the digital planning workflow.

Section 4.3.3 shows physical models used within the development and their contribution.

Section 4.3.4 gives deep insight into decisive engineering problems and solutions.

Section 4.3.5 displays the process of assembly and erection.

Section 4.3.6 compares measurements and simulation for validation.

The *Kinetic Umbrella* was managed, designed, and engineered by Jonas Schikore. The project was further supported and consulted by Prof. Rainer Barthel, Prof. Eike Schling and Prof. Pierluigi D'Acunto. The physical modeling was extensively supported by Fabian Matella (Student assistant) and the cover system was developed together with Clemens Lindner and Tao Sun, as part of their architectural bachelor thesis. The construction of the steel parts and the erection (lift up) was conducted and sponsored by the steel manufacturer *BRANDL.* Other sponsors are GEPOTEX GmbH (textile fibers) and *FACTUREE cwmk GmbH* (aluminum components at nodes). On site, the assembly was supported by a team of students and assistants: Merlin Bieling, Frederic Chovghi, Sebastian Dietrich, Sebastian Hoyer, Clemens Lindner, Maria Rau, Fabian Matella, Sanziana Maximeasa, Sarah Sendzek, Tao Sun, Frauke Wilken

---

[1] *The term „Research by Design" goes back to the Faculty of Architecture in Delft (Technische Universiteit Delft (2001))*

4.3.1 Design and Construction

This section shows the basic concept of the *Kinetic Umbrella* and systematically describes all structural components.

Concept

The general idea of an umbrella, to protect from sun or rain, goes back to ancient times (Sangster, 1871). Structurally, umbrellas are characterized by a central pole, where the structure is supported. Umbrellas may be classified by their portability or their ability to deploy. There is a wide range in sizing, and there are various mechanical approaches for deployment. (Figure 116: e.g.: transformable membrane, inflatable, and "origami"-folding).

Figure 116 *Various Umbrellas utilizing different mechanical approaches: a) Umbrellas by Frei Otto at the Bundesgartenschau Köln 1971, Photo: Atelier Frei Otto Warmbronn b) Inflatable Umbrellas World Expo, Osaka 1970 (Blümel, 1972) c) Umbrella Study using origami folding (Jaksch & Sedlak, 2011)*

The *Kinetic Umbrella* provides an alternative solution regarding the type of mechanism: A semi-compliant mechanism of a rotational asymptotic grid structure, fixed at the bottoms circular edge. The open funnel shape can be "packed" to a slender bundle. The design is guided by various criteria: The structure doesn't aim at a specific location and thus represents a "stand-alone" object in an architectural sense. The Umbrella fits into medium size courtyards and provides space for a small group of people underneath. Furthermore, the grid structure fits onto standard transportation vehicles or into standard containers. A rather small base radius is considered to minimize the space taken by the structure on site, but still providing stability. The *Kinetic Umbrella* is a movable structure. Accordingly, it is supported via movable weights to prevent from tilting, rather than fixed ground connections.
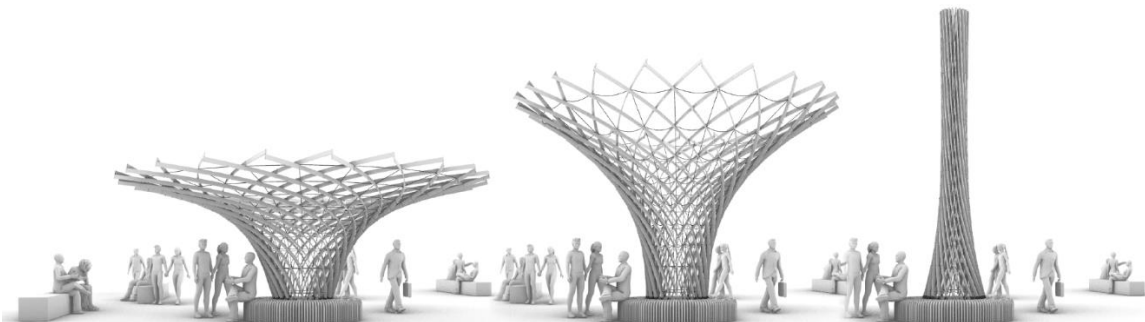
Figure 117 *Visualization of the Kinetic Umbrella conceptual design at open, intermediate, and closed state (Vis.: E. Schling)*

Components Overview

The components of the *Kinetic Umbrella* can be assigned to basic functions: The double layered lamella grid structure serves as load-bearing structure. Its structural parameters define the transformation. The attached textile cover provides shadow and adapts to the grid structure's transformation. Three circular fixed cables are locking the transformation at open state. The transformation as actuated by an additional circular cable, led down to a winch. The steel base connects the structure via uniaxial hinges to the concrete bodies, that resist global tilting. Timber panels covering the concrete bodies and steel base provide sitting accommodation. Figure 118 gives an overview on the components.
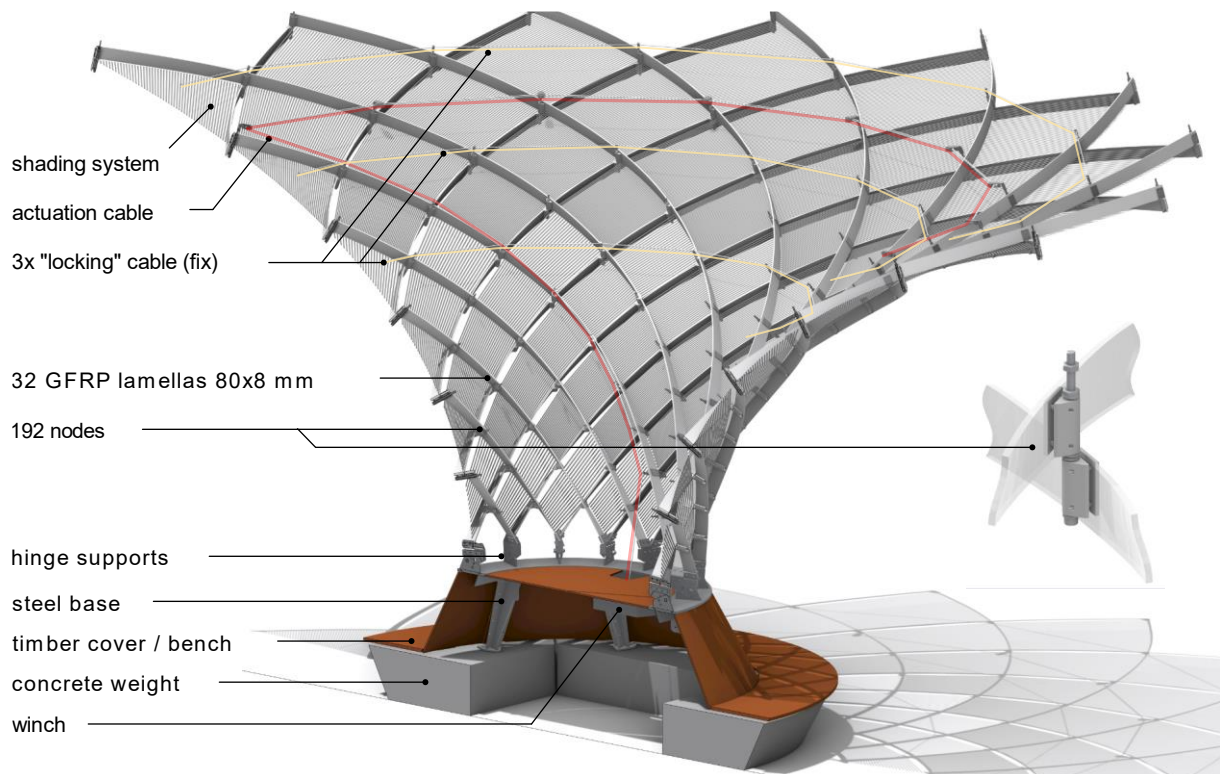
Figure 118 *Overview of the components of the Kinetic Umbrella. (Visualization by S. Maximeasa and M. Bieling)*

Dimensions

The *Kinetic Umbrella* has a diameter of 7,6 m and a height of 3,8 m at open state. Closed, the structure is transformed to a slender bundle of 6,8 m height and 0,8 m diameter. Dimensions are shown in Figure 120.

When the umbrella opens, the area of the reference surface increases from 12,8 m^2 to 50,9 m^2 (~400 %), and at open state, an area of 41 m^2 is covered (projected area).

The following table lists the components masses:

Component	Mass per unit	Pieces/dimension	Total mass [kg]
Textiles	3,7g/m	3017,8 m	11,12
Textile connection plates / bolts	-	-	~ 2
GFRP lamella profile	1,116 kg/m	182,94 m	204,17
Standard node	0,412 kg/p	192 p.	79,1
Ring cables	0,0350 kg/m	45,27 m	1,6
Actuation cable	0,0643 kg/m	(max) 28 m	1,8
Add. Cable/Actuation components	-	-	~ 5
Total (umbrella structure)			**305**
Steel structure base	7,85 t/m^3	0,03 m^3	235
Timber cladding	-	-	~ 70
Reinf. Concrete base	2,4 t/m^3	1,414m^3	3394
Total (base)			**3699**
Total			**4004**

Table 6 *component masses of the Kinetic Umbrella*

Grid Structure
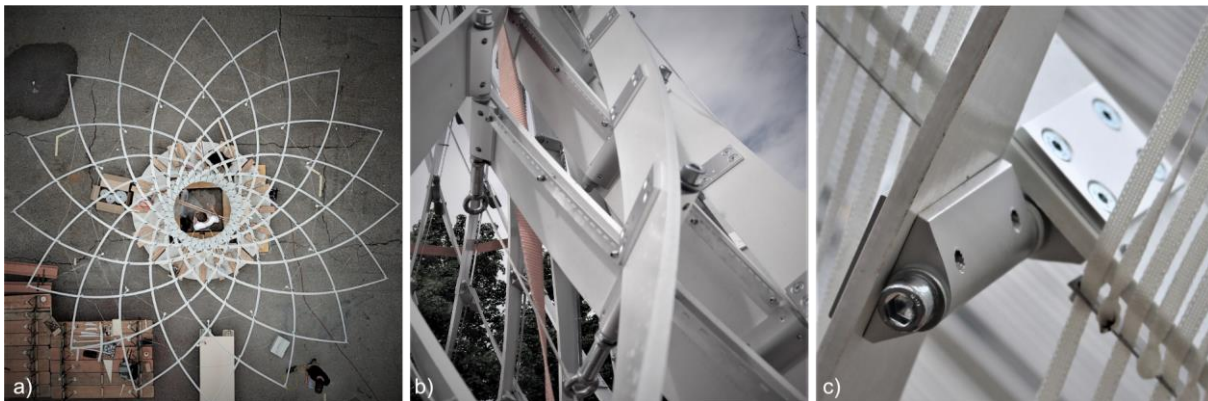
Figure 119 *Grid Structure of the Kinetic Umbrella: a) Detailed view - The bolts are eccentric b) The double layered lamella grid*

The grid is compound of 32 8x80 mm white GFRP lamella profiles of 571 cm length each. These extruded profiles are UV-resistant. The system is rotational symmetric, and all profiles are equal in length and node positions. The grid structure is double layered (in surface normal direction), and the rotational axis of the hinged nodes is eccentric to allow continues profiles.

The node consists of aluminum connectors that are fixed to the lamellas using M6 screws. The profiles are perforated by 4 holes (screws) of 6mm diameter to provide double sided aluminum connectors (adapters, see section 4.1.3, p.116) with clamping effect. These connectors guide eccentric M10 bolts with sleeve bearings to allow rotation and to provide a connection for additional components such as bracing cables or the actuation system.

side view
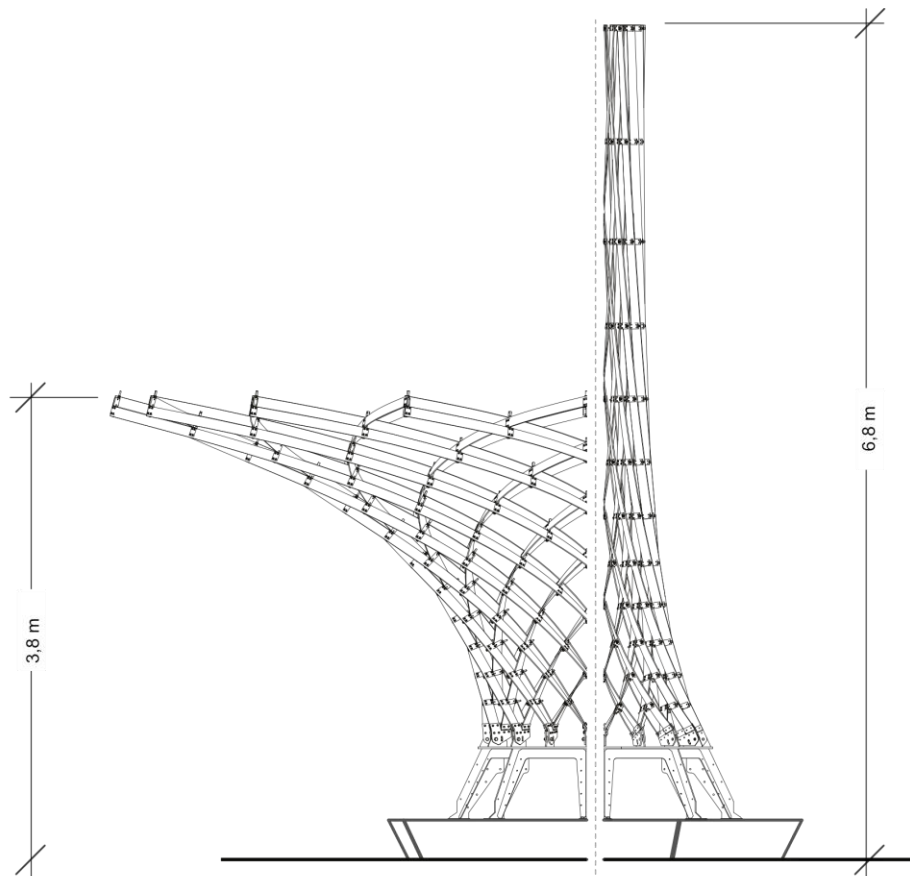
top view
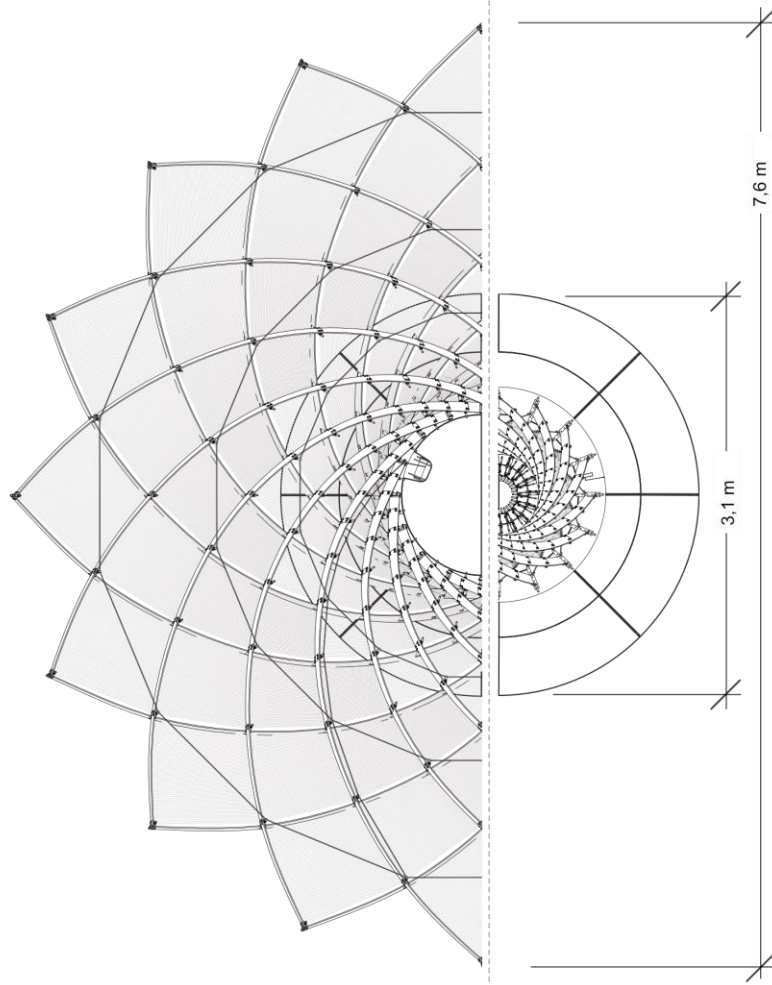
Figure 120 *Global dimensions of the "Kinetic Umbrella": side view (top), top view (bottom), at open (left), and closed state (right)*

137
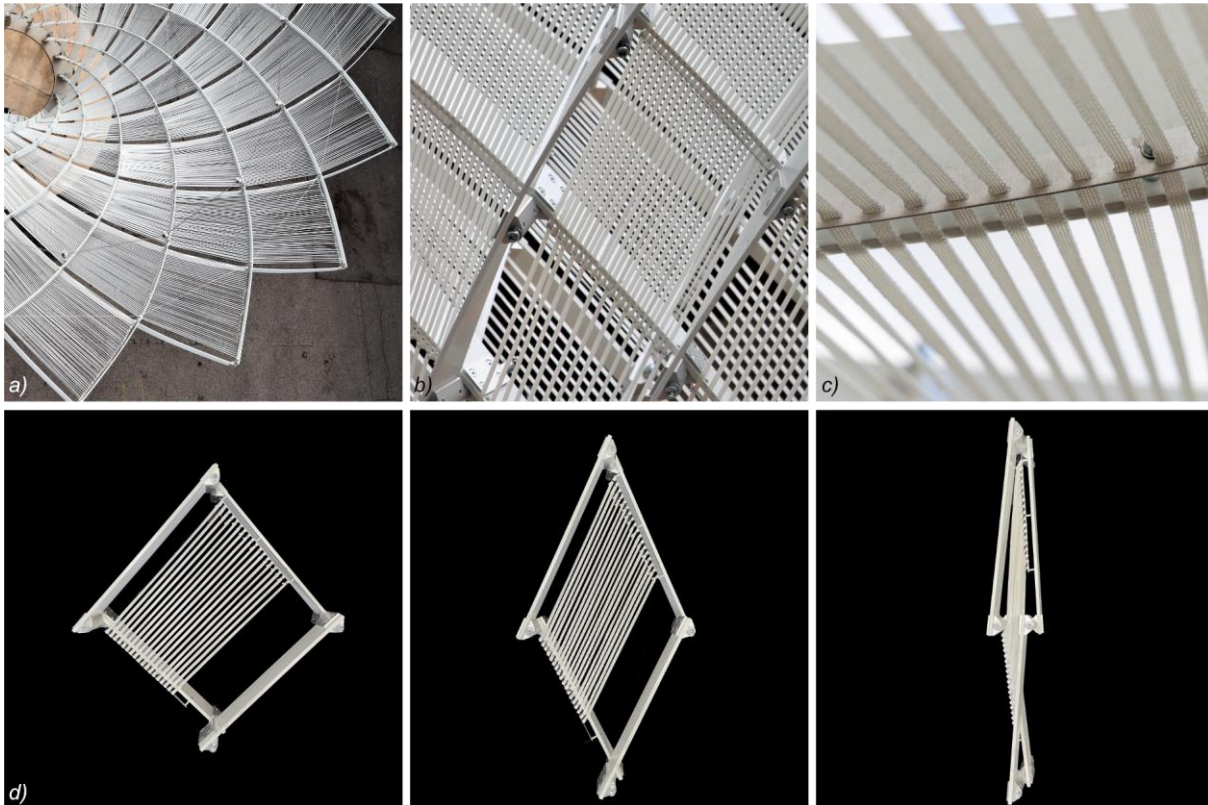
Cover System

Figure 121 Textile cover system layout: a) Pattern (top view) b) Open pantograph cell c) Aluminum profile with slots for fiber guidance d) Pantograph transformation of a unit cell with textile strips attached from open to close (left to right)

The structure is covered by an adaptive shading system. The development of this system is scope of the bachelor thesis of C. Lindner and T. Sun (Lindner & Sun, 2021).

A set of textile strips follows the grid's transformation as these are aligned with the outer set of lamellas. The custom made[1] textile fibers of 5mm width are UV-resistant, hydrophobic, and elastic to a small extend. They are fixed on aluminum profiles, attached to the inner lamella set. These aluminum profiles are positioned eccentric to the lamella profiles, but centric to the hinge axes at the nodes (Figure 121). The fibers follow the pantograph transformation of the unit cells. This configuration allows the use of textiles without folding or overlapping mechanisms. As the strips are guided along the asymptotic path, change in length during transformation only occurs due to tolerances and are neglectable.

The fiber layout follows a parametric pattern. This principle allows to fully control density and shading quality.

Actuation and Locking System

Due to self-weight, the umbrella is pushed into its open state (see section 4.3.4, p.149). The transformation is controlled via a cable system that ties the structure together at closed state and can be released for opening. The cable is winded on a winch located at the umbrellas base (Figure 122a) and guided (b) to a circular cable ring in the top part of the structure (d, e). In this ring, the cable runs in two parallel lines to decrease the cable force (c) (pully tackle).

---

[1] *The strips are sponsored, designed, and fabricated by GEPOTEX GmbH, Emskirchen (GER)*
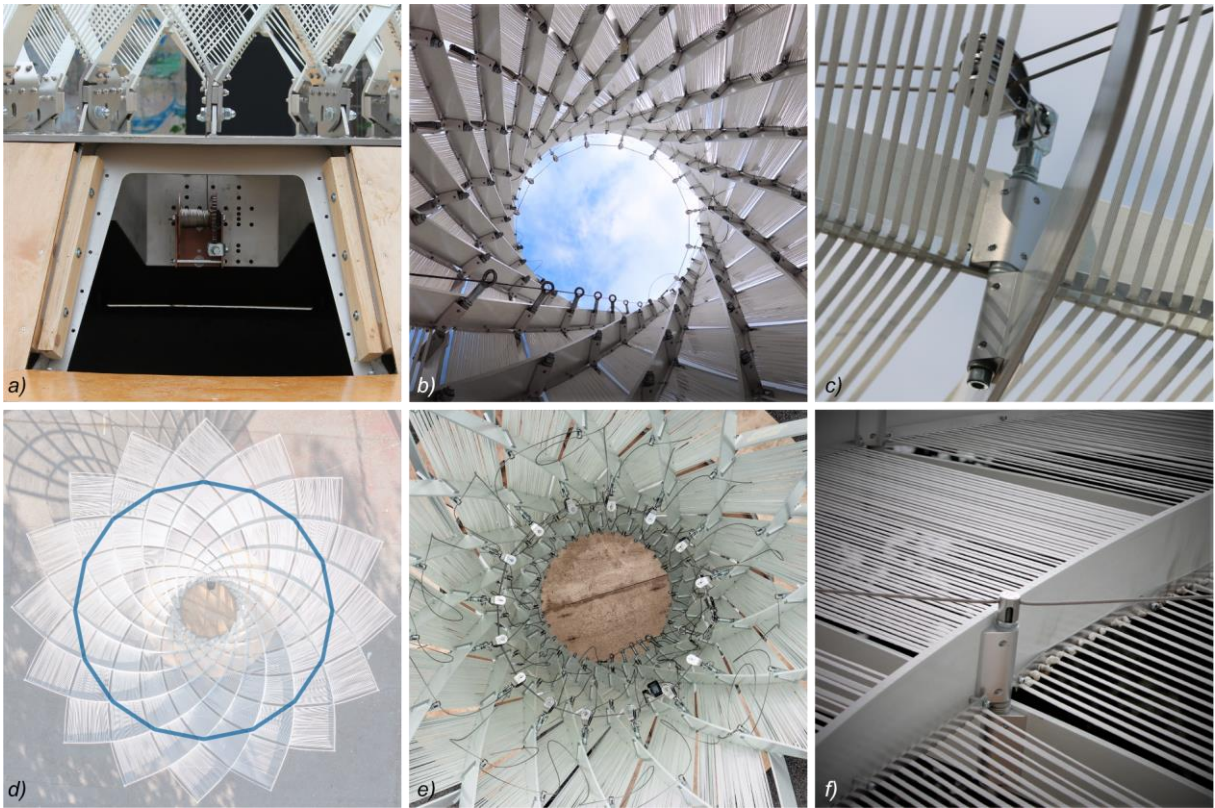
Figure 122 *Cable System for actuation: a) Winch at the base, b) Cable guiding at the grid structure following a lamella to reach the upper cable ring, c) Double pulley for the circular cable guide at an upper grid area d) Location of the actuation cable from top view, e) Inside view with locking and actuation cables at closed state, f) Connection of locking cables at nodes*

At open state, the transformation is locked by three circular cables of 3 mm diameter, fixed at each node in rows 8,10, and 12 (Figure 122f). Closed, the umbrella is tied by the actuation cable, that is held by the worm gear of the winch. Additionally, an external belt can be attached for shutter holdback.

Support (Base)

Figure 123 *Base of the Kinetic Umbrella: a) Concrete bodies and stees support, b) Grid support detail (hinge)*

The *Kinetic Umbrella* is a movable structure and its base can be possibly dissambled and transported. Four concrete bodies prevent the structure from titling in case of horizontal loads. A steel structure, fixed on top of the concrete provides precise support connections for the grid structure. Figure 123 shows the concrete and steel base (a) and grid connection detail (b). At the supports, the lamellas ends are rigidly fixed, but the support allows uniaxial rotation.

The base structure is designed to serve as sitting accommodation, covered with timber.

4.3.2 Digital Modelling

Digital models and tools are necessary to handle the highly interdependent design and iterative engineering steps, as shown in section 4.1.4. In the following, the essential models for planning and analysis are described. Figure 124 gives an overview of these models and modelling steps.

The **Initial Geometric Model** includes the geometric design of the grid at open service state (Figure 124a-c). The reference surface describes the most essential initial design parameters, from where the grid layout and any transformed states are derived using geometric operations or mechanical simulations. For the *Kinetic Umbrella*, a funnel shaped (anticlastic) rotational surface is defined by a rotated curve, (Figure 124a). An asymptotic curve can be found on the reference surface using appropriate algorithms[1] (Figure 124b). On a rotational symmetric surface, an asymptotic network can easily be generated by using simple rotational copy and mirror operations. The orientation of the grid members based on asymptotic curves can be either derived by the curve's curvature or by the reference surface normal, as these matches. The network's density is the only design parameter in this step (Figure 124c).

Network and orientation are the geometric base for the **ideal and kinetic transformation models** (System lines and profile orientation). Adding hinges (DoFs), support conditions, eccentricities and profile parameters completes the mechanical model that was used for ideal transformation and kinetic analysis using IGA. (Figure 124d+e).

The **Static Model** was setup using conventional FEM. To generate the FEM-model, the Initial Geometric Model was meshed, and all mechanical constrains were defined. The analysis was performed for the open state only, as this is the decisive state regarding wind (Figure 124f).

Finally, the geometric **Construction Model** is completed with details and additional components to provide plans for construction (Figure 124g).

---

[1] *E.g.: The Rhino/Grasshopper Plugin "Bowerbird" by Thomas Oberbichler (Oberbichler (2021)*

Initial Geometric Model (geometric)	a) Draw design curve to create an anticlastic rotational reference surface	
	b) Find asymptotic curve on reference surface	
	c) Generate asymptotic network by copy/mirror functions; Find orientation of asymptotic curves normal to the reference surface	
Ideal and Kinetic Transformation Model (numerical IGA)	d) Assembly of mechanical model. Definition of mechanical parameters (Support conditions, hinges, etc.)	
	e) Find states of transformation using IGA simulations	
Static Model (numerical FEM)	f) Assembly of mechanical model for single state static analysis using FEM (including load cases at service)	
Construction Model (geometric)	g) Complete geometric model including details and base to generate plans for fabrication and construction.	

Figure 124 Digital modelling process

4.3.3 Physical Modeling

The development of the *Kinetic Umbrella* went along with various physical models in different scales. These models were used to test the global kinetic behavior and to identify technical challenges. All models are made from GFRP.

Model 1:10 (Concept)

Figure 125 *Model 1:10 of the Kinetic Umbrella with centric hinge axis.*

The first model build is in a 1:10 scale using 8x1 mm lamellas and it is based on a preliminary geometry to test transformation in general. Figure 125a shows the model at closed, intermediate (natural) and open state.

This model proved fluent transformation by actuating two nodes only. This confirms the restriction of the transformation to its predicted path and the quality of the mechanism. The model is double layered and centric hinges are used (Figure 125b).

Model 1:3 (Kinetic Performance, Offsets and Actuation)

The second model was built at 1:3 scale, with a height of ~2 m (Figure 126). The reference surface (including the asymptotic network) and the eccentricities at the nodes exactly reflect the proportions of the built Structure. The model was used to successfully test the performance with eccentricities and to provide an experimental playground for testing actuation or cover systems. The circular cable configuration (see also Figure 136, p. 150) performed fluently, actuated by hand.
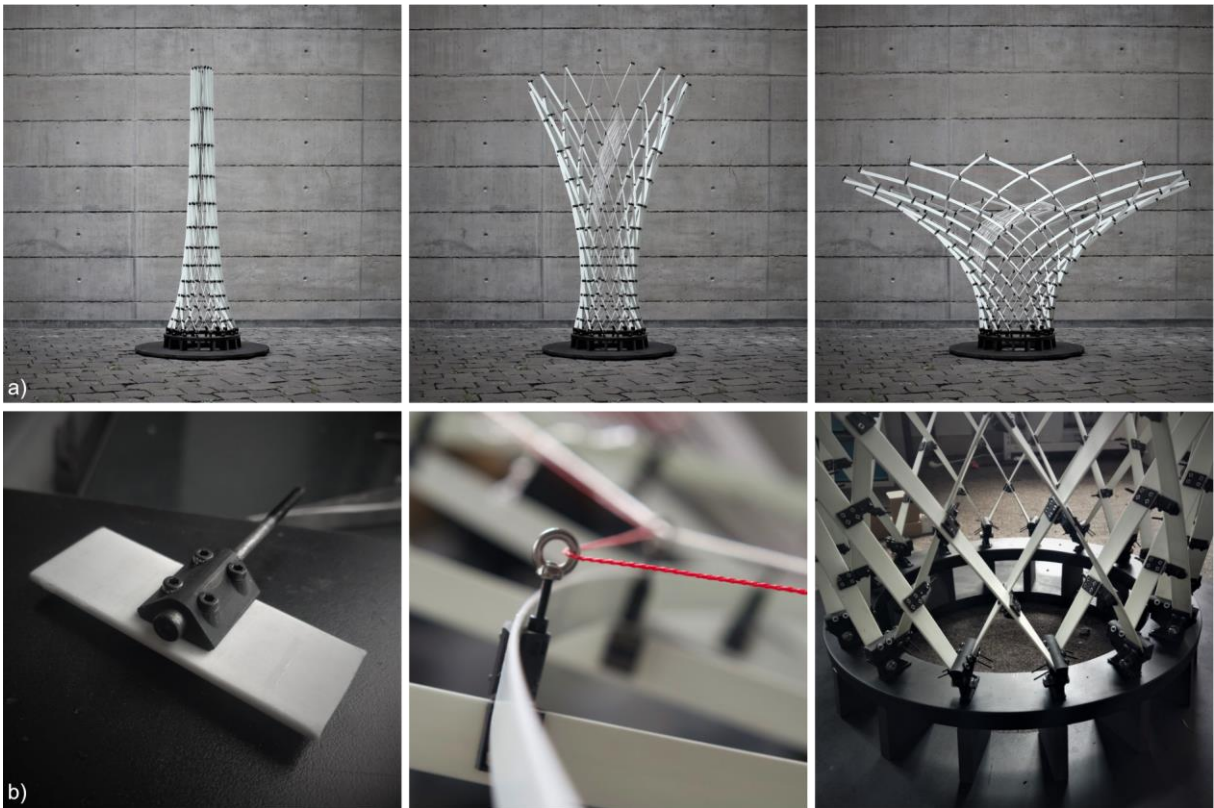
Figure 126 *Model 1:3 of the Kinetic Umbrella with eccentric nodes and final geometry: a) closed (left) to open (right) state of transformation (Photo: F. Matella), b) node detail (left), cable actuation for testing (middle) and supports with uniaxial hinges.*

Model 1:1 (Details)
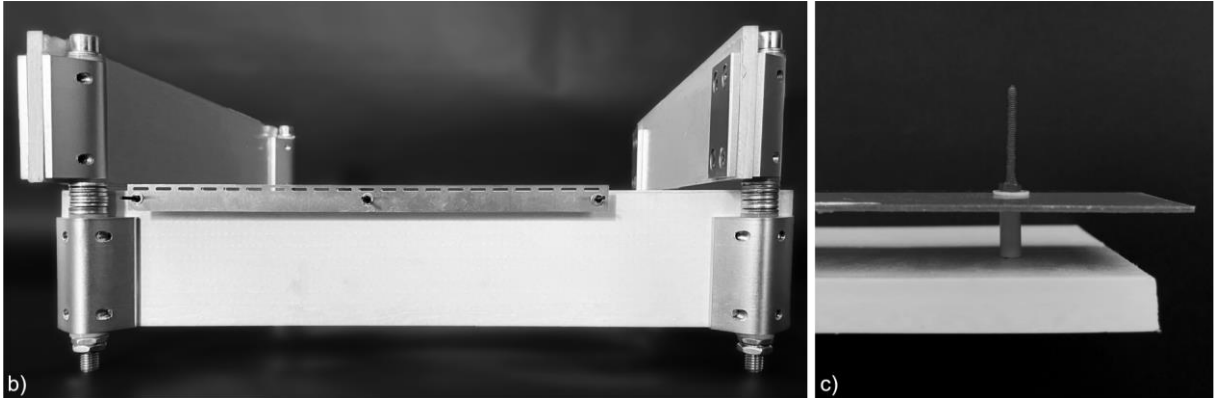
Figure 127 *Unit cell Model: a) pantograph mechanism of the textile adaptive shading system b) detailed construction model c) spacer for eccentric aluminum profile positioning, (Model Setup and Photo: C. Lindner and Tao Sun)*

Several detailed models in scale 1:1 were used to test the assembly, collision, and local performance. The unit-cell-model in Figure 127 tested the nodes and cover systems performance during transformation (see Figure 121d). This model revealed important collision issues regarding the node kinematics and cover system, caused by eccentricities. As a result, the textile strips for shading are located with distinct distance to the nodes, and they offset in bi-normal direction (Figure 127c, and see section 4.1.3 for offset description).

4.3.4 Engineering the *Kinetic Umbrella*

The engineering process of the *Kinetic Umbrella* refers to the workflow described in section 4.1.4. Various analytical and numerical calculations, and model studies were performed iteratively with the goal to find a suitable geometry, profile, actuation system, and suitable details.

In the following, the key processes and their results are described. These are not clearly divided in practice, as they are highly interdependent.

Mechanical Concept and Design

Umbrellas are characterized by a central support and free edges. The ability to deploy refers to the vertically projected area underneath. The rotational types of semi-compliant grid mechanisms provide useful morphologies and promising kinetic characteristics for this application. For the *Kinetic Umbrella*, the rotational "asymptotic" setup was chosen because of two key advantages against the "double ruled" or "geodesic" setup:

- The base circle must not transform synchronic to the top circle and thus allows fixed supports at the base. This constraint restricts the deformability. Furthermore, sliding supports are complex devices and more difficult to handle.

- The "upright" lamella orientation is suitable to stabilize free edges (see section 3.3.1), which suits to umbrella geometries.

The *Kinetic Umbrella* was designed from its open state. The rotational surface is defined by rotation of a "design"-curve. Asymptotic networks were analyzed in real time using a parametric workflow, by modification of the "design"-curve.

The following geometric criteria were set for the initial network design:

- The global proportions must show architectural qualities.

- The open shape must provide reasonable distance to accommodate people sitting or standing underneath.

- The min. and maximum density need to stay in a reasonable ratio. Small internodal distances may lead to constructive problems and large distances may cause buckling. A higher density at the base area is in line with higher normal forces due to self-weight.

- The number of nodes must be in reasonable relation the structure.

- The beams curvatures and twists must stay in a reasonable range to allow elastic deformation.

- The grid's members must be inclined at any location to generate resistance against global torsional deflections.

Figure 128 shows three exemplary design variations of the initial, open state.
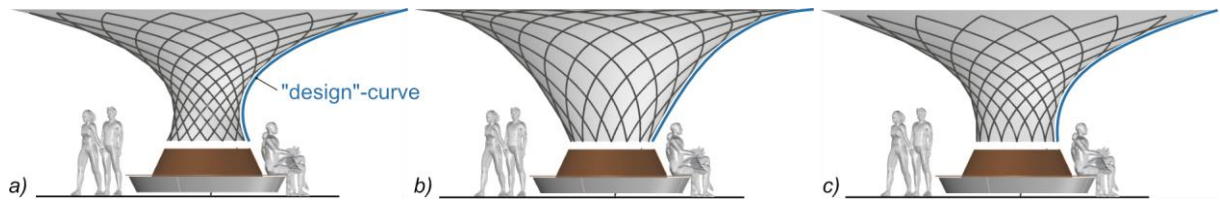
Figure 128 *Variations of asymptotic networks defined by a rotated "design"-curve (blue): a) Waisted shape, b) Conical base shape with curvature concentrated at the top area, c) Vertical and straight start of the "design"-curve at the base.*

The waisted surface in Figure 128a results to a dense network at the bottom area and numerous nodes. In contrast, the variation in Figure 128b results to a more spacious network, but architecturally, an overwhelming impression. Figure 128c shows a design with reasonable density and proportions. In this variation, the "design"-curve is vertical and has no curvature at the bottom, which results to a surface of zero gaussian curvature (developable) at the bottom, and consequently, the asymptotic curves start in the same (vertical) direction, with no horizontal component.
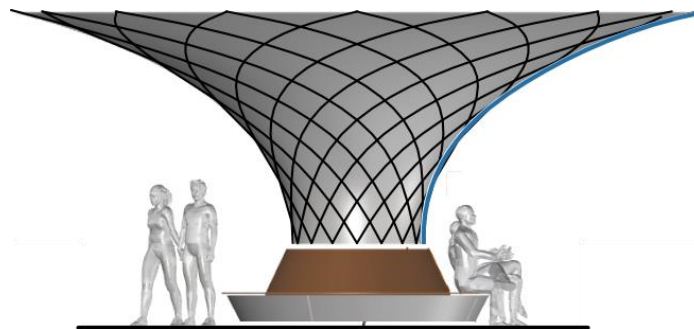
Figure 129 *Final reference surface and asymptotic network layout*

Figure 129 shows the final reference surface and network layout, that satisfies all design criteria mentioned, similar to the variation in Figure 128c, but with an intersection angle $\varphi > 0$ at the bottom, and horizontal force components at any location of the grid.

This study shows the impact of the initial shape on several design criteria. It underlines the importance of parametric workflows to allow iterative design loops, that run from shaping the initial reference surface to detailed design.

Transformation Design and Analysis

The transformation of the *Kinetic Umbrella* was simulated using ideal mechanical parameters for the grid members. The initial, one-layered grid without any offsets and a lamella ratio of h/t = 100/1 was used in this preliminary transformation analysis using IGA (section 2.3.2, p.34). The actuation for this simulation was applied according to the "central" configuration (see Figure 136).
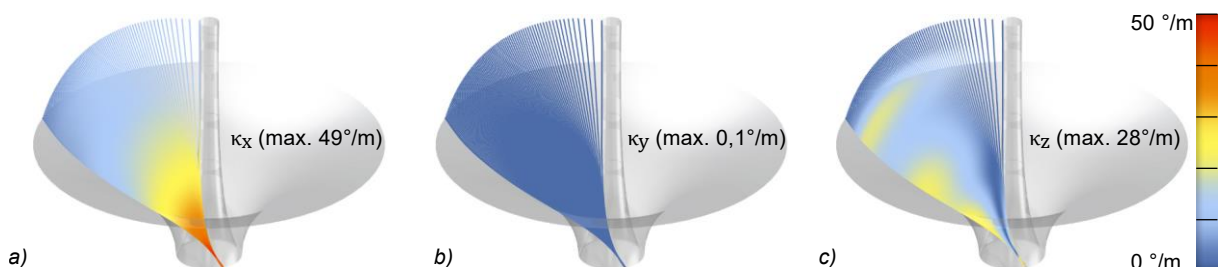
Figure 130 *Curvature analysis of the Kinetic Umbrella at all transformation states: a) Geodesic torsion, b) Normal curvature, c) Geodesic curvature*

145

Due to rotational symmetry, this analysis is valid for all grid members. The local curvatures of a single grid member are displayed in Figure 130 throughout transformation.

Note, there is normal curvature measured, that does not match with the asymptotic definition. However, the value is very small and results from a given stiffness in this axis, which is not infinite but high in relation. Nevertheless, the value is later applied for predimensioning.

The curvature-square analysis maps valuable information regarding the internal kinetic performance during transformation. Figure 131 shows the curvature-square graphs (top) and the graph of the height of the gravity center (bottom). The outer Diameter d of the Umbrella used as a reference parameter to allocate transformation states.
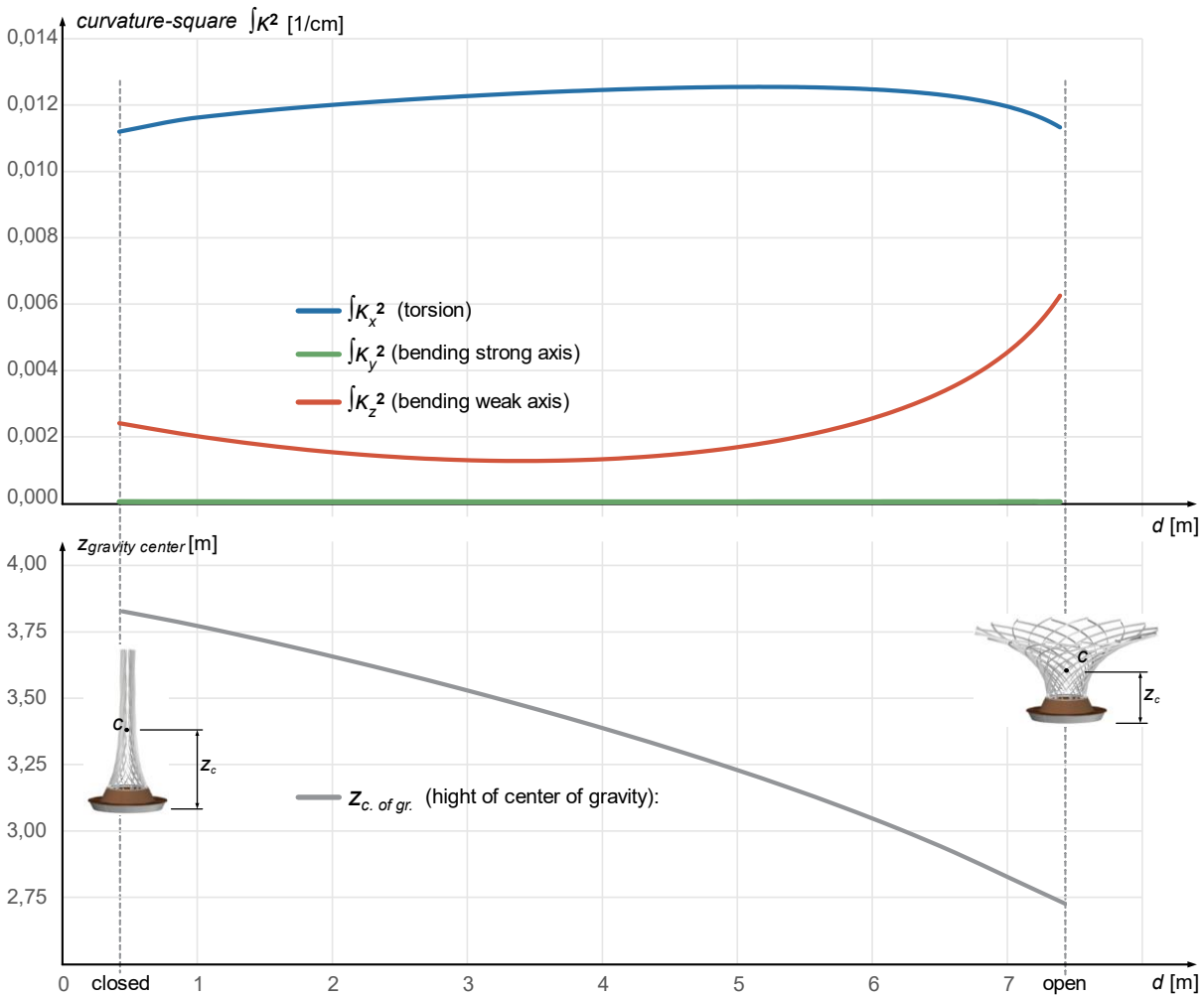
Figure 131 *Graphs showing the curvature-square (top) and height of gravity center (bottom) of the Kinetic Umbrella during transformation.*

Th graphs show opposing minima. The self-weight will pull the Umbrella into an open state (bottom, grey). The curvature-square graphs reveal that the torsional energy decreases in either open or closed state (blue), and weak axis bending finds its minimum somewhere in between (red). Strong axis bending is nearly non-existent.

Beam (Pre-) **Dimensioning**

For kinetic grid structures, profile dimensioning is a decisive step at early planning state. Besides load-bearing, the beams must perform and resist elastic deformation, and the transformation must be handled by an actuation system (see section 4.1.1, p.120).

For the *Kinetic Umbrella*, single lamella profiles made of GFRP were chosen. The GFRP-profiles are produced by *FIBROLUX*[1]. The following characteristic values are provided by the producer and used for structural analysis:

Stiffness

Elastic Modulus for Bending	$E_{bending,c}$	2500	kN/cm²
Elastic Shear Modulus	G_c	280	kN/cm²

Strength

Bending strength	$f_{bending,c}$	40	kN/cm²
Shear strength	τ_c	3	kN/cm²

For preliminary dimensioning, the maximum values of the curvature analysis are used. With the 80x8mm GFRP profile, the following maximum stresses occur:

shear stress due to κ_x (St. V.)	$\tau_{\kappa x}$	*(Equation 16)*	1,9	kN/cm²	(63%)
normal stress due to κ_y	$\sigma_{\kappa y}$	*(Equation 9)*	0,2	kN/cm²	
normal stress due to κ_z	$\sigma_{\kappa z}$	*(Equation 9)*	4,9	kN/cm²	
normal stress due to $\kappa_y+\kappa_z$	$\sigma_{\kappa y+z}$		5,1	kN/cm²	(10%)

This preliminary analysis of stresses shows, that for additional loads, 90% of normal stress capacities and 37% of shear stress capacities are hold available.

These values do not include effects due to helix torsion. However, the impact of helix torsion on this profile can be analyzed. Figure 132 shows the impact for twists up to 90°. The torsional moment and energy portions caused by helix torsion effects are very low in this comparison (~3-4%) and are neglected for further analysis and dimensioning.
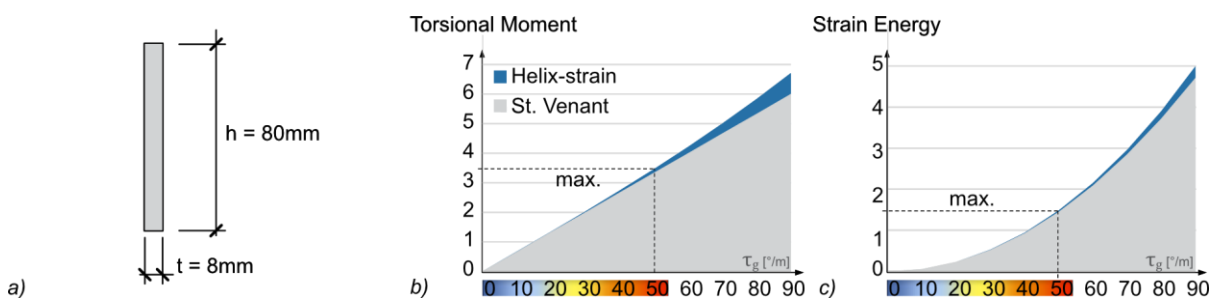
Figure 132 *Impact of helix torsion on the profiles of the Kinetic Umbrella: a) Section b) Torsional moment due to St. Venant and helix torsion, c) Strain energy for a lamella of 1 m length*

The beams stiffness is relevant for the actuation of the umbrella and the profile shape defines constructive solutions. In this context, the beams profile and material choice remain issues throughout the complete engineering processes.

---

[1] *Fibrolux GmbH, Hessenstr. 18, 65719 Hofheim – Wallau, Germany*

Constructive Design

This planning step looks at detailed constructive criteria and solutions, especially those, that have an impact on the systems kinetics (see section 4.1.4, p.121).

The development of profile, node, layering, or offsets is highly interdependent. The grid of the *Kinetic Umbrella* has internodal spacings of 22,2 cm in its most dense area at the bottom. This rather dense grid does not suit for nodes where profiles are cut and attached to a connective component, as such connections need space along the beam. In this case, the design focused on lateral solutions to allow continuous profiles.
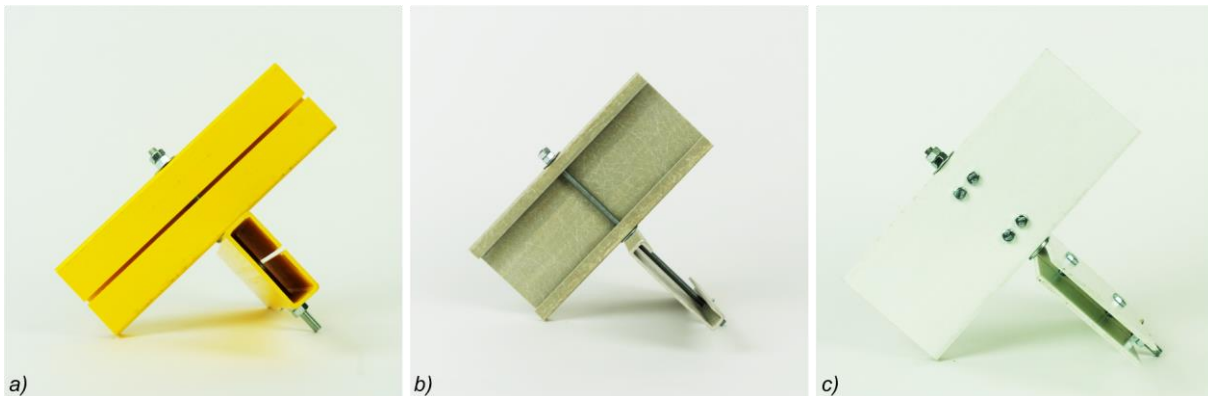
Figure 133 *Alternative, central nodes with hollow or split profiles: a) Slotted hollow section (high Iz), b) C-profile (low Iz), c) Double layered profile*

Figure 133 shows profile and node solutions that allow a central rotational axis with only minimal profile perforation. Using hollow profiles or C-Profiles (Figure 133a, b) allows rotational hinges just by drilling holes. In Figure 133c, the profile is split in two lamellas and a connective component is used as bolt sleeve. These solutions hold constructive advantages. However, such profiles are potentially stiffer and bearing of holes have a weakening effect.
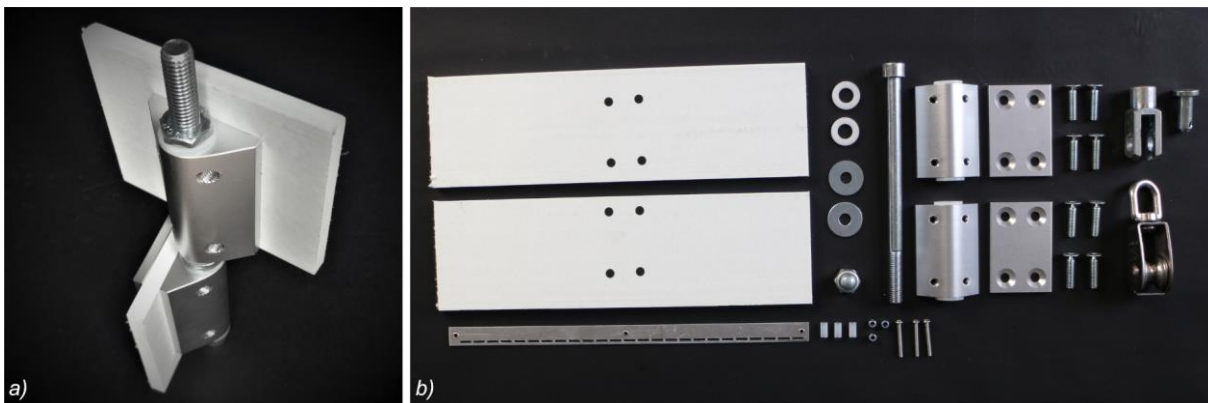
Figure 134 *Grid node: a) 1:1 Model of the hinged node, b) Disassembled joint*

An eccentric solution, in contrast, disconnects profile dimensioning and constructive aspects, as the connective component (bolt) must not stay within profile. Figure 134 shows the node with 12 mm eccentric bolt and all components. This offset follows the geometric design principle of eccentric lamellas, and nodes placed at the original, ideal network intersection (according to Figure 101b, p.116). The two lamella layers have an offset of 85mm using 80x8 mm lamella profiles. These offsets influence the kinetic performance and must be considered in further analysis.

Kinetic Design and Analysis

The kinetic analysis aims to fully understand and control the transformation process, with respect to any geometric constraints, offsets, beam parameters and the actuation system (see section 4.1.4, p.121)

The analysis of internal energy based on the ideal transformation analysis (curvature-square and height of gravity center) gives an approximation of the kinetic performance. The curvature-square values are simply multiplied by the beam's stiffness parameter (EI) and the height of the gravity centre is multiplied by the profiles specific weight. Figure 135 shows the graph of strain, potential and the total energy when the *Kinetic Umbrella* opens. Note, that for the potential energy shown here, only the mass of the grid members, and no additional components are considered.
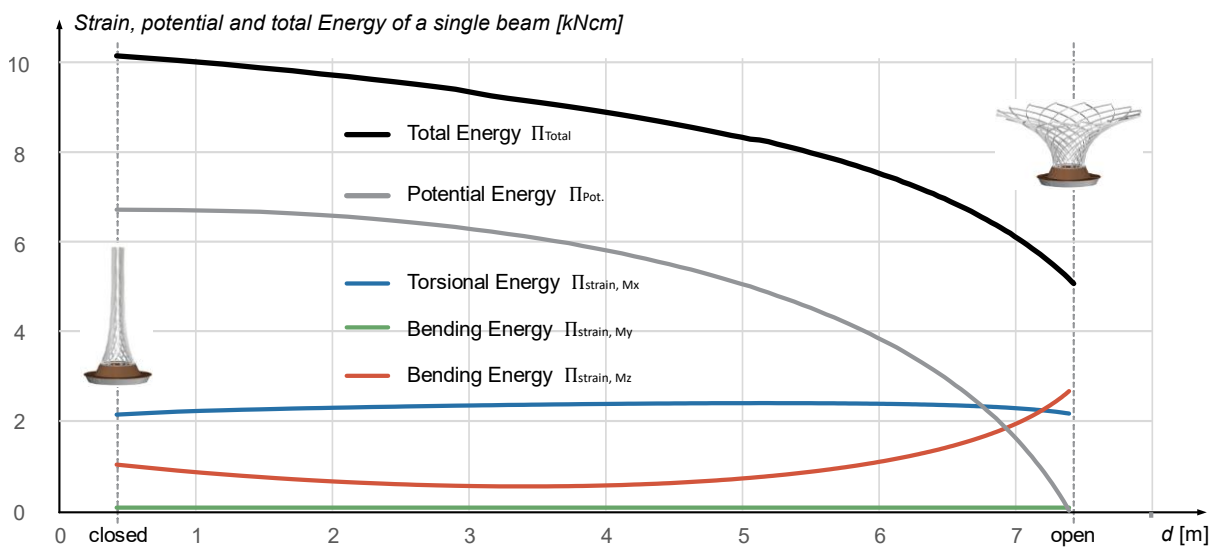
Figure 135 Strain, potential and total Energy Graph of a single 8x80 GFRP Lamella profile during transformation

The graphs show, that using the 80x8 mm GFRP profiles, self-weight is dominant. The total energy graph (Figure 135, black graph) is decreasing and the umbrella opens naturally. To close the umbrella, energy input is needed.

There are multiple options to actuate the system. Distances can be controlled either by a cable (tension only) or by an electric linear actuator exemplarily. The required force is furthermore called "actuation"-force. Three basic geometric approaches with specific characteristics regarding the kinetic performance of actuation were identified for rotational symmetric grids: the "central", "meridian" and "circular" configuration. Potentially, also others, or combinations are possible. Figure 136a shows these three configurations applied at node 11 of the *Kinetic Umbrella*.

In the "central" configuration, the distance to a central point located at the rotational symmetry axis of the grid is controlled. Note, that this configuration cannot be integrated within the grid structure, as an external point is connected. The "meridian" path is planar on a vertical plane. Note, this path is a geodesic curve and represents one of two "diagonal" paths of the asymptotic network. The "circular" configuration represents the other "diagonal" path. The circle is horizontally planar and embedded into the grid.
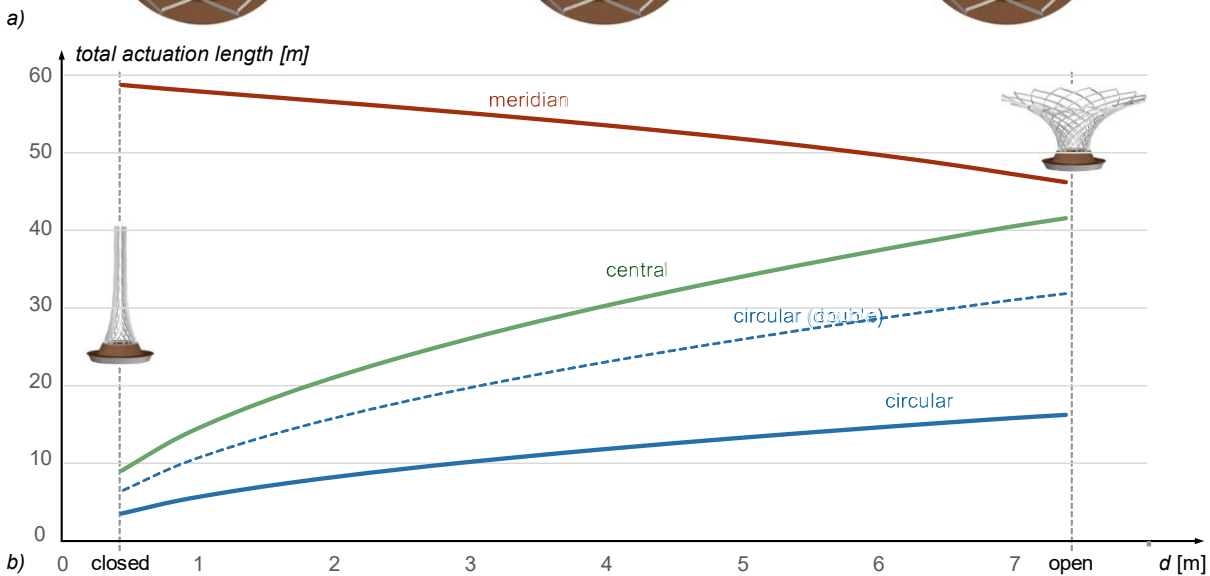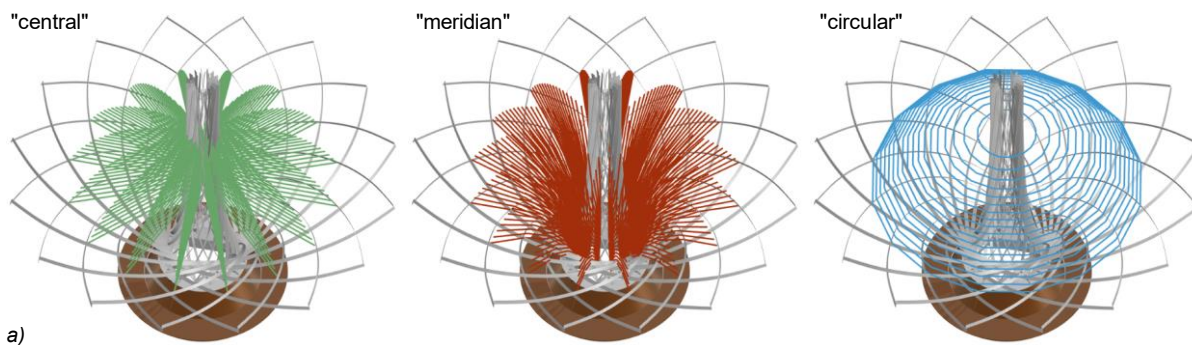
Figure 136 *Basic configurations of actuation systems on the Kinetic Umbrella: a) "Central, "meridian" and "circular" setup b) Geometric analysis of the transformation of the Kinetic Umbrella: total distance of the basic configurations "central", "meridian" and "circular" applied at node 11 from the Kinetic Umbrella*

The geometric analysis of path-controlled configurations of the actuation system gives some valuable indications for the design. The work to be done to close the umbrella can be carried out by actuation of long distances and low force or short distances with high forces (see Equation 29). The graphs in Figure 136b describe the total length of the three basic configurations at any state of transformation. A low gradient means low change in length and thus high actuation forces.

The "**central**" configuration (green) shows the largest change in length from start to the end of transformation, indicating low forces consequently. The length is increasing with lowering energy level (while opening), and the other way round. This indicates tensile forces, that allow the use of a cable system accordingly. The gradient (indicating force) is lower at the open state (t=0) and higher at the closed state. This does not coincide with the potential energy gradient referred to the gravity-center-height graph. In other words: This configuration is not effective, where needed, as the "gear-transmission"-ratio is inverted. The system performs like a car, driving horizontally at low gear and driving up a hill on a high gear.

The length at the "**meridian**" configuration is decreasing while the potential energy is lowering, and increasing, while the energy level is rising (closing). This actuation must work in compression, and thus involves the use of linear compressive actuators. The gradient (change in total length) is smaller compared to the "central" configuration, and higher forces are expected accordingly. The gradients of the potential energy (height of center of gravity) and actuation length coincide, which may pose a general advantage using actuators rated for constant force.

The "**circular**" setup involves tensile forces. The total change in length is similar to the "meridian" configuration and the gradient characteristics are similar to the "central" configuration. Although these characteristics are not ideal, the circular setup was chosen, as a simple cable system, attached to the grid can be used (internal actuation). To decrease the cable force (and actuation force), a circular pully system was developed. In this system, the cable ring and thus the length of cable to be actuated is doubled, which results in half the actuation force. Figure 137a,b show the principle of the pulley system and the application at the *Kinetic Umbrella*. Figure 137c shows the cable force taken from the numerical analysis (IGA). At open state, the force is increasing as expected from geometric investigation in Figure 136b, when the cable is released.
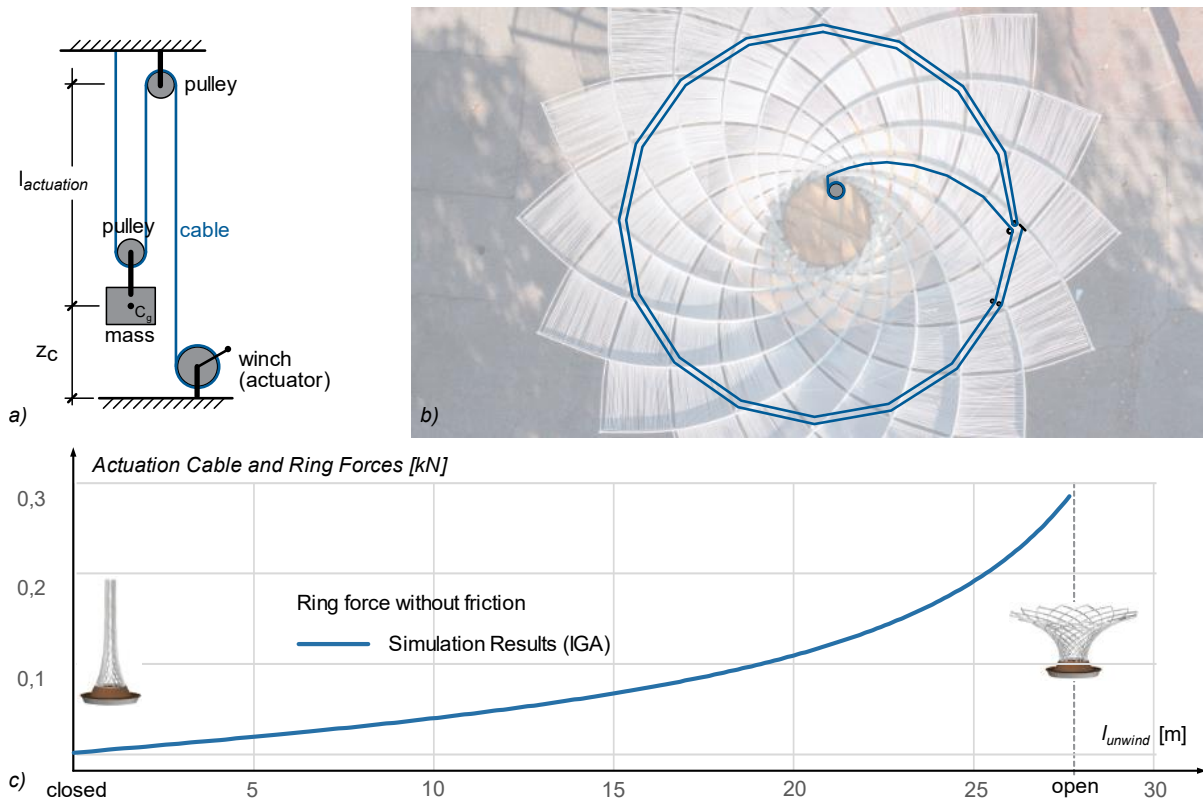
Figure 137 Circular cable system: a) Cable pully principle, b) Circular pulley configuration of the actuation cable, c) Cable force during transformation from closed to open

Note, apart from the shown configurations, there are numerous geometric possibilities for path-controlled systems: These could be assigned to other or more node rows, or geometric configurations can be combined.

The shown analyses underline the significance of the geometric and kinetic progression for further engineering: The energy progression is a decisive criterion for the actuation concept. It defines, where energy must be induced and clarifies whether compressive or tensile systems are suitable, or if the actuation is uni- or bidirectional (section 3.1.1, p.59).

The morphological sequence (geometric progression) is used to analyze various concepts of path-controlled actuation systems, without the necessity of numerical simulations for each variation. This allows quick conceptual decisions.

The fact, that the energy level of the structure is lowering when opening is beneficial as this allows a unidirectional system. Together with the "circular", path-controlled concept, a cable system is possible.

Static Analysis

This planning step looks at the closed and open service state (see section 4.1.4, p.121). In these, the structure must resist conventional external loads, such as wind. The goal is to prove load-bearing at these states. For this, static analysis was performed using the "inverse" FEM method[1]. The open state was modelled and analyzed analogous to the case studies shown in section 4.2. The analysis of the closed state is not shown here, as this state is not decisive.

The following investigations and results focus on the external load cases self-weight (SW) and Wind (W) in addition, which is applied as a globally projected line load 0,05 kN/m at all grid members. Prestress due to bending and torsion is present at all load cases. Note, a critical state is analyzed, where locking cables are not activated, and the structure is tied by the actuation cable only (representing a worst-case scenario). The calculations are run in theory of 3rd order. Given the results in Figure 139, some decisive observations and interpretations can be stated:

- The maximum stresses within the grid structure (SW:4,8 ; SW+W: 5,5 kN/cm^2) lead to an utilization of 14 % regarding material strength. The load case Self-Weight (including residual stresses) causes 87 % of the absolute, maximum utilization in load case SW+W.

- Under self-weight, the grid structure is under axial compression, under wind, tensile forces occur at the side facing the wind. The normal forces within the grid structure increase at the bottom, where maxima are reached (SW -0,33 kN ; SW+W: -1,35 kN). The load case Self-Weight causes 19% of the absolute, maximum normal force.

The relation of forces and stresses at different load cases leads to the following interpretation: The grid structures stresses are predominantly caused by initial deformation. Globally, load-bearing works through axial grid forces. In consequence, further analysis aims on stability:

In calculations, run in theory 3rd order, nonlinear behavior is generally considered, and stability failure can be derived. However, a simplified investigation provides a backup for stability evaluation. According to section 3.3.2, the critical Euler-Load provides a useful indication for the axial load capacity in compression. In this investigation, only internodal spacing is considered. Figure 138 shows all internodal spacings and the calculated critical Euler-Load as a reference capacity. These values underline the sensitive effect of internodal spacing on the compressive capacity and stability can be stated as decisive failure effect. The critical Euler-loads are not exceeded.

l_{12} = 89,2 cm, F_{crit} = 1,1 kN
l_{11} = 78,7 cm, F_{crit} = 1,4 kN
l_{10} = 66,5 cm, F_{crit} = 1,9 kN
l_9 = 57,6 cm, F_{crit} = 2,5 kN
l_8 = 50,1 cm, F_{crit} = 3,4 kN
l_7 = 42,9 cm, F_{crit} = 4,6 kN
l_6 = 37,9 cm, F_{crit} = 5,9 kN
l_5 = 34,3 cm, F_{crit} = 7,2 kN
l_4 = 31,3 cm, F_{crit} = 8,6 kN
l_3 = 29,7 cm, F_{crit} = 9,5 kN
l_2 = 26,5 cm, F_{crit} = 12,0 kN
l_1 = 22,2 cm, F_{crit} = 17,1 kN
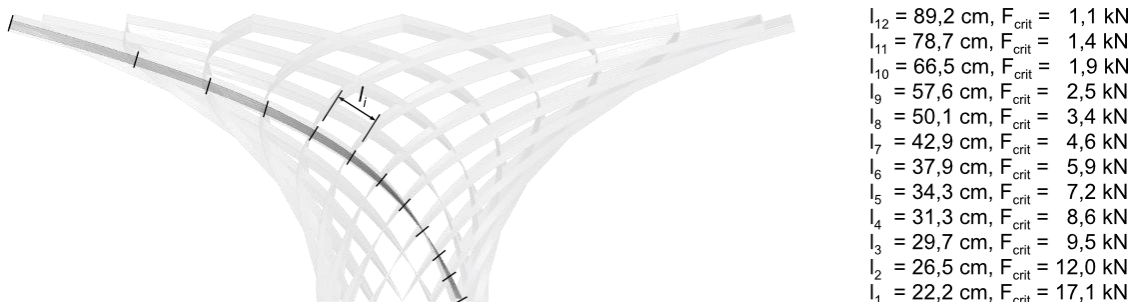
Figure 138 *Critical Euler Load as reference indication for the load-bearing capacity at each internodal segment*

---

[1] *Dlubal R-FEM 5, see also section 2.3.2, p.34*

SELF-WEIGHT (SW)

Stresses:

6,0 kN/cm²

-6,0 kN/cm²

Normal Forces:

compression
tension

0,56 kN

-0,33 kN

SW + WIND

Stresses:

6,0 kN/cm²

-6,0 kN/cm²

Normal Forces:

compression
tension

1,25 kN

-1,35 kN
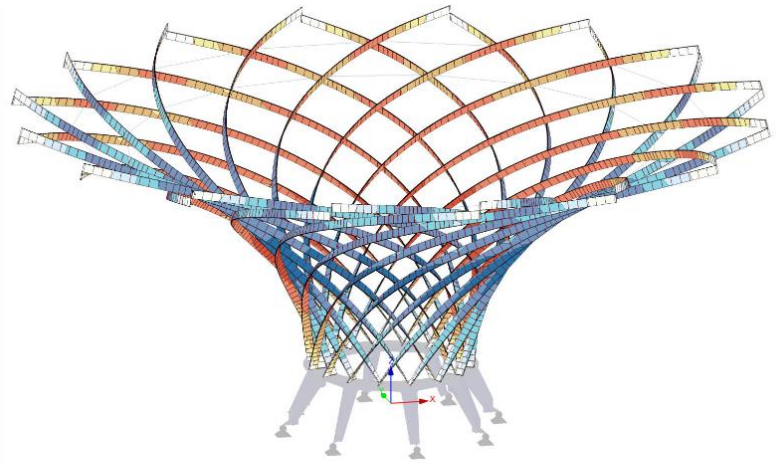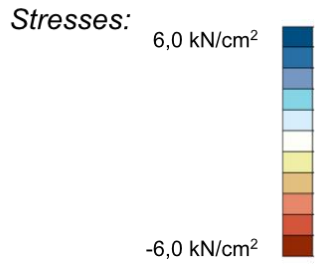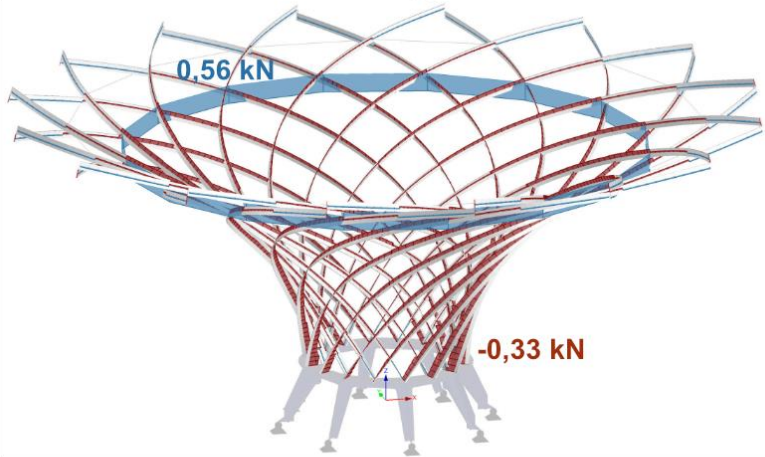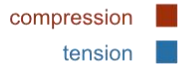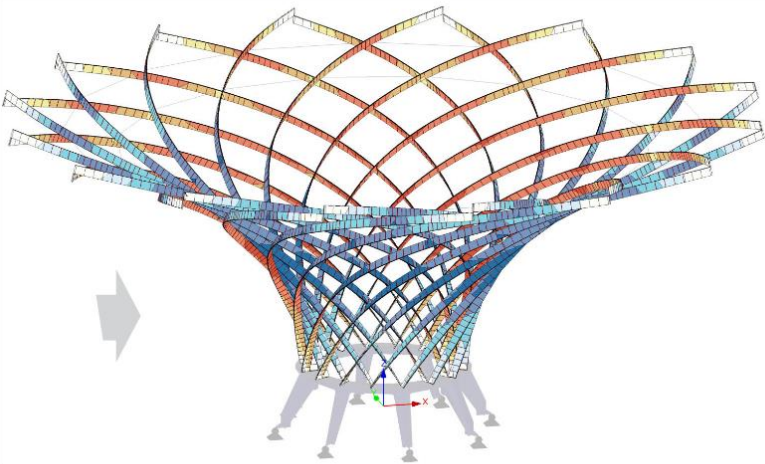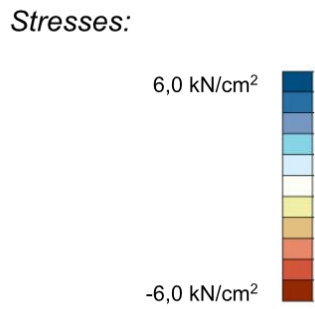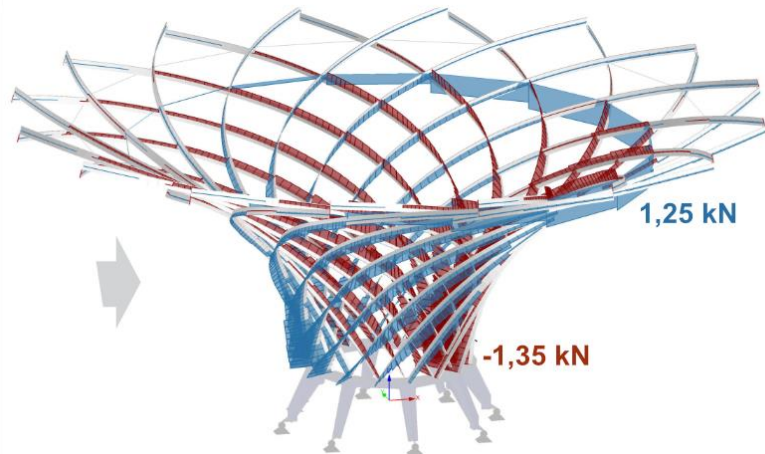
Figure 139 *FEM-analysis: Stresses and normal forces of the Kinetic Umbrella for Self-Weight (SW) and additional Wind (W)*

Construction Planning

This planning step aims to provide strategies and data for assembly and erection (see also section 4.1.4, p.121).

The Construction Model was set up including all details. From this geometric 3D-model, all plans for workshop and fabrications are derived. Figure 141 gives an overview on key plans and details relevant for the construction. These can be separated into a falsework plan for the grid assembly, drill plan for the lamellas (a set of distances to define the node locations), steel table plans (laser data and assembly/welding instruction), and concrete base plans (formwork planning).

Figure 140 shows the drill plan used to fabricate all lamellas. The distance set given in this single drill plan defines the complete special shape of the structure (due to rotational symmetry). Along the single lamella, all 13 nodes are numbered.
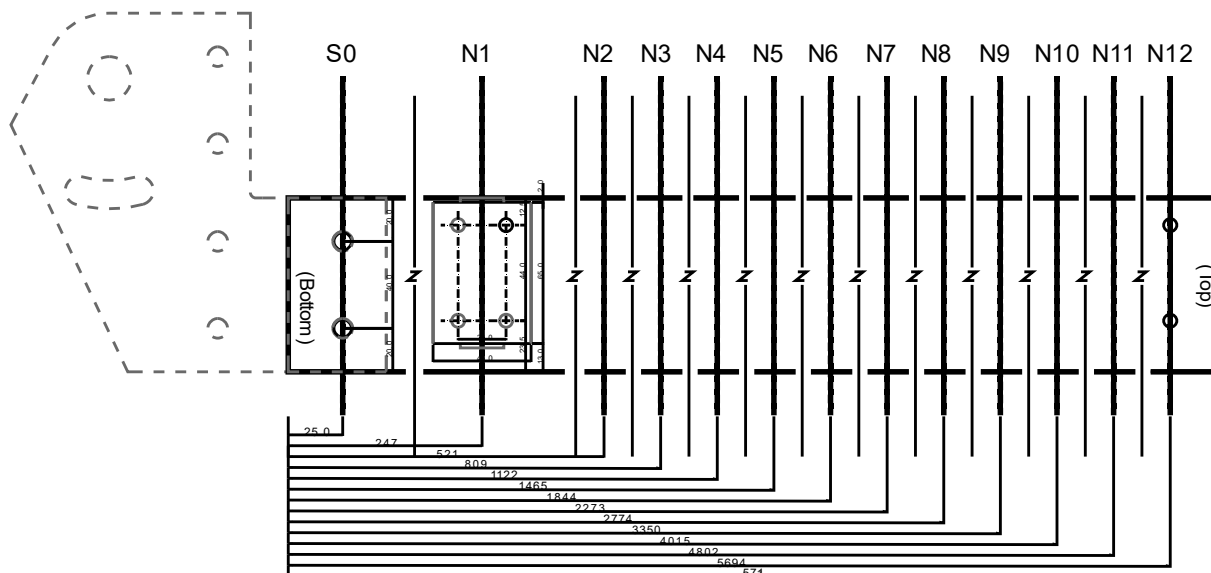
Figure 140 *Drill plan valid for all lamellas*

The assembly of the grid structure requires a falsework. The idea was to assembly the grid structure horizontally (see also Figure 142f), by placing the lamellas of the inner layer of the grid into slots of a circular falsework. For this, a specific state (nearby the closed state) was chosen, and the geometry of this state was taken from the digital model (Figure 141a). Two circular plates were positioned in the grid structure to collide with the inner grid layer, but not with node details (Figure 141c). These plates were supposed to be slotted to easily place the inner grid layer into position, and later attach the outer layer.

The steel table is welded together from 5 to 15 mm laser cut steel plates. The laser data is shown in Figure 141e. The in-situ concrete base underneath was poured into timber formwork, shown in Figure 141d.

The Construction Model helped to avoid mistakes when these components were brought together. It gives clear insight into potential collisions or reveals other potential problems.

154

N12
N11
N10
N9
N8
N7
N6
N5
N4
N3
N2
N1
S0

(Top)

(Bottom)

Drillplan lamellas

Falsework for grid structure

a)

b)

Ø880

c)

steel table

formwork concrete weights (base)

d)

e)
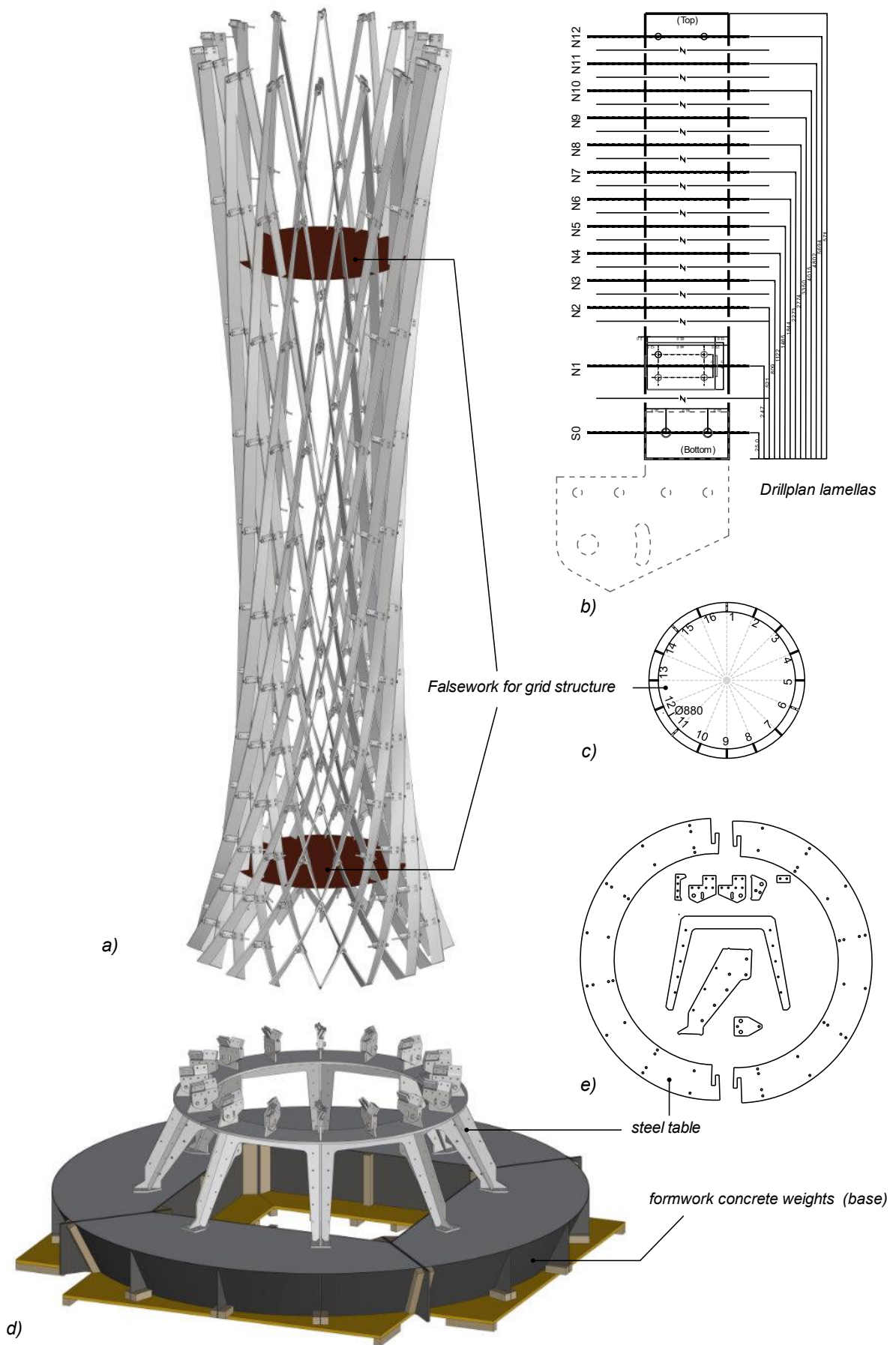
Figure 141 *Overview on key construction plans: a) Grid structure in state for horizontal assembly, b) Drill plan for lamellas, c) Saw plan falsework for grid assembly, d) Concrete formwork and steel table detail, e) Data for laser cutting (steel base)*

4.3.5 Assembly and Erection

The construction process of the Kinetic Umbrella lasted about two months. The following descriptions give insight into the construction process chronologically. The pictures in Figure 142 illustrate this process.

The **base** includes concrete weights at the bottom, a steel table as structural support for the grid structure, and timber covers for sitting accommodations. The concrete was poured on site, directly from a concrete mixer into the timber formwork (Figure 142a). The steel table was welded together by the steel manufacturer *BRANDL*[1] and mounted on top of the concrete bodies (b).

The **grid structure** is made of 32 GFRP lamellas, produced by *FIBROLUX*[2] and delivered in a single package. Figure 142c shows the lamella material used in total. The lamellas were drilled according to the drill plan (see Figure 140), and the aluminum connectors were attached. All lamellas are equally prefabricated using a full table drilling template (d).

The **grid was assembled** in a spatial, nearby closed state. A falsework was used (see Figure 141a) to successively insert the inner layer first, and then attach the outer grid layer (e,f). Note, the lamellas must be bent and twisted for assembly. This requires some force that could be managed by hand. Large timber forks were used to induce twist and bending when connecting the grids nodes.

The **locking cables and support connectors** were already mounted in the assembly state.

The **erection** was performed using a crane. The grid structure was transported horizontally in its mobile falsework and lifted at selected nodes. This falsework kept the grid structure at the supports in correct position (radius) to mount the lifted grid onto the steel base (g). Once connected, the timber falsework was removed, and the structure secured with a temporary belt until the actuation cable was threaded and connected to the winch at the base.

The **cover system** was prepared in advance. All aluminum profiles tor textile guiding (see section 4.3.1, p.138) were milled, and trimmed textile fibers were prepared (h). The profiles and fibers were mounted onto the grid structure by hand (i).

Finally, the **timber cover** was attached to concrete and steel parts of the base.

Conclusion

The assembly and erection process were performed without notable disruptions. However, the major challenges were to keep tolerances of the grid structure at a small level and to mount the lamellas at an initially stressed state. The tolerance could be faced by a precise template for prefabricating the lamellas.

For mounting, it was necessary to access the structure inside, which was possible due to the steel table design with openings.

---

[1] BRANDL Eitensheim (Germany) , www.brandl-eitensheim.de
[2] FIBROLUX GmbH (Germany), www. Fibrolux.com
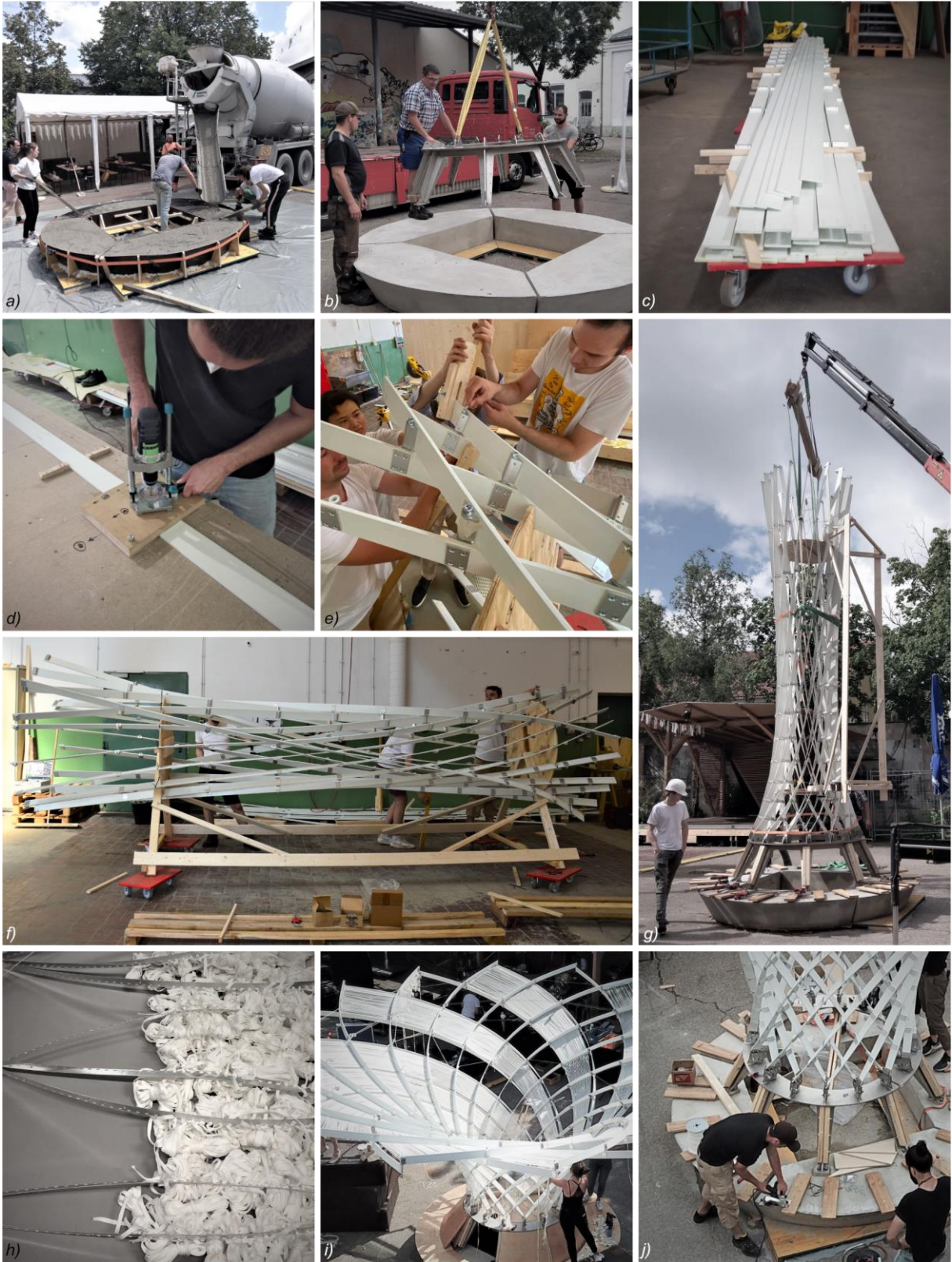
Figure 142 *Fabrication, assembly, and erection of the Kinetic Umbrella: a) Pouring concrete base, b) Placing steel base, c) Lamellas ready for prefabrication d) Prefabrication of lamella beams (drilling holes for connective components), e) Connecting grid members in falsework f) Assembly of grid structure horizontally in falsework g) Lift-up and connection of grid structure to base, h) Prepared textiles for the cover system, i) Mounting of textiles (cover system), j) Placing timber at base for sitting accommodation.*

4.3.6 Geometric and Kinetic Validation

Figure 143 *Measurements at the Kinetic Umbrella: a) Setup of lasers scan, b) Force meter interconnected at actuation cable*

The design and engineering of the Kinetic Umbrella involved several simulations to predict the transformation in both geometric and kinetic quantities. After the Structure has been completed, measurements were taken to validate the simulation results. The geometry was measured using a 3D lasers scan, and the actuation force was measured using a force meter (Figure 143). In the following, the scanned geometry and measured forces are compared with simulation results.

Geometry Validation

The data received from the laser scan and the simulated geometry of the kinetic transformation analysis are overlayed using CAD. The scanned geometry was aligned with the steel base structure of the 3D-model, as this component is built in high precision and therefor provides a reasonable reference. A transformation state of the 3D-model was chosen to receive a state of "best fit" at the grid structures top and deviations are measured at selected positions. Figure 144 shows various views of the geometry overlay. Deviations are measured up to 20 mm.

Although deviations of 20mm are much in conventional building, for a transformable lightweight structure, this value is satisfactory. Geometric deviations might be caused by tolerances in drilling and hinges, by not perfectly adjusted locking cables, or by deviations in load assumptions (self-weight). The latter is less likely, as masses were carefully recorded.
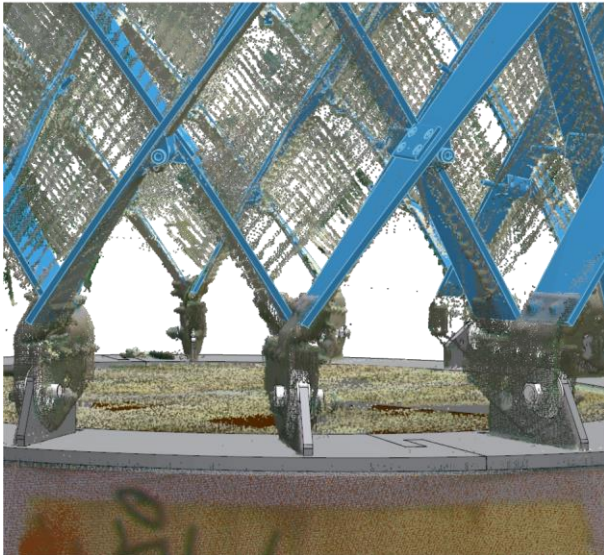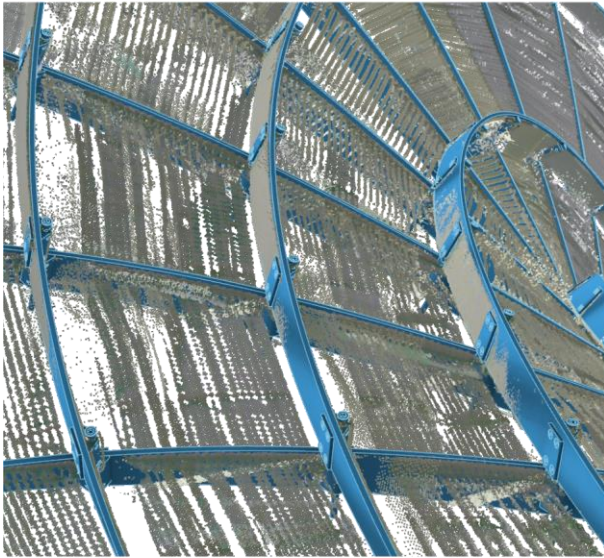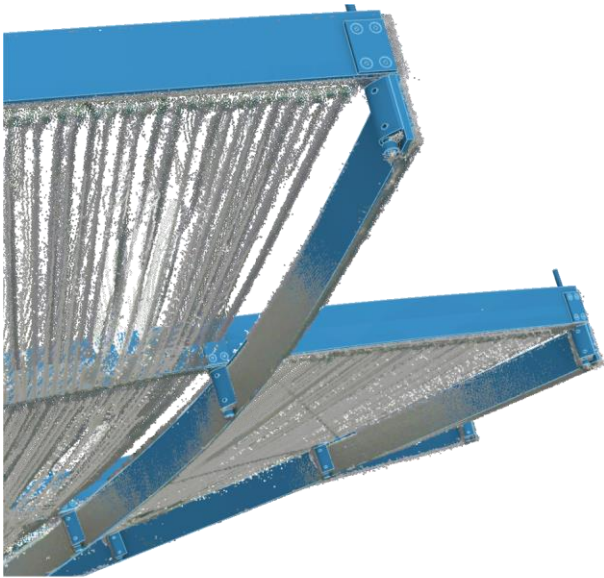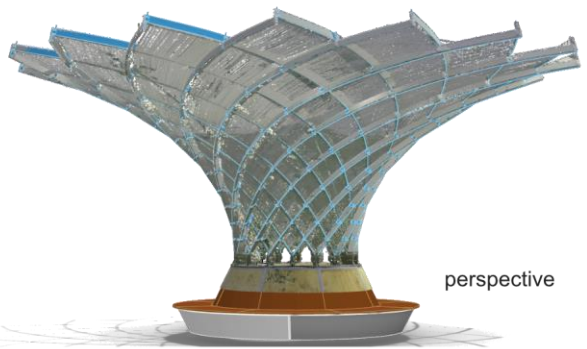
Figure 144 *Overlay laser scan (original color) and simulated geometry (blue) (IGA, self-weight)*

159

Force Validation

The tension at the actuation cable was measured at 22 transformation states with an interconnected force meter (Figure 143b). Each measurement was done twice: Once when winding (closing) and another when unwinding (opening) the actuation cable. These two measurements differ considerably, and the only reasonable explanation for this difference is friction. To understand these effects, a simplified but distinguished model of force components is set up schematically. In this model, forces either work opening or closing, and the following assumptions are made:

- At any specific state of transformation, forces due to self-weight and strain are not dependent on the direction of transformation (opening or closing). Hence, accelerations are ignored.

Forces due to self-weight and strain are nonlinear throughout transformation (see also section 4.3.4 Friction always works in opposite transformation direction.

- Friction is caused at two positions: At hinges (nodes) and at the actuation cable (pulleys). Friction at node rotation does not depend in quantity on the transformation direction and friction at the actuation cable depends on the actuation cable force, which does depend on the transformation direction, due to involved hinge friction (at nodes).

- The friction at the cable is linear dependent on the actuation force via the friction constant μ, to be set. This friction is generated, where the actuation cable runs downwards to the base via sliding guidance. The force in the cable ring at the top is not influenced by friction.

This model, together with measurements and friction-free simulation results, allows to back-calculate friction to its components. Figure 145a shows the abstracted actuation model at winding and unwinding process (see also section 3.1.1. for model definition). On the right, the equilibrium of both situations is shown in a force diagram. This model is used to evaluate the forces measured. In Figure 145b, several forces are mapped along transformation. The horizontal axis in this graph describes the length of winded/unwinded actuation cable. The measured values (dots) are approximated via polynomial regression (dotted blue curve). The force in the cable ring F_{Ring} is calculated using the friction coefficient μ:

$$F_{Ring} = (1 - \mu)F_{Act.}$$

Equation 67

Because friction at hinges is equal in absolute quantity for winding and unwinding, the friction-free force in the cable ring lies exactly in between the winding and unwinding values. This friction-free value of the cable-ring force is compared with simulation results from the kinetic transformation analysis (4.3.4, also free of friction) and the friction coefficient μ can be set to achieve best fit. Here, the value of $\mu = 0{,}2$ is set.

The simulated values (green curve) fit well together with the measured and back-calculated values (black curve) of the cable ring force. Deviations occur, at nearby closed states. These deviations are likely due to inaccurate measurements of low forces and other, smaller friction effects that become sensible at states of low actuation forces (<0,15 kN). However, with these results, the numerical simulations can be validated.

Figure 145 *Force validation: a) Abstracted actuation mode, b) measured actuation, ring and simulated forces (bottom)*

For the *Kinetic Umbrella*, friction has a noticeable impact on internal forces, especially on the actuation system. At open state, the real forces including friction are doubled, and when opening, the real forces are only one third due to friction compared to the results of numerical investigations.

161

Figure 146 *Kinetic Umbrella (closed)*

5 SUMMARY AND CONCLUSION

This work reveals the morphologies and the kinetic performance of semi-compliant grid structures with restricted compliancy, using both physical and computational modeling and simulation. Supported by various case studies, novel approaches and engineering strategies are developed and applied to implement semi-compliant grid structures at architectural scale.

5.1 Results and Significance

In the following, key results, interpretations, and the scientific significance are summarized, following the structure of this work.

2 STATE OF THE ART

This chapter aims to provide decisive fundamentals and to give an overview on the related research environment.

Section 2.1 recaps geometric fundamentals. It orientates at basic geometric objects, from points to networks on surfaces. Decisive geometric parameters of these objects are specified.

Section 2.2 recaps mechanical fundamentals of elastic beam deformation and related strain energy, on both profile and beam element level. Furthermore, the basic phenomena of large elastic deformations are described.

Section 2.3 provides an overview on computational and physical modeling techniques, used in this work. These are generally suitable for the design and analysis of semi-compliant grid structures. The focus lies on computational, parametric modeling methods, that support the iterative character in the design of such structures.

In *Section 2.4*, selected topics of research and development are presented, that highly relate to this work. The selection includes the research areas of architectural geometry, transformable, compliant, or active bending structures. A selection of build strained gridshells shows the current state of development at architectural scale. These topics have a large common ground but originate from different perspectives. Finally, the research environment of compliant grid transformations is displayed, and research gaps identified.

3 MECHANICAL STUDIES

This chapter discovers geometric-mechanical relations of semi-compliant grid structures in various physical and computational analyses.

Section 3.1 describes the anatomy of the research object, the structural components of semi-compliant grid structures and thus provides a structural framework. Furthermore, the structural scope for subsequent investigations is defined: Quadrilateral grid structures on smooth surfaces with restricted beam compliancy and uniaxial hinges at intersections.

Section 3.2 includes a kinematic (rigid body), and two kinetic transformation analyses:

The kinematic analysis (section 3.2.1) investigates rigid-body transformations of four two-dimensional cutouts of quadrilateral grid structures. Each cutout represents a basic case of how members can be oriented to an induced, directed deflection. The ratio of orthogonal compression and extension is geometrically derived. Grid layouts that are not symmetric to an induced compression/extension also involve shear-like transformation. If both grid member families are sloped in the same direction in a qualitative sense, an auxetic behavior appears. In a nutshell: This study reveals a simple geometric relation, that in its basis also applies to semi-compliant grid transformation. It describes the "lateral strain" of such structures on a macro structural level, using trigonometric formulas. Although these are purely kinematic relations, they are likely to exist also within compliant, curved configurations, that also (at least partly) perform through axial forces.

The kinematic relations directly express the static force relations within the grid, and thus influences the actuation and static performance. From this perspective, the intersection angle (the network layout) can be used as a design parameter.

The first kinetic analysis systematically investigates the morphology and transformability of semi-compliant grid structures with varying axial compliancy. This analysis is carried out using numerical simulations of an equilateral, flat grid structure, supported at four points, and transformed into spatial. The reference surfaces of the transformed grids are then analyzed regarding shape and curvature. This investigation covers three types: triaxial, biaxial, and uniaxial compliancy of the grid's members. Simulations involve either path-controlled deflections or eigenmode analyses, depending on the suitability for this investigation. The following is stated:

- Triaxial compliancy: The grid is transformed by controlled displacements at selected nodes. This grid type allows full adaptivity to any doubly curved smooth surfaces. This is in line with common practice in strained gridshell erection. However, this freedom of shape comes with a low controllability of the transformation, and such grids need to be physically forced at multiple positions to reach into desired shapes.

- Biaxial compliancy: There are three possibilities to configure biaxial compliancy, each has one axis rigid, the other two compliant. The simulations run for all configurations and two corner nodes are displaced to force a spatial transformation. All transformed shapes show constant gaussian curvature on their reference surfaces. However, their sign is characteristic: If torsion is rigid, the reference surface is synclastic and spherical. If bending at normal axis is rigid, the curvature is constantly negative, and thereby pseudospherical.

If the bi-normal axis is rigid, the reference surface's Gaussian curvature is zero, and thereby developable (Note, only valid for equilateral geodesic grids).

These observations are in line with geometric expectations for equilateral networks on curved surfaces. The simulations show that these shapes can be generated mechanically in a fluent transformation process, and that this transformation can be induced by local actuation, a crucial quality and requirement for the applicability of mechanisms.

- Uniaxial compliancy: There are three possibilities to configure uniaxial compliancy, each has one axis compliant, the other two rigid. This type is analyzed not by forced displacements, but through an eigenmode analysis. The following is observed: If only torsion is compliant, there is no global transformation possible (except for non-equilateral grids, e.g.: rulings of a hyperbolic paraboloid). If bending at bi-normal axis is compliant (creating normal curvature), the transformed shapes are developable. If only normal axes are compliant (creating geodesic curvature), the transformed shapes remain planar.

  These observations are also in line with geometric expectations for equilateral networks on surfaces. The high level of restriction in transformability is a beneficial quality for shape control, but the spectrum of shapes is low. The equilateral setup does not allow any doubly curved transformation.

The geometric expectations for all semi-compliant equilateral grid structures are fulfilled. This verification underlines the suitability of geometrically derived assumptions on structural morphology, not only for selected states, but for entire transformations.

However, there is still a wide spectrum of global transformability. Exemplarily, transformations shown for uniaxial compliancy (see Figure 64) are also valid for biaxially compliant structures, as these represent a morphological subset.

Altogether, the cases of biaxial compliancy (section 3.2.2, B and C) and uniaxial compliancy (C) on doubly ruled surfaces show the greatest potentials in their abilities to be punctually actuated and regarding geometric feasibility at section level. These are further investigated.

The second kinetic analysis (section 3.2.3) aims at the progression of internal strain energy. The systems chosen for this analysis, and their axial compliancy, are mechanically feasible in terms of profile stiffness ratios. The analysis includes lamella grids (biaxial compliancy - bending and torsion) and cross-sections (uniaxial compliancy – torsion only). For each type an open and rotational grid structure is modeled, and transformations are simulated. The internal strain energy progression, apportioned into its axial components is tracked using the integrated curvature-square value, representing the geometric factor of the strain energy term.

The curvature-square analysis gives insight into the internal balance of strain energy portions and their progression. It reveals possibly "natural" states of minimum strain energy, and how local profile stiffness ratios can influence the internal strain energy balance. The curvature-square graphs are mapped for bending and torsion separately to provide a clear differentiation.

The "double ruled" structures show distinct strain energy minima (natural states), e.g., at bundled state or for the hyperbolic paraboloid.

The natural state of structures with two compliant axes potentially depends on the compliant

stiffness ratios. Some structures show an increase (or decrease) of both torsion and bending when transformed. Their "natural" state of equilibrium cannot be modified by tuning the compliant axes bending stiffnesses. Other structures show countering curvature-square graphs. Their natural state can be modified accordingly.

The curvature-square analysis can be used for beam dimensioning as part of an iterative engineering process (see section 4.1.4 p.120). The curvature-square progression is specifically useful for kinetic morphologies that do not depend on local stiffness ratios, or at least, when dependencies are neglectable. This is the case for highly constraint structures, either by internal stiffnesses or constraints (e.g., stiff bending axes or limited DoF at hinges), or by external constraints (supports, etc.). Once determined, the graphs depict the unique kinetic behavior of a specific setup. It is the kinetic fingerprint of a compliant grid mechanism.

Section 3.3 investigates the performance of semi-compliant grid structures in a static, locked state in two numerical studies, aiming on global and local stiffness:

The first study compares the global stiffness of grids with biaxial profile compliancy, represented by lamella profiles with "upright" or "flat" orientation, when different locking principles are applied. Each configuration is locked using either a full edge support, four single corner supports, or corner supports combined with internal bracings. The stiffness of these structures is evaluated in an analysis of eigenfrequencies. The following is concluded: The "upright" lamella configuration leads to higher "out-of-plane" stiffness, whereas the "flat" orientation leads to higher "in-plane" stiffness. The "upright" configurations show higher global stiffnesses in all tested setups, and, in contrast to a "flat" orientation, their in-pane-softness can be effectively countered using "in-plane" bracing systems.

In general, the global stiffness also indicates global stability. In this context, the eigenfrequencies indicate resistance in terms of global stability phenomena and the modal shapes refer to buckling modes.

The second study aims on the local performance of curved compliant beams under compression. Elastically curved multi-span beams with varying constant radii and varying internodal spacing (span) are compressed in a numerical simulation, and the load-displacement paths are systematically recorded and evaluated. It is shown that the performance of curved members relates to the behavior of a straight, multi-span reference configuration. The shapes of deformation in curved configurations relate to buckling modes of straight multi-span beams and the resistance relates to critical buckling loads. The simulations show snap-through phenomena in between deformation modes, until the first buckling mode of a multi-span beam (Euler-case 2) appears. These findings support a simplified and early evaluation of the local capacities in terms of stability, using the simple critical Euler-load for early pre-dimensioning of profiles or grid density.

Section 3.4 includes physical model explorations on semi-compliant transformability, morphology, and actuation. Investigated are selected systems based on asymptotic networks, rotational geodesic systems, and rotational scissor systems. Their transformability was explored in a design studio, including actuation systems. These designs were successfully implemented at model scale. Finally, the designs were compared regarding their components based on Section 3.1. and evaluated in key statements.

4 ARCHITECTURAL IMPLEMENTATION

This chapter includes engineering strategies, dimensioning aspects, and design methods. These are developed and applied in various case studies at architectural scale. All built structures are dealing with asymptotic grid structures.

Section 4.1 extracts decisive requirements and parameters for dimensioning in context with the stiffness paradox, that compliant structures hold in general, and interconnects these. The ability to actuate and to deform are presented as additional basic user requirements, that emerge specifically for compliant structures. The complexity of these competing requirements is displayed and dissolved.

The stiffness paraoxon marks a special challenge for compliant structures. However, in section 4.1.2 detailed strategies for dimensioning are provided to tackle this problem, either on profile geometry level or at material level. It is shown how geometric profile modifications impact the beams deformability and stiffness. Furthermore, a decisive material index is revealed, that quantifies the material's potential to create elastically curved beams with maximum stiffness.

Constructive criteria are elaborated systematically, aiming at offsets, layering and discontinuities. The principles of offsetting as a constructive strategy and the geometric consequences are shown. Furthermore, the effect of local discontinuities in elastically curved members is elaborated and quantified. The length and stiffness of discontinuities are decisive for their impact.

All requirements and criteria are considered in an overall engineering process, that includes key processes: "Concept", "Formfinding", "Transformation Design and Analysis", "Beam Dimensioning", "Constructive Design and Analysis", "Kinetic Design and Analysis", "Static Design and Analysis", and "Construction Planning". These processes are integrated in an iterative workflow and connected via a coupled digital model environment. This engineering workflow is developed to manage the complexity of compliant grid structures.

Section 4.2 gives insight into three case studies, that utilize semi-compliant transformation for asymptotic gridshell erection. These projects supported the developments of section 4.1 and demonstrate feasibility of semi-compliant transformation at architectural scale.

Three projects are presented:

The *Inside/Out* pavilion marks the initial motivation for this topic. The erection of this structure utilized the constrained transformability of asymptotic steel patches and demonstrated the potentials. Furthermore, the FEM-inverse method was developed to analyze the static performance.

The *Hotel Intergroup Canopy* is the first commercial asymptotic steel structure. In this project, the kinetic performance when the grid structure transforms from flat to spatial was planned using novel simulation methods (IGA). The effect of helix torsion is analyzed in detail, as these depict a relevant portion.

The *Asymptotic Geodesic Timber Vault* is the latest project. It demonstrates the feasibility of timber for structures of this kind. The erection was performed similar to the *Inside/Out* pavilion, although, this structure has some geometric features: In addition to an asymptotic grid

structure, is includes geodesic members (flat orientated timber lamellas).

Transformability in all these build structures emerges from tolerances at the nodes and other connections.

Section 4.3 describes the development and realization of the *Kinetic Umbrella*, a reversibly transformable asymptotic grid structure. This case study includes detailed kinetic analyses and introduces GFRP to this kind of transformable structures.

The *Kinetic Umbrella* is a rotationally symmetric structure of 8 m diameter that can be closed to a slender cylindric shape. The base of this structure serves as sitting accommodation, and the compliant grid structure is covered with an adaptive shading system. The *Kinetic Umbrella* can be opened using a winch at the base of the structure.

The grid structure is double layered, and the lamellas are coupled with lateral connective components, hence, the structure involves offsets, considered in simulation, but with neglectable impacts on the kinetic performance.

The whole design and development of this project was performed in a coupled digital model environment, including a high level of parametrization. Simulations are run with using the IGA inverse approach. Detailing was integrated in this workflow.

Various physical models were used at three different scales (1:10/1:3/1;1) for the development. These models tested effects and feasibility of the basic morphological concept, offsets, and other geometric-mechanic characteristics. The 1:10 model demonstrated the mechanical quality, as the grid could be transformed by actuation of two nodes only (by hand). The 1:3 model showed that eccentricities and offsets do not essentially manipulate the kinetic performance. The 1:1 model was used for practical prototyping, to test the node, cover system, and assembly.

The engineering of the *Kinetic Umbrella* utilized the theory described in chapter 3. The characteristics of structures with biaxial compliancy are beneficial for the application of semi-compliant mechanisms, as they are constrained and restricted in deformability, and thus pose stiffness. Asymptotic grids tend to show beneficial stiffnesses at free edges (section 3.3.1). The curvature-square analysis reveals the kinetic character of this structural system. The state of minimum strain energy is theoretically adjustable using profile stiffness modification, but using reasonable sections and materials, strain energy is dominated by bending, and the minimum energy state is in between open and close. However, the self-weight pulls the structure down to the open state, and thus, actuation becomes unidirectional.

The simulated morphology (sequence of states) was used to quickly derive mechanical concepts for actuation. The "circular" cable configuration was used, as this allows an internal actuation system. Furthermore, a circular pulley system was developed to manipulate cable forces (and cable friction).

The static analysis verified the safety of decisive load cases. The FEM-"inverse" approach was used again and matched with the critical Euler-load using internodal spacings as buckling length. This approach relates to section 3.3.2, where the analogies are revealed.

The structure was assembled and erected without notable disruptions. However, the major

challenges were to keep tolerances of the grid structure at a small level and to mount the lamellas at an initially stressed state. The tolerance could be faced by a precise template for prefabricating the lamellas. For the assembly of the grid structure, large timber forks were used to induce twist and bending when connecting the grids nodes.

The internal forces and the physical state of the *Kinetic Umbrella* throughout transformation are compared with simulation results, and thus, used engineering approaches are verified. The deviations in geometry and force are in a reasonable range and give confidence to the methods used.

The Kinetic Umbrella is the first reversible compliant grid structure of this kind. It demonstrates the architectural and mechanical potentials given by this constructive approach and shows how the complexity of designing compliant grid structures can be handled.

5.2 Final Reflection

This thesis supports a novel type of transformable structure: the semi-compliant grid. These structures allow spatial transformations of doubly curved, smooth surface like structures. Compliant, kinematic, and ridged components are strategically combined to create feasible mechanisms. Findings in differential and architectural geometry provide a fundamental basis, and novel computational methods are necessary for the development of such systems.

This work systematically classifies semi-compliant grid structures and identifies its decisive parameters, geometric characteristics, kinematic relations, static, and kinetic behavior patterns. These explorations informed novel computational approaches and methods.

The challenge of semi-compliant grid structures lies in the implementation at architectural scale. This thesis provides a systematic engineering workflow that guides from initial design to service of structure. The various case studies did not only support these developments, but also demonstrate the concept and feasibility of semi-compliant grid structures in architecture.

5.3 Future Research

The implementation of compliant grid structures in architecture involves multiple and diverse competences. Potentials for future developments are found in any related field:

- **Architecture:** Transformable structures pose a niche in architecture. Nevertheless, their potentials are high for multifunctional buildings or adaptive building components, as these provide another dimension: time. The concept of semi-compliant grid structures is new in this field, but in future, architects may integrate such systems into their designs. Currently, architects and clients show increasing interest in transformable lightweight structures in context with climate change, urban heat islands, urban greening, etc.

- **Morphology:** The morphologies and grid configurations treated in this work represent a sample of possible systems. The parameter-set and combinatorics suggests that there is a wide spectrum of shapes to be discovered. This includes exemplarily modifications in nodal DoFs or rotational axis orientations, non-constant beam stiffnesses or inclined, global, or other beam orientations, non-traversal, or angulated nodes, such as used for scissor-systems, etc.

  Such explorations can be performed using numerical simulations, but also differential geometry poses great potentials to systematically discover further network morphologies that can be translated into mechanical systems.

- **Material:** The elastic capacities and parameters of compliant beams are dominantly limited and constrained by material parameters. Conventional material developments aim at high strength and stiffness. Compliant systems however aim at high maximum strain. Composite materials have shown high potentials in this characteristic, but specific research and development in this direction is still not present.

  Furthermore, such material developments may include aspects of sustainability. Natural materials, known for their sustainability, such as bamboo or timber products show great mechanical potentials for compliant structures.

- **Computational Methods:** The analyses and developments presented in this work involved extensive computational modeling and simulation. In this course, new techniques were developed: The *Bowerbird* Tool by T. Oberbicher (Oberbichler, 2021) supports the design of curvature networks. Novel coupling types and the "inverse" method used in IGA were developed by Anna M. Bauer (Anna Maria Bauer, 2020). These tools are important to support a fluent workflow. However, they can be improved, simplified, and extended.

- **Scale:** In this work, the semi-compliant grid structure was brought into the architectural environment for medium size structures. However, the mechanical concept is transferable to other mechanical fields and other applications, and generally not bound to any scale. The use for smaller applications, or devices might even be more likely, as self-weight does less impact the systems kinetic performance.

- **Details and Cover:** The Node, support, or actuation details and systems leave great potentials for further development and commercial use. Especially suitable, closed cover systems are not yet developed.

Nomenclature

This list includes the most fundamental signs and quantities.

Curves

κ	Curvature	$[m^{-1}]$
τ	Twist	$[m^{-1}]$
r	Radius of curvature	$[m]$
t	Tangent vector	
n$_c$	Normal vector	
b	Bi-normal vector	
t	Curve parameter	

Surfaces

κ_1	Max. principal surface curvature	$[m^{-1}]$
κ_2	Min. principal surface curvature	$[m^{-1}]$
K	Gaussian curvature	$[m^{-2}]$
H	Mean curvature	$[m^{-1}]$
k$_1$	Max. principal surface curvature vector	
k$_2$	Min. principal surface curvature vector	
n$_s$	Surface Normal vector	
$U\,/\,V$	Surface parameter	

Curve on Surface

κ_n	Normal curvature	$[m^{-1}]$
κ_g	Geodesic curvature	$[m^{-1}]$
τ_g	Geodesic torsion	$[m^{-1}]$
t	Tangent vector	
n$_s$	Normal vector	
u	Bi-normal vector	

Geometric Profile Quantities

w, h, t, d	Profile dimensions (width, height, thickness, diameter)	$[cm]$
e	eccentricity	$[cm]$
A	Profile area	$[cm^2]$
$W_{T/y/z}$	Sectional Moment (torsional, around y/z-axis)	$[cm^3]$
$I_{T/y/z}$	Moment on Inertia (torsional, around y/z-axis)	$[cm^4]$
I_P	Polar Moment of Inertia	$[cm^4]$
I_r	Helix area moment	$[cm^4]$

Mechanical Profile Quantities

$N, V_{y/z}$	Internal forces (normal force, shear force)	$[kN]$
$M_{T/y/z}$	Internal moments	$[kNcm]$
σ	Internal normal stress	$[kN/cm^2]$
$\tau_{y/z}$	Internal shear stress	$[kN/cm^2]$
ε, γ	Normal strain / shear distortion	$[-]$
$\kappa_{x/y/z}$	Twist / curvature due to torsion / bending	$[cm^{-1}]$

Energy

Π_i	Internal strain energy	$[kNcm]$
Π_e	External Work	$[kNcm]$
$\Pi_{pot.}$	Potential energy	$[kNcm]$

Material

E	Elastic Modulus	$[kN/cm^2]$
G	Shear Modulus	$[kN/cm^2]$
ν	Poisson ratio	$[-]$
σ_{Rd}	Strength (limit of linear elastic stress)	$[kN/cm^2]$
τ_{Rd}	Shear strength (limit of linear elastic shear stress)	$[kN/cm^2]$

Abbreviations

This list includes all abbreviations used in this work.

DoF   Degree of Freedom

SLS   Scissor Like Systems

IGA   Isogeometric Analysis

FEM   Finite Element Method

References

Ashby, M. F. (2011). *Materials selection in mechanical design* (4th ed.). Butterworth-Heinemann. http://www.sciencedirect.com/science/book/9781856176637

Barthel, R. (2019). *Structural Design: Flächen und Raumtragwerke.* Chair of Structural Design, Technical University of Munich.

Bauer, A. M [Anna M.], Wüchner, R., & Bletzinger, K.-U [Kai-Uwe] (2019). Isogeometric Analysis in the Design Process of Lightweight Structures. In International Centre for Numerical Methods in Engineering (Chair), *IASS,* Barcelona.

Bauer, A. M [Anna Maria]. (2020). *Cad-integrated isogeometric analysis and design of lightweight structures* [Dissertation, Technische Universität München, München]. WorldCat.

Bavarel, O., Feraille, A., Tayeb, F., Cravero, J., Tchiguirinskaia, L., Versini, P.-A., Caron, J.-F., & Mesnil, R. (2020). Structure Elastique et Procede de Mise en Place Correspondant(3080390). France. https://patentimages.storage.googleapis.com/42/42/a6/a97712115d1389/FR3080390 B1.pdf

Beckh, M. (2012). *Hyperbolische Stabwerke: Suchovs Gittertürme als Wegweiser in den modernen Leichtbau* (Erste Auflage). *DETAIL Special*. DETAIL. https://ebookcentral.proquest.com/lib/kxp/detail.action?docID=1383633

Bentley, D., Pottmann, H., Asperl, A., Hofer, M., & Kilian, A. (Eds.). (2007). *Architectural geometry* (First edition). Bentley Institute Press.

Bi, Z. (2020). *Computer Aided Design and Manufacturing*. *Wiley-ASME press series*. WILEY-BLACKWELL. https://ebookcentral.proquest.com/lib/kxp/detail.action?docID=6037150

Blümel, D. (Ed.). (1972). *Mitteilungen des Instituts für Leichte Flächentragwerke (IL): Vol. 5. Wandelbare Dächer: Convertible Roofs*. Institut für Leichte Flächentragwerke; Krämer [in Komm.].

Borrmann, A., König, M., Koch, C., & Beetz, J. (Eds.). (2015). *VDI-Buch. Building Information Modeling: Technologische Grundlagen und industrielle Praxis*. Springer Vieweg.

Burkhardt, B., & Bächer, M. (Eds.). (1978). *Mitteilungen des Instituts für Leichte Flächentragwerke (IL): Vol. 13. Multihalle Mannheim: Zugleich ein Bericht des Teilprojektes "Erfahrungen am Bauwerk" des Sonderforschungsbereichs 64 "Weitgespannte Flächentragwerke" der Deutschen Forschungsgemeinschaft*. Krämer.

Chengcheng Tang, Martin Kilian, Pengbo Bo, Johannes Wallner, & Helmut Pottmann (2016). Analysis and design of curved support structures. In S. Adriaenssens, F. Gramazio, M. Kohler, A. Menges, & M. Pauly (Eds.), *Aag 2016: Advances in Architectural Geometry 2016.* vdf Hochschulverlag AG an der ETH Zürich.

Chris Williams. (2014). What is a shell. In S. Adriaenssens, P. Block, D. Veenendaal, & C. J. K. Williams (Eds.), *Shell structures for architecture: Form finding and optimization* (pp. 21–31). Routledge.

D'Acunto, P., & Kotnik, T. (2013). *AA/ETH Pavilion*. Zürich, Switzerland. Chair of Structural Design, DARCH, ETH Zurich.

Dankert, J., & Dankert, H. (2006). *Technische Mechanik*. Teubner.

Du Peloux de Saint Romain, L. (2017). *Modeling of bending-torsion couplings in active-bending structures : application to the design of elastic gridshells* (2017PESC1209) [Theses, Université Paris-Est]. BibTeX. https://pastel.archives-ouvertes.fr/tel-01795135

ENPC (Ed.). (2020). *Corolle – a Vegetated Gridshell.* Think Shell. www.thinkshell.fr/corolle-a-vegetated-gridshell/

Escrig, F. (1996). General survey of deployability in architecture. In *Mobile and Rapidly Assembled Structures !!* (Vol. 21). WITpress. https://www.witpress.com/elibrary/wit-transactions-on-the-built-environment/24/9423

Fernández-Serrano, M. P. *The `movable Theatre ´ from Emilio Pérez Piñero. A space-time journey.* UPCT - Arquitectura y Tecnología de la Edificación.

Finsterwalder, S. (1899). Mechanische Beziehungen bei der Flächendeformation. In D. Mathematiker-Vereinigung (Ed.), *Jahresbericht der Deutschen Mathematiker-Vereinigung* (Vol. 6, pp. 43–59). Teubner; Reimer.

Goldbach, A., & Bletzinger, K.-U [K.-U.] (2019). CAD-integrated Parametric Design Cycle for Structural Membranes. In International Centre for Numerical Methods in Engineering (Chair), *IASS,* Barcelona.

Hernandez, E. L. (2016). *Design and Optimisation of Elastic Gridshells* [Dissertation, UDK, Berlin]. BibTeX. https://opus4.kobv.de/opus4-udk/frontdoor/index/index/docId/994

Hoberman, C. (1993). *Chuck Hoberman fonds, circa 1980-2006, Drawings and other graphic material, 1989-1999, predominant 1989-1994.* Canadian Centre for Architecture. www.cca.qc.ca

Howell, L. L. (2001). *Compliant mechanisms. A Wiley-Interscience publication.* Wiley. http://www.loc.gov/catdir/description/wiley039/2001026196.html

Ihde, A. (2018). *Kontrolle der Planungskomplexität bei Entwurf, Analyse und Konstruktion von Tragwerken* [Dissertation, Technische Universität München, München]. BibTeX.

Jaksch, S., & Sedlak, V. (2011). A Foldable Umbrella Structure – Developments and Experiences. *International Journal of Space Structures*, *26*(1), 1–18. https://doi.org/10.1260/0266-3511.26.1.1

Johnson, S. (2002). *Downland Gridshell.* www.thearchitectureensemble.com/collaborations_gridshell_5.html

Kassabian, P., You, Z., & Pellegrino, S [S.] (1999). Retractable Roof Structures. *Proceedings of the Institution of Civil Engineers - Structures and Buildings*, *134*(1), 45–56. https://doi.org/10.1680/istbu.1999.31252

Kinsey, L. C. (1993). *Topology of surfaces. Undergraduate texts in mathematics.* Springer.

Kleefisch-Jobst, U. (2017). *Vom Raumwunder und seinen Ingenieuren: die Multihalle in Mannheim.* Baukultur Nordrhein-Westfalen e. V. www.baukultur.nrw/artikel/vom-raumwunder-und-seinen-ingenieuren-die-multihalle-in-mannheim/

Krishnan, S., & Li, Y. (2019). Geometric Design of Axisymmetric Spatial Structures Using Planar Angulated Members. *Journal of Architectural Engineering*, *25*(2), Article 04019007. https://doi.org/10.1061/%28ASCE%29AE.1943-5568.0000348

Lehmann, T. (1985). *Elemente der Mechanik IV Schwingungen, Variationsprinzipe* (2., durchgesehene Auflage). Vieweg+Teubner Verlag. https://doi.org/10.1007/978-3-322-89571-4

Levien, R. (2008). *The elastica: a mathematical history.* USA. www.eecs.berkeley.edu/Pubs/TechRpts/2008/EECS-2008-103.html

Lienhard, J. (2014). *Bending-active structures: Form-finding strategies using elastic deformation in static and kinetic systems and the structural potentials therein.* Zugl.: Stuttgart, Univ., Diss., 2014. *Forschungsberichte aus dem Institut für Tragkonstruktionen und Konstruktives Entwerfen, Universität Stuttgart: Vol. 36.* ITKE. http://nbn-resolving.de/urn:nbn:de:bsz:93-opus-94838

Lindner, C., & Sun, T. (2021). *Transformable Cladding Systems: Research, Design and Fabrication* [Bachelor Thesis]. Technische Universität München, München.

Lumpe, G., & Gensichen, V. (2014). *Evaluierung der linearen und nichtlinearen Stabstatik in Theorie und Software: Prüfbeispiele, Fehlerursachen, genaue Theorie. Bauingenieur-Praxis.* Ernst.

Maden, F., Aktaş, E., & Korkmaz, K. (2015). A Novel Transformable Structural Mechanism for Doubly Ruled Hypar Surfaces. *Journal of Mechanical Design, 137*(3), Article 031404. https://doi.org/10.1115/1.4029231

MARCH. (2020). *Plate Rolling Workshop in Vyksa.* Moscow Architecture School (MARCH). https://en.march.technology/vyksa

Museum of Modern Art Archives. (1994). *Installation View of the exhibition "projects 45: Chuck Hoberman".* The Museum of Modern Art. www.moma.org/calendar/exhibitions/3080?

Novacki, Z. (2014). *Wandelbare lineareTragsysteme: Analyse und Neuentwicklung* [Dissertation]. Technische Universität München, München.

Oberbichler, T. (2021). *Bowerbird* (Version 2.8.0) [Computer software]. Github. https://github.com/oberbichler/Bowerbird

Panetta, J., Konaković-Luković, M., Isvoranu, F., Bouleau, E., & Pauly, M [M.] (2019). X-Shells. *ACM Transactions on Graphics, 38*(4), 1–15. https://doi.org/10.1145/3306346.3323040

Pflüger, A. (1964). *Stabilitätsprobleme der Elastostatik* (2nd ed.). Springer Berlin / Heidelberg. https://ebookcentral.proquest.com/lib/kxp/detail.action?docID=6594930

Pillwein, S., Kübert, J., Rist, F., & Musialski, P. (2020). Design and Fabrication of Elastic Geodesic Grid Structures. In E. Whiting (Ed.), *ACM Digital Library, Symposium on Computational Fabrication* (pp. 1–11). Association for Computing Machinery. https://doi.org/10.1145/3424630.3425412

Pillwein, S., Leimer, K., Birsak, M., & Musialski, P. (2020). On elastic geodesic grids and their planar to spatial deployment. *ACM Transactions on Graphics, 39*(4). https://doi.org/10.1145/3386569.3392490

Pillwein, S., & Musialski, P. (2021). Generalized deployable elastic geodesic grids. *ACM Transactions on Graphics, 40*(6), 1–15. https://doi.org/10.1145/3478513.3480516

Pottmann, H., Eigensatz, M., Vaxman, A., & Wallner, J. (2015). Architectural geometry. *Computers & Graphics, 47*, 145–164. https://doi.org/10.1016/j.cag.2014.11.002

Quinn, G. (2018a). *SheltAir.* UDK. www.udk-berlin.de/studium/architektur/aktuelles/sheltair/

Quinn, G. (2018b). *Pneumatic Erection of Elastic Gridshells: Design, Simulation & Realisation* [Dissertation]. UDK, Berlin. https://opus4.kobv.de/opus4-udk/frontdoor/deliver/index/docld/1209/file/Doctoral_thesis_Gregory_Quinn.pdf

Sangster, W. (1871). *Umbrellas and their history.* Cassell, Petter, and Galpin.

https://hdl.handle.net/2027/iau.31858044407512

Schikore, J. (2022). Mobile, Convertible and Adaptive Structures. In E. Möller (Ed.), *Edition Detail. Manual of structural design: Structural principles - suitable spans - inspiring works* (pp. 136–141). Detail Business Information GmbH; Walter de Gruyter GmbH.

Schikore, J., Bauer, A. M [Anna M], Barthel, R., & Bletzinger, K.-U [K.-U.] (2019). Large Torsion on Elastic Lamella Grid Structures. In International Centre for Numerical Methods in Engineering (Chair), *IASS,* Barcelona.

Schikore, J., Schling, E., Oberbichler, T., & Bauer, A. M [Anna Maria] (2020). Kinetics and Design of Semi-Compliant Grid Mechanisms. In O. Baverel, C. Douthe, R. Mesnil, C. Mueller, H. Pottmann, & T. Tachi (Eds.), *AAG 2020 // Advances in architectural geometry 2020: Advances in Architectural Geometry 2020* (pp. 108–129). Ecole des Ponts ParisTech; Université Gustave EiffeldDL 2021. https://mediatum.ub.tum.de/doc/1631486/document.pdf

Schleicher, S. (2016). *Bio-inspired Compliant Mechanisms for Architectural Design: Transferring Bending and Folding Principles of Plant Leaves to Flexible Kinetic Structures* [Dissertation]. Universität Stuttgart, Stuttgart.

Schling, E. (2018). *Repetitive structures* [Dissertation, Technische Univerität München, Fakultät für Architektur, Lehrstuhl für Tragwerksplanung, Prof. Dr.-Ing. Rainer Barthel, München]. Deutsche Nationalbibliothek.

Schling, E., & Barthel, R. (2021). Šuchov's bent networks: The impact of network curvature on Šuchov's gridshell designs. *Structures*, *29*, 1496–1506. https://doi.org/10.1016/j.istruc.2020.12.021

Schling, E., Hitrec, D., & Barthel, R. (2018). Designing Grid Structures Using Asymptotic Curve Networks. In K. de Rycke, C. Gengnagel, O. Baverel, J. Burry, C. Mueller, M. M. Nguyen, P. Rahm, & M. R. Thomsen (Eds.), *Humanizing digital reality: Design Modelling Symposium Paris 2017* (pp. 125–140). Springer Singapore; Imprint; Springer. https://doi.org/10.1007/978-981-10-6611-5_12

Schling, E., Hitrec, D., Schikore, J., & Barthel, R. (2017). Design and Construction of the Asymptotic Pavilion. In K.-U. Bletzinger, E. Onate, B. Kröplin (Ed.), *Structural Membranes 2017* (Vol. 8, pp. 178–189). Artes Gráficas Torres S.L., Huelva 9, 08940 Cornellà de.

Schling, E., Kilian, M., Wang, H., Schikore, J., & Pottmann, H. (2018). Design and Construction of Curved Support Structures with Repetitive Parameters. In L. Hesselgren, A. Kilian, S. Malek, K.-G. Olsson, O. Sorkine-Hornung, & C. Williams (Eds.), *AAG 2018: Advances in Architectural Geometry 2018* (Vol. 7, pp. 140–165). Klein Publishing GmbH; Klein Publishing GmbH (Ltd).

Schling, E., & Schikore, J. (2022). Morphology of Kinetic Asymptotic Grids. In C. Gengnagel, O. Baverel, G. Betti, M. Popescu, M. Ramsgard Thomsen, & J. Wurm (Eds.), *Towards radical regeneration: Design Modelling Symposium Berlin 2022* (pp. 374–393). Springer. https://doi.org/10.1007/978-3-031-13249-0_31

Schling, E., Schikore, J., & Oberbichler, T. (2021). D-Nets on rotational surfaces. Equilibrium gridshell layout, symmetric to the principal stress directions. In International Centre for Numerical Methods in Engineering (Chair), *IASS,* Surrey.

Šljivić, A., Miljanović, S., & Zlatar, M. (2021). *A new classification of deployable structures.*

University of Sarajevo. E3S Web of Conferences. https://doi.org/10.1051/e3sconf/202124405016

Soriano, E., Sastre, R., & Boixader, D. (2019). G-shells: Flat collapsible geodesic mechanisms for gridshells. In International Centre for Numerical Methods in Engineering (Chair), *IASS,* Barcelona.

Tan, L. T., & Pellegrino, S [Sergio]. (2006). Thin-Shell Deployable Reflectors with Collapsible Stiffeners Part 1: Approach. In *AIAA Journal* (Vol. 44, pp. 2515–2523). https://authors.library.caltech.edu/11120/1/TANaiaaj06.pdf

Technische Universiteit Delft. (2001). *Research by design: International conference, Faculty of Architecture, Delft University of Technology in co-operation with the EAAE/AEEA, November 1 - 3 2000*. DUP.

TESS. (2011). *Forum Café, Festival Solidays: Construction d'une structure provisoire en gridshell*. www.tess.fr/projet/forum-cafe-festival-solidays

von Braunmühl, A. (1891). *Christoph Scheiner als Mathematiker, Physiker und Astronom*. *Bayerische Bibliothek: Vol. 24*. Buchnersche Verlagsbuchhandlung. www.digitale-sammlungen.de/de/details/bsb00127419

Figures

178